MODEL REFERENCED CONDITION MONITORING OF HIGH PERFORMANCE CNC MACHINE TOOLS

SEBASTIAN SZTENDEL

A thesis submitted to the University of Huddersfield in partial fulfilment of the requirements for the degree of Doctor of Philosophy

December 2016

The University of Huddersfield

Copyright statement

i. The author of this thesis (including any appendices and/or schedules to this thesis) owns any copyright in it (the “Copyright”) and s/he has given The University of Huddersfield the right to use such copyright for any administrative, promotional, educational and/or teaching purposes.

ii. Copies of this thesis, either in full or in extracts, may be made only in accordance with the regulations of the University Library. Details of these regulations may be obtained from the Librarian. This page must form part of any such copies made.

iii. The ownership of any patents, designs, trademarks and any and all other intellectual property rights except for the Copyright (the “Intellectual Property Rights”) and any reproductions of copyright works, for example graphs and tables (“Reproductions”), which may be described in this thesis, may not be owned by the author and may be owned by third parties. Such Intellectual Property Rights and Reproductions cannot and must not be made available for use without the prior written permission of the owner(s) of the relevant Intellectual Property Rights and/or Reproductions

Declaration

I declare that this thesis is my own investigation, and is not being concurrently submitted in candidature for any other degree.

Sebastian Sztendel

ACKNOWLEDGMENTS

I am deeply grateful to Dr Andrew Longstaff for his invaluable support, patience, kind encouragement, mentorship, and long hours without which I could have never accomplished this project. I owe much to him for his willingness to devote time and energy to my work, but words cannot describe how thankful I am. His constant feedback on every aspect of the project helped me in honing my knowledge. He has continuously provided me with enthusiasm, vision, and wisdom. I would like to thank Dr Crinela Pislaru for giving me the opportunity to undertake this so interesting project. This dissertation could not have been completed without her guidance and help, to whom I am extremely grateful. Her professionalism and immense knowledge helped me in all the time.

There are no words to convey my appreciation for Klaus Meck and John Crane in supporting the project and providing hardware throughout the duration of AE work.

It is a pleasure to express my sincerest gratitude to Andrew Bell who has supported me throughout my dissertation with his patience, time and knowledge and my colleague Moschos.

My mentors ideas and vision have helped guide, shape and inspire my postgraduate studies. They have been a constant source of brilliant guidance and support during every stage of my project. I admire them for their wide knowledge, creative thinking, and deep insight in machine tools and control theory.

Sebastian Sztendel

Huddersfield

2016

ABSTRACT

Generally, machine tool monitoring is the prediction of the system's health based on signal acquisition and processing and classification in order to identify the causes of the problem. The producers of machine tools need to pay more attention to their products life cycle because their customers increasingly focus on machine tool reliability and costs. The present study is concerned with the development of a condition monitoring system for high speed Computer Numerical Control (CNC) milling machine tools.

A model is a simplification of a real machine to visualize the dynamics of a mechatronic system. This thesis applies recent modelling techniques to represent all parameters which affect the accuracy of a component produced automatically. The control can achieve an accuracy approaching the tolerance restrictions imposed by the machine tool axis repeatability and its operating environment. The motion control system of the CNC machine tool is described and the elements, which compose the axis drives including both the electrical components and the mechanical ones, are analysed and modelled. SIMULINK models have been developed to represent the majority of the dynamic behaviour of the feed drives from the actual CNC machine tool. Various values for the position controller and the load torque have been applied to the motor to show their behaviour.

Development of a mechatronic hybrid model for five-axis CNC machine tool using Multi-Body-System (MBS) simulation approach is described. Analysis of CNC machine tool performance under non-cutting conditions is developed. ServoTrace data have been used to validate the Multi-body simulation of tool-to-workpiece position.

This thesis aspects the application of state of art sensing methods in the field of condition monitoring of electromechanical systems. The ballscrew-with-nut is perhaps the most prevalent CNC machine subsystem and the condition of each element is crucial to the success of a machining operation. It's essential to know of the health status of ballscrew, bearings and nut. Acoustic emission analysis of machines has been carried out to determine the deterioration of the ballscrew. Standard practices such as use of a Laser Interferometer have been used to determine the position of the machine tool.

A novel machine feed drive condition monitoring system using acoustic emission (AE) signals has been proposed. The AE monitoring techniques investigated can be categorised into traditional AE parameters of energy, event duration and peak amplitude. These events are selected and normalised to estimate remaining life of the machine. This method is shown to be successfully applied for the ballscrew subsystem of an industrial high-speed milling machine.

Finally, the successful outcome of the project will contribute to machine tool industry making possible manufacturing of more accurate products with lower costs in shorter time.

ABBREVIATIONS

AE	Acoustic Emission
AET	Acoustic Emission Testing
ACC	Adaptive Control Constraint
AD	Accidental Damage
AS	Airborne Sound
CAD	Computer-aided Design
CBM	Condition Based Monitoring
CNC	Computer Numeric Control
CG	Center of Gravity
CS	Coordinate System
DAC D/A	Digital-To-Analogue
DBN	Dynamic Bayesian Networks
DC	Direct current
DoF	Degrees of Freedom
DTC	Direct Torque Controller
ED	Environmental Damage
EGF	Empirical Green's Function
FD	Fatigue Damage
FDTD	Finite Difference Time Domain
FE	Finite Element
FEM	Finite Element Method
FFT	Fast Fourier Transform
FMM	Flexible Multibody Models
FRF	Frequency Response Function
GMS	Generalized Maxwell-Slip
GPC	Generalized Predictive Control
GUI	Graphical User Interface
GUM	Guide to the Expression of Uncertainty in Measurement
HIL	Hardware-In-the-Loop
HMI	Human Machine Interface
HSM	High Speed Machining
HTML	Hypertext Mark-up Language
I/O	Input – Output
MBS	Multibody Simulation
MCP	Machine Control Panel
MFBD	Multi-Flexible-Body-Dynamics
MID	Modulation Intensity Distribution
MIL	Model-In-the-Loop

MRR	Material Removal Rate
NCK	Numerical Control Kernel
NCU	Numerical Control Unit
NDT	Non-Destructive Testing
ODE	Ordinary Differential Equation
PCA	Principal Component Analysis
PDE	Partial Differential Equation
PID	Proportional–Integral–Derivative
PIL	Processor-In-the-Loop
PLC	Programmable Logic Controller
PMSM	Permanent-Magnet Synchronous Motor
PWM	Pulse Width Modulation
PZT	Piezoceramic lead-zirconate-titanate
RMS	Root Mean Square
RT	Real time
RTI	Real-Time Interface
RTW	Real-Time Workshop
S-wave	Shear/transverse waves
SD	Standard Deviation
SIL	Software-In-the-Loop
SK	Spectral Kurtosis
SMC	Sliding Model Control
SOM	Self-Organization feature Map
SV	Surface Vibration
TLC	Target Language Compiler
TMF	Thermal Mechanical Fatigue
TLM	Transmission Line Matrix
WGs	Ultrasonic Waveguides
WMRA	Wavelets based Multi-Resolution Analysis
VR	Virtual Reality
VRML	Virtual Reality Modelling Language

LIST OF PUBLICATIONS

Sztendel, S., Pislaru, C. – Development of Control Graphical User Interface (GUI) for a dSPACE Real-Time System. Proc. School of Computing and Engineering Research Festival, Huddersfield, 7 Mar 2008.

Pislaru, C., Sztendel, S., Ford, D., Myers, A. - Real -Time Implementation of a Novel Transmission Line Matrix (TLM) Model for High Speed Feed Drives, Proceedings of Int. Conference on Machine Tools, Automation and Robotics in Mechanical Engineering MATAR 2008, Prague University, Sept 08, pp. 25-30.

Sztendel, S., Pislaru, C., Ford, Derek G., Myers, Alan - Development of Experiment Control Graphical User Interface for Hardware in the Loop (HIL) Simulations. Proceedings of Int. Conference MATAR 2008, Prague University, Sept 08, pp. 123-128.

Sztendel, S., Pislaru, C., Poxton, A., Ford, D.G., Myers, A. - Developing Mechatronic Models Of Modern CNC Machine Tools For Real-Time Implementation. Proc. 9th Int. Conf. on Laser metrology, machine tool, CMM and robotic performance (LAMDAMAP 2009), 30June - 2 July 2009, Brunel University, pp. 147-155.

Sztendel, S., Pislaru, C., Longstaff, A., Ford, D., Myers, A., Poxton, A. – Linking Feed drive Models with Structural Models for CNC Machine Tools. Proc. School of Computing and Engineering Research Festival, Huddersfield, Mar 2010.

Sztendel S., Pislaru C., Longstaff A.P., Fletcher S., Ford, D.G., Myers A., - *Analysis of complex interactions between mechanical elements using ANSYS and SIMULINK,* Computing and Engineering Researchers' Conference, University of Huddersfield, March 2012

Sztendel S., Pislaru C., Longstaff A.P., Fletcher S., Myers A. - *Five-Axis Machine Tool Condition Monitoring Using dSPACE Real-Time System* Proceedings of Int. Conference COMADEM 2012

Sztendel, S., Papananias, M. and Pislaru, Crinela (2015) Improving the Dynamic Performance of Five-Axis CNC Machine Tool by using the Software-in-the-Loop (SIL) Platform. In: Laser Metrology and Machine Performance XI, LAMDAMAP 2015. EUSPEN, Huddersfield, UK, pp. 170-180. ISBN 978-0-9566790-5-5

Papananias, M., Sztendel, S. and Pislaru, Crinela (2015) Development of a Novel Multi Body Mechatronic Model for Five-Axis CNC Machine Tool. In: Laser Metrology and Machine Performance XI, LAMDAMAP 2015. EUSPEN, Huddersfield, UK, pp. 379-389. ISBN 978-0-9566790-5-5

LIST OF TABLES

TABLE OF CONTENTS

LIST OF FIGURES

CHAPTER 1 INTRODUCTION

Having the ability to detect mechanical parts degradation to the point where a replacement can be planned is invaluable to a manufacturer who utilizes Computer Numerical Control (CNC) machines. This thesis looks into the possibility of utilizing mathematical modelling techniques in the field of condition monitoring of mechatronic systems. The focus of this work was to develop a system to monitor in order to minimise their off times Machine tools are chosen as an example.

1.1 MOTIVATION

Manufacturing industry demands increased product quality, batch production, limited development times and just-in-time production. Increased productivity and profitability is seen only when production is reliable and without disturbances, which is possible if there is complete control of the machining process with optimal degree of computerisation. Industry's aim is to perfectly produce parts, "right first time", with tight tolerances in the lowest total processing time. Therefore, there is a noticeable trend for companies to scale down their process development efforts and to plan processes on the machine, which imposes further constraints on process reliability.

Machine tool manufacturers aim to produce precise machine tools to increase the value of manufactured goods. Machine tool accuracies directly impact load capacity, quality, and efficiency of manufacturing processes. A negative impact of requiring a very high accuracy of machine is the potential downtime required to maintain that state. The quality and functionality of each element is an important part in the chain that contributes to the accuracy.

Buying new machines and tooling requires large capital investments and it doesn't solve production profitability problems if they are underutilized. There is a trend in manufacturing systems to a structure consisting of small, intelligent and flexible units with monitoring capabilities which increases the demand to monitor quality and performance by solutions integrated into intelligent systems like Computer Numeric Control CNC machine tools.

The typical CNC milling machine feed drive consists of several elements that can influence precision. To predict and eliminate the faults in a precision engineering process requires computationally fast and efficient algorithms that mathematically model the system, which replicates the dynamic behaviour of the process. The design of CNC machine feed drives involves expensive and time-consuming calculations and therefore the modelling and simulation techniques become beneficial for the design process.

Computational modelling and analysis tools play a key role in high performance machining and have become essential parts of engineering design, especially for complex continuous dynamic systems which incorporate nonlinearities, such as friction and backlash. This thesis presents the mathematical equations used to develop the model of the axis drive for a five-axis CNC machine tool. A five-axis gantry machine existing at the University of Huddersfield is used as a case study. The motion control system, which consists of the controller, electrical drives, guide-ways, transducers and transmission, is one of the most important elements of the CNC machine tool since it governs the relative tool-to-workpiece position that is vital to the form of the finished product.

This thesis is focused on the development of advanced techniques for monitoring the machine tool with reference to the derived simulation model. The real-time control and monitoring is concerned with sensor application during the dry-run processes. Sensors are devices which convert physical properties into electrical signals. Indirect computer supported techniques such as: sensor base monitoring and control and virtual machining process simulation have been accepted for real-time decision making and system developments (Hujun 2013).

A machine tool is an electrically powered mechatronic system equipped with cutting tools used to remove material. Machining is a metal-cutting operation, which is performed by shaving away metal in small pieces to achieve a desired form. A machine tool controls the movements of the axes to move the relative position of the cutting tool and workpiece to achieve a desired product shape. The modern CNC machine tool has the ability to achieve high accuracy and precision, if is utilized efficiently.

SIMULINK block diagrams represent an insightful object-orientated programming language Thus, specific aspects such as axis feed, spindle speed, movement of the tool can be investigated (Neugebauer 2012). SIMULINK is used to reproduce the workspace of the machine tool in model. The accuracy of the model depends on the model structure and the model parameters. The difference between the actual positions of the drive and model will be monitored continuously. Simulated results compare well with the experimental data measured from the actual machine so that the proposed model is validated. This represents the first step in developing a software-in-the-loop model of the machine including the horizontal, vertical and rotary axes drives.

The detailed computer-aided design (CAD) model for the CNC machine in SolidWorks and development of Multi-Body-Simulation (MBS) approach provides useful information about the interactions which occur between the machine components and their dynamic properties obtained in elapsed time. The combination of MATLAB/SIMULINK/SimMechanics and SolidWorks software packages has been proven as a fast and efficient solution for developing a multi-body mechatronic hybrid model for the five-axis CNC machine tool. This novel model containing blocks from SimPowerSystems, SimDriveline, and SimMechanics fulfils the main purpose of this work - making possible the performance evaluation of machine tools and the production of more accurate products with lower costs and time.

This thesis describes the steps for data acquisition using ControlDesk and SIL software-in-the-loop implementation of the drive models in dSPACE. The real time system provides a block library to access the controller board interfaces (analogue and digital in-/outputs, encoder inputs, etc.), that are used like source and sink blocks in the SIMULINK model of the control algorithm. Process control (Start, Stop), data acquisition, online visualisation and software project management is supported by a configurable “Control Desk” where the experiment control graphical user interface (GUI) has been completely developed. Real time operating system is mainly used to guarantee that a process runs within a specified time interval. The integration required accessing dSPACE Data acquisition DAQ cards and command transfer via machine interface to the SINUMERIK 840d sl controller.

Gantries include many crucial electrical and mechanical elements. One of the major problems with a gantry is misalignment which causes uneven and distorted motion. Condition monitoring is one of the methods to prevent that. Other causes of ballscrew failure is insufficient lubrication and its contamination. Without condition monitoring gantry misalignment may cause short system life, downtime, high maintenance costs and decreased accuracy. (Eidelberg 2015)

Condition Monitoring (CM) is a technique that is used to monitor the operational state and health of a machine, and to detect potential machine degradation before they develop into a failure. The procedure involves periodically timed or continuous data acquisition and analysis. CM forms an essential part of a Condition Based Maintenance System (CBMS). It enhances operational effectiveness and reliably predicts the remaining useful life (RUL) of equipment. CBMS optimizes equipment readiness while reducing maintenance and man-hours therefore techniques are being progressively implemented in the industry providing additional time to plan necessary maintenance procedures. (Mathew 2006)

The transient elastic waves produced by release of energy produced by the friction, rubbing, material loss damage can be detected for CM purposes. Mechanical deformation is accompanied by the motion of a large numbers of atomic displacements which produces such energy with varying frequencies. Lower frequencies are usually examined with vibration analysis using accelerometers. Acoustic Emission (AE) is used to detect energy released in the higher frequency range. AE is one of a non-destructive testing (NDT) technique method based on the detection of those high frequency elastic waves. High sensitivity is the main unique capability so sensors can detect small-scale damage long before failure. AE was first developed for NDT of architectural structures, but has been used to monitor the health of rotating parts like bearings, pump impellers and gearboxes. (Walsh 2015)

AE can produce either impulsive or continuous signals high frequency signals therefore it can be used to detect defects much earlier compared with other conventional NDT methods (Theobald 2016). The AE monitoring techniques can be characterised into AE parameters of: RMS, energy and peak amplitude. Once the initial signal processing has been completed, analysis of the measurement data begins. To track and quickly detect faulty or broken machine tools, the

measurement curves are tracked with defined limits. When a limit on the curve is violated, the system can respond by switching operation of the machine.

Measurement uncertainty expresses incomplete knowledge of a measurement and can directly affect the confidence with which reaction can be taken to changes in data. To evaluate the uncertainty of the data coming from the AE sensor, the signal is measured using a procedure described in the “Guide to the Expression of Uncertainty in Measurement” GUM BIPM (2012) to determine the likelihood function. This function depends on the AE measurement problems and the measuring system uncertainties.

AE technique brings the capability of novel real time continuous monitoring for the ballscrew assembly. Therefore, a machine tool feed drive condition monitoring system combining acoustic emission signals and model is proposed.

1.2 AIMS AND OBJECTIVES

The aims of the thesis are:

- the development of a novel multi-body mechatronic model for five-axis CNC milling machine tool which represents the behaviour of the electrical and mechanical elements in a single simulation environment and which can be used for condition monitoring purposes.
- the integration of acoustic emission signals into the condition monitoring systems.

OBJECTIVES:

Modelling

- Produce a multi-body mechatronic model for a 5-axis milling machine and validate it by comparing the simulation values with data from the inbuilt monitoring tools (ServoTrace)
- Build a Software-in-the-Loop (SIL) platform using dSPACE real-time system and machine model.

Acoustic Emission

- Determine Data Acquisition (DAQ) system to record the outputs of AE sensors for the analysis of the high frequency signals.
- Use Bayesian uncertainty assessment to evaluate the uncertainty related to the estimates obtained from measured data and to evaluate the performance of AE sensors for suitability for machine tool condition monitoring
- Validate the system by correlating the AE measurements with laser measurements.

Condition monitoring

- Define the CM strategy which employs the dSPACE real-time system and machine model and investigate the degradation of a ballscrew subsystem of a machine tool using Acoustic Emission (AE) sensors

1.3 THESIS OUTLINE

The work presented in this thesis consists of nine chapters, the first three of which provide the necessary background material, the fourth to eighth chapters detail the main original work, and the last chapter includes conclusions and suggestions for further work. Figure 1-1 show overall thesis layout.

Chapter 1 introduces the research background and importance of the research, scientific contributions aims and objectives, and structure of this thesis.

Chapter 2 reviews state-of-the-art and relevant fundamental theoretical background of the presented literature review in field of condition monitoring and acoustic emission

Chapter 3 describes in detail the CNC controller, a Siemens SINUMERIK 840D sl and Drive-CLiQ real-time serial digital interface. Basic theory and general equations of the associated components are outlined. It also introduces the CNC machine tool feed drives of the studied system. It concentrates on modelling and describing the components of CNC machine tool axis drives including both the electrical and the mechanical elements.

Chapter 4 presents the implementation and working of the SIMULINK model. Models for the CNC machine tool axis drives are developed in SIMULINK and tested. Variable load torques are applied to the motors to simulate the behaviour of feed drives. The 3D assembly of the machine tool is done in SolidWorks, imported into SimMechanics and modified to fit the needs of the CNC milling machine. Feed drive models drive the SimMechanics model of the CNC machine tool. The mechatronic hybrid model based on MBS simulation approach is controlled in SimMechanics which runs within the SIMULINK. The complete model contains blocks from Simscape which comprises SimPowerSystems blocks, SimDriveline blocks and SimMechanics blocks.

Chapter 5 presents development of software in the loop platform on dSPACE real time system hardware This section present the steps of performing data acquisition using ControlDesk from dSPACE real-time system and the development of SIL implementation which is used the validated proposed drive model.

Chapter 6 This chapter will first review the theory and previous application of acoustic emission (AE) monitoring. Then it presents details of a typical AE System: the principle of the AE sensors, preamplifier and data acquisition system. This chapter includes a description of how couplant material is determined by the particulars of the application. Details of the experimental setup and

procedure to determine uncertainties are explained. A statistical Bayesian model is developed to describe the relationship between the uncertainty parameters.

Chapter 7 proposes a machine tool condition monitoring system using AE signals. A ballscrew with nut is perhaps the most widely used CNC machine subsystem and their condition is critical to the operation of CNC machine. Various AE parameters including RMS, energy etc. are extracted from continuous AE events. These events are ordered and normalized using Matlab software

Chapter 8 describes how real-time system can be used for the development of machine tool diagnosis and prognosis systems that facilitate the improvement of maintenance activities. This chapter presents the definition of a ballscrew remaining useful (RUC) life algorithm.

Chapter 9 draws conclusions arising from investigation and proposed suggestions for further work.

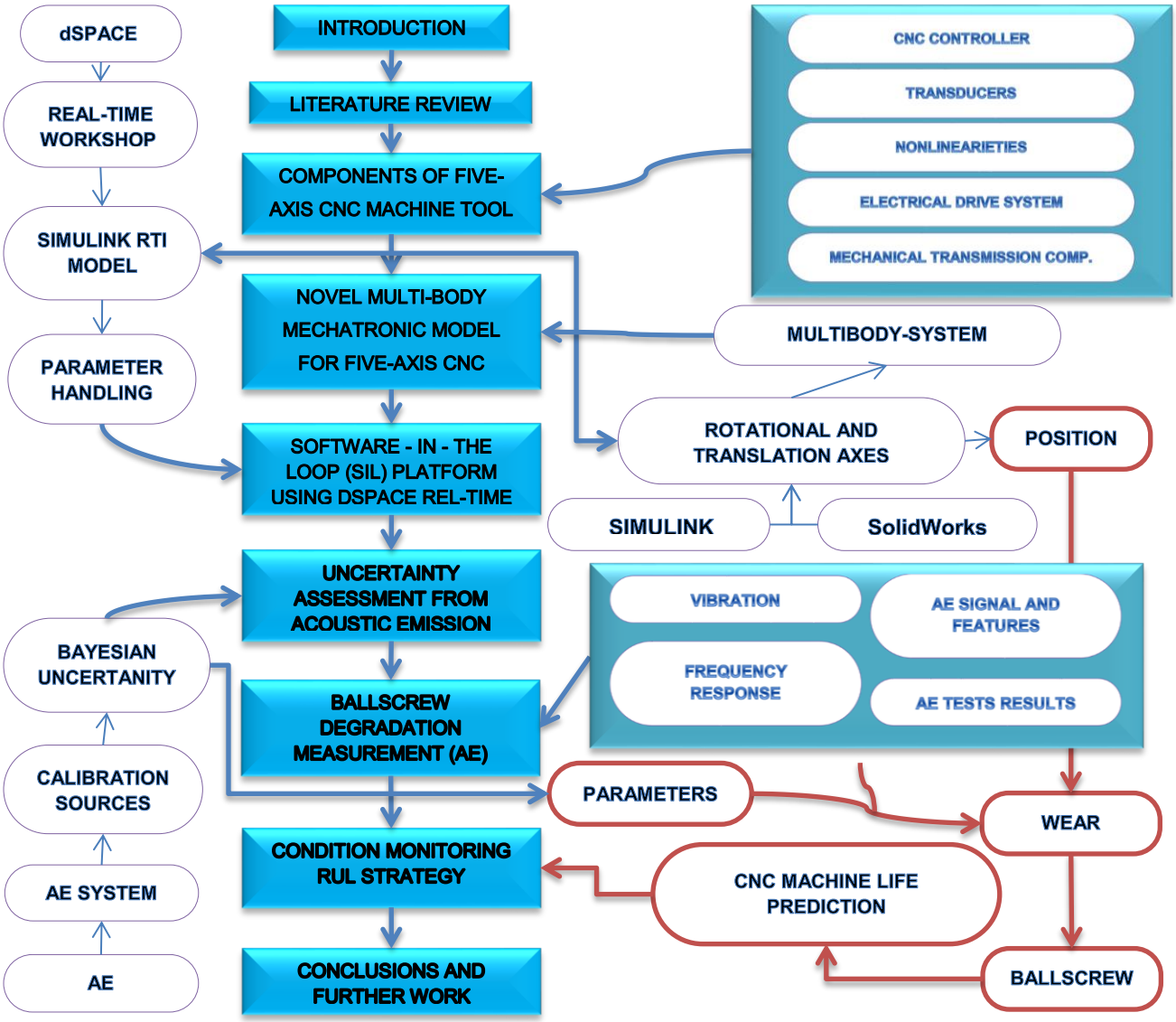

Figure 1-1 Thesis layout

Additionally, the dissertation includes eight appendices – AE sensor review, the SIMULINK parameters, results and Matlab code and results.

1.4 RESEARCH METHODOLOGY

The scope of this thesis is to evaluate the condition monitoring methods used for metal-cutting machine tools. The methodology in the first instance was to obtain knowledge about machine tools, modelling, instrumentation and other industrial processes. Detailed discussions were held with the machine tool experts of the department and CNC controller suppliers to explore their knowledge and acquire in-depth understanding of the points of failure, measurement and monitoring strategies, influencing parameters, etc. This face-to-face learning was supplemented by in-depth academic literature research into the very broad areas of machine tool measurement and modelling, condition-based monitoring, etc. This review of the body of knowledge led to the choice of modelling technique. The previous work in literature had concentrated on 3-axis machine tools. For this research, a 5-axis gantry machine was chosen for modelling.

5-axis gantry milling machine displayed in is constructed of 3 linear and 2 rotary axes. This consists of the left and right had sides of the gantry (Y master and slave) on top of which is placed the X axis (left to right) and on top of that the Z-axis (vertical column). GEISS trimming spindle is equipped with an open machine table and orthogonal trimming head. Figure 1-2 shows the five-axis machine existing at the University of Huddersfield which has been used for practical measurements.

a) Actual five-axis machine b) Rotational B and C axes

Figure 1-2 Actual five-axis machine and the rotational B and C axes.

Ballscrew transforms the rotary motion into the liner motion of the gantry axis. The gantry is composed of Y1 and Y2 axis. The unique feature is that the gantry axis consists of two 1FK7 driving motors with a beam between them. It has direct drives so the servo-motors are joined directly to the load with no transmission devices. These motors allow the dynamic direction changes for high velocities and excellent accuracy.

Feed drive performance is dependent on transmission devices, ballscrew, electronics, mechanical structures and feedback sensors. One of the major problems with a gantry axis is missalingment.

Tilted gantry will cause uneven and distorted feed drive motion. Real time condition monitoring is one of the ways to prevent that. In order to produce a feed drive model, MATLAB and SIMULINK work has been used. In Figure 1-3 methodology tree is presented. Choice of suitable analysis methods was made based upon analytical and experimental verification of the basic dynamic and static characteristics and parameters of the system and analysis of previous work Widiyarto (2005) Pislaru (2001), where it had been shown to be effective. Furthermore, the proposed software-in-the-loop (SIL) system would rely upon the dSPACE data acquisition system, so the native MATLAB language was the obvious choice. Experimental data was collected from the chosen CNC milling machine and used in a database for the SIL modelling. Novel multi-body mechatronic model for five-axis CNC including the horizontal, vertical and rotary axes drives which represent the behaviour of electrical and mechanical elements in a single simulation environment has been developed in this work. Design a detailed CAD model for the GEISS machine in SolidWorks and develop Multi-body simulation MBS approach in SimMechanics to examine interactions that occur between machine tool components and the motion dynamic properties obtained with regard to elapsed time. This approach to modern maintenance practice can be used on various CNC machines with similar feed drive systems

Condition monitoring solution relies on the capabilities of simulation software such as SIMULINK. Software in the loop (SIL) simulation reproduce the NC control unit which reacts to errors between real input from CNC and model. The approach has been shown to be scalable to other axes, giving it widespread applicability. The steps for data acquisition using ControlDesk and SIL implementation of the feed drive models in dSPACE real-time system has been described. It has been explained how the experimental data obtained from the data acquisition process using dSPACE ControlDesk can be used for developing machine tool diagnosis and prognosis systems.

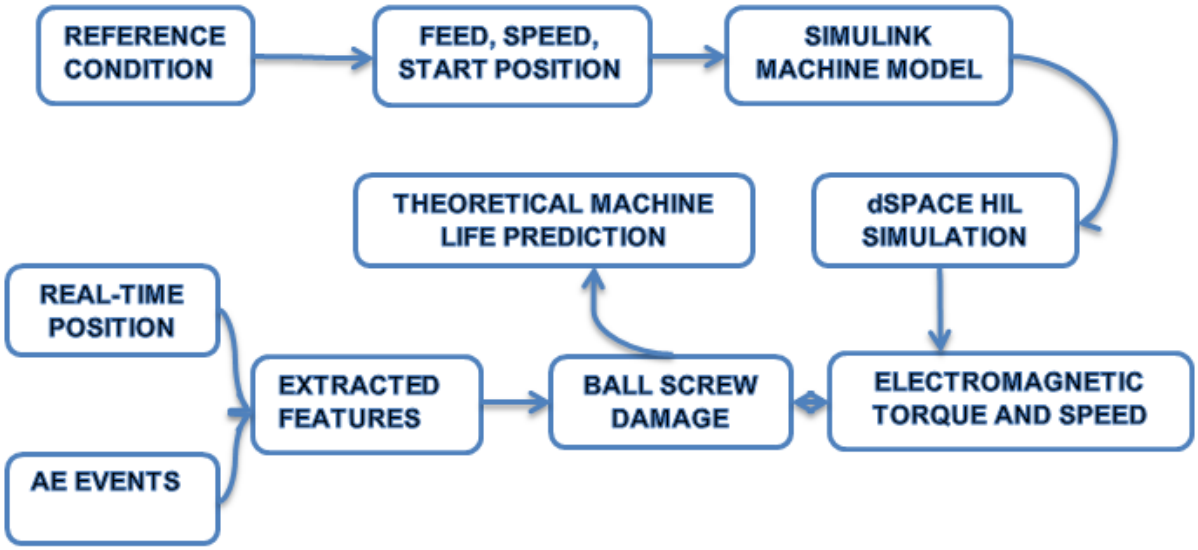

Figure 1-3 Methodology tree

Vital phase of detection and Condition Monitoring requires a robust identifier which simulates dynamic measuring systems by extracting relevant AE features. Bayesian uncertainty assessment and study in influences of external factors on AE measurement. In this work acceptable degree and locate higher AE peaks on the ballscrew has been established.

Reference condition and real time data like feed, speed and start position has been used in dSPACE simulation. The motion and behaviour of ballscrew provide very useful information, such as degree of wear, lubrication and breakage. Real time estimation of the position is and model parameters are used to quantify the damage in precise point. The extracted AE features (relation between contact AE energy and ballscrew wear calculated) and used to estimate the life. The prescribed levels are based on theoretical results.

The most used non-destructive testing like vibration and acoustic emission (Theobald 2016) methods for inspection purposes have been evaluated for reliability and accuracy. This down-selection led to acoustic emission (AE) being explored more deeply for this application due to its promising initial results and it not being previously used for this application with reference to the uncertainty of measurement. Limitations, advantages and disadvantages of the sensor have been discussed. The calibration test procedures are described and AE monitoring is conducted physically on the chosen machine. Mathematical evaluation of the AE signal features in the time domains and the frequency response of the system is carried out using software. The results from the experimental data were significant.

A theoretical approach is described for predicting the remaining life for the ballscrew. Its life prediction based on AE signal compared to electromagnetic torque is discussed. Laboratory testing of a faulty feed-drive system and comparing their output signals with those obtained in a hardware-in-the-loop (HIL) model should be the next stage of research.

CHAPTER 2 LITERATURE REVIEW

Modelling and simulation are essential parts of engineering design especially for complex continuous dynamic systems which incorporate non-linearity. Various factors affect the performance of machine tool motion control system and the appropriate choice of motor technology and various elements of machine tools contribute to a high-performance system structure. The motion control system, which consists of the controller, electrical drives, guide-ways, transducers and transmission, is one of the most important elements of the Computer Numeric Control (CNC) machine tool. The accuracy and repeatability of the CNC machine tool depends upon the performance of the motion control system, which governs the tool-to-workpiece relationship. Therefore, the motion control system has to respond accurately. As industrial applications increasingly require higher performance machining, reliability and lower cost, there is the need for more precise models of the motion control systems.

2.1 ADAPTIVE CONTROL AND REAL-TIME TECHNIQUES USED FOR CONDITION MONITORING PURPOSES

Computationally fast and efficient algorithms are required for the prediction, computation, and elimination of the instantaneous error in high precision engineering processes. In order to achieve this, a mathematical model is required that adequately reflects the true dynamic behaviour of the various components and of the complete assembly of machine tool.

The requirement for a true “real-time” solution for monitoring can impose severe constraints on the cost of hardware and complexity of algorithm that can be processed, based upon the speed of the processor. A “deadline miss” describes the case where a processing algorithm has failed to complete “in real time.” Hansen and Drews (2006) maintain that the design of “hard” real-time systems, assuming that the system could fail from a single deadline miss, leads to significant waste of resources because this assumption in quite drastic in the case of majority of practical systems. The authors recommend that a small fractions of missed deadlines be allowed without loss of system integrity. Adopting this approach, the required resources will be reduced dramatically and the “soft/firm real-time systems must focus on more than just minimizing the mean delay” meaning addressing the task delay distribution with respect to a fixed deadline or through a time/utility function.

2.2 MODELLING, SIMULATION AND CONTROL OF MACHINING PROCESS AND MACHINE TOOLS

Various applications have been developed, which take advantage of the Virtual CNC's accurate simulation capability in predicting and improving the dynamic performance of real CNC machine tools.

Yeung (2006) experimentally verified various tracking control schemes, such as proportional–integral–derivative PID, Sliding model control SMC, Generalized Predictive Control GPC on the Virtual CNC system. A comprehensive virtual model of a Modular CNC was presented. The Virtual CNC allows modular integration of trajectory planning and interpolation routines, mathematical models of ballscrew and linear drives, friction, feedback sensors, amplifiers, digital-to-analogue converters (DAC) and flexible motion control laws.

The potential of the virtual machine concept in an optimization study of the complete machine tool has been shown by Fredin et al. (2012). They presented an efficient optimization strategy for solving complicated optimization problems. More specifically, a combination of optimization algorithms was used for achieving an efficient way to solve the complicated task of optimization of a complete machine tool. Gradient based algorithms, genetic algorithms, and more traditional hands-on engineering were used in order to solve the optimization problem. For extracting as much information as possible from optimization results, post processing and data mining was suggested. One of the significant conclusions was that the virtual machine should reinforce the decision making in product development, not replace the product developers.

Neugebauer, Klimant, and Witt (2012) presented a Virtual Reality (VR) based realistic machine tool simulation which extends the traditional content of machine tool simulation systems like collision detection and material removal. A HIL (hardware-in-the-loop) coupling between the controller SIEMENS SINUMERIK 840Dsl and a VR model of a three-axis milling machine was used for achieving the objective of this research. Furthermore, it was shown, how it is possible to calculate and integrate into the VR simulation environment process-related deviations in the workpiece by means of the inertia of the moving masses, as well as by means of the tool deflection. To achieve this, a Multibody simulation model MBS observed the moving masses of the machine tool, and a bending beam model calculated the deflection of the tool because tool deflection and static flexibility can be calculated with the knowledge of the process forces and axial values through MBS simulation.

A comprehensive review of the existing virtual systems has been realized by Kadir, Xu, and Hammerle (2010) with emphasis on VR, mathematical modelling, Web-based techniques, hardware interactions, and STEP-NC-based methodologies. They also categorized the systems into different groups in accordance with their application domains for better understanding. They concluded that although simulation functions have increased constantly from simple predictions to more complex outputs, there is no specific system which can complete a suite of simulations. Most

researchers had mainly focused on material removal simulation, numerical control code interpretation functions, tool-path generation, and techniques for modelling the machine tool behaviour. VR-based systems alone are not capable of performing complex simulations, due to the fact that they lack advanced data input and output functions. However, VR offers a realistic sense of real machining through realistic animations, advanced visuals, and acoustic interfaces. Many advantages are provided by Web-based systems against non-Web-based simulation systems. Although most Web-based systems are able to incorporate the ordinary computer-aided design (CAD) schemas into the Web-based modelling schemas, it requires extraordinary effort and time for the implementation. The HIL and programmable logic controller (PLC) simulation approaches coupled with the virtual mechatronic systems of machine tools provide a more realistic sense of the machine tool and PLC behaviour in comparison to the use of ideal numeric control (NC) codes. Dramatically improved results can be provided by precise algorithms coupled with real-time simulation which also allow the study of process machine interaction in a real-time simulation environment.

Hanwu & Yueming (2009) proposed a virtual operating system based on the Virtual Reality Modelling Language (VRML). The authors studied the system framework, concept models, and structure models and presented a communication approach based on VRML, HyperText Markup Language (HTML). A CNC milling machine was taken as an example for the validation of the proposed prototype development, which is platform independent and does not need some special program on the client computer in comparison with the traditional standalone CNC machine simulation system.

Lee & Lin (2009) proposed a new methodology for constructing a universal five-axis virtual machine simulation system. In this virtual environment, provided by the OpenGL library, all motions of the virtual machine tool are displayed. In this paper, a modified D-H notation was adopted so that universal construction procedures can be achieved and user interfaces were developed for the configuration of machine tool. This method provides a number of extendable applications for virtual CNC machine tools. More specifically, new design configurations can be assembled and verified by machine tool designers. In addition, for machine tool makers, the virtual machine tool capability can be evaluated by the virtual machine tool. To sum up, this method enhanced the use of virtual machine tool simulation systems.

Movements on flexible structures have to be calculated to predict the machining results. Zaeh (2007) used a finite element study to understand the properties of machine tool components. Simple static analyses were carried out. Examination of the structural dynamics with a finite element method (FEA) was developed. In this model, a three-axis machine was chosen for simulation of large movements. The author integrated finite element and multi-body simulation. The simulation system is based on the relative nodal method for large deformation problems. The model parts for the linear guide ways, ballscrew drives and the controller were implemented.

The mechatronic model presented by Maj and Bianchi (2006) allows the reproduction of a typical Experimental Static Stiffness Test, also evaluating the effects of linear position sensor location and drive-tuning on static stiffness at the tool and disturbance rejection. Time simulation results are then elaborated to in Matlab to obtain the corresponding information in the frequency domain. It is therefore possible to investigate the effect of tuning parameters on the dynamic compliance of the tool Frequency Response Function (FRF).

Boer, et al. (2013) proposed a reduction method for the efficient time-integration of planar compliant mechanism models FMM flexible multibody model which endure considerable deflections. Detailed description of geometric non-linearities are typically included in models of this class of mechanisms since stiffness characteristics may modify dramatically during deflection. An FE flexible multibody simulation approach was used for analysing compliant mechanisms regarding independent coordinates. Geometric transfer functions were applied for expressing the configuration of the mechanisms regarding independent coordinates. The authors observed that serious changes in eigenfrequencies during simulation were accurately described by the reduced models in both examples. The demonstration of their method was carried out by two planar examples; a compliant straight guidance which endures considerable deflections and a flexible manipulator.

The analysis of Multi-Flexible-Body-Dynamics (MFBD) plays a key role in computational dynamics. In addition, the dynamic analysis of a variety of mechanical systems may involve contacts among flexible and rigid bodies. However, the contact study in the MFBD still remains a tremendously challenging area. Choi (2013) used a compliant contact force model based on the Hertzian contact theory in order to simulate the contact phenomena. In this study, contact algorithm, which is called General GEOMetry contact due to the fact that, it can use general rigid and flexible geometries, was proposed for developing the robust and efficient general purpose contact algorithms for the rigid and flexible bodies. The contact algorithms were divided into four basic parts; a surface representation, a pre-search, a detailed search, and a contact force generation. A comparison between the GGEOM and RecurDyn (2013) contact elements was carried out and it was demonstrated that GGEOM contact is able to handle contact problems defined as rigid and flexible surfaces.

Delgado, Ozturk, and Sims (2013) developed and simulated an FE model of a high speed spindle with variable bearing preload in ANSYS and SpindlePro for analysing the effect of preload on stiffness and Frequency Response Function (FRF). In order to observe the thermal effects on back-to-back bearing configuration, a simplified thermal model was simulated in SpindlePro. For the practical scenario that was considered, it was concluded that gyroscopic moment is effective at lower damping ratios and stiffness. The largest influence on the dynamic response was shown to be the bearing preload. For various preload scenarios, FRF was measured, while stability lobes were calculated for analysing the preload effects. Finally, they concluded that further analysis is required in order to execute an accurate thermal analysis.

Nowadays, a variety of modelling and simulation architectures, which are based on the discrete matter approach and on FEA method, are well established. The basic setup of the kinematics of the feed drives and a dynamic optimized dimensioning of all the fundamental structures and subsystems of the machine are rapidly produced by these methods. Fortunato & Ascari (2013) reported the latest developments of virtual design of machines for High Speed Machining (HSM). The final result of this research was the development of a software architecture for assembling and integrating all the design tools around a common project database. Thus, they presented a single-axis (Y axis) optimization of a gantry machine in order to demonstrate the potential of this innovative and open design platform which is particularly suitable in industrial applications.

Law, Altintas, and Srikantha Phani (2013) presented a computationally efficient methodology for evaluating and improving the dynamic performance of a machine tool at the design stage. Thus, an efficient position-dependent MBS dynamic model of a machine tool was developed based on reduced model sub structural synthesis. It was demonstrated that this model efficiently simulates dynamic response with considerably less computational effort than FE models. Reduced order sub structural model was applied for the identification of weak components of an unproductive machine due to machine tool chatter. Although this methodology was used to a specific kinematic configuration and for a given set of machining operations, the rapid redesign and analysis of unproductive components due to low compliance is generic and can be extended to virtual evaluation of any CNC machine tool.

The machine tool dynamics at different worktable feed speeds have been infrequently studied. Li et al. (2013) proposed an output-only modal identification method to predict the modal parameters of a machine tool at different feed speeds using the inertia force sequence caused by random idle running of the worktable. They carried out a comparison between the extracted modal parameters and the modal parameters of the machine tool in a static state which were evaluated by hammer tests. The experimental results indicated that the modes in which the worktable vibrates are influenced by the running state of the worktable. It was also concluded that as the feed speed increases, the estimated damping ratios and natural frequencies both decrease. Finally, it was concluded that, the proposed technique can be efficiently used for the prediction of the dynamic behaviour of the machine tool at different feed speeds for the entire working volume, due to this technique can determine the operational modal parameters by measuring the response of the structure of the machine tool without using any artificial input.

Whalley, Abdul-Ameer, and Ebrahimi (2011) derived a hybrid model (distributed-lumped model) for the X-and Y- axes of a machine tool and presented the model validations using experimental results. More specifically, the lead-screw, which was considered to include a uniformly distributed, mass-inertia and stiffness element, was approached using a distributed model. Lumped parameter models were employed for the remainder of the system. The model for the Z axis was provided by the adaptation of the model. The total X, Y, and Z axes response of the system was detailed for circular and cylindrical cutting processes. Finally, resonance conditions were investigated and

adverse cutting frequencies were identified. The dynamic amplification and the time-domain system's performance was therefore determined.

The theoretical modelling of non-proportional damped mechanics for a biaxial-single spindle-vertical lathe has been demonstrated by Neugebauer, et al. (2010). An approach was shown to treat non-proportional damped systems with typical software tools of the mechatronic simulation. More specifically, local damping effects were introduced into an FE model for the state-space description of a mechanical system in MATLAB/SIMULINK software related to the coupled simulation of structural dynamics and control.

Although typical five-axis machine tools include three translational (two horizontal, X and Y axes and one vertical, Z axis) and two rotary axes (C and B axes), as the studied CNC machine tool, different combinations can be found, such as a horizontal spindle machine. Yang & Altintas (2013) presented a generalized kinematics model which allows automatic configurations of all five-axis machine tools using screw theory, where all the coordinates and vectors are relative to the base coordinate system, instead of using Denavit-Hartenberg notations. Thus, a generalized kinematics module was developed for all possible configurations of five-axis machine tools, which is capable of giving complete inverse kinematics solutions for both rotary and translational motions. Each kinematic element was modelled, as a revolute joint, prismatic joint, workpiece or cutting tool and they were mathematically assembled through screw theory. The singularities in five-axis contouring were avoided by deforming splined tool orientation vectors. Thus, they concluded that the screw theory provides computational and modelling advantages when developing generalized models for different five-axis machine tool configurations. Finally, when the proposed kinematic module is coupled with tool path generation algorithms, it becomes possible to detect and avoid the kinematic singularities by deforming the splined tool paths while accomplishing smoother velocity, acceleration, and jerk.

MODELLING USING BLOCKS

Nassehi & Newman (2012) proposed a novel methodology in order to represent individual machine tool components as smart interlocking software blocks which are dynamically structured based on predefined ontology and then combined in order to form holistic models of machine tools. These models can be used for the assessment, simulation, and optimization of the machine tools against a range of criteria. Finally, a prototype implementation of the proposed methodology was demonstrated using two test cases for kinematics and power usage.

Sztendel, et al. (2012) developed a lumped parameter model of a rotational axis of the studied five-axis CNC machine tool existing at the University of Huddersfield, and described the steps required for data acquisition using ControlDesk and HIL implementation of the drive models in the dSPACE real-time system. The operation of the machine tool was analysed and mathematical equations which describe the dynamic behaviour of the machine tool was derived and explained. The implementation of the model was carried out in SIMULINK using the SimPowerSystems toolbox.

Moreover, they explained how it is possible to use the experimental data, which has been obtained from the data acquisition process using dSPACE real-time system, in order to develop systems for machine tool diagnosis and prognosis. Finally, the implementation of the HIL system was validated by comparison between the simulated angular rotor position and experimental data.

FEA/CONTROL

Uhlmann, Eβmann, and Wintering (2012) presented a novel design- and control-concept for highly dynamical precision CNC machine tools which aims for lightweight design. A Kalman-Bucy filter including the mechanical structure's model was applied. It was demonstrated that the model is accessible from FE models by using the Krylov-subspace method for model order reduction. It was shown that the bandwidth of the controller is not limited by the first mechanical eigenfrequency of the frame. In addition to this, it was demonstrated that it is even possible to reduce the dynamic dislocation by the first mechanical natural frequency of the frame. It was concluded that, although the proposed concept has been applied on a test stand offering idealised conditions, it can also be applied to real CNC machine tools. Finally, the concept was proposed for direct-drive CNC machine tools which are used for micro-milling.

A review of the design, analysis, and control of machine tool feed drives have been performed by Altintas, et al. (2011).Machine tool guides based on roller bearing, friction, hydrostatic and magnetic levitation principles were presented as well as mechanical drives based on ballscrew and linear motors, along with their compliance models. Electrical motors and sensors used in feed drives and the virtual modelling of feed drive systems was discussed. Also, the control of rigid and flexible feed drives was presented. It was noted that the recent developments in power electronics, digital computers, electrical motors, actuators and sensors have significantly benefited the speed limits of spindle and feed drive systems. Furthermore, it was underlined that there is the need for computationally efficient, accurate and realistic models of machine tools with feed drives so that design concepts can be appropriately tested in the virtual environment. They concluded that a major research effort is required for modelling of machine tool and feed drive structures using multi-body dynamics.

2.3 MODELS FOR MACHINE TOOL STRUCTURE

The structural analysis can be divided into three stages

1. structures resistance capability to withstand static forces,
2. analysis of natural frequencies analysis and
3. dynamic analysis of the machine tool.

The structural behaviour of the CNC machine tool under static or inertial loads is executed with the FEM (Finite Element Method) considering the maximum values as inputs for the three-dimensional

model. Because it is very difficult to estimate some construction details problematic procedure in FEM includes the contacts between structural components along the degrees of freedom (DoF). While it is easy to run the analysis of natural frequencies it is difficult to make modifications in reality. Despite the fact that in real CNC machine tools damping comes primarily from the contact in the guideways, it is included as an input which means it is an approximate value in finite element models. Furthermore, thermal analysis is carried out by using the thermal capabilities of FEM software packages by Lopez de Lacalle & Lamikiz, (2009). A model using Pro-Engineer three-dimensional CAD software represents major structural features of a machine tool. In addition, an FE model offers complete and accurate results for a wide range of analyses: static (linear and non-linear); dynamic (modal, harmonic, and transient) and; thermal (steady-state and transient). Some of the FEM commercial software packages which are widely used are ANSYS, MSC.Nastran, ABAQUS, and COMSOL.

Finite Element Method

Frey, Dadalau, and Verl (2011) presented an approach which aims at finding a sufficient model for expressing the most relevant characteristics of ballscrew feed drive systems used for CNC machine tools. More specifically, a hybrid and a discrete model for a ballscrew feed drive system was derived and verified by experimental data. The hybrid model, which combines discrete and continuous formulation elements, was developed in FEM combining dampers, springs, Timoshenko beam elements and mass-elements. The distributed model was directly developed with Computer-Aided-Control-Engineering-Tools (CACE-Tools) using standard blocks such as gains, integrators and basic mathematical operations because of its simplicity. A comparison of the approaches concluded that the simplified lumped parameter model was well suitable for the prediction of the most relevant eigenfrequencies of the feed drive system over a variety of parameters. Through simulation results, it was shown that the ballscrew shaft has a crucial influence on the overall dynamics of such a feed drive. Finally, they concluded that, in most cases, the lumped parameter model due to its simplicity and the intuitive synthesis offer fast and reliable simulations.

2.4 MULTIBODY SYSTEMS

The name multibody stands as a general term which encloses a broad variety of systems such as mechanisms, industrial machinery, robots, trains, automobiles and trucks, space structures, satellites, antennas, and others (Garcia de Jalon & Bayo, 1994). Multibody Simulation (MBS) can be conceived as an assembly of component bodies connected to each other with a range of connecting elements, and upon which external and internal forces act. Concerning the material properties of the bodies and connecting elements, a distinction can be made between rigid (inflexible) and elastic (flexible, deformable) elements (Janschek, 2012).

An MBS model is used for modelling the dynamic behaviour of interconnected rigid and elastic bodies. Mathematically speaking, systems of ordinary differential equations are used for the

description of the dynamics of rigid bodies (the concepts of rigid body mechanics), while systems of partial differential equations are used for the description of the dynamics of elastic bodies (the concepts of continuum mechanics) (Janschek, 2012).The connections of the bodies can be modelled with classical force elements like spring-dampers or realized by kinematical constraints, such as joints.

2.4.1 MULTIBODY SYSTEMS SIMULATION

Prevost, Lavernhe, and Lartigue (2010) have modelled the feed drives of the five axis CNC machine. The main focus was to create a model for the feed drive dynamics during trajectory follow-up including the position, velocity and current loops as well as the feed forward terms which describe classical feed drives on actual HSM machines. In addition, an identification procedure was implemented, and model performances were assessed by the comparison between the simulated and experimental results. Finally, experimental verifications of the virtual axis model were detailed for both three and five axis trajectories, presenting a variety of geometrical discontinuities.

2.4.2 MECHATRONIC MODELLING

The much-used word “mechatronics" hints at a tight interaction between the classical mechanics (mechanical engineering) and electronics (electrical engineering).In other words, mechatronics can be defined as the synergistic combination of mechanical engineering, electronic control and intelligent computer control in the design of products and manufacturing processes (Janschek, 2012).

The static and dynamic properties are considered as key evaluation criteria when designing machine tools. A machine tool is a non-linear, mechatronic system. For this reason, accurate identification of the feed drives dynamics is a crucial step in the design of high precision CNC machine tools. Mechatronic modelling, which takes into account the coupling of elastic mechanic structure with the control system, is of great importance and recently has become an advanced tool (Neugebauer et al. 2011).

On the one hand, the main focus of modelling the mechanics is on rigid or elastic multibody systems. On the other hand, the transfer of high-quality mechanics models (e.g. FEM results) via modal reduction into control engineering software is a typical modelling technique for machine tools. In other words, mechatronic simulation can be achieved either by coupling a mechanic simulation system (FEM software) and a control engineering software (e.g. MATLAB/SIMULINK), which is the so-called co-simulation or by using only one simulation environment (FEM software packages e.g. ANSYS) for a complete mechatronic simulation (Neugebauer et al. 2011).

2.4.3 FRICTION MODELLING

Friction stick-slip vibrations lead to energy dissipation, noise, excessive wear and premature failure of machine parts. Friction characteristics is nonlinear. It’s known to be sensitive various factors-like temperature, lubrication. Up till now several friction models have been proposed. The absence

of accurate friction models has been exposed to be a limiting factor in developing friction compensation in real time. Lubricant reduces the groove surface friction, and exchange heat generated by the balls passing between shaft and nut. Improper lubricant can cause the ball screw failure, as the improper lubricant will contaminate the ball screw internal surface and cause further damage. When the contact geometry and the operating conditions are such that the load is fully supported by a fluid film, the surfaces are completely separated. A theoretical analysis of hydrodynamic lubrication was carried out by Osborne Reynolds (1886).

Canudas de Wit et al. (1995) proposed the LuGre accurate model that is based on various physical aspects of the friction. His model is able to capture experimentally observed pre-sliding displacements, break-away force, and stick-slip motion associated with the Stribeck effect. LuGre model (when linearized) is shown to be equivalent to a linear spring/damper arrangement.

The General maxwel slip model friction model described by Al-Bender (2005) is a qualitatively new formulation of the rate-state approach applied to the Maxwell-slip model. The GMS model retains the (original) Maxwell-slip model structure, which is a parallel connection of different elementary slip-blocks and springs, but replaces the simple Coulomb law governing each block, by another state equation to account for sliding dynamics.

Yanada and Sekikawa (2008) deal with modelling of dynamic behaviour of friction in the sliding regime. Using a hydraulic cylinder, friction characteristics are experimentally investigated under various conditions of velocity variation. It is shown that the modified LuGre model can simulate the real dynamic behaviour of the friction of the hydraulic actuator with a relatively good accuracy. The model can simulate not only lasting stick–slip motion but also its decay. It may be useful for simulating and analysing friction-induced vibrations. It is believed that the proposed model can express the friction behaviour observed in many types of contact surfaces and can apply to many mechanical systems

Laxalde and Thouverez (2009) work mostly deal with friction nonlinearities but the method is applicable to any generic type of nonlinearities. Large-scale systems can also be treated as demonstrated in an industrial application dealing a turbomachinery compressor blade with dry-friction at its root interface. On this example, a detailed description of the treatment of two-dimensional frictional motion through complex variables is given for two particular friction models.

2.5 ACOUSTIC EMISSION

AE piezoelectric sensors are most widely employed in industry. It characterizes through a wide-range frequency response, sensitivity. Piezo ceramic is used to build AE sensors for the reason that it’s high sensitivity and robustness. Two main types of the sensors are recognised wideband and resonant- accordingly to their frequency response. Resonant sensors are narrowband to one

main frequency. High frequency wideband sensors provide flat frequency output. Usually wideband sensors have lower sensitivity than resonant sensors.

2.5.1 PIEZO-ELECTRIC PHENOMENON

The piezo-electric effect is described as a mechanical deformation caused by an applied electric field, or conversely an electric field caused by mechanical deformation. This happens due to a macroscopic polarization of the material. For a structure with aligned dipole moments within the crystal lattice, an applied electric field will distort the dipoles and will change the lattice density in certain directions. This leads to a macroscopic deformation of the mechanical structure. The polarization can be induced in different ways. The most important piezo-electric materials are crystals or semi crystals. Due to the circulation of ions in their crystal structure they show a natural polarization. Furthermore piezoelectricity can be induced to a material by applying strong magnetic fields.

Kholkin, A. L. (et al.) (2008) describes that piezoelectricity has commonly been used for more than a century to describe the ability of materials to develop electric displacement, D, that is directly proportional to an applied mechanical stress, σ. Piezoelectric effect in crystalline materials to a large extent is defined by the crystal symmetry. The symmetry considerations are indispensable for understanding the piezoelectric properties of single crystals, ceramics, and thin films. By varying the orientation of the applied field with respect to the crystallographic axes, it is possible to enhance the piezoelectric response of some crystals drastically.

Kholkin, A. L. (et al.) (2008) mentioned that above a certain temperature, *T*c (the Curie point), the spontaneous polarization vanishes, and the ferroelectric crystal changes into the para-electric state. Many ferroelectrics lose their piezoelectric properties above *T*c completely, because their para-electric phase has Centro-symmetric crystallographic structure. The measured piezoelectric response generally contains not only the intrinsic contribution determined by the lattice properties, but also an extrinsic contribution caused by movements of non-180◦ domain walls. Recently, it has been shown that the piezoelectric properties can also be improved by cutting the crystal at some angle to the polarization direction.

2.5.2 ACOUSTIC EMISSION PHENOMENA

Acoustic emission is a phenomena where transient frequency stress waves over 20 kHZ are emitted by the rapid discharge of energy from materials and AE sources. AE was recognized by Kaiser (1953). Investigations using an anodic etching technique with polarity reversals and AE monitoring proved that emissions from metals were mainly due to disruption motion-related plastic deformation, rather than being totally due to grain boundary slipping. The application of acoustic emission to non-destructive testing of materials, typically takes place between 100 kHz and 1 MHz, as shown in Figure 2-1.

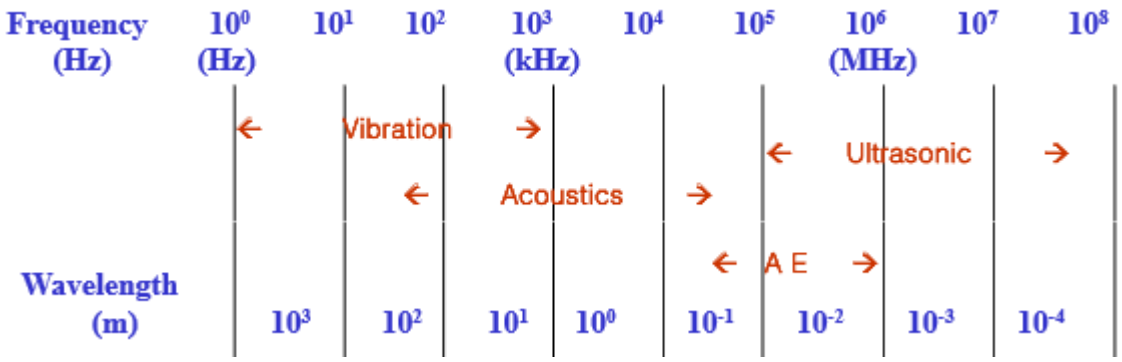

Figure 2-1 Elastic Waves for various Wavelengths (Essid El-Alej M (2014))

As deformation occurs energy transmits to the contiguous material and dissipates as an elastic wave. The distance from the source of AE at which it can be detected depends on its initial amplitude and the acoustic characteristics of the material in which it is travelling. Acoustic emission monitoring can indicate an unexpected or a continued failure and can provide information on the reason of the failure. (Beattie 2013)

The excitation of a sensor indicates events on the specimen, the amplitude specifies the level of the disturbance. Noises are present in applications where the AE testing environment is disturbed by mechanical vibrations airborne and in solid, electrical and other background noise. Electrical noise can be filtered, where mechanical noises are high frequency signals and digital filters are not effective to extract the AE signal.

2.6 CONDITION MONITORING

There are several types of condition monitoring methods for machine tools. Vibration is a cyclic or pulsating motion of a machine or machine component from its point of rest. Acoustic Emission Testing (AET) is a condition monitoring technique that is used to analyse emitted sound waves caused by defects or discontinuities. Ultrasound condition monitoring is defined as “sound waves having a frequency above the limits of human hearing, or in excess of 20,000 cycles per second. (Theobald 2016).

Lee (2014) states that condition based maintenance (CBM) is a maintenance program that can provide maintenance decisions based on the information collected through condition monitoring. It can reduce maintenance cost by avoiding unnecessary scheduled preventive maintenance operations and also lower manufacturing cost caused by the unexpected breakdown.

Jardine (2006) mentions that in order to save high maintenance costs and to increase manufacturing system’s operating ratio, condition-based maintenance (CBM) method has been developed. CBM is carried out with indicators, which show equipment’s faults and performance deterioration.

Temperature is one of the most common indicators of the structural and functional health of equipment and components. Infrared thermograph is used to find faulty machineries, corroded electrical connections, damaged material components, etc., can cause abnormal temperature distribution. Lubrication oil is used in electrical and mechanical machines to reduce friction between moving surfaces. Lubrication oil analysis is important source of information for early machine failure detection. After a detailed study of each technology, it is concluded that the most suitable condition monitoring technique is AE which is described in chapter seven. (Theobald 2016)

2.6.1 ACOUSTIC EMISSION IN CNC MACHINE TOOLS

Designed CBM (condition based monitoring) systems acquire Acoustic Emission (AE) data over few steady running conditions, e.g. during periods of steady feed rate and speed, to provide diagnostics for drive-train components including nut, bearings and a ballscrew. Time and frequency domain Condition Indicators (CIs) are mined from the acquired raw Acoustic emission signals and from the signals after processing them. The CIs are extracted after subtracting the average of the signal from the raw or processed AE signal under consideration. The time domain CIs can include: the Root Mean Square (RMS) of the signal, the four statistical moments of the signal (average, standard deviation, skewness, and kurtosis), the maximum value, the minimum value, the difference between the maximum and minimum values, and the maximum rate of change. The frequency domain can include the magnitudes of certain frequencies, the power of certain frequencies, the integral of the power spectrum of a processed signal, etc.

2.6.2 BACKGROUND TO AE IN CNC CONDITION MONITORING

Srinivasa (2013) has developed an adaptive control constraint system for computer numerical control (CNC) turning based on the feedback control and adaptive control/self-tuning control. In an adaptive controlled system, the signals from the online measurement have been processed and the feedback to the machine tool controller adjusted the cutting parameters so that the machining can be stopped once a certain threshold is crossed. The main focus of the work is to develop a reliable adaptive control system, and the objective of the control system is to control the cutting parameters and maintain the displacement and tool flank wear under constraint valves for a particular work piece and tool combination. Using MATLAB and SIMULINK, the digital adaption of the cutting parameters for the experiment has confirmed the efficiency of the adaptively controlled condition monitoring system, which is reflected in different machining processes at varying machining conditions. This work describes the state of the art of the adaptive control constraint (ACC) machining systems for turning.

Prasad et al. (2011) presented an investigation for a tool condition monitoring system, which involves a fast Fourier transform pre-processor for generating features from online acousto-optic emission (AOE) signals to develop a database for appropriate decisions. A fast Fourier transform (FFT) decomposes AOE signals into different frequency bands in the time domain. This method has also been widely used in the field of metal cutting. It detects process changes like displacement due to vibration, tool wear, etc.

Bhuiyan et al. (2012) placed an acoustic emission sensor and a triaxial accelerometer on the shank of the cutting tool holder to monitor the cutting tool condition in machining. The acoustic emission sensor assesses the internal change whereas the vibration sensor demonstrates the external effect on tool state. AE and vibration components effectively respond to the tool state and the different incidences in turning.

Urbanek et al. (2014) described a method for recognition of modulations in vibroacoustic signals, named modulation intensity distribution (MID), which is a function that combines multiple spectral correlation densities in one way or another, depending on the application. Liang et al. (2013) applied a self-organization feature map (SOM) neural network to acoustic emission (AE) signal-based tool wear monitoring for a micro-milling process. They presented a monitoring system that integrates AE signals obtained from the workpiece and the SOM algorithm. Signal analysis shows that tool wear increased along with time.

Nasha Wei et al. (2015) focuses on the investigation of using AE to characterize the friction online. To separate the effect relating to friction sources, wavelets multi-resolution analysis is used to suppress interfering AE events due to valve impacts and combustion progress. Then a wavelet envelope indicator is developed to highlight AE contents from friction induced AE contents. The authors report a method to monitor the engine friction online based on characterization of AE signals. As AE signals have strong non-stationary contents and there are a number of distinctive AE sources in the engine, wavelets based multi-resolution analysis (WMRA) techniques is used to extract the weak AE events that are relating to friction process. The envelope of extracted signals is used to develop diagnostic parameters for monitoring engine lubrication condition.
The current research trend of using AE sensors relies on integration of the sensor with intelligent algorithmic methods. The simplest algorithmic method uses the root mean square value (RMS) of the captured data using AE sensors. Advanced techniques includes artificial neural networks and signal processing approaches like time domain analysis.

Standard AE sensors tailored for tool condition monitoring applications are available from vendors like Artis, Brankamp, Kistler, Montronix. Description of AE sensors and manufactures are described more in Appendix A.

2.6.3 AE IN BEARINGS

Li et al. (2012) listed the common sources that generate AE in a gearbox, including plastic deformation, micro fracture, wear, bubbles, friction and impact.

Loutas et al (2011) combined vibration, acoustic emission and oil-debris monitoring for rotating machinery. The authors applied principal component analysis (PCA) to reduce the number of parameters extracted from the three methods, and concluded that the AE method is not sensitive to gear wear, but detects the tooth crack earlier than the vibration method.

Ozevinet et al. (2014) recorded AE data during the initial crack growth from the notched spline, and recorded high frequency data in five second intervals for the entire 130 hours of gearbox testing. Four AE sensors were mounted on the gearbox housing at different positions in order to understand the influences of sensor type/location and gearbox operational conditions to the AE characteristics. It is observed that the AE features extracted from the AE signals are influenced by the sensor type and location. As the pattern recognition methods rely on the AE features as the descriptors, they should be developed for a specific sensor type and position. The primary features sensitive to potential flaws are identified as the frequency domain features including frequency centroid and partial powers

Non-intrusive measurements such as surface vibration (SV), airborne sound (AS) and acoustic emission (AE) measurement are appropriate monitoring methods for early stage journal bearing fault in low, medium and high frequency. Raharjo et al. (2012) focused on the performance comparison using SV, AS and AE measurements in monitoring a self-aligning spherical journal bearing for normal and faulty (scratch) conditions. They examined the signals in the time domain and frequency domain and identified the frequency ranges for each measurement in which significant changes were observed. The results of SV, AS and AE experiments indicate that the spectrum can be used to detect the differences between normal and faulty bearing. The statistic parameter shows that RMS root mean square value and peak value for faulty bearing is higher than normal bearing.

Feng et al. (2015) developed an accurate envelope analysis algorithm for a wireless sensor node. The proposed algorithm down-samples and cascades the analysed envelope signals to construct a relatively long one. Thus, a relatively higher frequency resolution can be obtained by calculating the spectrum of the cascaded signal. In addition, a 50% overlapping scheme is applied to avoid the distortions caused by the envelope calculation based upon a Hilbert transform. The proposed method has been tested successfully for detecting an outer race fault of a rolling bearing.

Gu et al. (2014) developed an adaptive filter technique by combining SK with envelope analysis for rolling bearing fault detection and diagnosis. They modelled the vibration sources from bearing defects as an impact process with constant size, but three different lengths corresponding to outrace fault, inner race fault and roller fault, respectively. An experimental study followed to evaluate this model. The conventional envelope analysis of the measured vibration signals from the tested faulty bearings is optimized by spectral kurtosis (SK) for automatic and reliable fault detection and fault category diagnosis.

2.6.4 MACHINE TOOL LIFE

Multi body simulation offers the possibility to investigate the realistic load spectra of machine components when performing the simulated operation of a given CNC program. Fleischer (2009) describes that load levels can be accounted, and the overall wear time can be accumulated and allocated to wear regions on the components. Thus, the progress of component life consumption can be obtained by simulation, which is useful for the appropriate requirements towards the

machine's components at the point of the machine design. He presents a practical approach to the estimation of machine tool component life based on simulation.

Jin (2013) focuses on the fault diagnosis of ball screw system components. In order to classify multiple failure modes, one full size ball screw testing machine is set up to replicate different health conditions including four failure modes — lubrication starvation, preload loss, ball nut wear, and re-circulation system failure. In this paper, the first two failure modes are introduced. Time domain and frequency domain features have been extracted from the vibration and temperature signals. A classification modeling method is used to establish a ball screw system health map. Author shows that the direction of the threads on the screw shaft causes different vibration patterns when ball nut travels forward and backward. Thus, failure signatures from both traveling directions are investigated in the paper. Based on the developed health map for the ball-screw, the health values can be calculated to quantify the failure severity.

Unlike traditional maintenance that needs to be carried out on a regular time basis, the CBM detects any system defect early and identifies the cause of failure efficiently through use of indicator signals that reflect the actual operation condition of systems and accordingly reduces unnecessary costs and maintenance efforts. For this process, Lee (2015) derives normal and defect frequencies were from the common failure of the ball-screw. Then a vibration signal acquisition module has been implemented in the diagnosis system. The normal and defect signals were obtained and then the derivation was investigated. Also the amplitude change of defect signal was found according to the progress of failure. Lee (2015) applies Wavelet transformation to the signal so that the system identifies the defect frequencies and estimates their progress. The system is stand-alone and PC-based one so that it can be applied to various manufacturing equipment pieces or facilities.

Ball-screw is a typical linearly reciprocating part and is widely used in industry, it has not gained attention to be diagnosed compared to rotating parts such as motor, pump, and bearing. The components of the ball screw can fail either at the beginning due to their low manufactured quality, or wear out in time during continuous operation because of high friction, increasing heat. All issues caused by increased temperature limits smooth circulation of balls so it may break and damage the nut or spindle groove. Qiu Ha (2003)

Maier (2011) describes the methodology of condition monitoring that can be based on controller CNC and additional sensors. Two main methods for assessment are signal analysis based exclusively on measurement data and a model based method. The method uses positioning data to generate characteristics for describing wear of the mechanical components of the ballscrew drive. As input signals the rotatory position and the linear position are used. The rotatory position is taken from the servo motor’s encoder the linear position is the machine table’s direct actual position.

2.7 CONCLUSIONS

Machine tools cost thousands of pounds. Faulty systems can lead to expensive, sometimes dangerous maintenance. In some of industries predictive maintenance. Research has been carried out in modern years in the context of the application of condition monitoring technologies for monitoring machine tool drives.

Liao (2012) states that “Two analysis approaches are generally available to the engineer: model-based and data - driven analysis. Physics-based modelling of machines and other equipment provides good insight into mechanical mechanisms and produces very accurate prognostic information if the machine is well understood. Well-built model may not be easily adaptable to other machines, especially complex machines.”

Real time machine data needs to be used with developed machine model to estimate loads on the system in order to establish remaining useful life of the feed drive system. Condition monitoring using a SIMULINK model of feed drive and position errors is influenced by precise knowledge of the dynamic properties of the drive system. Acoustic emission can be used to monitor faults, like cracking or plastic deformation of balls and track, and detect the effectiveness of the lubrication system in a ballscrew. It therefore has a high potential of early fault detection. AE incident counts and peak values can be used in a wider extent with a semi-real time machine tool model. The effect on machine tool performance and simplicity need to be taken into attention.

Condition based maintenance (CBM) is a maintenance program that can help to make a decisions based on the information collected during condition monitoring. It can reduce maintenance cost by avoiding unnecessary scheduled preventive maintenance operations and also lower manufacturing cost caused by the unexpected breakdown.

Important methodology for mechanical analysis is model-based approach. These approach utilize physics specific and explicit mathematical model to simulate the mechanism of monitored machine

The model-based approach is more effective if the accurate model is established; the accurate physical model can replicate the machine structure and the machine’s performance can be simulated. C. C. Wei (2003) shows kinematic analysis for ball screw mechanism and evaluate the influence of different friction coefficient, normal force and contact angle on the ball screw’s mechanism.

By combining the modelling, condition monitoring, data acquisition and fault detection identification and localization it should be possible to provide feed drive systems that possess better tolerance and performance and the ability to detect deterioration earlier. In future there is a need to develop a condition monitoring system for variable machining conditions. However, more research should be undertaken in this area in order to improve the monitoring condition of ballscrew.

CHAPTER 3 MODELLING COMPONENTS OF FIVE-AXIS CNC MACHINE TOOL AXIS DRIVES

3.1 MODELLING METHODS

There are two basic principles by which a system can be approached - continuous matter or modular approach and the discrete matter or lumped mass approach (Holroyd, 2007). Generally, when a mass can be defined as a rigid body or, in other words, when a system has a finite number of degrees of freedom, it is more efficient to be modelled as a discrete (lumped parameter system). On the other hand, when a mass is non-uniform or, in other words, when a system has an infinite number of DoFs, it is best to be modelled as a continuous distributed parameter system. There are also: hybrid models, which combine lumped and distributed parameters and provide more realistic dynamic performance; and Transmission Line Matrix (TLM) models based on Transmission Line modelling, which is in essence a space-and time-discretising method normally used for computation of electromagnetic fields.

3.1.1 LUMPED PARAMETER MODELS

A lumped parameter model is a lumped system which, mathematically speaking, is solved by a set of ordinary differential equations (ODEs) because all the dependent variables of interest are only a function of time. Lumped parameter models simplify the description of the behaviour of spatially distributed physical systems solved by a set of partial differential equations (PDEs), where all dependent variables consist of more than one independent variable. Despite the fact that all systems are actually distributed in nature, ordinary differential equations can approximate distributed systems for practical modelling.

The forced-damped method can be used for solving the non-homogeneous equation of motion. According to this method, the steady-state response to exciting forces is calculated by transfer matrices. Moreover, this method uses fewer elements than the lumped mass approach in order to create a realistic model. This method contains terms which are dependent on frequency, thus it requires the frequency of excitation to be specified. Thrust and torsional loads are transmitted by the ballscrew as the nut is guided lengthwise the screw (Holroyd, 2007). Unlike lumped parameter models, modularized models allow the easy exchange of components when changes in any system component occur. Finally, drive shafts and concentrated assemblies, such as bearings, gears, couplings and load platforms are relatively “long” distributed elements employed in CNC machine tools (Pislaru, 2013).

3.1.2 HYBRID MODELS

One type of hybrid models of machine tool feed drives combine lumped and distributed parameters, thus providing more realistic dynamic performance. CNC machine tools are complex systems. Therefore, hybrid modelling, which considers explicit damping factors, distributed load and

measured non-linear effects (backlash and Coulomb friction), are better able to represent the dynamics of CNC machine tool feed drives (Pislaru, 2001).

3.1.3 TRANSMISSION LINE MATRIX MODELS

The Transmission Line Method (TLM) is based on the analogy between the electromagnetic field and a mesh of transmission lines. It is an important numerical method in computational electromagnetics, and its application involves the division of the screw shaft into various identical elements. TLM methods are used to solve time-dependent or transient problems (Russer, 2000).

The three-dimensional TLM method allows modelling of complex electromagnetic structures by modelling the electromagnetic field by wave-pulse propagating in a three-dimensional mesh of lines (Russer, 2000).TLM links and TLM stubs can be used for modelling distributed and lumped parameter elements, respectively (Pislaru, 2001).The TLM scheme has been derived from Maxwell's equation using the finite difference approximation, the finite integration approximation, and the method of moments. It is considered as one of the most powerful time-domain methods along with the Finite Difference Time Domain (FDTD) technique (Russer, 2000).

There are two basic principles for looking at the bodies of a mechanical system: the discrete matter or lumped mass approach; and the continuous matter or modular approach. A lumped parameter model is solved by a finite number of ordinary differential equations derived by considering the equations of motion of each element of the system, because all the dependent variables of interest are only a function of time Transmission line matrix model is more complex therefore is not used in this work.

The lumped mass approach is a very convenient technique for modelling some parts because the mass is focused on the centre of a specific component. However, the behaviour and interaction of individual components of an electromechanical system cannot be examined with lumped parameter models. On the one hand, the lumped mass approach, which is in essence a finite element method (FEM), models the mechanical system under lumped consideration of masses and springs. Modelled parts with simple equations are presented in next paragraph.

3.2 MODELLING TOOLBOXES

Few modeling softwares has been rewieved (Appendix B). LMS gives direct coupling of multibody model with MATLAB and Simulink, based on FEA modes. NI INSIGHT environment through LabVIEW automation can be used for live measurements directly to CAD/CAE models for instant design validation and simulation verification. Ricardo API is used in field of engine and vechicle. It links ANSYS FLUENT and WAVE to execute simultaneously.

MATLAB with Solidworks software packages and real time dSPACE hardware system has been used in this research work. dSPACE specializes in real-time hardware and software products,

markets a complete set of tools for use with the Real-Time Workshop (RTW). These tools are primarily intended for rapid prototyping of control systems and HIL applications. The dSPACE product line includes a variety of A/D and D/A boards, encoder boards, and digital I/O boards.

3.2.1 SIMMECHANICS TOOLBOX

The design and modelling of systems can be carried out by SimMechanics, which is part of physical modelling and provided by MathWorks Inc. SimMechanics runs within SIMULINK environment and interfaces with the rest of MATLAB software. Self-contained modelling blocks characterise physical components. The purpose of SimMechanics is the engineering design and simulation of mechanical systems of rigid bodies which are connected by joints with the standard Newtonian dynamics of forces and torques. SimMechanics simulates rotational and translational motion in three dimensions and offers a number of tools for defining bodies and their mass properties, their possible motions, coordinate systems, kinematic constraints, and the means of initiating and measuring motions (University of Copenhagen, 2014).

A number of block libraries and special simulation features support SimMechanics. The connection of SimMechanics blocks to normal SIMULINK blocks is becoming possible through special “sensor” and “actuator” blocks. These blocks are the elements of a platform for modelling mechanical systems which consist of any number of interconnected rigid bodies representing rotational and translational DoF. It can also encompass hierarchical subsystems as in normal SIMULINK models. The internal visualization tools of SimMechanics can display and animate simplified representations of three-dimension mechanical systems, before and during simulation in MATLAB. It can handle graphics windows and a “virtual world” rendered in a virtual reality viewer (University of Copenhagen, 2014).

3.2.2 SIMPOWERSYSTEMS TOOLBOX

SimPowerSystems, another package also available within the MATLAB (2014) system, also works together with SIMULINK and offers a set of libraries and analysis tools for simulating electrical, mechanical and control systems. These are a combination of electromechanical devices and circuits. Models of electrical power components can be utilised for developing control systems and testing system-level performance. Simscape is an integral part of MATLAB-Simulink to model low-level mechanical, pneumatic, hydraulic physical components. The development of models to HIL systems is supported by C-code generation. Both SimPowerSystems and SimMechanics share a modelling block used for line interface.

3.2.3 SIMDRIVELINE TOOLBOX

SimDriveline MATLAB (2014) provides component libraries for modelling /simulating 1DoF mechanical systems. The SimDriveline library contains models of translational and rotational components including: planetary gears; differential gears; worm gears with meshing and viscous losses; lead-screws; rack and pinions; translational friction; various clutches; etc. These components can be used for modelling the transmission of mechanical power in industrial

machinery, vehicle powertrains, helicopter drivetrains, and so on. SimDriveline models can also be converted into C code for other simulation environments, including HIL systems, for real-time testing of controller hardware (MathWorks, 2014).

3.3 CNC CONTROLLER

For a single machine tool, the CNC is a self-contained system which includes a special form of processor controlled by stored instructions for executing the essential numerical control functions. At least three programs compose the software of a CNC controller; the part program, the service program, and the control program. Regarding the part program, it is based on a description of the geometry of the workpiece being created and the cutting conditions. The service program aims at checking, editing, and correcting the part program. Finally, the control program receives the part program and generates signals in order to drive the rotational and translation axes (Pislaru, 2001).

The signal for moving the axis of a machine tool passes in sequence through the interpreter, the interpolator, the Acceleration/Deceleration controller. Finally is transmitted to the position controller for minimizing the position error. The three-tier CNC system architecture portrayed in the **Error! Reference source not found.** represents the general architecture for the axis control module of a CNC machine tool and consists of the following modules (Suh, Kang, Chung, & Stroud, 2008):

- adaptive control module
- error compensation module
- interpolation module
- spindle control module
- servo control module

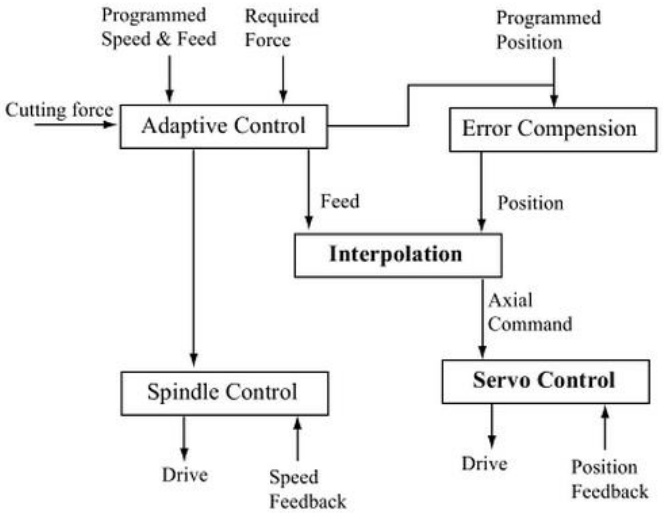

Figure 3-1 Three-tier CNC system architecture (Suh et al., 2008)

The adaptive control module produces optimized cutting conditions such as spindle speed and feedrate. The error compensation module performs the compensation of error factors which cause deviation from the programmed path. Such errors can be the volumetric error of CNC machine tools, the heat from moving elements, tool wear and tool deflection. The interpolator receives the optimized feedrate from the adaptive control module and compensated position instructions for each axis from the error compensation module and sends axial commands to the servo control module. The spindle speed is optimized by the adaptive control module and is transmitted to the spindle control module. (Suh et al., 2008).

Although a fully functional CNC system includes the various control modules which have been described above, the majority of CNC systems consist of control systems containing only the interpolation module and the servo and spindle control modules (Suh et al., 2008). The fact that the CNC controller of the studied five-axis gantry CNC machine tool is a digital computer yields a lot of advantages such as the possibility to access the control and compensation of loops through time sharing. The required control response can be achieved by changing parameters in software. Supervisory applications, such as scheduling required applications, can be executed by the controller.

3.3.1 CNC CONTROLLER SINUMERIK 840D SL

Milling machines represent a large category of machine tools with many variations and configurations available to meet the needs of complexity, capacity and access. Milling machines have capability to machine various surfaces by feeding the work piece against the rotating cutter to enable the machining of closed angles and contoured surfaces. A GEISS 5-axis gantry CNC high-speed milling machine tool (described in methodology section - Research Methodology has been used as the case study in this research. The controller of this machine tool is the SIEMENS SINUMERIK 840D solution line. The machine tool controller processes the part program and realizes its conversion into signals which control a number of actions of the CNC machine tool. In addition, the CNC controller can generate the position demand signal from input instructions entered manually from the operator of the machine tool via the Machine Control Panel (MCP) which also contains data displays for the machine operator (Boothroyd & Knight, 2006).

The SINUMERIK 840D integrated into the SINAMICS S120 and SIMATIC S7-300 automation system forms a new complete digital system. The SINUMERIK 840D sl has a high number of applications for high-speed cutting that are managed by the Numerical Control Unit (NCU), which combines Numerical Control kernel (NCK), HMI, Programmable Logic Control (PLC). The corresponding HMI Human Machine Interface software is already integrated in the NCU software for operating, programming, and visualization. Regarding the connections, DRIVE-CLiQ cables from Siemens are used. The typical topology of the SINUMERIK 840D sl complete system is illustrated in the following Figure 3-2 (Siemens, 2012).

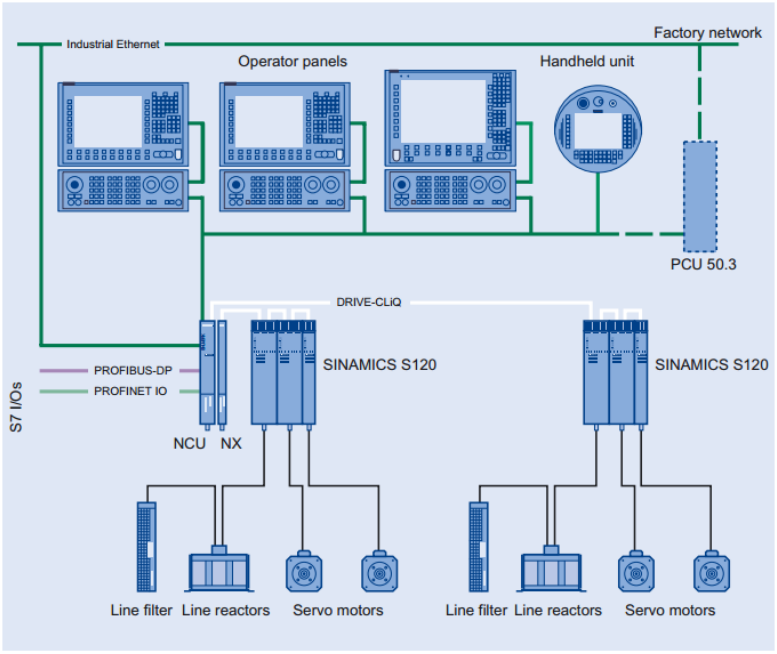

Figure 3-2 Typical topology of the SINUMERIK 840D sl complete system (Siemens, 2008)

Technical specifications for the SINUMERIK 840D sl with NCU 730.1 are presented in Siemens (2008). The drive-end computing performance for the SINAMICS drives within the SINUMERIK 840D sl can be increased with the numeric control extension NX10.

3.3.2 DRIVE-CLIQ REAL-TIME SERIAL DIGITAL INTERFACE

The power supply with required system components are connected via a series of interfaces of the control unit. The components of the SINAMICS S120 are connected with the control unit via DRIVE-CLiQ - depicted in the Figure 3-3. Drive click needs to be used to integrate Siemens terminal module. TM41 allows the encoder position actual value of another drive is output as incremental encoder emulation position measurement. TM41 can be implemented in the real time hardware in the loop system.

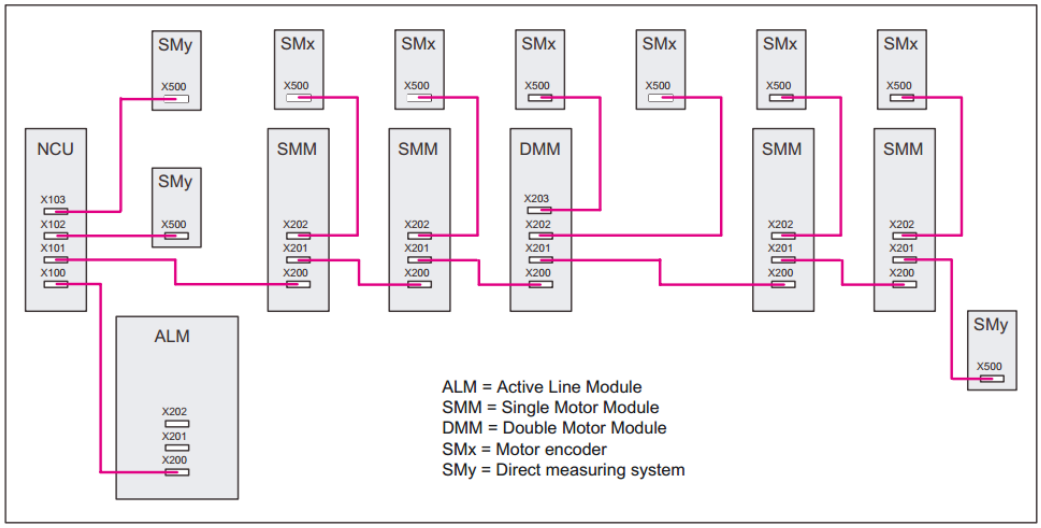

Figure 3-3 DRIVE-CLiQ wiring (Siemens, 2007)

According to manufacturer's manual, the rules for wiring DRIVE-CLiQ are the followings:

- Ring wiring is not allowed.
- Individual components must not be double-wired.
- Up to eight nodes may be connected in one row.
- A maximum of one line module, six motor modules, and three direct measuring systems can be connected to one control unit.

3.4 INVERTER

Historically, synchronous motors and induction motors were used for constant speed drives. It was not possible to use them for variable speed applications as they were less efficient or too expensive. Hence DC motors were employed variable speed drives. A pulse width modulation device is used to obtain variable frequency voltage. AC power converter has been shown on Figure 3-4.

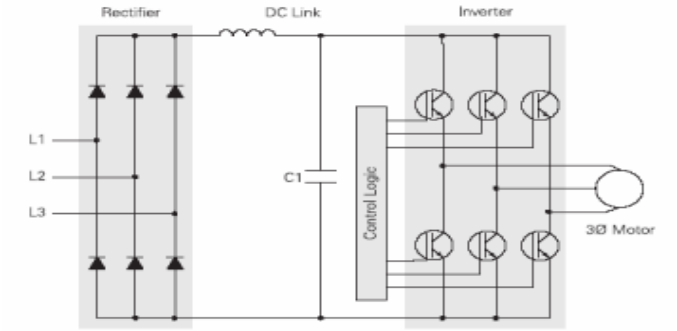

Figure 3-4 Three phase inverter with rectifier and DC link (Nelson 2012)

A three phase power supply is provided to the rectifier. The DC link comprising of an inductor and a capacitor holds a fixed voltage. The inverters can employ various types of semiconductor devices like thyristors, bipolar junction transistors, MOSFET's etc. based on the nature of usage. They are basically used as switching units. The frequency of switching depends on the gating signal applied. Once a trigger is applied the semiconductor unit which is at forward bias due to the DC link starts to conduct until the gate voltage falls below a certain threshold voltage. The control logic block is a pulse width modulation generator driven by the feed drive. The Figure 3-5 taken from Widiyarto's thesis (2006) elaborates on the number of pulses and how they work synchronously to generate the AC current. The figure below shows how the impressed AC signal is generated using pulse width modulation. System control the width of the triggering pulse to generate an AC wave at the output of the inverter.

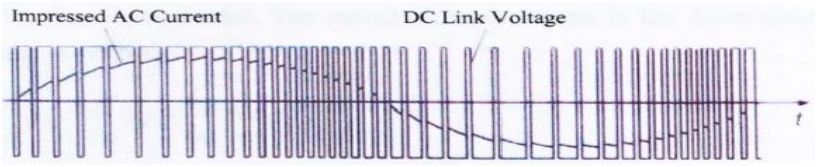

Figure 3-5 Pulse with modulation (Widiyarto 2006)

Nelson (2012), in his white paper, discusses using a common DC bus for multi axis drives. What this essentially means is that the two motor modules that govern the motion control of a gantry axis (mentioned in methodology) will have a shared rectifier unit and DC link. This can help in reducing the size, wiring, cabinet space, assembly time and cost of the drive system.

Triangle comparison based Pulse Width Modulation PWM technique has been employed. The SIMULINK implementation of inverter is shown Figure 3-6 below.

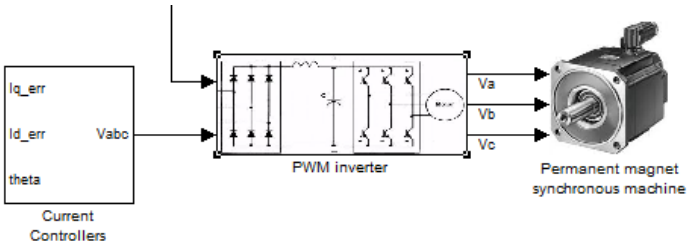

Figure 3-6 PWM Inverter model

The PWM inverter subsystem in SIMULINK model takes two parameters: Vabc, which is the multiplexed three phase voltage signals generated by the current controller and; Vref_abc, which is the reference three phase multiplexed signal fed back from the motor. The functionality of the block is illustrated in the following detailed diagrams of the subsystem.

Three phase multiplexed signals are passed to the Control Logic subsystem in the model. This subsystem generates the control pulses for the following section. Owing to the size and quantity of wiring involved in Inverter subsystem, tags (variables) have been implemented to link one section of the subsystem to the next.

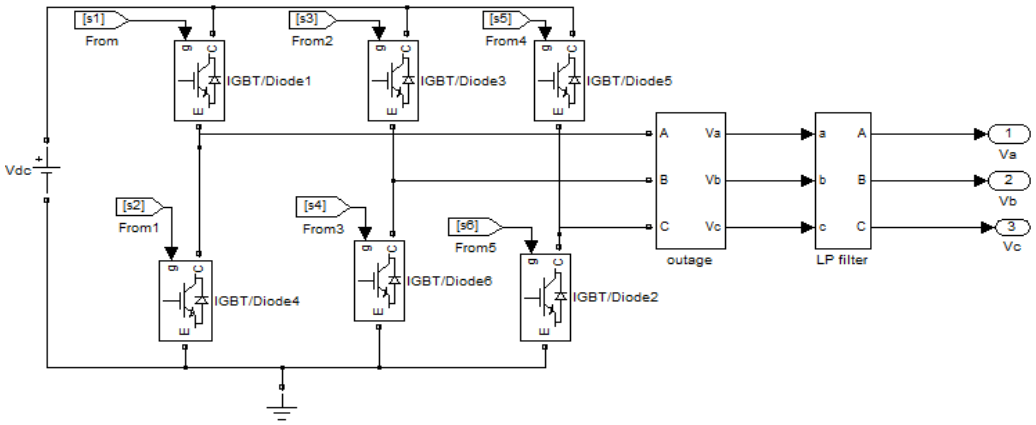

Figure 3-7 Rectifier model

The control pulses generated from the Control Logic are used to turn ON/OFF a set of 6 thyristor-based switches. Based on the sequence of switching (of the thyristor gates) the power transferred to the motor can be regulated. As speed of the motor depends on the power transferred to it, by controlling the switching frequency control the speed of the motor and therefore the displacement as well in the Y axis. The SIMPOWER library provided in MATLAB has been widely used in inverter subsystem.

3.5 PERMANENT MAGNET SYNCHRONOUS MOTOR MODEL

The model number of the permanent magnet synchronous motor (PMSM) used in the project is 1FK7083 – 5AF71 – 1DG0. The technical details for the motor are provided in Appendix C.

As mentioned in the technical specifications, the PMSM has 4 poles and uses a 22-bit incremental encoder. The concerned motor has been illustrated in the Figure 3-8.

Figure 3-8 PMSM motor (Siemens 2013)

They have extremely high dynamic response owing to the low rotor moment of inertia. The motor comes with an integrated DRIVE-CLiQ interface (DQI) encoder. Based on the nature of mounting of the permanent magnets, the PMSM could be surface permanent magnet motor or interior permanent magnet motor.

3.5.1 OPERATION AND MODELLING

Since the rotor has permanent magnets, a permanent magnetic field is induced. The stator winding is energized by a sinusoidal voltage from the inverter. The three phase sinusoidal excitation creates a rotating magnetic field. This field cuts the permanent magnets in the rotor and they start to rotate. The speed of the motor is dependent on the number of rotor poles and the input frequency. The stator current is switched at a higher frequency as opposed to the motor's actual speed.

The space vector equations governing the motor are given below.

$$V_s = r_s i_s + \frac{d\lambda_s}{dt} \qquad \text{Equation 3-1}$$

$V_s, i_s \& \lambda_s$ are the three phase stator voltage, current and flux linkages, respectively.

r_s is the stator resistance

For modelling d q model over a rotor reference frame is used. Figure 3-9 expresses the model.

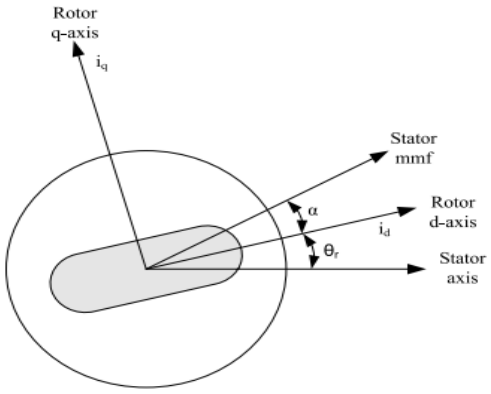

Figure 3-9 D-Q model (E. L. C. Arroyo 2006)

Further few assumptions are made to generate a model: Field dynamics are absent; there are negligible losses from eddy current and hysteresis; Saturation and a sinusoidal waveform for the induced EMF are neglected.

The equations governing the voltage are given by:

$$V_d = r_s i_d - \omega_r \lambda_q + \frac{d\lambda_q}{dt} \qquad \text{Equation 3-2}$$

$$V_q = r_s i_q - \omega_r \lambda_d + \frac{d\lambda_d}{dt} \qquad \text{Equation 3-3}$$

The equations governing flux are given by:

$$\lambda_d = L_d i_d + \lambda_f \qquad \text{Equation 3-4}$$

$$\lambda_q = L_q i_q \qquad \text{Equation 3-5}$$

Relating the equation governing flux and voltage results is following:

$$\begin{pmatrix} V_q \\ V_d \end{pmatrix} = \begin{pmatrix} r_s + L_q \frac{d}{dt} & \omega_r L_d \\ \omega_r L_q & r_s + L_d \frac{d}{dt} \end{pmatrix} \begin{pmatrix} i_q \\ i_d \end{pmatrix} + \begin{pmatrix} \omega_r \lambda_f \\ \frac{d\lambda_f}{dt} \end{pmatrix} \quad \text{Equation 3-6}$$

The equation for torque is given by

$$T_e = \frac{3}{2}\left(\frac{P}{2}\right)\left(L_d i_q - L_q i_d\right) \quad \text{Equation 3-7}$$

Equation governing mechanical torque is as follows

$$T_e = T_L + B\omega_m + J\frac{d\omega_m}{dt} \quad \text{Equation 3-8}$$

The angular velocity of the motor in terms of velocity of the rotating magnetic flux in the stator is as follows

$$\omega_m = \omega_r \left(\frac{2}{P}\right) \quad \text{Equation 3-9}$$

V_d is the voltage due to direct current, V_q is the voltage due to quadrature current, r_s is the resistance in the stator winding i_d is the direct current, i_q is the direct current, ω_r is the angular velocity of the rotating magnetic flux in the stator, ω_m is the angular velocity of the motor, λ_q is the flux linkage due to quadrature current, λ_d is the flux linkage due to direct current, λ_f is the field flux linkage, T_e is the developed torque, T_L is the load torque, B is friction, J is inertia, P is the number of poles, L_d is the self-inductance in the direct axis, L_q is the self-inductance in the quadrature axis and I_m is the supply current peak value.

3.5.2 PERMANENT MAGNET MOTOR CONTROL

An efficient method for controlling a PMSM is the field oriented control. The stator coils of the motor are excited using sinusoidal waveforms from the inverter. The frequency and phase of the signal are varied to control the speed of the motor. Information is required about the present position of the instantaneous flux of the rotor or rotor position of the permanent magnet. An absolute encoder is therefore used.

The choice of control depends on the rated speed and the inverter. The information about the speed at which the constant torque operation ends and the flux weakening is quintessential. Plot between steady state torque and speed is illustrated on Figure 3-10.

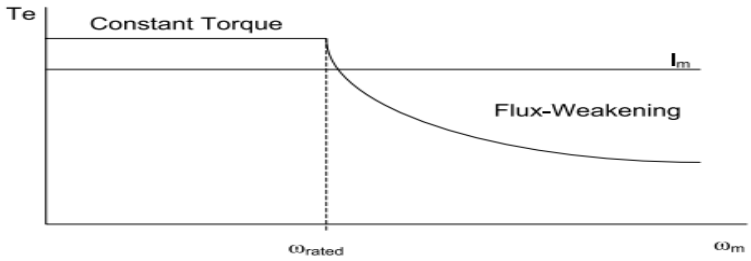

Figure 3-10 Torque speed characteristics (Siemens 2008)

The current equations for the three phases are

$$i_a = I_m \sin(\omega_r t + \alpha)$$ Equation 3-10

$$i_b = I_m \sin\left(\omega_r t + \alpha - \frac{2\pi}{3}\right)$$ Equation 3-11

$$i_c = I_m \sin\left(\omega_r t + \alpha + \frac{2\pi}{3}\right)$$ Equation 3-12

Therefore from the equation above values of direct and quadrature current in terms of the supply current will be:

$$\binom{i_q}{i_d} = I_m \binom{sin\alpha}{cos\alpha}$$ Equation 3-13

The following equation is a representation of the developed torque in terms of the supply current. This is obtained from equations above

$$T_e = \frac{3}{2}\left(\frac{P}{2}\right)\left(\frac{1}{2}(L_d - L_q){I_m}^2 sin2\alpha + \lambda_f I_m sin\alpha\right)$$ Equation 3-14

Or

$$T_e = \frac{3}{2}\left(\frac{P}{2}\right)\left((L_d - L_q) i_d i_q + \lambda i_q\right)$$ Equation 3-15

The second version of the equation is quite the favourite in SIMULINK representation of the permanent magnet synchronous machine.

Constant Torque Operation

In this strategy, the maximum possible torque always being used. Quadrature current is proportional to the torque producing current. If α will be 90^o then quadrature current will be equal to the supply current and the direct current will be equal to zero. Therefore the torque equation would now be modified as follows:

$$T_e = k_t . i_q$$ Equation 3-16

Where k_t is the torque constant and is given by

$$k_t = \left(\frac{3}{2}\right)\left(\frac{P}{2}\right)\lambda_f$$ Equation 3-17

The direct current is responsible for generating flux. Therefore speed of the motor can be increased reducing the flux. Initially the motor operates at a rated value of flux linkage up to a definitive speed where in the v/f (voltage and frequency ratio) ratio is maintained as a constant. Beyond a definitive value of frequency V/f ratio would decrease once inverter limit is attained. In order to retain the ratio the flux linkages need to be weakened. In the constant power region the torque decreases proportionally to the decrease in flux. Since rotor is made up of permanent magnets its flux cannot be reduced. Hence it is required to increase the d axis current in the negative direction. Now using armature reaction the flux in the air gap can be reduced. The equivalent flux is reduced or weakened. The angle α may be deduced as

$$\alpha = tan^{-1}\left(\frac{i_q}{i_d}\right)$$ Equation 3-18

Also the relation between the direct quadrature and supply current is as follows

$$I_m = \sqrt{{i_d}^2 + {i_q}^2}$$ Equation 3-19

The load torque may therefore be adjusted to a given value of reference angular speed against the maximum rated value of torque. This is described by the equation:

$$T_L = T_{e(rated)}\left(\frac{\omega_{rated}}{\omega_r}\right)$$ Equation 3-20

Regarding the construction of a PMSM. The permanent magnet is placed inside this shallow rotor core in order to maintain the rotor magnetization. In the beginning, the rotor flux is restricted to the core. Afterwards, as the speed rises, there is a reduction of the rotor frequency, while the rotor flux builds up, producing a pulsating torque with the magnetic field. When the motor comes to the full speed, the impressed field comes into step with the magnetic field, the rotor rotates at the same speed as the rotating magnetic field in the stator or in other words, the machine runs as a synchronous motor. PMSM's exhibit constant speed with varying load (zero slip) and offer high efficiency and power factor, as well as lower current draw than comparable synchronous motors.

Created for purpose of research SIMULINK Model Figure 3-11 illustrates in detail the function of the Control Logic subsystem implemented within the Inverter subsystem.

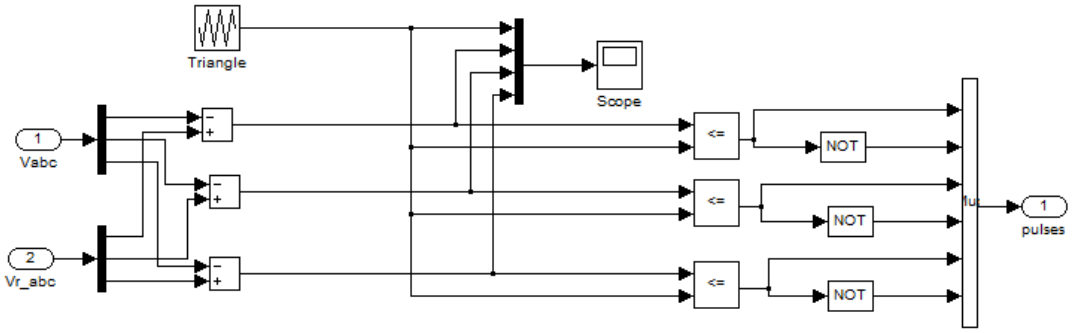

Figure 3-11 Detailed model of Control logic sub system

The multiplexed three phase voltages generated from the current controller and the referenced voltages fed back from the motor are de-multiplexed and compared against each other (Va with Vref_a, Vb with Vref_b & Vc with Vref_c). This is compared against a triangular carrier wave generated from the triangle block. This block has a customized functionality. It generates a triangular wave at a frequency of 2 Khz and to do that it uses a repeatable table. The frequency used is 2Khz. This implies that the time period is 0.0005s. In the table, the output values at 4 critical points within the time period are specified. The interpretation of the sequence is as follows – at time 0 the value of the wave is zero, at quarter of the time period the triangle attains the positive peak, at three quarters the time period the negative peak is attained and finally at 0.0005s it goes back to zero. This block generates a repeating sequence of these values to create the triangular wave. The error between the reference and actual values of the three phase voltages are compared against the triangular wave.

The switching logic from the thyristor circuit drives an outage subsystem. The SIMULINK drawing of the subsystem in Figure 3-12. The current from the thyristor-based rectifiers are measured using a SIMPOWER current measurement block. Two ports out of the current block are used to calculate the voltage using voltage measurement block. Only the phase voltage is obtained so far. To evaluate the line voltages it is necessary to subtract them from one another as shown in the SMULINK.

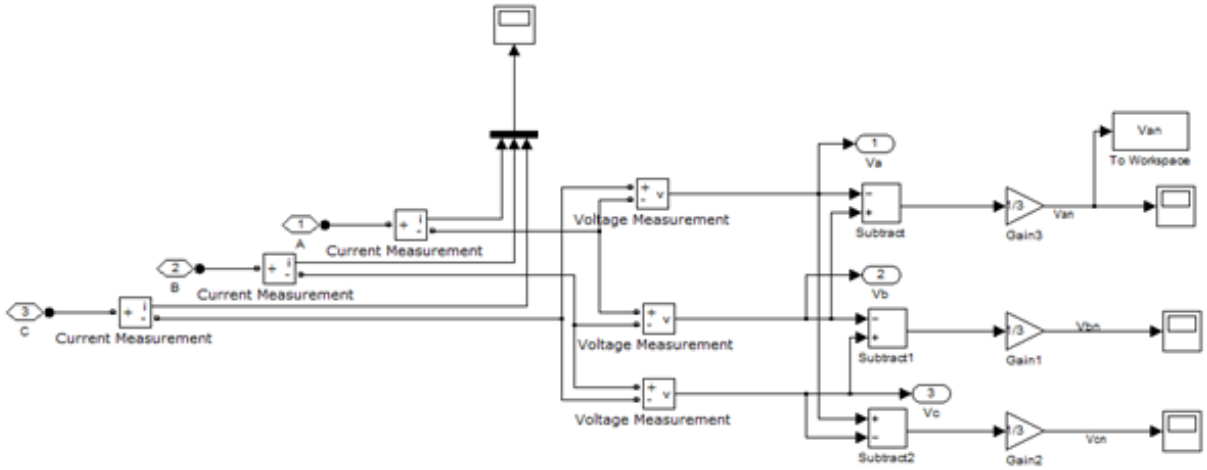

Figure 3-12 Detailed model of the outage sub system

A filter subsystem within the inverter smooths the response. It contains three sets of third-order low-pass Butterworth filters.

3.5.3 SIMULINK MODEL OF PMSM MOTOR

Operation, working and potential equations governing the PMSM motor have been discussed. This section will present a SIMULINK implementation of the theoretical model of the PMSM motor discussed so far. The signals obtained from the inverter are transferred to the motor subsystem as shown in Figure 3-13 SIMULINK representation.

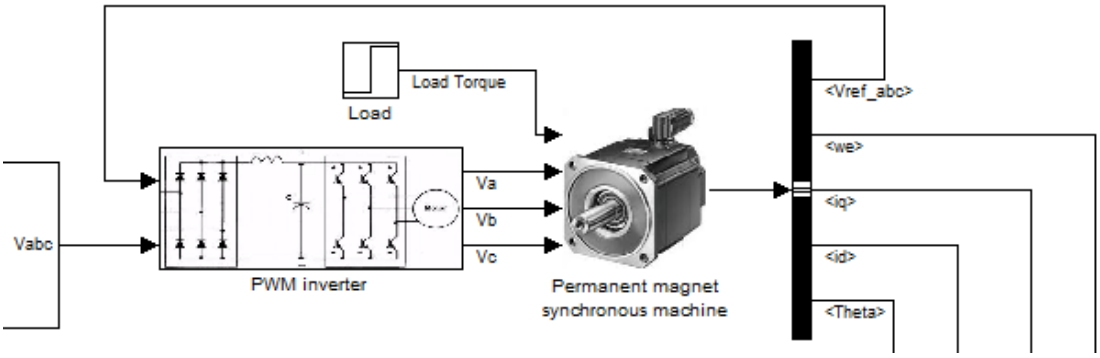

Figure 3-13 Permanent magnet synchronous machine control model

The PMSM subsystem takes four input parameters V_a, V_b, V_c and Load torque. For the purpose of simulation, Load torque is assumed to be a step load having an initial value of 0 Nm and attaining a torque value of 4Nm at 0.025s (calculated through trial and error and tested for good torque response)

The PMSM has three subsystems, or three stages of operation. The first subsystem takes the three phase voltage parameters and performs a coordinate transformation. It transforms them into direct and quadrature axes. This step is crucial as most of the analysis performed is based on the direct and quadrature quantities. It provides the user the ease to control an AC motor like a normal DC motor without having to control directly the three phase varying quantities. The direct and quadrature voltages are then used by up by the second subsystem to generate the current (direct and quadrature) along with other relevant mechanical quantities such as torque, angular speed and theta (angle). The angle theta is the electrical angle which can also be closely approximated to the actual angle of the rotor. The value of theta is very important and is used internally by the subsystems 'V_abc to Vdq'& 'Vdq to V_abc'. The third subsystem transforms the voltages in the direct and quadrature axis back into the three phase domain. The multiplexed three phase voltage signal Vabc is then fed back from the motor to the inverter.

The working of the first stage (V_abc to Vdq) within the permanent magnet synchronous machine model. The SIMULINK representation shown Figure 3-13 Permanent magnet synchronous machine control model is simply the mathematical representation of the abc to dq transformation governed by the following equations.

$$V_d = \frac{2}{3}(V_a sin\,\theta + V_b \sin\left(\theta - \frac{2\pi}{3}\right) + V_c \sin\left(\theta + \frac{2\pi}{3}\right)) \quad \text{Equation 3-21}$$

$$V_q = \frac{2}{3}(V_a cos\,\theta + V_b \cos\left(\theta - \frac{2\pi}{3}\right) + V_c \cos\left(\theta + \frac{2\pi}{3}\right)) \quad \text{Equation 3-22}$$

$$V_0 = \frac{1}{3}(V_a + V_b + V_c) \quad \text{Equation 3-23}$$

The value of θ, as discussed earlier, is obtained from the subsequent section. θ is the electrical angle and it is computed in the next stage. The first subsystem computes the voltages V_d&V_q and transfers them to the second subsystem within the permanent magnet synchronous machine subsystem. The SIMULINK representation of the subsystem is given on Figure 3-14.

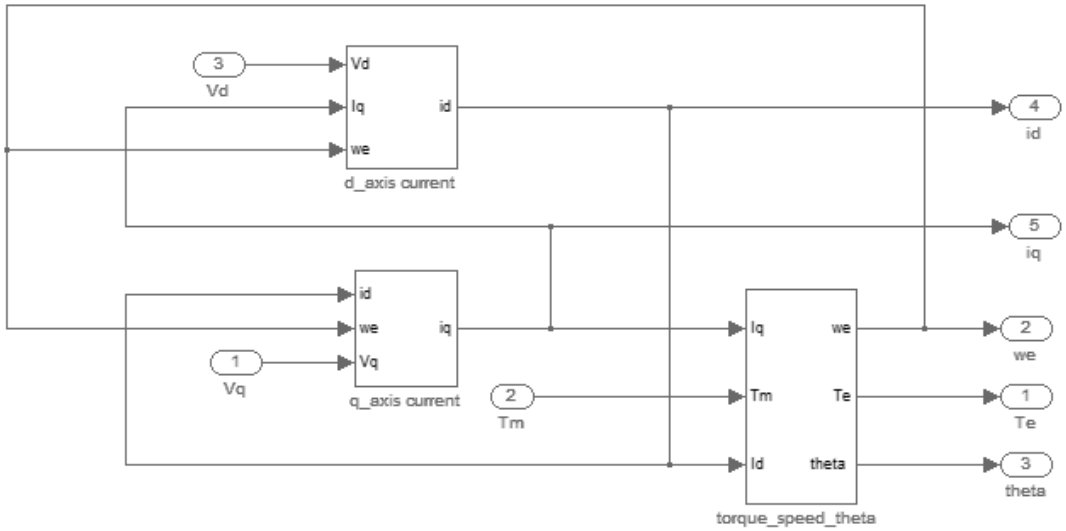

Figure 3-14 Detailed model of PMSM_Current sub system

There are again three blocks to this subsystem. The d_axis current block as shown on (Figure 3-15) computes the value of i_d using the following equations.

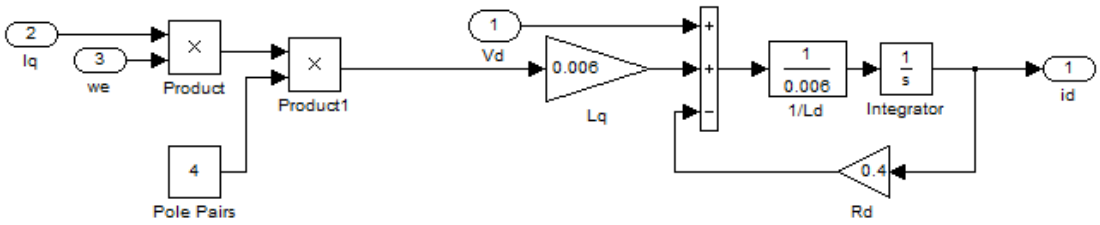

Figure 3-15 Detailed model for d_axis current sub system

Although equations relating V_d&i_d for the purpose of modelling have been discussed, the model uses a slight variant of the same equation as provided by SIMULINK.

$$\frac{di_d}{dt} = \frac{1}{L_d}\left(V_d - r_s i_d + \frac{P}{2} L_q \omega_r i_q\right) \quad \text{Equation 3-24}$$

Taking Laplace transforms for the above equation:

$$si_d(s) = \frac{1}{L_d}\left(V_d(s) - r_s i_d(s) + \frac{P}{2} L_q \omega_r i_q(s)\right) \qquad \text{Equation 3-25}$$

$$\therefore i_d(s) = \frac{1}{s}\left\{\frac{1}{L_d}\left(V_d(s) + \frac{P}{2} L_q \omega_r i_q(s) - r_s i_d(s)\right)\right\} \qquad \text{Equation 3-26}$$

The values for L_d, L_q&r_s (R_d $in\ the\ model$) are provided by Siemens (2012) in the manual for their 1fK7 motor. These are appropriately inserted into the model as shown above. This model can determine the value of direct current at any given instant of time. In a similar sense, the q_axis current block computes the value for quadrature current based on the SIMULINK model shown in Figure 3-16.

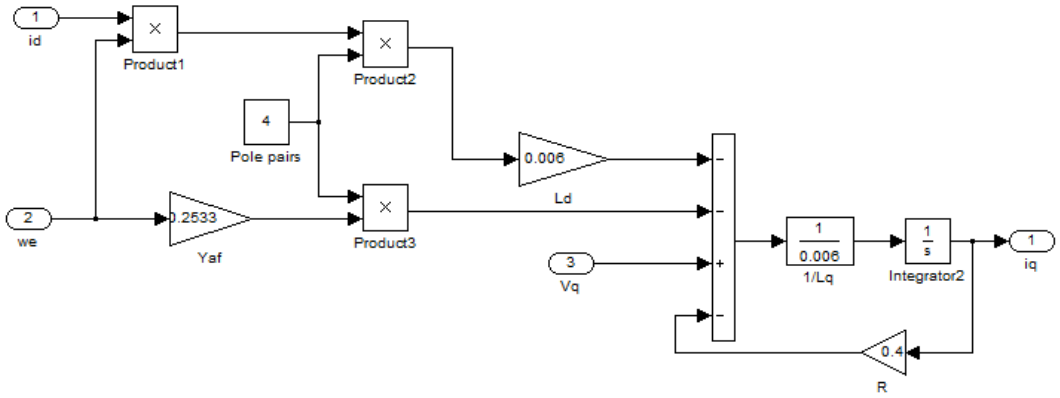

Figure 3-16 Detailed model of q_axis sub system

To compute the values relating V_q&i_q for the quadrature current, the equations governing the relation is used and given below.

$$\frac{di_q}{dt} = \frac{1}{L_q}\left(V_q - r_s i_q + \frac{P}{2}\left[-L_d \omega_r i_d - \lambda_f \omega_r\right]\right) \qquad \text{Equation 3-27}$$

Taking Laplace transforms for the above equation :

$$si_q(s) = \frac{1}{L_q}\left(V_q(s) - r_s i_q(s) + \frac{P}{2}\left[-L_d \omega_r i_d(s) - \lambda_f \omega_r(s)\right]\right) \qquad \text{Equation 3-28}$$

$$\therefore i_q(s) = \frac{1}{s}\left\{\frac{1}{L_q}\left(V_q(s) - r_s i_q(s) + \frac{P}{2}\left[-L_d \omega_r i_d(s) - \lambda_f \omega_r(s)\right]\right)\right\} \qquad \text{Equation 3-29}$$

This equation has been implemented in the SIMULINK diagram shown Figure 3-16 above and therefore computes instantaneous values of the quadrature current. Note that the values for L_d, L_q, $\lambda_f(Yaf\ in\ the\ model)$, $P(number\ of\ poles)$ and r_s ($R\ in\ the\ model$) are appropriately replaced with values obtained from the 1FK7 motor manual and its included in Appendix C. The third subsystem, torque_speed_theta, illustrated in the SIMULINK model Figure 3-16 above takes the load torque (T_m), direct and quadrature values of current as inputs. So basically, the values of direct and

quadrature current computed by the d_axis current subsystem and q_axis current subsystem are transferred to the torque_speed_theta subsystem to compute quantities like angular speed, angle and electromagnetic torque. The detailed illustration of the subsystem is given on Figure 3-17.

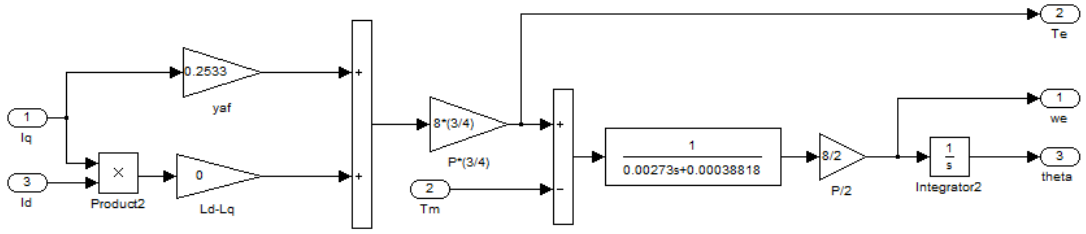

Figure 3-17 Detailed model of torque_speed_theta subsystem

The first half of the model shown Figure 3-17s the simple implementation of the electromagnetic torque equation for the PMSM motor given by

$$T_e = \frac{3}{2}\left(\frac{P}{2}\right)\left((L_d - L_q)i_d i_q + \lambda i_q\right) \qquad \text{Equation 3-30}$$

Note that for the given model of the 1FK7 motor the values for L_d and L_q are the same. This may not always be the case. Most manufacturers differ when they provide a response for this query. Alternatively, a series of tests may be performed to compute the theoretical values for L_d and L_q. For the scope of this project, equal values for the inductances have been assumed.

After computing the torque, a transfer function block is connected in series to determine the angular speed. This is based on the following equation.

$$T_e = T_L + B\omega_m + J\frac{d\omega_m}{dt} \qquad \text{Equation 3-31}$$

Taking Laplace transforms for the above equation:

$$T_e(s) = T_L(s) + B\omega_m(s) + Js\omega_m(s) \qquad \text{Equation 3-32}$$

$$\therefore T_e(s) - T_L(s) = \omega_m(s)(B + Js) \qquad \text{Equation 3-33}$$

$$\therefore \omega_m(s) = \frac{T_e(s) - T_L(s)}{Js + B} \qquad \text{Equation 3-34}$$

The Load torque from the electromagnetic torque is subtracted and multiplied with a transfer function of the form$\frac{1}{Js+B}$. The values for J are obtained from the motor's specification manual. However, the value for damping requires extensive computation. Once the angular speed is computed, it becomes relatively easy to calculate the value of theta. It is obtained by integrating the angular speed signal.

So far, the 1st and 2nd blocks in the permanent magnet synchronous machine have been discussed. The final block within the subsystem is the Vsq0-V_abc subsystem. This block takes $V_d, V_q \& theta$ signals as input and transforms the voltages from the dq0 domain to the three phase abc domain.

The Vdq to V_abc subsystem is the simple representation of the given transformation equations from the dq0 to the abc domain.

$$V_a = V_d cos\theta - V_q sin\theta \quad \text{Equation 3-35}$$

$$V_b = V_d \cos\left(\theta - \frac{2\pi}{3}\right) - V_q \sin\left(\theta - \frac{2\pi}{3}\right) \quad \text{Equation 3-36}$$

$$V_c = V_d \cos\left(\theta + \frac{2\pi}{3}\right) - V_q \sin\left(\theta + \frac{2\pi}{3}\right) \quad \text{Equation 3-37}$$

So basically, three phase voltages have been converted into dq0 domain values. This helps to analyse and determine the physical parameters such as electromagnetic torque, angular speed & theta. Once these values are calculated, thne the dq0 domain voltages are reversed back into 3 phase signals which are then fed back to the inverter to perform PWM.

3.6 MECHANICAL TRANSMISSION COMPONENTS

The purpose of a transmission is to convert mechanical power energy from motor to linear/rotary movement of the axis. In this subsection of the thesis a model will be derived. The coupling guide way and ballscrew are the main transmission components of CNC machine feed drive systems.

3.6.1 COUPLING BETWEEN MOTOR AND BALLSCREW

A belt drive is a motion transmission mechanism which consists of a pair of pulleys (wheels) and a belt. A series of cylindrical pulleys connected by a flat belt form the simplest configuration of a belt drive in which the transmission of torque is achieved, because of the friction developed between the pulley and contact.

Belt drives can be divided into: friction belt drives where the transmission depends on the principle of the rope friction; and toothed belt drives in which a constant transmission is achieved because the tangential forces are produced without slip. According to Isermann (2003), an equivalent model describing the dynamic behaviour of the belt drive is depicted in Figure 3-18. It is necessary to take into account a few simplifying assumptions:

- The belt is massless
- The shaft distance is constant
- The effect of centrifugal forces is neglected
- The deformation of the wheels and the shafts is neglected compared to the belt deformations

- For a certain load status, the modulus of elasticity is constant over the total belt length, such that Hooke's law applies
- For friction belts, extension slip only occurs.

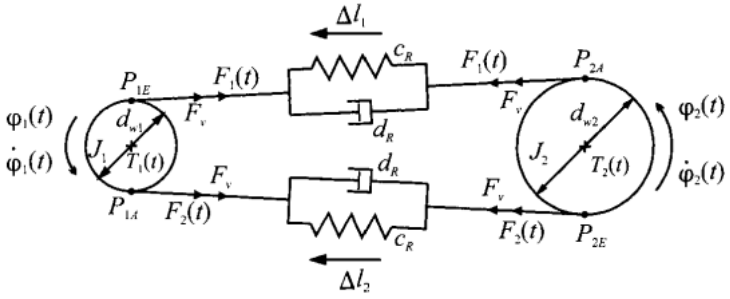

Figure 3-18 Equivalent model of a belt drive (Isermann, 2003)

It becomes possible to estimate the belt spring stiffness C_R using the following formula :

$$C_R = \frac{EA}{l_R}$$ Equation 3-38

Where $EA$is the belt stiffness factor and l_R the belt length on tight or slack side.

The following formula calculates the belt-damping coefficient d_R:

$$d_R = \frac{\psi C_R}{2\pi\dot{\varphi}_{10}}$$ Equation 3-39

Where $\dot{\varphi}_{10}$is the angular speed of the driving pulley at the operating point and ψ the relative damping of the belt. Considering the above equations and equivalent model of the belt drive in the Figure 3-18 the following angular momentum balances at the driving pulley and at the driven pulley can be defined as follows (Isermann, 2003):

At the driving pulley:

$$J_1\ddot{\varphi}_1(t) = T_1(t) - \frac{d_{W1}}{2}\big(F_1(t) - F_2(t)\big)$$ Equation 3-40

At the driven pulley:

$$J_2\ddot{\varphi}_2(t) = -T_2(t) + \frac{d_{W2}}{2}\big(F_1(t) - F_2(t)\big)$$ Equation 3-41

Where the indices 1 and 2 define the tight side belt, driving pulley and slack side belt, driven pulley, respectively, with,

$$F_1(t) = F_v + C_R\Delta l_1(t) + d_R\Delta i_1(t))$$ Equation 3-42

and

$$F_2(t) = F_v - C_R\Delta l_2(t) - d_R\Delta i_2(t)$$ Equation 3-43

With Δl_1 as the increase of the length of the tight side and Δl_2 as the decrease of the length of the slack side.

By inserting $F_1(t)$ and $F_2(t)$ into$J_1\ddot{\varphi}_1(t)$ and $J_2\ddot{\varphi}_2(t)$ respectively, the following equations for the belt drive can be obtained (Isermann, 2003):

$$J_1\ddot{\varphi}_1(t) + \frac{d_{w1}}{2}\left[C_R\left(\Delta l_1(t) + \Delta l_2(t)\right) + d_R\left(\Delta i_1(t) + \Delta i_2(t)\right)\right] = T_1(t) \qquad \text{Equation 3-44}$$

$$J_2\ddot{\varphi}_2(t) - \frac{d_{w2}}{2}\left[C_R\left(\Delta l_1(t) + \Delta l_2(t)\right) + d_R\left(\Delta i_1(t) + \Delta i_2(t)\right)\right] = -T_2(t) \qquad \text{Equation 3-45}$$

The pre-tensioning F_v disappears.

The motor is coupled to the ballscrew using a timing belt, as illustrated in Figure 3-19.

Figure 3-19 Details about the timing belt (Rexroth Bosch Group 2006)

In the Geiss machine, the toothed timing belt used has a gear ratio of 1:1.5. The objective of the physical model is to transform the rotary motion into the translator motion of the gantry axis. This transformation is made possible through a ballscrew.

For synchronous belt drives, the mathematical model can be defined as follows by Isermann (2003):

$$J_1\ddot{\varphi}_1(t) + d_{DT}\left(\dot{\varphi}_1(t) - i\dot{\varphi}_2(t)\right) + c_{DT}\left(\varphi_1(t) - i\varphi_2(t)\right) = T_1(t) \qquad \text{Equation 3-46}$$

$$J_2\ddot{\varphi}_2(t) - i\left[d_{DT}\left(\dot{\varphi}_1(t) - i\dot{\varphi}_2(t)\right) + c_{DT}\left(\varphi_1(t) - i\varphi_2(t)\right)\right] = -T_2(t) \qquad \text{Equation 3-47}$$

Where c_{DT} is the dynamical torsional stiffness in Nm/rad,

$$c_{DT} = \frac{{d_{w1}}^2}{2}\, c_R \qquad \text{Equation 3-48}$$

andd_{DT} is the damping factor in Nm/rads,

$$d_{DT} = \frac{{d_{w1}}^2}{2}\, d_R \qquad \text{Equation 3-49}$$

The simplified implemented model of the synchronous belt drive is illustrated in Figure 3-20.

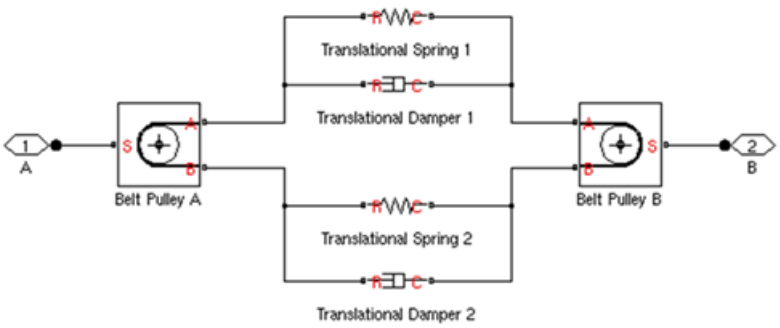

Figure 3-20 The belt drive block (MathWorks, 2014)

The spring and damper blocks which are depicted in the above schematic account for compliance in the belt, and the connections A and B of the same schematic are the conserving mechanical rotational ports which are associated with the shafts of pulleys A and B, respectively. The friction coefficient is equal to the friction velocity threshold between the belt and each of the pulleys (MathWorks, 2014). All these transmission devices have limited mechanical stiffness and increase the inertia that has to be overcome by the acceleration of the servo motor.

3.6.2 BEARINGS

Many translation axis of a CNC machine tool includes shafts supported by bearings which are a source of frictional torque. When the ballscrew is loaded, the bearings, which support the ballscrew, are axially loaded. The torque caused by friction in bearings can be computed by the following formula (Pislaru, 2001):

$$T_{b=}T_f + T_d \qquad \text{Equation 3-50}$$

whereT_f and T_d are the load-free and load-dependent components of the total frictional torque (Nmm), respectively.

Bearing mounting stiffness model is presented on Figure 3-21:

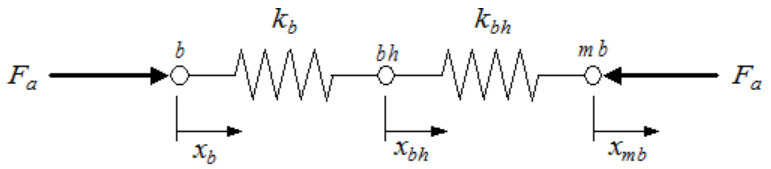

Figure 3-21 Bearing mounting stiffness (Pislaru, 2001)

where, k_b the bearing stiffness, k_{bh} the bearing housing stiffness, x_b the displacement of the contact point with screw shaft, and $x_{mb}$the displacement of the contact point with the machine bed.

3.6.3 BALLSCREW

The function of a ballscrew is to translate the rotary motion of the screw to linear motion of the nut. This transformation is accomplished with a number of other screw mechanisms. The ballscrew, which is a precision assembly usually is supported by a set of rolling elements (balls) mounted between the screw and the nut.

Holroyd (2007) describes that two basic components of a ballscrew are the screw and the nut, supported by rolling elements. The screw is a long cylindrical solid or hollow rod with helical grooves on its outer cylindrical surface. The rolling elements roll in these grooves, as they are close to being a part-circular section. In most cases, axial movement of the parts of the ballscrew is achieved by rotating the screw and holding the nut. Nevertheless, axial movement of the parts of the ballscrew can also be achieved by rotating the nut and holding the screw. In the last case, it is required that the screw is clamped at one or both ends Figure 3-22.

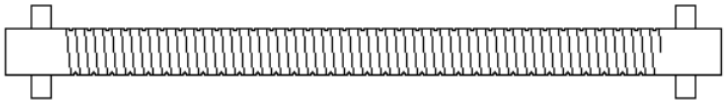

Figure 3-22 The “fixed-fixed” screw clamping arrangement (Holroyd, 2007)

In the case where it is rotated, the screw has provision for bearings, at one or both ends. In order to provide axial constraint, at least one of these bearings has to be a thrust bearing. There is also a provision at one end of the screw for mounting the means of its driving, such as an elastic coupling, a gear wheel, or a belt drive pulley as in the studied CNC machine tool. The maximum tolerable axial forces, as well as the maximum possible linear speeds are usually limited by the length of the screw and the design of the end bearings (Holroyd, 2007).

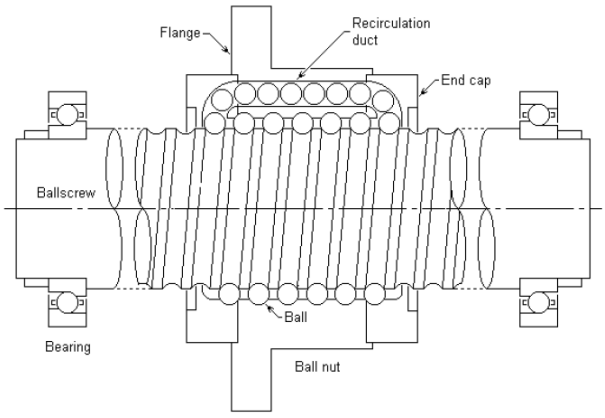

Figure 3-23 Ballscrew nut (Holroyd, 2007)

The second basic component of a ballscrew is the nut presented on Figure 3-23. Its inner surface is a short hollow tube. The diameter of this tube is bigger than the outer diameter of the screw. Cylindrical tube with a pair of parallel flat surfaces with an attached flange at one end is a quite

usual arrangement. The nut in its inner surface has grooves which match those on the screw. Rolling elements fill the space between these two main components which fit into the grooves. The movement of the nut will be an axial movement along the screw. This system can be applied to either the fixed nut or the fixed ballscrew method.

3.6.4 BALLSCREW MODEL

In this section the modelling of a FAR-B-S driven nut ballscrew is discussed. The driven nut model is different from the traditional model of the ballscrew. In the traditional models the screw of the ballscrew rotates and the nut travel on the rotation of the screw. In the driven nut model the screw is fixed and the balls in the nut rotate allowing the nit to travel along the length of the screw. Driven nut ballscrews have higher values of stiffness and allow accurate translator motion. The technical details for the driven nut ballscrew are given in APPENDIX C.

For the sake of simplicity model of the master axis and replicated model for the slave neglecting any minute variations in mechanical parameters. The physical model under discussion is given on Figure 3-24. Zirn (2008) talks about this model in detail. He has divided the system into 4 point masses. Friction for motor bearings and linear guides are available from the manual for motor. The slider and the nut are considered as one body connected to the second screw part by the nut stiffness k_M. All inertia has been transformed into equivalent masses $m_{eq,i}$.

$$m_{eq,i} = \left(\frac{2\pi}{h_S}\right)^2 . J_i \qquad \text{Equation 3-51}$$

Since there is an additional gear between ballscrew and motor the motor and motor belt wheel inertia have to be transformed to the screw axis

$$J_{M'} = u^2 . J_M \qquad \text{Equation 3-52}$$

With the gear ratio defined as

$$u = \frac{\omega}{\omega'} \qquad \text{Equation 3-53}$$

The stiffness of the pre-stressed belt gear depends on the geometry

$$k_{Ktor} = \frac{{r_2}^2}{a} . k_R \qquad \text{Equation 3-54}$$

Where k_R is the spring constant of a belt piece with a length of 1m.

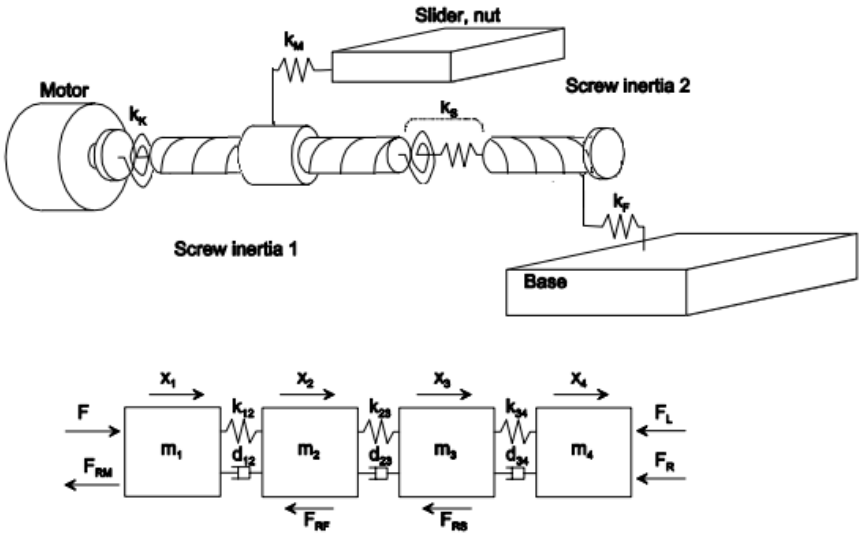

Figure 3-24 Ballscrew model (Zirn 2008)

All flexibilities given as torsion springs $k_{tor,i}$ must be transformed into equivalent translatory spring constants k_i

$$k_i = \left(\frac{2\pi}{h_S}\right)^2 . k_{tor,i}$$ Equation 3-55

Thus the springs in the physical model according to Figure are given as

$$k_{12} = \left(\frac{2\pi}{h_S}\right)^2 . k_K$$ Equation 3-56

$$k_{23} = k_S$$ Equation 3-57

$$k_{34} = k_M$$ Equation 3-58

The point masses $m_{1\ldots4}$ in the physical model according to Figure are given by

$$m_1 = \left(\frac{2\pi}{h_S}\right)^2 . \left(J_M + \frac{J_K}{2}\right)$$ Equation 3-59

$$m_2 = \left(\frac{2\pi}{h_S}\right)^2 . \left(\frac{J_S}{2} + \frac{J_K}{2}\right)$$ Equation 3-60

$$m_3 = \left(\frac{2\pi}{h_S}\right)^2 . \frac{J_S}{2}$$ Equation 3-61

$$m_4 = m_M + m$$ Equation 3-62

Friction torques $M_{RM,S}$ and motor torque M have to be transferred to equivalent forces

$$F_{RM,S} = \left(\frac{2\pi}{h_S}\right).M_{RM,S}$$ Equation 3-63

$$F = \left(\frac{2\pi}{h_S}\right).M$$ Equation 3-64

Oliver Zirn (2008) mentions in his paper that the dominant influence for the feedback control performance results from the eigenmode with the lowest resonant frequency. Therefore it is sufficient to model the servo drive with flexible transmission devices as a 4th-order system with one DOF for the input variable (motor torque/force) and a second DoF for the output variable (slider/load position). Zirn (2008) discusses a reduction method based on a simplified Guyan method which turned out to be very effective and accurate for drive chains like ballscrews and belt gears. Flexible transmission devices are part of the feedback control loop. The Figure 3-25 given below illustrates the case scenario.

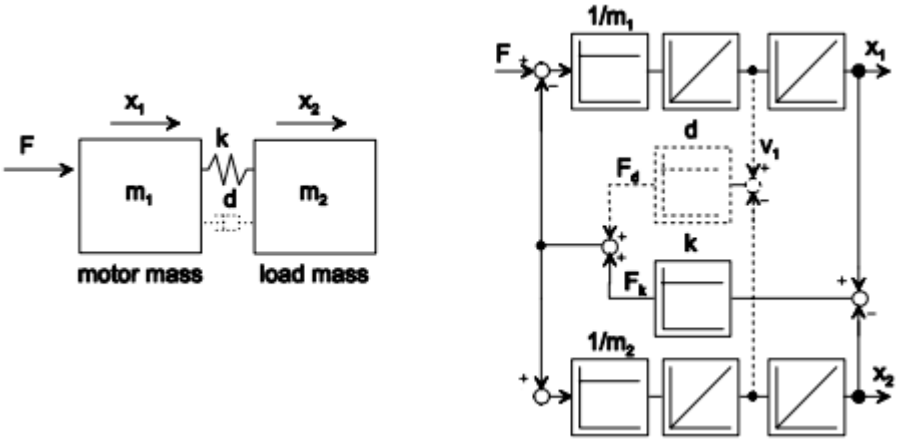

Figure 3-25 Reduced mass spring model of the ballscrew system (Zirn 2008)

Therefore all inertia on both sides of the dominant flexibilityk_{ij}, i.e. smallest stiffness in the physical model in Figure, is coupled together. The remaining equivalent stiffness of the simplified model results from the chain of all springs:

$$k = \frac{1}{\frac{1}{k_{12}}+\frac{1}{k_{23}}+\frac{1}{k_{34}}}$$ Equation 3-65

Relative damping D_{ij} of the dominant flexibility k_{ij} defines the damping constant d of the simplified model:

$$d = 2.D_{ij}.\sqrt{m_2.k}$$ Equation 3-66

The spring force F_k depends on the relative position of the two remaining masses

$$F_k = k.(x_1 - x_2)$$ Equation 3-67

The damping force F_d depends on the relative velocity

$$F_d = d.(\frac{dx_1}{dt} - \frac{dx_2}{dt})$$ Equation 3-68

The above mathematical model is expressed in created SIMULINK model.

3.6.5 GUIDEWAYS AND SLIDES

Guideways or just guides are structural elements of machine tools which are used for guidance and positioning. In particular, they are sliding systems where two surfaces are in contact. One surface is the fixed known as the guide, while the other surface placed on the sliding component (carriage) is known as the counterguide. The guides, which are directly responsible for the smoothness and precision of the machine tool axis movements, can be divided into two basic types; the sliding type and the rolling type (Lopez de Lacalle & Lamikiz, 2009).

The classification of guideways presented on Figure 3-26 involves three main levels. The first level is based on the friction component, the second level is based on design configuration, and finally, the third level of classification is based on geometric configuration. Guideways with sliding friction are called slideways, which can be geometrically symmetrical, asymmetrical and open or closed concerning the design configuration. On the other hand, the rolling elements, either ball type or roller type, which are incorporated on guideways, compose anti-friction ways. The third level of anti-friction ways classification is defined by the exposure of rolling elements and circulation results. Frictionless guideways are considered to have no friction.

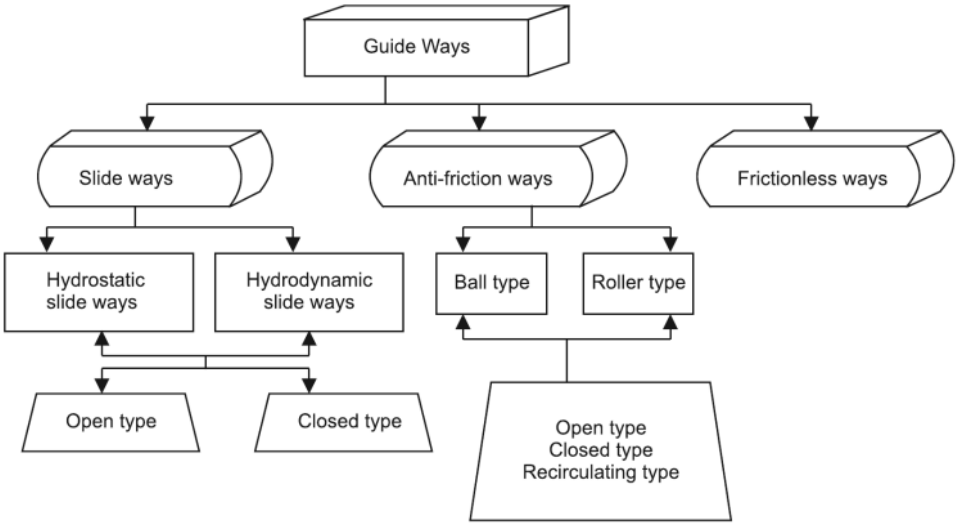

Figure 3-26 Classification of guideways

Forces acting on the carriage block of a guideway (Pislaru, 2014):

$$F_{gw} = F_{gw0} + \mu \cdot F_E + \mu \cdot v_l$$ Equation 3-69

$$F_E = X \cdot F_R + Y \cdot F_L$$ Equation 3-70

$$F_{gw} = F_0 + F_1$$ Equation 3-71

$$F_0 = F_{gw0} + \mu \cdot F_E$$ Equation 3-72

$$F_1 = \mu \cdot v_l$$ Equation 3-73

Where, F_{gw} is the force of friction, F_{gw0} is the frictional force under no-load, v_l is the velocity of the load, F_R is the radial load, F_L is the lateral load, F_E is the equivalent load, and X and Y are factors according to the design.

3.7 MODELLING OF NONLINEARIETIES

Computational modelling and analysis tools play a key role in high performance machining, and nowadays, they have become essential parts of engineering design especially for complex continuous dynamic systems, which incorporates nonlinearities, such as friction and backlash.

The accuracy of the model depends on the structure and parameters. Backalsh model has been simplified - an initial change in input has no effect on the output. The amount of side-to-side play - deadband is cantered about the output. Friction is categorized according to its pre-sliding and sliding regimes, and the simplest friction models consider only the sliding regime.

3.7.1 FRICTION IN MACHINE TOOLS AND MECHANISMS

Friction, by definition, refers to the resistance to motion during sliding of two opposing objects against one another. Friction is present almost everywhere and it brings benefit in various forms. Braking systems and clutches are two examples of friction effects that benefit us. However, friction is highly undesirable in most industrial and mechanical applications. Uncompensated friction force increases energy consumption and reduces efficiency of these processes.

The model proposed by Al-Bender and Horstein (2005) and used in this research work consists two main control modes. The first mode is dealing with the gross-sliding friction second mode of the controller is activated until the motion leaves the pre-sliding region again. Al-Bender (2005) developed Generalized Maxwell-slip (GMS) friction model and illustrate the superiority of the model with respect to simulation of friction behaviour in both the pre-sliding and sliding regimes. Its main advantage is that it contains a hysteresis function with non-local memory behaviour to describe the pre-sliding regime. The GMS friction model includes the following:

- the Stribeck curve for constant velocity,
- dependence of the friction force Ff on the velocity v = constant
- hysteresis function with non-local memory for the pre-sliding regime,
- frictional memory for the sliding regime.
- The friction force is constant and only depends on the direction of the velocity.
- The Coulomb friction models the dry friction case.

Stiction is minor in the model if the external force is known. The friction force simply counteracts the external force and precludes the object from moving. Static friction can usually reach higher magnitudes than dynamic friction and, naturally, it cannot be described as a function of velocity v. At some critical force value F_{static}, which is called breakaway force, the object starts to glide across the surface. If this happens, the friction force drops rapidly to a lower value and from then on has to be described in the context of dynamic friction. (Horstein (2005))

Combining static and dynamic leads to a multi-valued function:

$$F(\mathrm{f}) = \begin{cases} F_{static} = F_{\theta} \mathrm{if\ v} = 0 \\ F_{dynamic}(\mathrm{v}) = F_c * \mathrm{sign(v)} + F_{v\ else} \end{cases} \qquad \text{Equation 3-74}$$

All three functions are multi-valued in the region of static friction (v = 0m/s). Here the friction force is a function of the position rather than of velocity and cannot be properly displayed in the diagrams presended by Canudas et al. (1995). The dynamic behaviour of an elementary slip-block is described by a:

$$\frac{dF_i}{dt} = k_i \qquad \text{Equation 3-75}$$

ki spring model with stiffness

On the other hand, slipping occurs if the *Fi* equals a maximum value *Wi = αis(v),* of each element during sticking and. During slipping, equation describing the dynamic behaviour of the slip-block is represented on Figure 3-27 as

$$\frac{dF_i}{dt} = sign(v)C\left(\alpha_i - \frac{F_i}{s(v)}\right) \qquad \text{Equation 3-76}$$

αi is the normalized maximum friction force

s(*v*) is the Stribeck curve

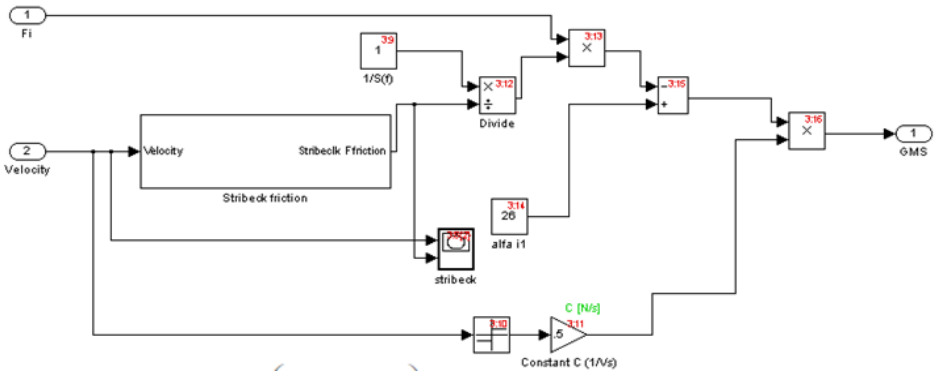

Figure 3-27 GMS friction SIMULINK model

The constant parameter *C* (equals to 1/*Vs*) in:

$$F_f(v) = \left\{F_c + (F_s - F_c)exp\left(-\left|\frac{v}{V_s}\right|^{\delta}\right) + \sigma|v|\right\} sign(v) \qquad \text{Equation 3-77}$$

In pre-sliding regime, friction is dominated by the displacement and behaves as a hysteretic function of displacement with non-local memory behaviour. This behaviour is characterized by the so-called virgin curve. The virgin curve is derived from a sinusoidal excitation of the system. The frequency and amplitude of the sinusoidal input signal are selected to minimize inertia effect and to remain in the pre-sliding regime. (Horstein (2005))

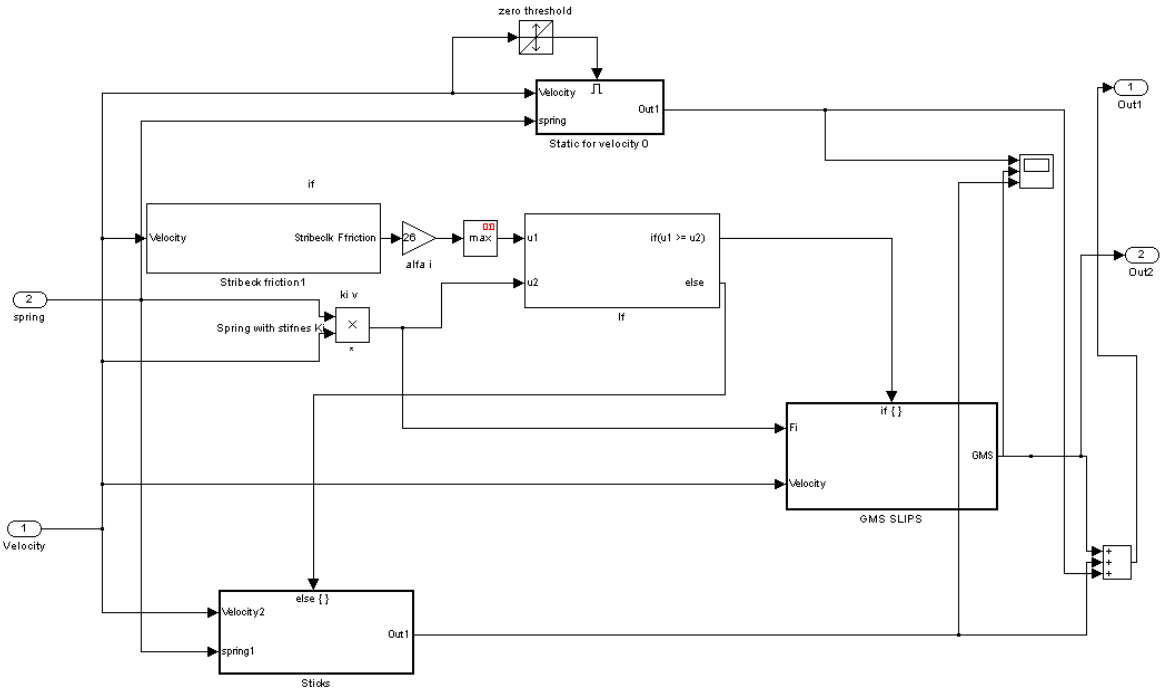

Figure 3-28 GMS Friction SIMULINK model

That indicates the rate at which the friction force follows the Stribeck effect in sliding. The ability to estimate the friction behaviour in pre-sliding regime is the superiority of GMS model, while it does not lose its ability to estimate the friction in the sliding regime. Therefore the GMS model can capture friction behaviour for any working range of displacement and velocity. Al-Bender (2005)

Simple experiment has been conducted by Horstein (2005). His model has been used in CNC feed drive model. It has been found that classical models like Coulomb friction and the Stribeck friction model give satisfactory results for accurate ballscrew system. However, at low displacements, which emphasize the pre-sliding regime, the classical models fail to give a satisfactory therefore it may be useful in future studies. AE features may be useful to investigate frictional parameters. The mayor disadvantage of the GMS model is complexity which complicates its application in real time analysis.

3.8 TRANSDUCERS

Geiss machines are compensated to a position accuracy of IT6 as per DIN 7151. Machining accuracy are achieved by utilising glass encoders and error compensation.

3.8.1 LINEAR ABSOLUTE ENCODER

The linear encoder implemented in Geiss machine is an absolute linear encoder manufactured by Heidenhain - model number LC 183 .The basic specifications are given in Appendix C. The LC183 absolute linear encoder is shown Figure 3-29.

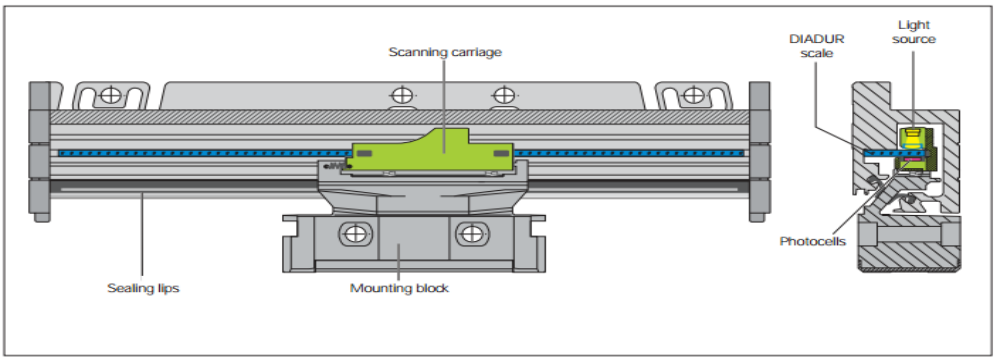

Figure 3-29 Absolute linear encoder (Heidenhain 2012)

The scale on the glass which is the scale of measurement. It includes of a specially coded pitch lines arranged in parallel. The Heidenhain LC 183 model uses an Image scanning standard. As the read head moves along the scale the light output obtained at the various read heads of the detector varies due to the presence of a coded substrate on the scale. For each position a unique value is acquired as the output. Different types of encoding may be used. J. R. Rene Mayer (2000) has elaborated some of them in the instrumentation and sensors handbook.

3.8.2 SIMULINK IMPLEMENTATION OF THE LINEAR ENCODER

The SIMULINK drawing illustrating the implementation of the linear encoder is given in the Figure 3-30.

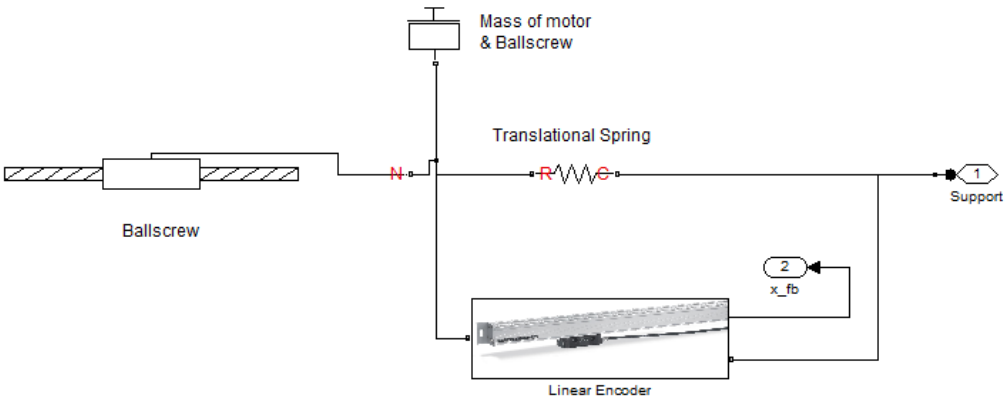

Figure 3-30 SIMULINK Implementation of the linear encoder

In order to measure the displacement of the Ideal translational motion sensor block (Linear Encoder) within SIMSCAPE is used. This block has two input ports Case and Rod. These ports are connected across an ideal spring like it's presented on Figure 3-31.

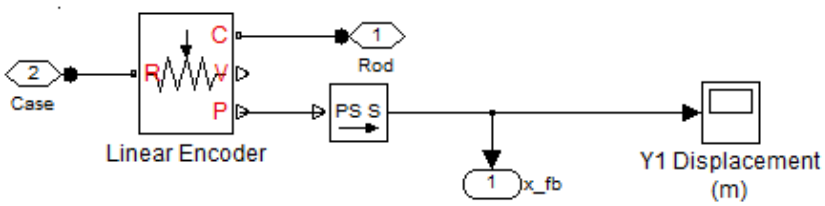

Figure 3-31 Detailed model of the linear encoder subsystem

Ideal mass block representing the mass of the ballscrew has been connected to an ideal spring. This spring has been given a value equivalent to the inverse of the acceleration due to gravity. The Case terminal is analogous to the negative terminal in electrical domain. The ideal translational motion sensor block can provide either an electrical signal or physical signal proportional to the displacement. The electrical signal can be obtained from port V and the physical signal is obtained from port P. The displacement of the ballscrew is the displacement of the gantry axis. The axis Y1 is treated as a master axis and this signal is fed back to the position controllers of both master and slave axis. Since the displacement obtained is still a physical quantity it is transformed back into a SIMULINK signal by using the PS-SIMULINK Converter block. The transformed signal is then fed back to the position controller.

3.8.3 ROTARY INCREMENTAL ENCODER

The rotary encoder used in the Geiss machine is an incremental encoder. This is an incremental encoder and makes use of mounted stator coupling. This encoder module is attached to the back of the SIEMENS 1FK7 motor. This instrument works on the image scanning principle similar to linear LC183 explained in the earlier section. Instead of absolute encoding it uses incremental encoding.

The Figure 3-32 illustrates a simple Incremental encoder. This encoder has a single track with slots. The slots are spaced apart by a degree. During one revolution of the disc light pulses are detected by the receiver.

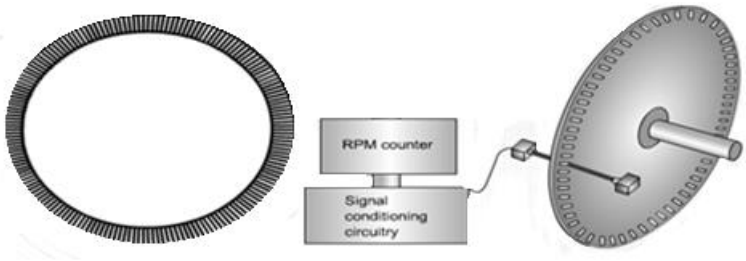

Figure 3-32 Encoder operation (Wisc-online 2013)

A solution is discussed in the online resources for rotary encoders in Wisc-online (2013). To overcome the problem another track is added to the encoder. As the disc rotates two set of pulses or square waves are obtained which are shifted in phase by 90 degrees. Received pules are leading in phase depending on whether the rotation is in the anticlockwise direction or reverse respectively. J. R. Rene Mayer (2000) illustrates a simple logic circuit to compute rotary position in her paper.

3.8.4 SIMULINK IMPLEMENTATION OF THE ROTARY ENCODER

This is very similar to the linear encoder model discussed before. The SIMULINK detailed drawing of the rotary encoder is shown on Figure 3-33.

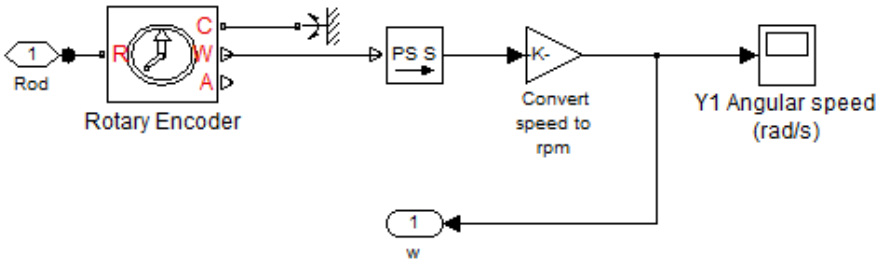

Figure 3-33 Detailed model of the rotary encoder

The only difference is that Ideal Rotational Motion Sensor to measure the speed of the motor. The angular speed is a physical signal and therefore is transformed into a SIMULINK signal using a PS-SIMULINK Converter block. This signal is then fed back to the speed controller.

3.9 CONCLUSION

Machine tools are main parts of whole manufacturing systems. The rapid advances in technology makes modelling more challenging mission than ever before. Maintenance personnel rely on

machine information, their past breakdowns as well as new research results in the area. They get access to information about the system by using nondestructive testing (NDT) or condition monitoring. CNC machine tools is complex mechatronic systems which incorporates non-linarites, therefore mechatronic modelling, which considers the coupling of mechanical structure and control system can be achieved by coupling a mechanic simulation with software (as in the present work) or by using only one simulation environment for a complete mechatronic simulation has been proved of great importance due to successful results. To be able to use a reference model approach for condition monitoring of a machine tool, it is important to understand not only the mechanical factors, but also the control elements which affect them. The responses of the system to deterministic inputs under profile following conditions are presented. It is important to use accurate modelling techniques to achieve model tool which can be used in Industry 4.0 to estimate remaining useful life.

When building the models level of the representation which reproduces the studied system fidelity needs to be considered. Exact replica and high level of accuracy of studied physical system can increase the cost to compute and build the model. Elements of the system are described as direct as possible. Simulation models of all described elements has been validated and verified. Simulink libraries and simplified equations presented in Chapter 3 has been used to achieve good accuracy with efficient computing power so the model can be easily implemented in real time system in model. The simulated machine tool system is presented in Chapter 4.

Application of a simple identification procedure for the Generalized Maxwell-slip (GMS) of the friction model that may produce superior friction compensation performance, especially at lower tracking velocity has been presented. The models are provided with all governing equations, parameter values and necessary conditions.

By modelling it’s possible to chart the system behaviour so costly complex testing scenario can be easily simulated. This is the primary reason for implementing the SIL in this type of machine tool. Results simulated results from the Simulink model and measured data are compared. This gives an insight into the nature of controller required and possibilities of fine tuning. Finally model can be applied to target hardware for performing diagnostic tests and simulation.

CHAPTER 4 DEVELOPMENT OF NOVEL MULTI-BODY MECHATRONIC MODEL FOR FIVE-AXIS CNC MACHINE TOOL

Current trends in mechanical engineering show the growing importance of costs for machine tool life cycles. The producers of machine tools need to pay more attention to their products' life cycle because the customers increasingly focus on machine tool reliability and costs.

Model can be used to dynamically identify the current status and predicts disruption of the desired performance. It's a cost-efficient method to create state-of-the-art condition monitoring (CM) system. The models should match the machine's physical components.

The other future goals in manufacturing engineering represent the design and realization of intelligent factories. Multi-body mechatronic model can be used to the design of machines, which are inherently more reliable and should degrade in predictable ways. The detailed CAD model for the GEISS machine in SolidWorks and development of MBS simulation model containing Matlab package blocks fulfils the main purpose of this work and contributes to modern machine tool industry making possible the performance evaluation of machine tools and the production of even more accurate products with lower costs and time, simultaneously.

Testing single axis avoids the coupling problems. Models are executed for rotational and translational axes. Whatever the axis, all the tests lead to similar results. Simulated data is close to the one measured by servo trace.

4.1 MODELLING OF ROTATIONAL AXIS FOR GEISS MACHINE

The results of the analysis of the operation of actual Computer Numerical Control (CNC) five-axis machine and the derivation of the mathematical equations describing the dynamic behaviour of machine will be presented. Implementation of C-axis drive model in SIMULINK and the simulated results are compared with the measured data. **Error! Reference source not found.** shows the main elements of the C-axis drive: position setpoint generator; position controller; speed controller; current (direct torque) controller; 3-phase inverter; induction motor with rotary encoder which generates a feedback signal proportional with the rotor speed. The angular position is obtained by integrating the speed values.

4.1.1 IMPLEMENTATION OF C-AXIS DRIVE MODEL IN SIMULINK

Accurate identification of the feed drives dynamics is an important step in designing a high performance CNC machine which is a mechatronic system (consisting of mechanical and electronic components and software).

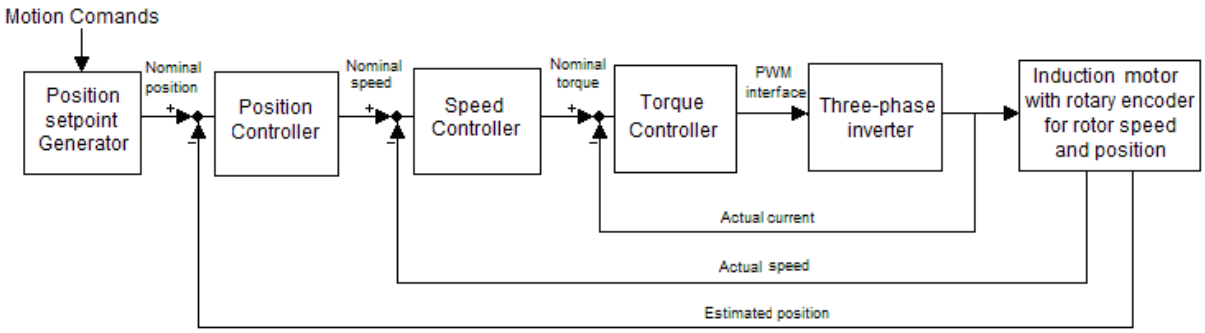

Figure 4-1 Block diagram representing C-axis drive

The input signals for 'Position Controller' block are nominal angular position and actual position from the motor. This block generates the nominal speed (SP) which is fed to 'Speed Controller' block together with actual motor speed (N) from the rotary encoder and the magnetic compensation constant (MagC). The 'Speed Controller' produces the values for flux and torque which is included in DTC (Direct Torque Controller) together with three-phase voltage V_abc and current I_abc. DTC block generates the command signals for the thyristors gates from the 'Three-phase inverter'. The induction machine receives the electrical energy from the three-phase power supply, diode rectifier, braking chopper and PWM inverter. The block 'Voltage Current Conversion' transforms the torque values into electrical current values. The 'Induction Machine' block produces the values for the rotor angular position, armature currents, rotor speed.

A rotational axis drive consists of six major elements; position setpoint generator, position controller, speed controller, direct torque or current controller, three-phase inverter, and motor with rotary encoder. The rotational *B* and *C* axes from the GEISS CNC machine tool contain direct drives. In this type of drive only one rotary encoder attached to the motor is used both for rotor speed and rotor angle. In comparison to standard servo-controllers which need one encoder for position measurement, and one encoder for velocity measurement. The feed drive models for the B-axis and C-axis are depicted in the following Figure 4-3. The SIMULINK blocks which compose a CNC machine tool rotational axis drive are a three-phase source *'400V 50Hz'*, a three-phase diode rectifier *'Rectifier_3ph'*, a *'Braking chopper'*, a *'Three-phase inverter'*, a *'Permanent Magnet Synchronous Machine'*, a *'Position controller'*, a *'Speed controller'*, and a vector controller *'VECT'*.

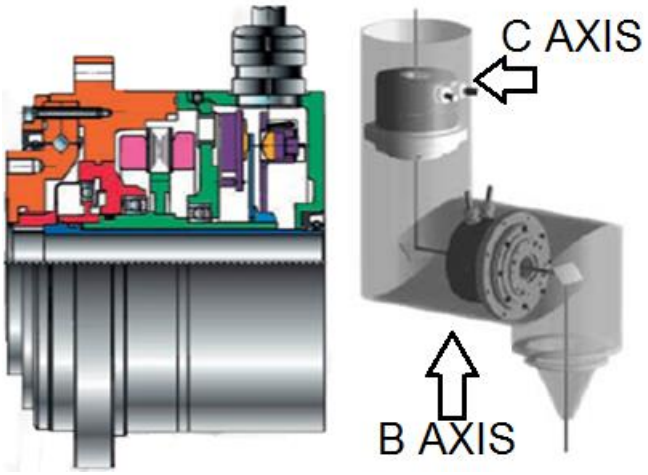

Figure 4-2 B and C axis drive

There is little difference between the *B*-axis and *C*-axis drive apart from planetary gearbox and data for the parameters of various elements that have been determined according to their corresponding datasheets and specified in each block's dialog box. Data for the parameters, which have been specified in each block's dialog box, is presented in the Appendix C. From the following figures, it can be noticed that, the C-axis drive is similar to B-axis drive. Data is presented only for the PMSM block of C-axis, because the parameters of other blocks are similar to those of B-axis.

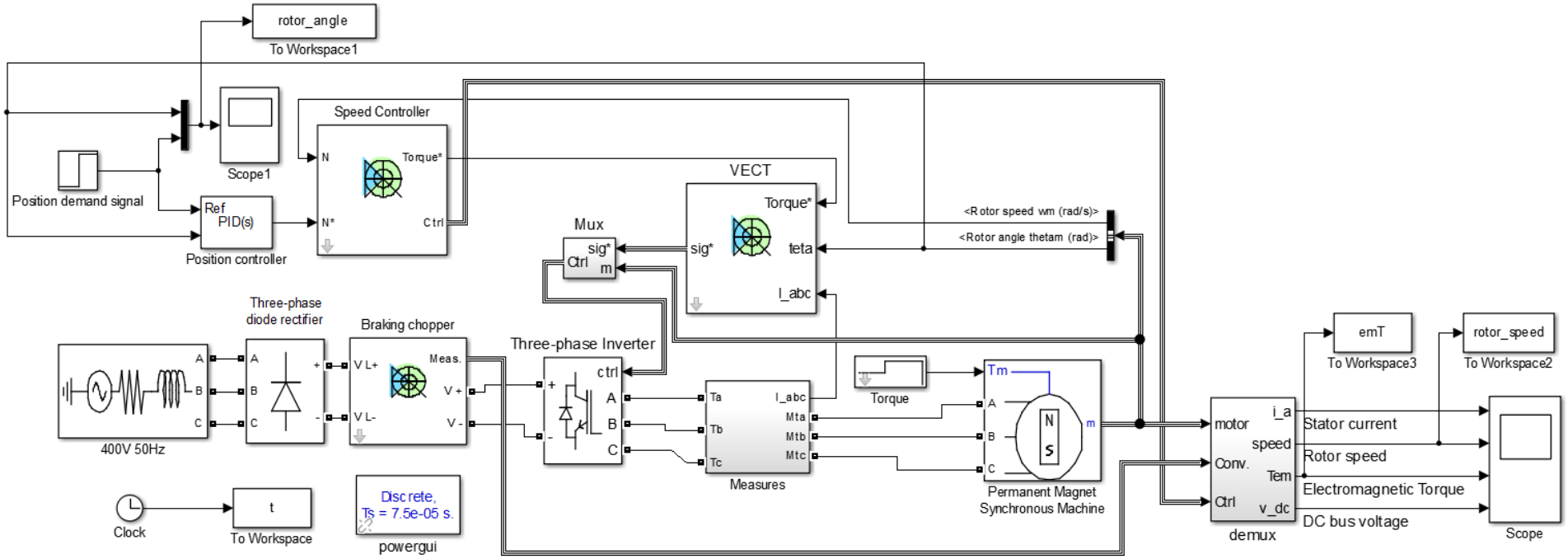

Figure 4-3 SIMULINK model for B or C axis

The speed controller is based on a PI regulator which generates a torque set point applied to the direct torque controller (DTC) estimates the motor flux components and the electromagnetic torque. The SIMULINK implementation uses the blocks from SimPowerSystems library. The power supply adjusts the AC input voltage to the intermediate circuit voltage. One intermediate circuit supplies several axis power modules, which makes possible the storage of braking energy and energy exchange between different axis operations. Braking chopper is used to absorb the energy produced by a motor deceleration. A, B, C are the three phase terminals of the drive.

Figure 4-4 shows the simulated angular position produced by the block 'Induction machine' from the SIMULINK implementation. A triangular signal was applied as a demand to the 'Position Controller' block and the model simulates the rotor angular position. The values for the demand signal were chosen in accordance with the measured data from the five-axis machine.

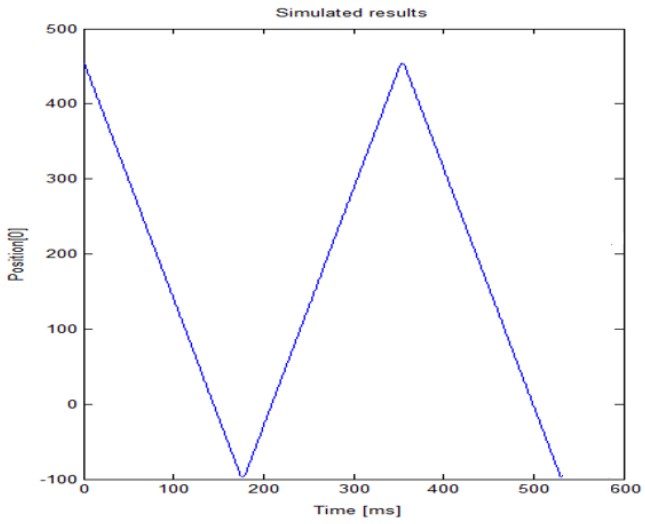

Figure 4-4 Simulated results obtained using SIMULINK model.

4.1.2 COMPARISON BETWEEN SIMULATED AND MEASURED RESULTS

The servo trace built-in function of the SINUMERIK 840D SL controller is used to measure the data from the actual five-axis machine. Manual commands are applied to achieve rapid traverse movements of the C-axis. Output signals are provided via rotary encoder mounted on the motor. Appendix H shows the steps used to obtain servo trace data. The approach behaviour at various speeds has been checked using the Human Machine Interface (HMI) servo trace software. The measured values for the angular position of the actual servomotor are presented on Figure 4-5.

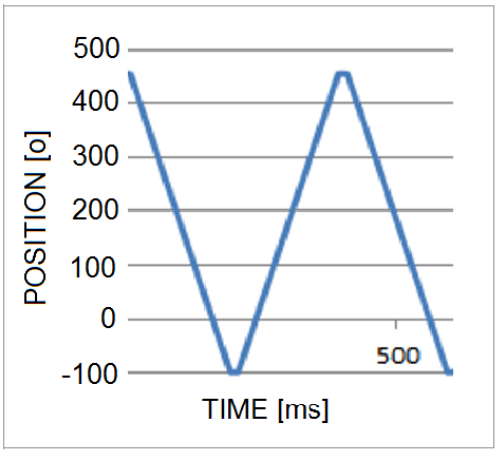

Figure 4-5 Measured rotor angular position using ServoTrace tool

The simulated results Figure 4-4 compares well with the measured data from the actual machine servo-trace system Figure 4-5. This represents the first step in developing a full model of the five-axis machine.

4.2 TRANSLATION AXES

A translation axis is categorized into two main parts, and more specifically, the control or electrical part, which has been already described in the previous section, and the mechanical including the mechanical transmission system which converts the rotary motion of the motor into linear motion of the nut using the ballscrew assembly driven by the belt drive system. The rotary encoder is used only for rotor speed. The feed drive receives feedback signals produced by the linear encoder (mounted on the slide) which directly measures the actual position of the machine tool, and by the attached rotary encoder which provides the rotor speed. The following Figure 4-6 depicts the realistic block diagram representing the principle of operation of translation axes.

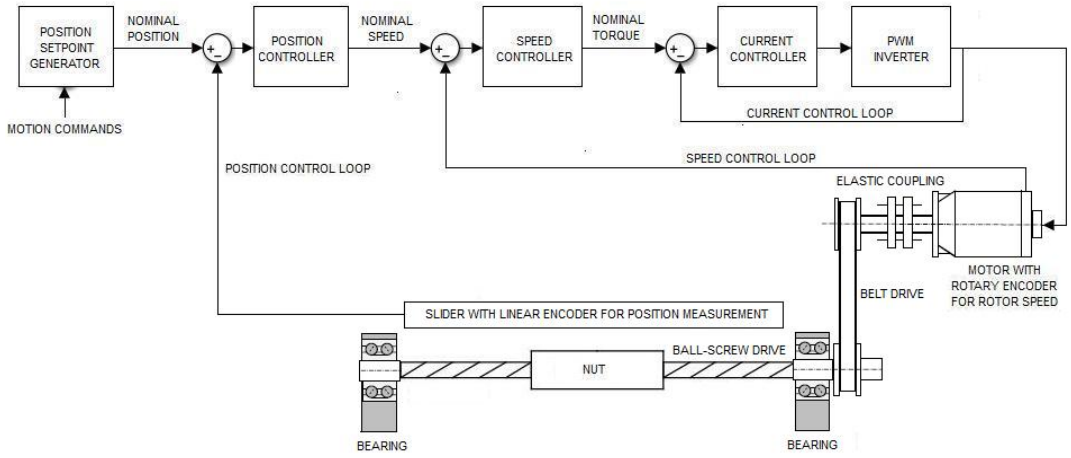

Figure 4-6 Realistic block diagram representing the translation axes

Accurate machine tool feed drive models have to contain values for the various damping coefficients and non-linarites such as, backlash and Coulomb friction. In high precision machining, friction between the moving components may cause serious errors. In most cases, the largest portion of friction, which is produced due to complex kinematics of the ball nut, is undesirable because it causes the errors. Though sometimes it might be desirable, because it offers damping (Widiyarto et al., 2005).

Finally, for convenient control of large mechanisms such as gantry robots, two motors may be required to drive a single axis. This split-axis option has also been adopted by the studied CNC machine tool for the gantry drive (Y-axis). The split-axis feature realizes control of such configurations transparent to the application software, due to the fact that, it automatically coordinates the drive of the two motors. In order to keep the mechanism aligned, the commands, which are sent to the motors, are coordinated. Regarding the point of view of the application, there is no difference between a single-motor axis and a dual-motor axis.

4.3 MODELLING OF GANTRY AXIS FOR GEISS MACHINE

SIMULINK model was designed to control a motor to generate the angular speed signal. For the gantry axis under discussion the motor is coupled to the ballscrew through a toothed timing belt. The ballscrew employed is a driven nut ballscrew. This essentially means that the rod or shaft is fixed and the nut rotates and moves along the shaft. Figure 4-7 is an illustration of the physical model of the gantry axis.

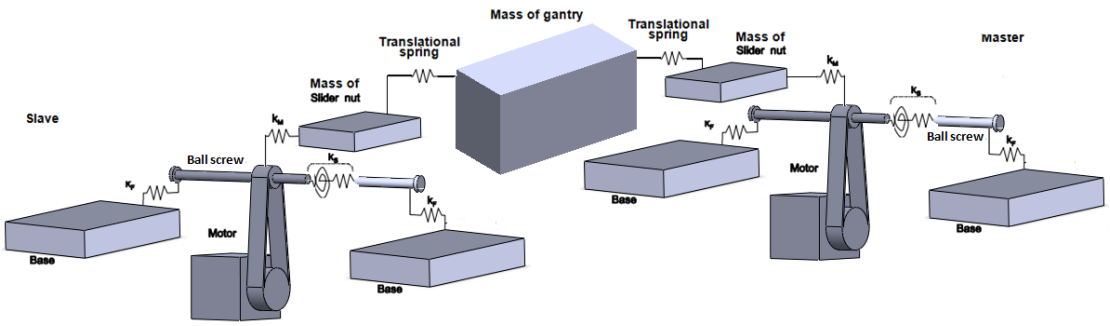

Figure 4-7 Mechanical model of the gantry axis

Notice that the shafts of the ballscrew are attached to a fixed based and not coupled to the motor as in the traditional model. The motor is coupled to the nut through a timing belt having a gear ratio of 1:1.5. The link between the motor & the nut through the timing belt generates the rotation of the nut (The screw is fixed).The rectangular prism adjacent to the nut symbolizes the mass of the nut. Both the nuts together drive the mass of the spindle along the y axis. Therefore it is represented as a mass of the gantry connected to the mass of nut on either side with a translational spring in between.

Gantry axes are mechanically grouped two machine axes. The position set points are inputted synchronously to both axis controllers. Due to several input variables, the gantry axis is less sensitive to machine parameter variations than is for a single drive. Modelling of gantry axis for GEISS CNC trimming machine should be accurate enough to represent all important influences, but at the same time some certain restrictions which exist under real working conditions will lead to a simplified system, that represent the direct effect of structures and transmission devices on the servo drive control.

SIMULINK block diagrams represent an insightful object orientated programming language so CNC gantry model will be developed in there. The difference between the actual positions of the drive and model will be monitored continuously.

4.4 CONTROLLER DRIVE MODEL – SINUMERIK 840D SL &SINAMICS S120

In this section the actual configuration of SINUMERIK 840d SL controller and SINAMICS S120 drives is described. As mentioned earlier this composite system enables motion control in the GEISS machine. The figure in the next page illustrates the entire graph of SINUMERIK and SINAMICS modules, how they are connected together to perform control on GANTRY axis. As observed at the heart of the system is the SINUMERIK 840d SL numeric control unit NCU730.3 module. This is the numerical controller that computes all the relevant control signals. The port numbers shown have a prefix of character X. This signifies a DRIVE CLiQ connection. The gantry is composed of Y1 and Y2 axis. They both have one 1FK7 motor each. Each of these motors is driven by a motor module. The motor modules and the NCU controller are both powered by the Active line module. The NCU perform the position control, speed control and current control and finally at the end of the cascaded control operations it generates the direct and quadrature voltages and passes them on to the Motor modules. The motor module is comprised of inverter. They generate the pulse with modulation (PWM) signals and control the motor in essence. Apart from driving the motor, it also performs acquisition activities collecting the encoder signals and the three phase voltage signals feeding it back to the NCU which operates on these signals and the respective set points to compute the error signals. The motor module gives angular position, speed and three phase voltage information to the NCU. But for the NCU to perform its position control activities it needs the linear position signals. This is provided by the Heidenhain LC 183 position encoder. Since this is an external encoder to communicate with the NCU it needs a middle man. Sensor module external (SME) serves this purpose. NCU has a limitation on the number of devices it can control. The NCU is connected to the HMI unit using Ethernet connectivity so the user can input the position and speed set points and perform diagnostic and trace operations.

4.4.1 AXIS POSITION CONTROL LOOP

The controller for an axis consists of the speed control loop, the current control loop and a position control loop like its presented on Figure 4-8

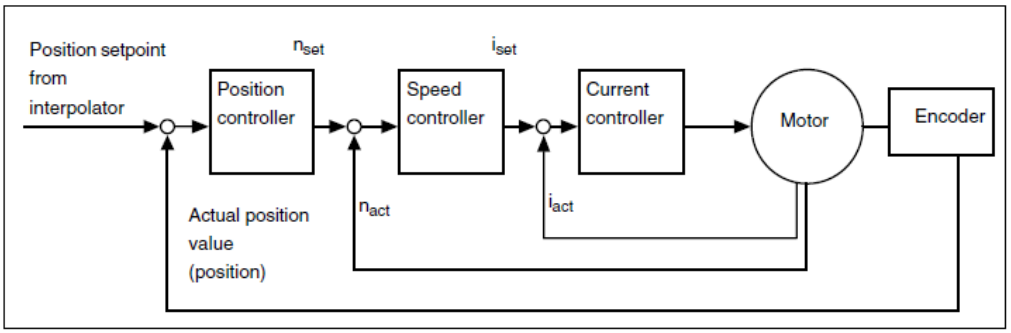

Fig. 6-15 Control loops

Figure 4-8 Siemens system control loops (Siemens 2012)

In order to obtain high contour accuracy with an interpolation, the loop gain factor (K_V factor) of the position controller must be large. If the K_V factor is too high, on the other hand, this leads to overshooting, instability and inadmissibly high loading of the machine. The maximum permissible KV factor is dependent on the design and dynamic response of the drive and the mechanical quality of the machine. (Siemens 2012)

Figure 4-9 shows a simplified model of the position control loop and a velocity control loop. The velocity control loop is represented by a first-order transfer function block (Zirn 2005) with the time constant:

$$T_v = \begin{cases} \frac{1}{k} & for\ indirect\ measurement \\ \frac{k+\omega_0}{k\omega_0} & for\ direct\ measurement \end{cases}$$ Equation 4-1

depending on the position capture location, the additional delay due to the flexibility between motor inertia and load can be assessed by the predominant resonant angular frequency ω_0.

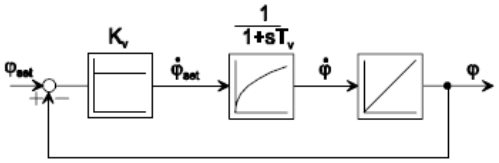

Figure 4-9 Simplified model of the position control loop (Zirn 2005)

The transfer function of the simplified position control loop is given by

$$G_x(s) = \frac{K_v}{T_v s^2 + s + K_v}$$ Equation 4-2

The position control gain is given by:

$$K_v \leq \frac{1}{4T_v} = \begin{cases} \frac{k}{4} & for\ indirect\ measurement \\ \frac{k\omega_0}{4(k+\omega_0)} & for\ direct\ measurement \end{cases}$$ Equation 4-3

Equation defines the maximum position control gain for one axis. A machine tool requires identical position control gains in all axes to eliminate the static path error. Thus the maximum position control gain has to conform to the “weakest” axis.

The loop gain is converted using the following formula:

$$K_v(e^{-1}) = K_v \frac{[m/min]}{mm} 16.6667$$ Equation 4-4

4.4.2 VELOCITY CONTROL LOOP

The velocity controller is responsible for damping (proportional gain K_p) and eliminating (integrator time constant T_n) static loads. The typical commissioning procedure is firstly to tune the proportional gain and afterwards to decrease the integrator time constant until a well damped control performance is reached. The drive frequency response contains redundant information. Due to the logarithmic scale, uncertainties concerning the current converter scaling factors and the noise in real measurements, the frequency response gain yields only a rough estimation for complete inertia θ and inertia ratio λ. As motor inertia $\lambda\theta$ is generally known with sufficient precision from the machine tool design, the inertia ratio can be computed using resonance frequency ω_0 and resonance frequency ω_N, which as a rule are clearly identifiable in the frequency response:

$$\lambda = \left(\frac{\omega_N}{\omega_0}\right)^2 = \left(\frac{f_N}{f_0}\right)^2$$ Equation 4-5

The closed velocity control loop transfer function is:

$$G_v(s) = \frac{K_p G(s)}{1+K_p G(s)} = \frac{\frac{\kappa}{\lambda}s^2+{\omega_0}^2\kappa}{s^3\frac{\kappa}{\lambda}s^2+{\omega_0}^2 s+{\omega_0}^2\kappa}$$ Equation 4-6

With the scaled proportional gain:

$$\kappa = \frac{\kappa_p}{\theta}$$ Equation 4-7

The small material damping in the structure is mostly negligible (damping constant $d \cong 0$) compared to the damping introduced by the feedback control loop. The root locus of the velocity control loop shows one pole on the negative real axis, which defines the set point response. The conjugated complex pole pair defines the vibration and damping performance. At first, increasing κ leads to an improved damping performance and a faster set point response. Overdrawing κ changes damping for the worse. Thus the commissioning criterion for κ is optimum vibration damping.

4.5 SIMULINK MODELS FOR X, Y, AND Z TRANSLATION AXES

As already mentioned in the second chapter for the translation axes, a translation axis is divided into the control or electrical part and the mechanical part. The control part has been already built and described in detail in the previous section building the SIMULINK models for the rotational axes. In this section, the mechanical part including the mechanical transmission system, which converts the rotary motion of the motor into linear motion of the of the nut using the ballscrew assembly driven by the belt drive system, will be built in SIMULINK and described in detail, as well.

The main block which form the mechanical part of CNC machine tool translation axes are the: Belt drive or belt and pulley (gear box), Ballscrew, Inertia, Mass and translational spring.

The five-axis CNC machine tool linear axes are modelled element by element for achieving a realistic to represent the actual dynamics of machine tool feed drives. X, Y Z models are presented on following Figure 4-10 and Figure 4-11 to simulate the motion of translational SIMULINK blocks.

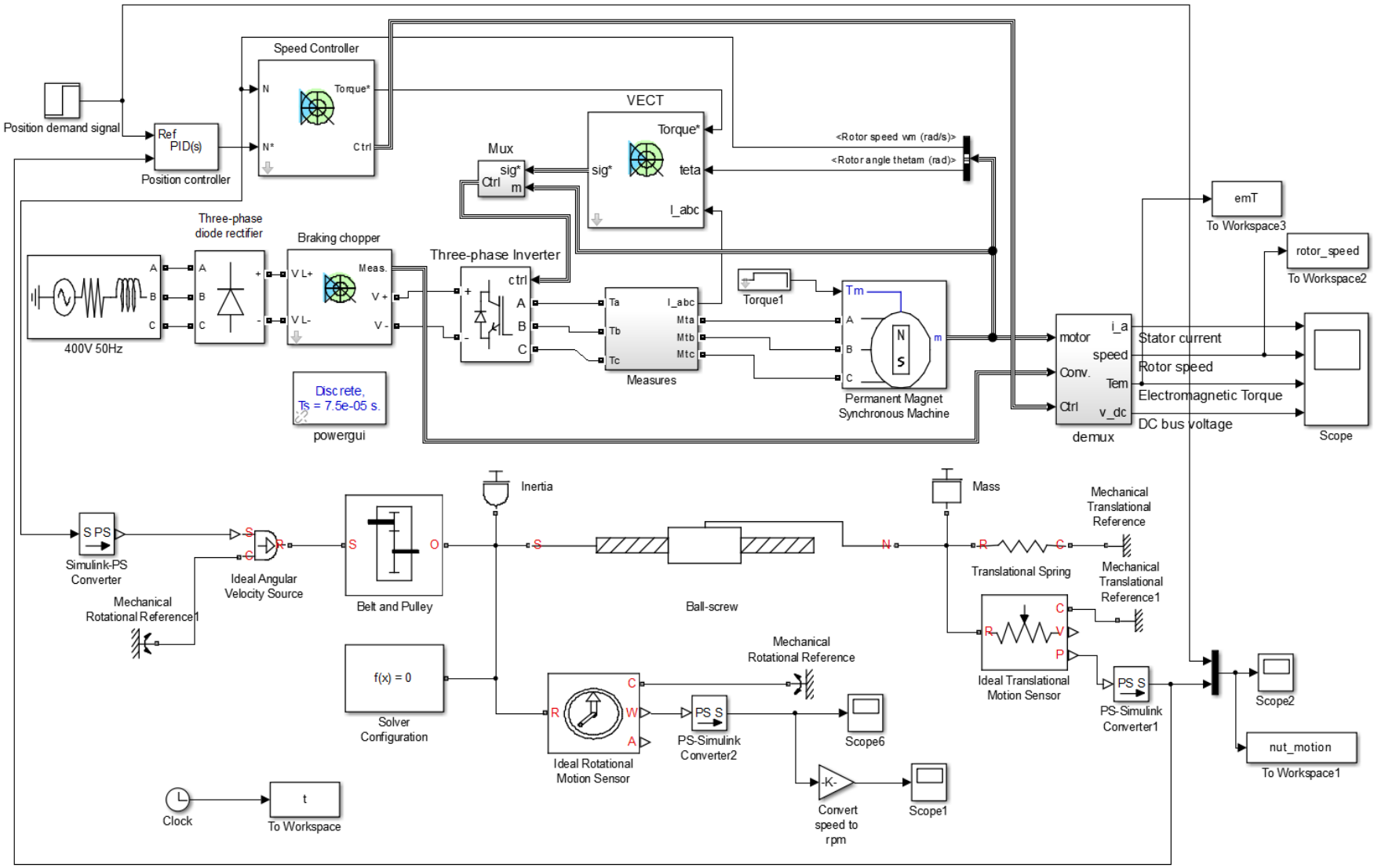

Figure 4-10 SIMULINK model for X and Z axis

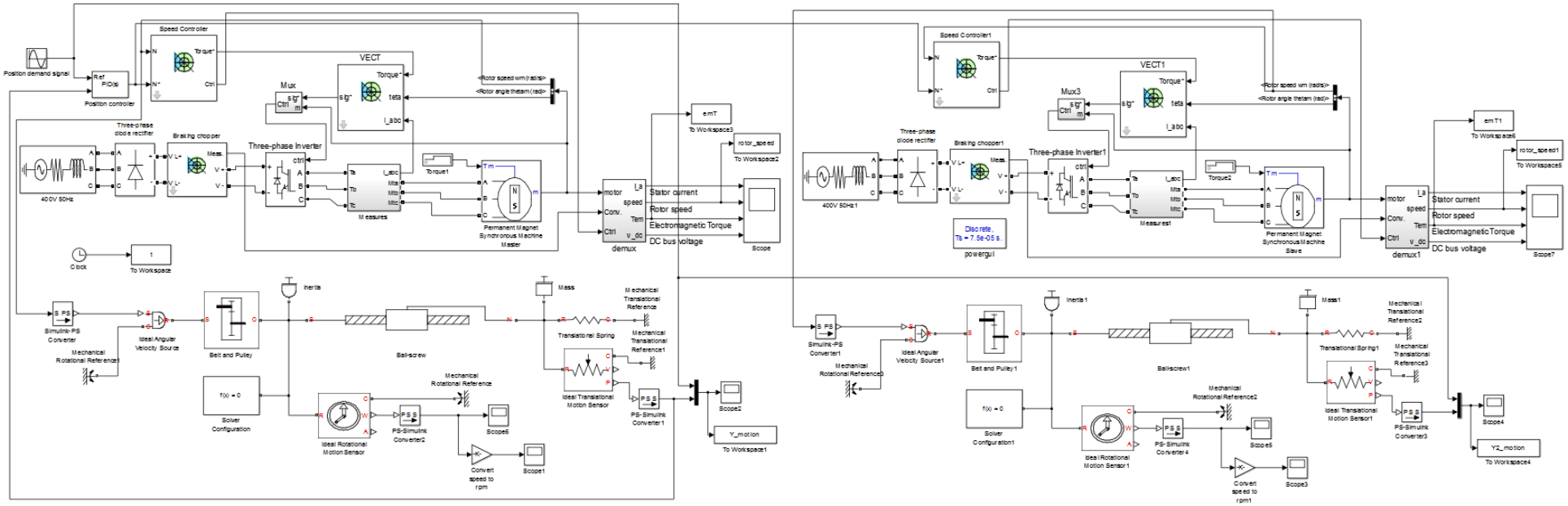

Figure 4-11 SIMULINK model for Y-axis

4.6 LINKING FEED DRIVE MODELS WITH STRUCTURAL MODELS FOR CNC MACHINE TOOLS

The model is implemented in SIMULINK using the technical details of the practical machine components so the simulated results represent the machine dynamic behaviour. Also the feed drives models are tested for variable load torques which occurs in the cutting processes. The 3D assembly of the CNC machine tool is built in SolidWorks and imported into SimMechanics.

Multi-body simulation environment for three-dimensional mechanical systems offered by MathWorks provides a number of benefits. It is possible to define bodies in terms of their mass, inertia, and connection points and import into SimMechanics models from CAD systems including mass, inertia, joint, constraint, and three-dimensional geometry. A multi-body system can be modelled with ease, and then SimMechanics formulates and solves the equations of motion for the complete mechanical system. The system dynamics can be visualized by the automatically generated three dimensional animation. The development of models to other simulation environments including Hardware-In-the-Loop (HIL) systems is also supported by C-code generation with SIMULINK Coder. Finally, it is possible to create libraries of components that can be reused in various different designs (MathWorks, 2014).

4.6.1 MULTIBODY SYSTEM SIMULATION APPROACH (MSSA)

The multi-body systems consist of interconnected rigid (inflexible) and flexible (deformable, elastic) bodies which undergo large relative translational and rotational displacements. Various physical and mechanical systems can be modelled as multi-body systems such as, machines, mechanisms, industrial machinery, robotic manipulators, trains, automobiles and trucks, space structures, satellites, etc. Mathematically speaking, on the one hand, systems of ordinary differential equations are used to describe the dynamics of interconnected rigid bodies (the concepts of rigid body mechanics). On the other hand, systems of partial differential equations are used for the description of the dynamics of interconnected elastic bodies (the concepts of continuum mechanics) (Janschek, 2012). The connecting elements can be modelled as classical force elements such as spring-dampers. However, the connections can be also realized by kinematical constraints such as joints. In most cases, the dynamic equations of motion of multi-body systems cannot be solved analytically, due to the fact that, these equations are highly nonlinear. Because of this, the numerical solution of the resulting dynamic equations, which govern the motion of multi-body systems, is used.

4.6.2 SOLIDWORKS

SolidWorks is a solid modelling CAD software which is produced by Dassault Systèmes SolidWorks Corp. It delivers robust three-dimensional design capabilities and performance. Fully detailed and

sophisticated parts, assemblies can be created quickly and efficiently. In addition, the tools which are required to produce complex surfaces can be accessed. It also includes wizards in order to automate designs, implement stress analysis, and define the environmental impact of components (SolidWorks).

4.6.3 3D ASSEMBLY MODEL IN SOLIDWORKS

The 3D assembly model for the machine tool Figure 4-12 has been built in SolidWorks. Advanced mates have been used to limit the maximum travel of translation axes in relation to the measurements, which have been taken moving the machine tool manually via the controller keyboard. The maximum travel for the X-axis is 2450mm, for the Y-axis is 1502mm, and for the Z-axis is 700mm.

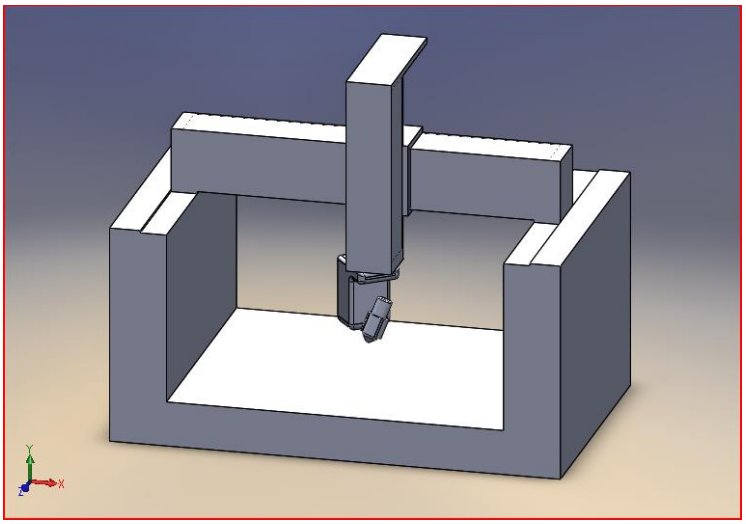

Figure 4-12 Five-axis CNC machine tool in SolidWorks

The export procedure of the machine tool 3D assembly from SolidWorks

The SimMechanics link in SolidWorks software is used to export the 3D assembly of the machine tool. The export procedure (SimMechanics link) generates one XML file which contains the structure of the assembly and the parameters that define each part, and a set of STL files which provide the visualization and specify the 3-D surface geometry of each CAD part. SimMechanics uses the structure and parameters to automatically generate a new SimMechanics first or second generation model during CAD import. The STL files are not required to generate the model, but they are required for visualization of CAD assembly. After opening the 3D assembly of machine tool in SolidWorks installation, the assembly is exported in SimMechanics first-generation format. The file has to be saved in a convenient folder, because this folder will be selected to import the machine tool assembly model into SimMechanics.

4.7 SIMMECHANICS MODEL

SimMechanics™ provides a multi-body simulation environment for mechanical system, formulates and solves the equations of the blocks representing bodies, joints, constraints motion. Models from CAD system are imported into SimMechanics. 3D animation visualizes the system dynamics. Once the export procedure has been completed, the 3D assembly of the machine tool is imported into SimMechanics using the following process:

The SimMechanics first generation model of the machine tool has been created as shown in the Figure 4-13.

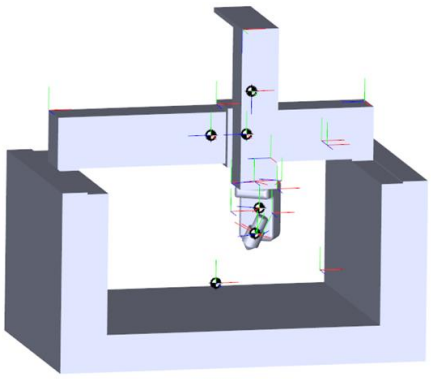

Figure 4-13 Five-axis CNC machine tool in SimMechanics

An imported model containing no STL files can be simulated, but the explorer visualization utility is unable to display a representation of the CAD model without STL files. Furthermore, if the 3D assembly of the GEISS machine tool had been exported from SolidWorks using SimMechanics link second generation. The following command would have been used to import the 3D assembly of the machine tool in to SimMechanics second generation format.

4.7.1 THE MODIFICATION OF THE MODEL TO FIT THE NEEDS OF THE GEISS CNC MACHINE

However, the SimMechanics model requires some modifications in order to fit the needs of the GEISS CNC machine tool as shown in the Figure 4-14.

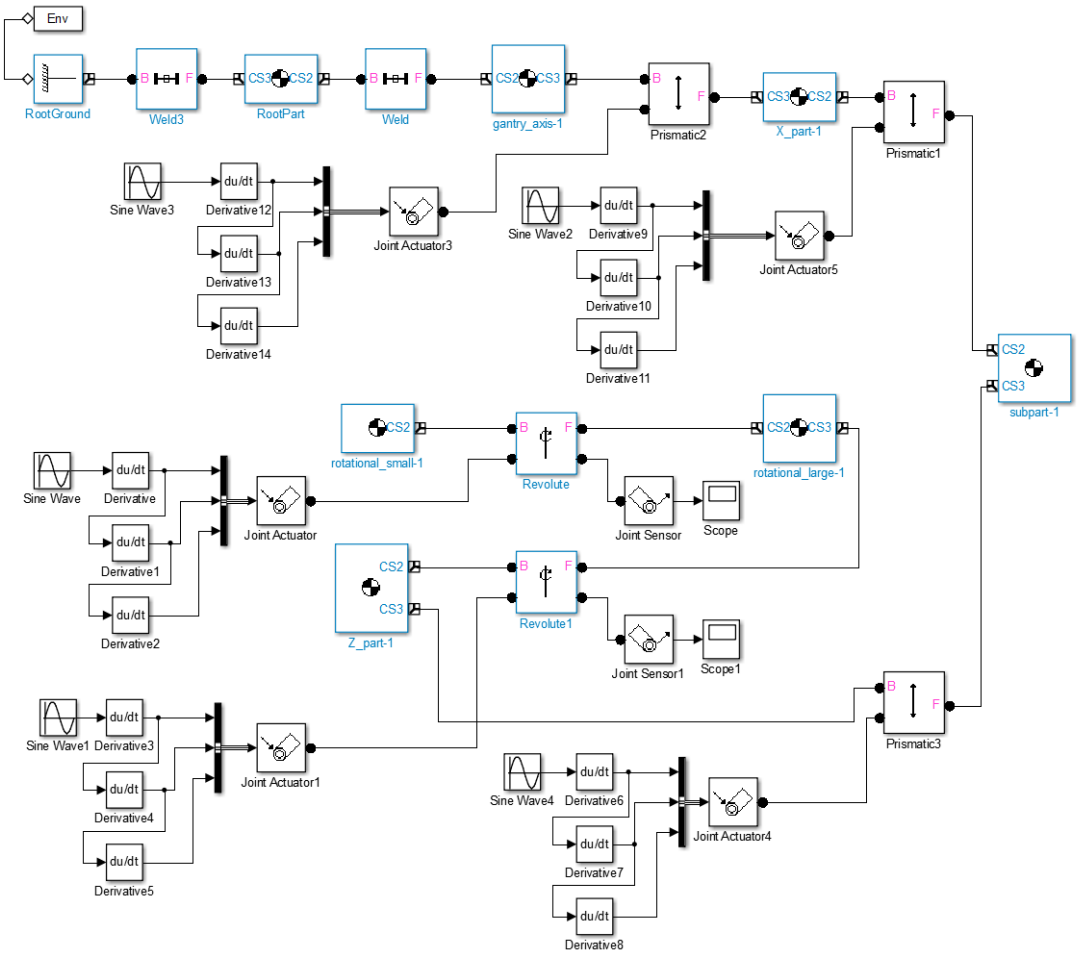

Figure 4-14 Modified SimMechanics first generation model of the machine tool

The SimMechanics model of the GEISS machine tool shown on Figure 4-14 consists of Machine environment (Env), Ground (RootGround), Weld, Body, Prismatic Revolute and Joint actuator blocks. The machine environment block defines the mechanical simulation environment for the machine to which the block is connected; gravity, dimensionality, analysis mode, constraint solver type, tolerances, linearization, and visualization. Due to the fact that, a SimMechanics model may consist of one or more machines, the mechanical environment settings is viewed and changed through the machine environment block for one machine in the model. A CNC machine is considered as a complete, connected diagram of SimMechanics blocks. In addition, each machine requires one or more ground blocks and can be a composite of submachines connected by shared environment blocks. The SimMechanics model is valid, when exactly one ground per machine is connected to a machine environment block.

The machine environment block is responsible for the simulation of the machine, the interpretation of mechanical constraints, and the linearization of simulation. The ground block represents a ground point. As a result, its connection with a joint prevents one side of that joint from moving. The weld block represents a joint with zero degrees of freedom (DoF). As a result, the two bodies, which are connected to either side of this block, are locked rigidly to one another, with no possible relative motion. The prismatic block represents one translational DoF along a specified axis between two bodies. The joint actuator block actuates a joint primitive with generalized force/torque or linear/angular position, velocity, and acceleration motion signals (MathWorks, 2013).

4.8 MECHATRONIC HYBRID MODEL FOR THE FIVE-AXIS CNC MACHINE TOOL USING MBS SIMULATION APPROACH

The complete mechatronic hybrid model based on Multi body (MBS) simulation approach is accomplished by combining the SIMULINK feed drive models with the SimMechanics model. SimMechanics does not recognize the advanced mates, which have been used to limit the maximum travel of translation axes in SolidWorks. For this reason, saturation blocks can be added to limit the input signal of joint actuator to the upper and lower saturation values. SimMechanics model has been developed which also can take into account the maximum travel of translation axes. Figure 4-15 includes this model which combines gain blocks and sine wave functions.

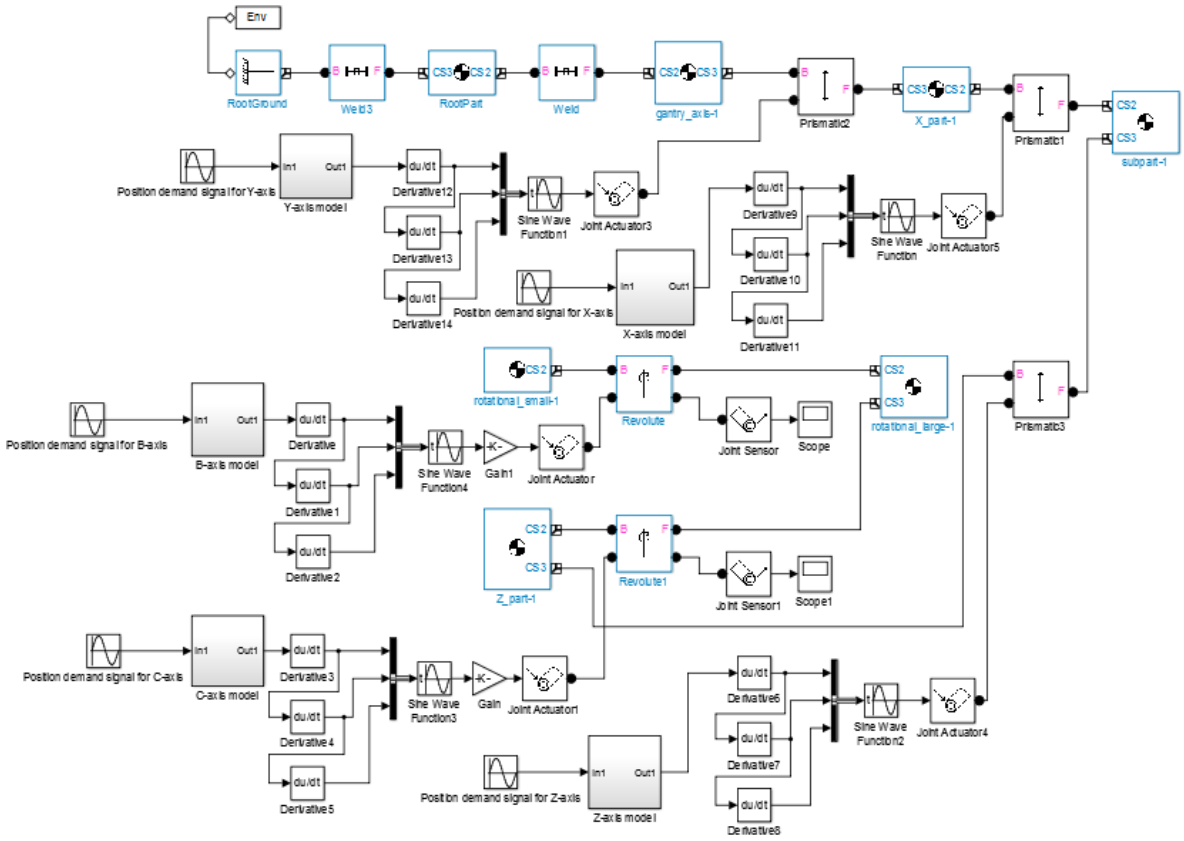

Figure 4-15 The mechatronic hybrid model for the five-axis CNC machine tool using MBS simulation approach combining gain blocks and sine wave functions

4.9 SIMULATION RESULTS

All models have been identified and described. A simulation experiments produces a defined set of results, which are presented in this part of this thesis. The combination of MATLAB/SIMULINK/SimMechanics and SolidWorks software packages was proved as a fast and efficient solution for developing a mechatronic hybrid model for the five-axis CNC machine tool using MBS simulation approach.

4.9.1 B-AXIS DRIVE MODEL

The unity step response of B-axis drive is depicted in the following figure where the rotor angle follows precisely the position demand signal (step input). Figure 4-16 present rotor speed with nominal speed (above) and electromagnetic torque with reference torque (below) for a step input, steady load torque 5Nm, and Kp=2 Rotor speed with nominal speed (above) and electromagnetic torque with reference torque for a step input, steady load torque 5Nm, and Kp=2 (zoom along the X-axis of the plot) On

Figure 4-16, the rotor angle follows precisely the position demand signal (step input). The following figures depict the rotor speed with the nominal speed and the electromagnetic torque with the reference torque. As it can be observed from the above two figures, the rotor speed and the electromagnetic torque follow precisely the nominal speed and reference torque, respectively. In addition, by increasing the proportional term, the response of the system becomes faster. The simulation results of C-axis drive are presented in the Appendix D due to the fact that, the B-axis drive is similar to C-axis drive.

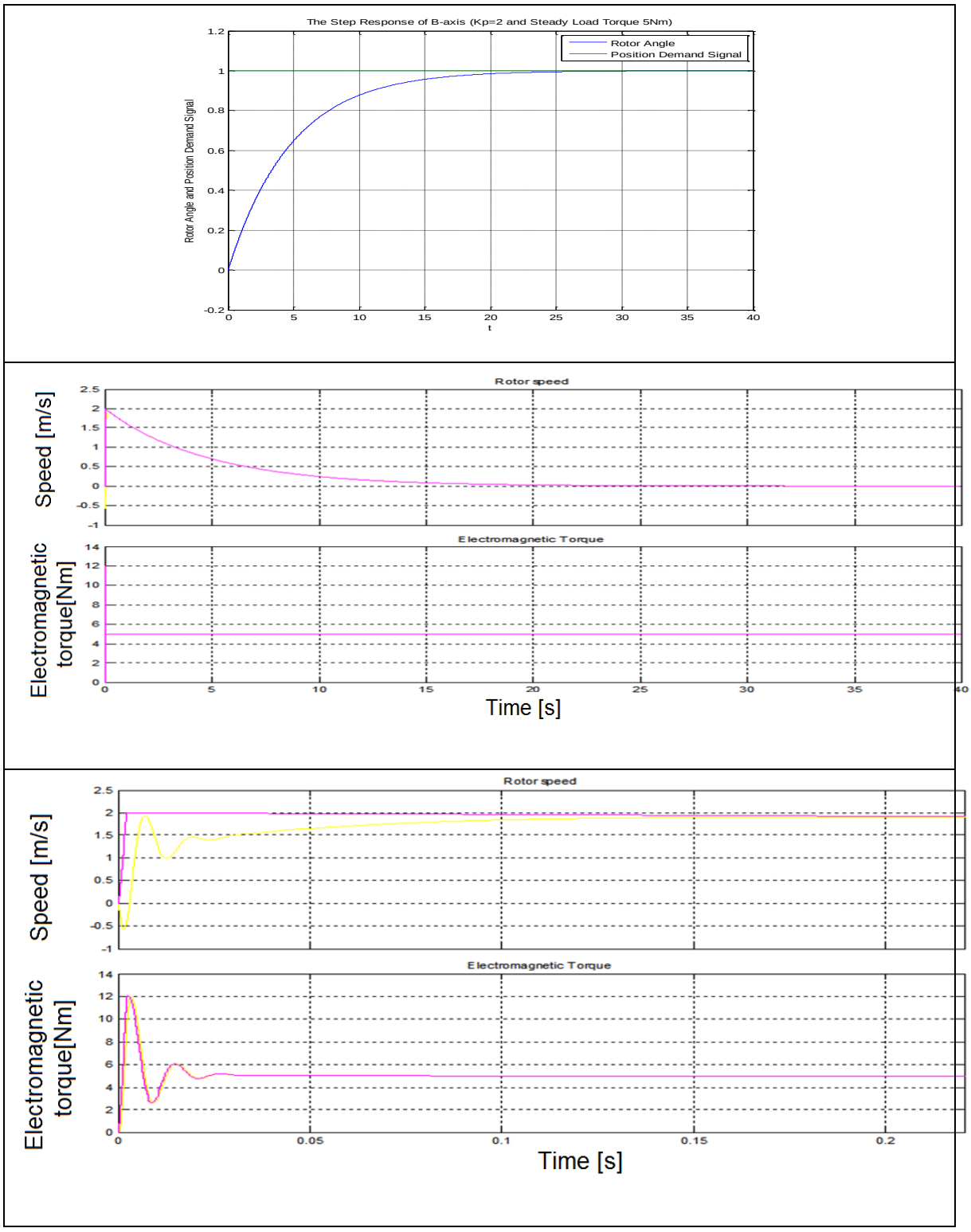

Figure 4-16 The unity step response of B-axis for a steady load torque 5 Nm and Kp=2

4.9.2 X-AXIS DRIVE MODEL

The unity step response of X-axis drive is depicted in the following figure where the motion of the nut follows precisely the position demand signal (step input).

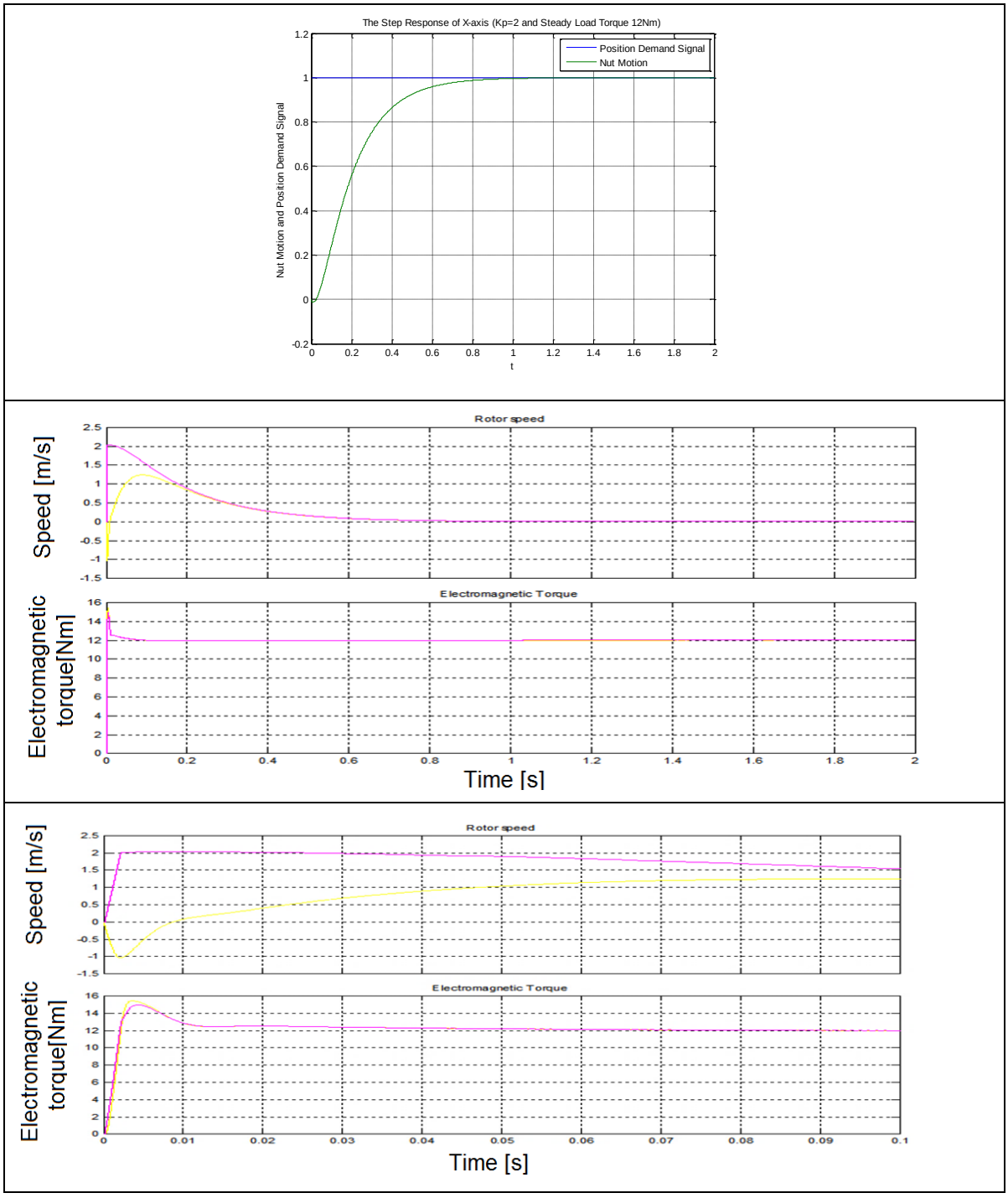

Figure 4-17 The step response of X-axis for a steady load torque 12Nm and Kp=2

Figure 4-17 presents rotor speed with nominal speed (above) and electromagnetic torque with reference torque (below) for a step input, steady load torque 12Nm, and Kp=2 Rotor speed with nominal speed (above) and electromagnetic torque with reference torque (below) for a step input, steady load torque 12Nm, and Kp=2 As it can be observed from the Figure 4-17, the motion of the nut follows precisely the position demand signal (step input). In the same way, the rotor speed and electromagnetic torque. In addition, by increasing the proportional term, the response of the system becomes faster, as shown in z-axis Appendix D.

4.9.3 Y-AXIS DRIVE MODEL

The unity step response of gantry drive (Y-axis/Master and Y2-axis/Slave) is depicted in the Figure 4-18 where the Y-axis and Y2-axis follow precisely the position demand signal (step input). For the Y-axis:

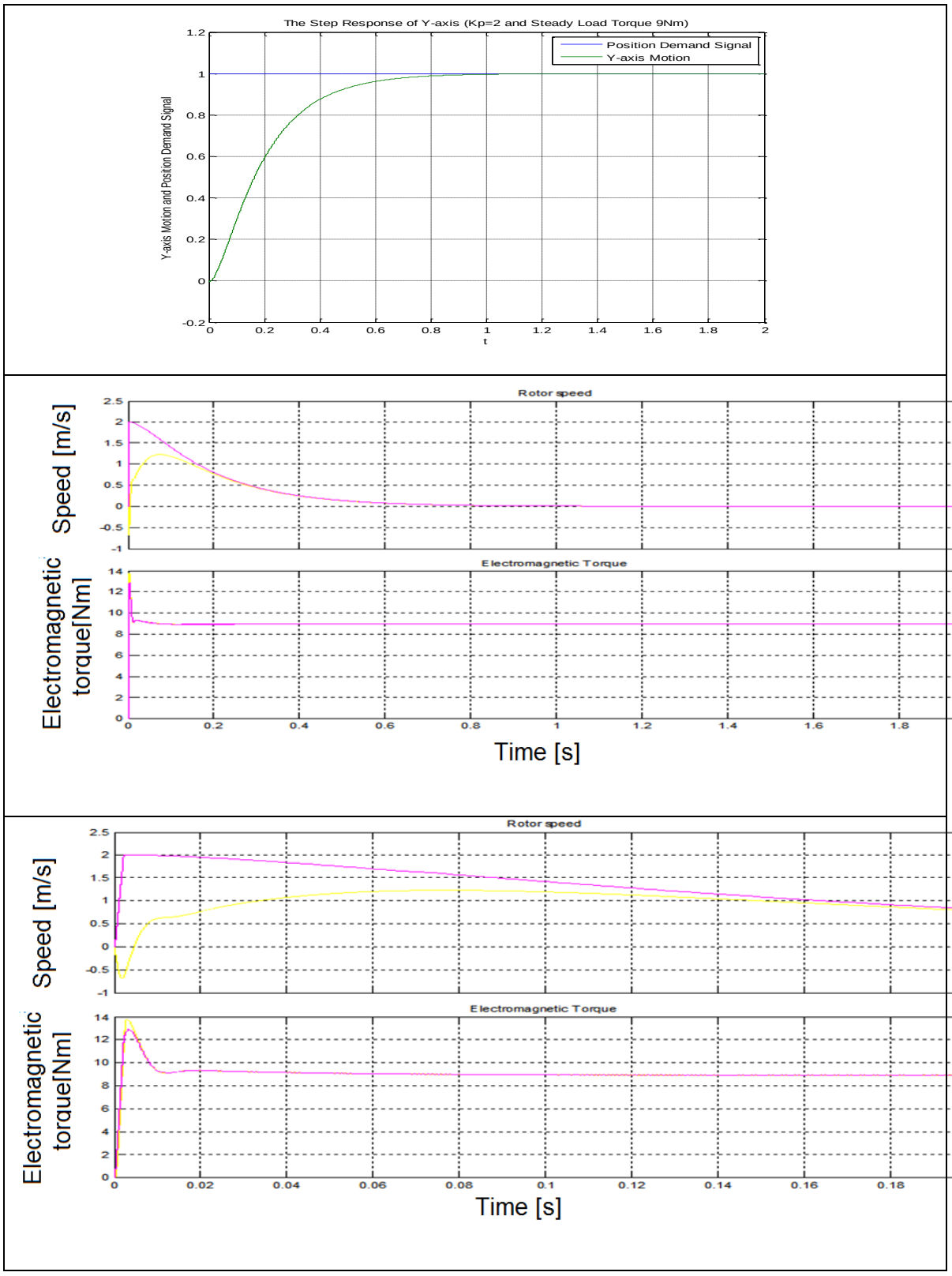

Figure 4-18 The step response of Y-axis for a steady load torque 9Nm and Kp=2

Figure 4-18 shows rotor speed with nominal speed (above) and electromagnetic torque with reference torque (below) for a step input, steady load torque 9Nm, and Kp=2. Rotor speed with nominal speed (above) and electromagnetic torque with reference torque (below) for a step input, steady load torque 9Nm, and Kp=2 (zoom along the X-axis of the plot). As it can be observed from the above figure, the motion of Y-axis drive follows precisely the position demand signal (step input). Similarly, the rotor speed and electromagnetic torque of Master PMSM.

For the Y2-axis position demand signal (step input). Similarly, the rotor speed and electromagnetic torque of Slave PMSM so the results can be found in Appendix D. In addition, by increasing the proportional term, the response of the system becomes *faster.* It is important to note that, at t=0.4s, the full load torque (2Nm) is applied to the motors (both to the Master PMSM and Slave PMSM). It is observed a small disturbance in the motion of the gantry drive, which stabilizes very quickly. At t=1.5s, the mechanical load passes from 2Nm to-2Nm.Themotion of the gantry drive stabilizes very quickly after a small overshoot. Correspondingly, for a sine wave input with angular frequency 10rad/sec and amplitude 1. As can be seen in the above figures the position commanded position is 1. The settling time and the time to peak were both extracted from the raw displacement data collected. It has been noticed that the smaller the movement the longer settle time. Difference between actual and commanded position is less than 0.1 % so it is a low steady state error. Low overshoot condition is noticeable after the position correction loop has completed.

4.10 CONCLUSIONS

The five-axis CNC machine tool has been modelled element by element for achieving a realistic model which represents the actual dynamics of CNC machine tool feed drives. Data for the parameters, which have been specified in each block's dialog box, is presented in the Appendix C. The main aim was the development of a mechatronic model for five-axis CNC machine tool using MSS multi-body-system simulation approach.

In the Appendix D data is presented for the mass and inertia blocks, because the parameters of other blocks are similar. From the following figures, it can be noticed that, the Z-axis drive is similar to X-axis drive and Y -Axis. For this reason, the simulation results of Z-axis drive are presented in the Appendix D.

SimMechanics toolbox allows to define the rigid bodies through the dialog box unfortunately, it does not recognize the advanced mates, and therefore *saturation* blocks are added to limit the input signal of joint actuator to the saturation values. Also SimMechanics first generation is proved more appropriate for modelling the studied system. The developed model can be included in SIL software in the loop implementation using dSPACE real-time system described in Chapter 5 . It's a fast and

efficient solution for developing a multi-body mechatronic hybrid model for the five-axis CNC machine tool.

The aims and objectives of this task have been successfully completed. The intermediate objectives were accomplished and the following conclusions reached. It would be extremely difficult to replicate properly the dynamic behaviour of the whole control system therefore model needs to use real time machine tool data to be able accurately calculate necessary variables (presented in last chapter).

Although the 3D assembly of the GEISS machine could be developed directly in SimMechanics defining the rigid bodies through the dialog box including the mass of the body and moment of inertial tensor, the coordinates for the centre of gravity of the body, and one or more body CS's, SimMechanics link was used as a simpler solution for building the 3D assembly of the CNC machine tool in SolidWorks.

Due to the fact that SimMechanics does not recognize the advanced mates, which have been used in SolidWorks to limit the maximum travel of translation axes, saturation blocks has been added to limit the input signal of joint actuator to the upper and lower saturation values or the combination of gain blocks with sine wave functions.

Although SimMechanics second generation introduces a simpler modelling paradigm with a new block library and an advanced computational engine and visualization utility was proved more appropriate for modelling the studied system.

The present project was concentrated on the development of a mechatronic hybrid model for five-axis CNC machine tool using multi-body-system simulation approach and has shown promising simulated results.

CHAPTER 5 DEVELOPMENT OF THE SOFTWARE-IN-THE-LOOP PLATFORM

The chapter presents the development of SIL (software in the loop) platform allowing the real-time simulation of the feed drive models for the gantry axis of the GEISS five axis CNC machine tool existing at the University of Huddersfield. The interfacing of modular dSPACE hardware on the actual machine and feed drive model in SIMULINK and dSPACE system are explored. The same procedure can be applied for the development of SIL platforms allowing the real-time simulation of feed drive models of remaining translational and rotational axes from GEISS machine.

In this chapter discussion how to implement in the platform this can be achieved using dSPACE is presented. The aim of this work is development of the SIL platform allowing the real time simulation and comparison with experimental results. Dougal (2000) mention that traditional software-based simulation has the disadvantage of being unable to exactly replicate real time operational conditions. One way to bridge the gap between simulation and real conditions is hardware-in-the-loop (HIL) simulation. Barcoss (2001) have been written outlining the basic fundamentals of HIL simulation. Tummescheit H. (2003) present “hardware-in-the-loop” definition as: “Process and tools for verifying the logical and temporal correctness of integrated control system hardware and software.” In his work he shows the “hardware-in-the-loop” key to Validation & Verification of controlled dynamic performance.

5.1 INTRODUCTION

In the past 20 years, there have been many projects that have validated the success that can be achieved using HIL system testing (mentioned later in this chapter). Some of the latest approaches can be found by perusing the websites of companies that produce control systems products, ADI, A&D, dSPACE, ETAS, Fujitsu-TEN, National Instruments, Opal-RT, and PhaseX systems.

The major advantage of LabVIEW and dSPACE over conventional high level languages, such as C, Pascal, or FORTRAN, is the graphical user interface, which is built in, intuitive in operation, and simple to apply. According to National Instruments (2015) LabVIEW Simulation Interface Toolkit software allows a MATLAB/SIMULINK model to be compiled into a LabVIEW accessible dynamically linked library (DLL) file that can be ported directly to the real-time hardware and real-time distributed simulation package (RT-LAB).

dSPACE gained significant capabilities in the assessment of the functions to accurately reproduce plant behaviour and developed the hardware needed for more accurate simulation capability. dSPACE system was chosen because it is uniquely modular and uses the same base components that can be multi-purposed throughout a wide range of experiment configurations. The system is built using the dSPACE real-time environment, which is based on a dSPACE 1005 board (2015) allowing the processor to interact directly with the sensors during real-time simulation. The real-time interface tool (RTI) connects SIMULINK and the Real-Time Workshop (RTW) with dSPACE's real-time systems to form a ready-to-use environment for real-time applications.

Hardware in the loop simulation is a technique that can be used to test complex embedded systems in real time. It comprises of a test platform that tries to represent the dynamics of the system through mathematical expressions. Hence the expressions are the simulation against which the system is tested. So instead of performing the complex and time consuming test on the actual machine prototype, simulations and understand the system behaviour can be done. The inputs from the system and the outputs of the controller are interfaced through the I/O modules with the simulation model. The Figure 5-1 illustrates the software development cycle for embedded control applications in aerospace defence and automotive arena. This is a general concept applied with slight variations across various applications.

Figure 5-1 V diagram of system engineering

This same model shall be considered in this project. The system modelling is done in SIMULINK after the first three steps of the V diagram. As mentioned earlier the Real Time Interface is used to interface with the SIMULINK model. This combined with UI tools from dSPACE is an effective interface option to view and control data. To acquire a thorough understanding of the system behaviour, apart from the software simulations user also has to perform Rapid Control Prototype testing. The controller is tested on the hardware prototype. To perform this step the SIMULINK model will have to be converted to C

code using the Real Time Workshop. Based on the test results, fine tuning is applied to the controller model if required and further tested. Now the model is ready to be applied in target hardware.

HIL simulation offers the lot of advantages like cost and downtime reduction, reusability and low risk testing capability. In this chapter the first four phases of the above V diagram have been completed and discussed.

5.2 PRACTICAL HIL SYSTEMS

Due to the characteristic advantages (discussed in the earlier section) offered by the HIL simulations they are widely used in the industrial arena of the various kind. Unmanned automotive systems where the controlling technique for instance, analysing performance and monitoring purposes.

H.Kim et al. (2008) have implemented HIL setup as a means to investigate dynamic characteristics of the active roll controller. Using the hardware-in-the-loop setup including the prototype roll control system and full vehicle model they have attempted to investigate nonlinear tire characteristics and control performance.

HIL systems are also used in the medical field, an area exhibiting complex dynamic behaviours. S.Herrmann et al. (2012) and B.M. Hanson et al. (2007) talk about how they used HIL systems to review dynamic behaviour model of artificial joints and cardiovascular system. Based on the simulations run they were able to evaluate the effectiveness of control techniques applied to the assist devices and suggest improvements.

Further examples of HIL simulation and implementation have been suggested by M.Montazeri et al. (2011) as a means for evaluation of Jet engine controller and by G.Randolf et al. (2006) for evaluating dynamic behaviour of proton exchange membrane (PEM) fuel cells and their auxiliaries

Implementing HIL eliminates the need for presence of actual machine component for complex real time testing. Complexity can arise from the system dynamics, environment interaction, nature of testing and even cost. By making use of an embedded controller, an electrical/electronic system and appropriate software capable of processing the dynamic model of the system a cost effective HIL simulation setup can be perfected.

5.3 DSPACE KIT

Kanaka Juvva (1998) defines a Real-Time System as a system in which the correctness of the system behaviour depends on the logical results of the computations and also on the physical instant at which these results were computed. Typically it comprises of computer based controlling system acquiring and processing information from various sensors and inputs and essentially defining the state of the system. This state information must corroborate with the actual state of the real time environment. Therefore periodic data acquisition in a logical, timely and delay less fashion is of the prime essence. Same author classifies the Real Time System into hard and soft Real-time systems. A default in hard Real-Time systems can cause catastrophe whereas in a soft Real-Time system it leads to significant loss. Therefore in either case predictability is essential. Predictability can be achieved by static or dynamic scheduling of real time tasks ensuring that they meet the deadlines. dSPACE is a pioneer in providing hardware and software solutions for the development of mechatronic control systems. They specialize in key technologies like rapid hardware-in-the-loop simulation and control prototyping.

For the scope of this project the modular hardware comprising of the DS1005 PowerPC 750 GX processor, I/O boards and encoders will be inspected. DS 1005 is a hardware prototyping board. It makes integrating existing hardware with dSPACE hardware easier. The ACE kit components are illustrated in the Figure 5-2.

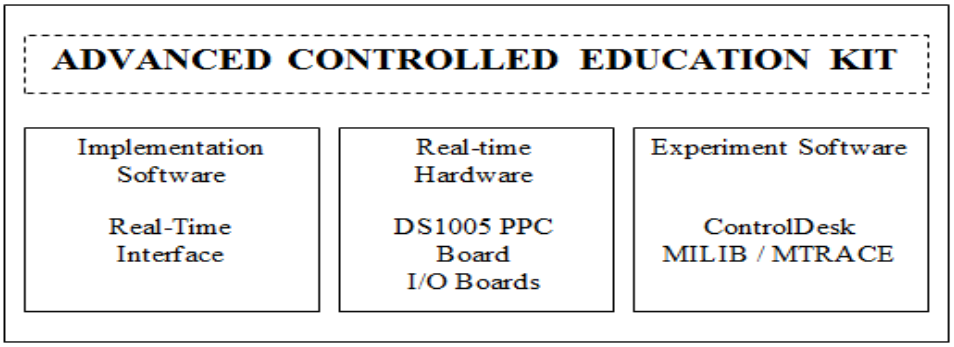

Figure 5-2 dSPACE ACE kit

5.3.1 HARDWARE

dSPACE (2013) provides an ACE (Advanced controlled education) kit. This primarily comprises of DS1005 PPC board. This is the core of the modular hardware. Based on requirement of the project additional I/O boards, cables and other accessories such as expansion box could be utilized. The list of the modular hardware that can be connected with PPC board is given in Appendix E. The processor employed is an IBM PowerPC 750GX at 1 GHz. The technical details have been specified in Appendix E. The block diagram connecting the various elements of the modular hardware has been shown on Figure 5-3.

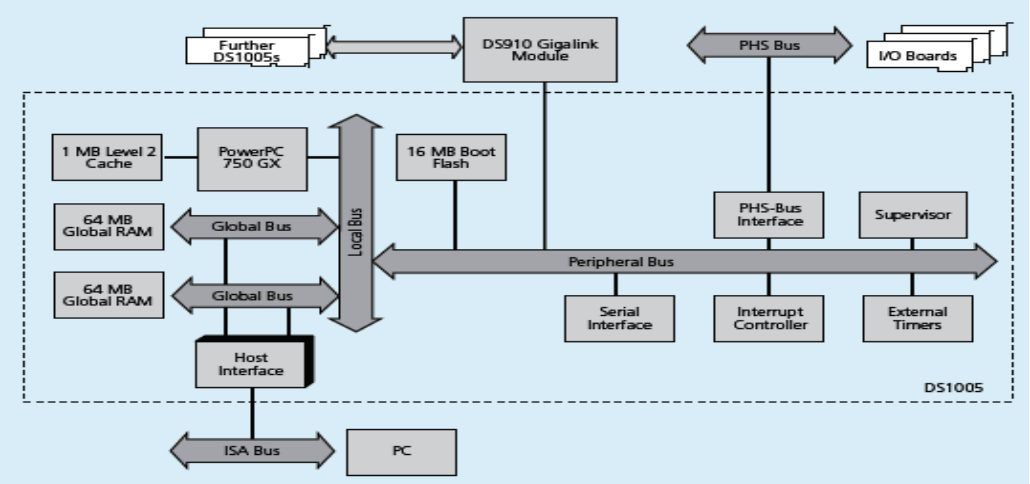

Figure 5-3 Block diagram for the modular hardware Liu (2010)

The DS1005 is interfaced with the other I/O boards through the PHS bus. The key benefits of modular hardware are wider choice and faster access to I/O therefore higher processing power. Initializing and configuring the I/O modules may be done through the GUI of SIMULINK. The dSPACE in addition has software packages with tools for monitoring the instruments connected to the system and data acquisition.

5.3.2 SOFTWARE

dSPACE comes with a whole suite of software's classified as System architecture, Implementation, Test, Automotive ECU software. As a general approach the following steps are followed for the implementation of the SIL in dSPACE.

1st Model with Real-Time Interface -The model of the system are designed in the MATLAB/SIMULINK development environment.

2nd Graphical I/O Structure - After testing the model in SIMULINK, it has to be prepared for implementation on the real-time hardware. An I/O model can be added by a simple drag and drop from the RTI I/O library to the model.

3rd Parameter Arrangement - I/O parameters are specified at the I/O block through a simple double click.

4th Implementation on dSPACE Hardware - Automatic implementation of the SIMULINK model on dSPACE hardware is possible. A single click on Build starts the implementation, including code generation, compiling, and downloading. An integration algorithm and a step size may be specified.

The dSPACE generates executable that can be cross compiled considering the fact it needs to interact with different devices and their respective drivers. However the user must still consider the compatibility of the devices with process board.

5.3.3 DSPACE SOFTWARE- CONTROLDESK

Using dSPACE experiment software the RTI ensures control over each separate variable after the implementation process. ControlDesk provides an instrument panel that enables changing parameters and monitor signals. It is capable of displaying the time histories of any variable used by in the application. Multiple signals can be acquired and displayed from a convenient GUI. Control Desk provides options for data decimation and data acquisition. It is also possible to save the acquired data in a .Mat file for Matlab.

The ControlDesk Package is powerful software which allows to see the variables, display their behaviour and change the simulation parameters by interacting with the dSPACE DSP board ControlDesk. Typical ControlDesk window provides access to the different parts of a real-time experiment and allows for the instructions to be given to ControlDesk.

5.4 REAL-TIME WORKSHOP

The Real-Time Workshop can generate code directly from SIMULINK models. They can be used for the following applications.

- Real-time control - The code generated from the block diagram model can be compiled and downloaded to target hardware.
- Real-time signal processing - The generated code for the signal processing algorithm can be compiled and downloaded to target hardware.
- Software-in-the-loop simulation —SIMULINK models that mimic system dynamics can be converted to code for target hardware. This sort of exercise is useful for control system validation, training simulation etc.
- Interactive real-time parameter tuning - Allows to change parameters during program execution.
- Generation of portable C code for export to other simulation programs.

Real-Time Workshop optimized code in C with appropriate comments using the Target Language Compiler. It maintains target files (ASCII text files) for the SIMULINK model describing how they must be converted to code. Therefore manual customisation is possible by accessing these target files. All blocks are converted to code except the ones that invoke M files. In this scenario these blocks should be rewritten as C MEX S-functions. Real-Time Workshop provides C code used in non-real-time

simulation environments or for real-time applications. Real-time program code generated for a dedicated real-time hardware. The requirement is to interface with an external clock source. High - performance stand-alone simulation used to generate an executable for stand-alone simulations. The executable produces a model.mat file that contains logged data of variables in SIMULINK.

An illustration of the Real-Time workshop's open architecture is given on Figure 5-4.

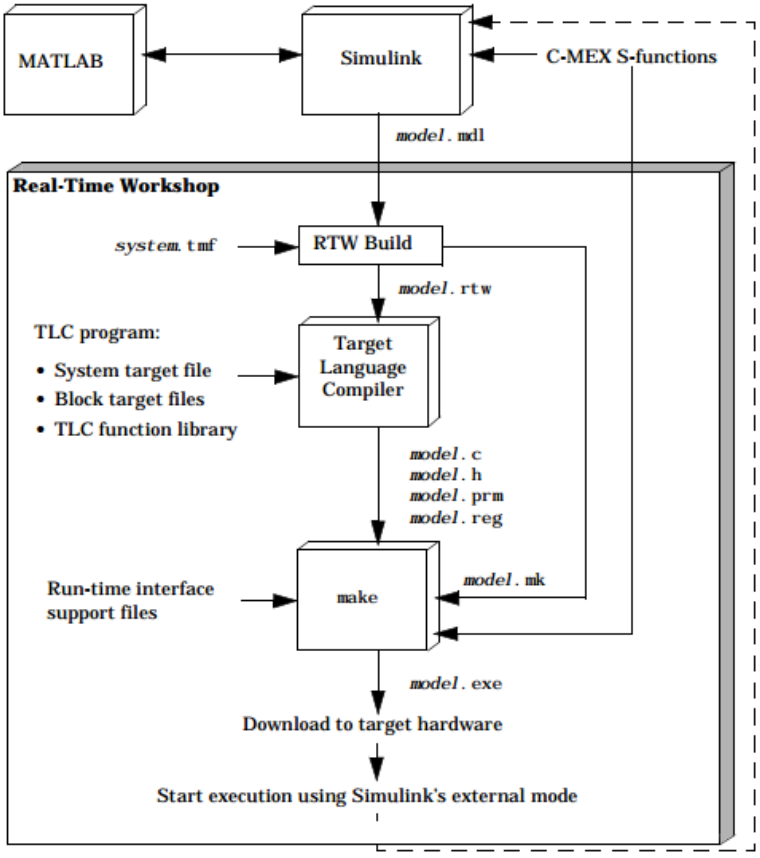

Figure 5-4 Open architecture of Real-Time Workshop (Hansen 2006)

5.5 MATLAB PRODUCTS AND DSPACE SOFTWARE

The Real-Time Workshop produces C-code from SIMULINK models and builds complex programs that can be run in a real-time systems or on processor. The Real-Time Workshop provides a library of functions that allow great flexibility in constructing real-time system models and generated code. It is used to run stand-alone simulations on on an external computer. Rapid prototyping procedure reduce costs and shorter development cycles. It has been used to implement software-in-the-loop (SIL) simulations.

The generated model is by default highly optimized and fully commented C code that can be generated from any SIMULINK model, including linear, nonlinear, continuous, discrete, or hybrid models. All SIMULINK blocks are automatically converted to code, with the exception of MATLAB function blocks and S-function blocks that invoke M-files. The Real-Time Workshop includes a set of target files that are compiled by the Target Language Compiler (TLC) to produce ANSI C code. The target files are ASCII text files that describe how to convert the SIMULINK model to code.

5.5.1 REAL-TIME INTERFACE

Real-Time Interface (RTI) links the real time system of the dSPACE with the SIMULINK models. In order to use Real-Time Workshop with dSPACE hardware target specific software must be developed. The target specific code is nothing but device drivers and interrupts service routines. As mentioned earlier the RTI has a Graphical user interface with a set of block libraries. A specific dSPACE I/O board can be represented using the respective block from the library. The model with the blocks replaced by the I/O blocks is then easily compiled by the RTI. Using RTI it is possible to set task priorities program event triggering and manipulate event interrupts.

To specify a dSPACE I/O board the corresponding I/O graphical modules from the RTI library are picked and parameterize within SIMULINK. After this, RTI compiles, downloads, and starts Real-time model. Different channels of the same I/O board can be used with different sample rates, and even in different subsystems. RTI supports aperiodic events, for example, software interrupts and external hardware interrupts, and allows to set task priorities for the execution of the interrupt-triggered subsystems.

5.5.2 DATA ACQUISITION

Instrument panels are used to visualize and control the parameters of real-time applications and SIMULINK simulations. Simulator variables are defined in two application-specific files - variable description files (SDF, TRC) and MAP files – that have to be loaded in ControlDesk to build data connections from instrument panels to the variables. SDF files provides information on how many

processors are used. TRC file of SIL simulation specifies the variables and blocks defined SIMULINK model. The MAP file maps symbolic names to system physical addresses.

Variable Browser within Control Desk display the SIL simulator variables and connect them to the instruments like on Figure 5-5. Variable description file needs to be loaded and variable's connected to an instrument.

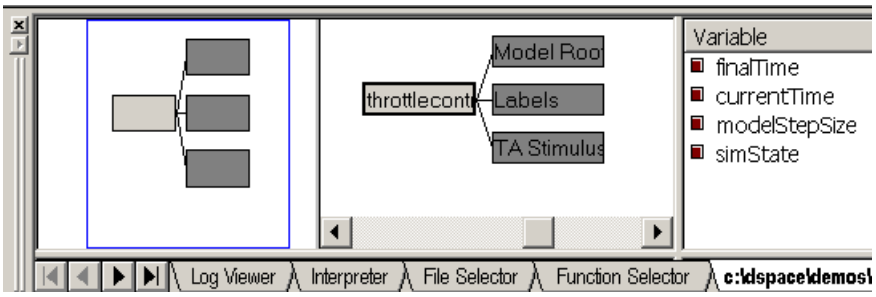

Figure 5-5 Variable Browser window

The next step is to establish data connections between the different elements. Data connections are used to send and receive data or control layouts. (Unknown 2008)

5.5.3 PARAMETER HANDLING

Parameter Editor is used to perform parameter studies. ControlDesk provide the "Parameter Editor" that allows saving, loading and modifying sets of parameters. Data connections between variables and instruments can be exported and imported to/from connection files. The Table Editor instrument displays the values of a connected vectors. ControlDesk automatically performs some preparatory steps including inserting call-back routines and some basic SIMULINK blocks.

Simulation Parameters dialog provided by SIMULINK or the Properties dialog provided by ControlDesk are used to specify the parameters. The latter is a subset of SIMULINK's simulation parameters, containing only dialogs relevant to ControlDesk. To monitor signals the corresponding variable description file is loaded and at least one variable is connected to an instrument some preparatory steps have to perform.

ControlDesk allows to monitor and control SIMULINK and real-time variables available from the corresponding variable description file. The variable the data connection is still accessible after migration from SIMULINK to real-time. The Parameter Editor allows saving parameter sets for later use.

5.6 SOFTWARE IN THE LOOP SIMULATION

The code is auto generated code therefore it is prone to errors and resolution loss. Due to errors behaviour might change from host to processor environment. It is crucial to check that the code produces identical results in both – SIMULINK and dSPACE 1005 processor by running known data.

Software-in-the-loop testing is used when expensive CNC hardware is not possible. It offers low cost but but its main disadvantage is that simulation time is not real time– it can be completely different than it is the case in hardware-in-the-loop (HIL) simulation.

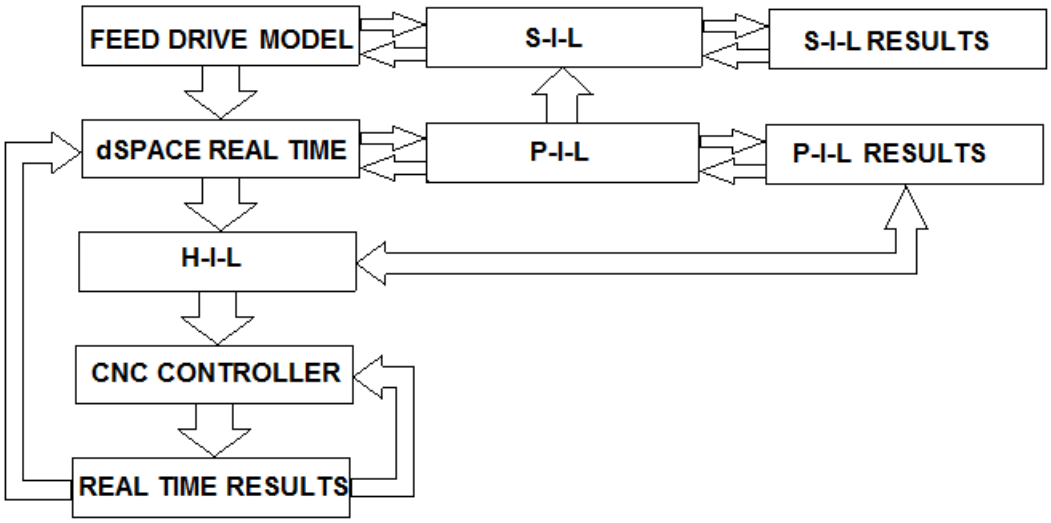

Figure 5-6 Simulation loops

The common simulation loops that are functional when model generating code is applied are highlighted in Figure 5-6. First simulation - model-in-the-loop has been done in SIMULINK environment to capture the specified behaviour of the model that is implemented using C code. The feed drive model is simulated on a block basis – like described in previous chapter and therefore with the highest possible precision. These act as the reference for the HIL steps.

A RTI provides the interface between the simulation and the generated code. The simulation plots are matching when compared to the results of model-in-the-loop simulation.

Processor-in-the-loop (PIL) and Software-in-the-loop are the part of whole testing process where the generated code executes on the actual embedded processor. The generated code runs on a DS1005 embedded processor. With PIL and SIL in place an opportunity arises to test the model in an environment closest to the HIL real time platform. PIL also addresses compiler related problems with the generated model code.

Software-in-the-loop simulation does not use any real control hardware. The behaviour of these components is reproduced and emulated. Zeah *et al.* (2008) shows a comparison of the SIL and HIL approaches Figure 5-7:

Properties of the approach	HILS	SILS
Low effort for modeling and adaption	●	○
Representation of real time behavior	●	○
Full integration of the control and human-machine-interface functionality	●	◑
Integration of real hardware components	●	○
High model complexity	◑	●
Widely accepted by users	●	◑
Independent from target control hardware	◑	●

● Fulfilled ○ Not Fulfilled ◑ Partially Fulfilled

Figure 5-7 Hardware versus SIL simulation Zeah *et al.* (2008)

Purzel et al. (2013) mentions that current programs which are used to simulate NC programs are desktop-based and consist of two software parts – the virtual machine and the NC control unit. These SIL systems include the workspace of the machine tool, speed, range of movement of the tool and the accuracy of the work pieces geometry. However, it is difficult to create NC control unit using a desktop-based SIL simulation.

SIL applications are prototyping simulations, prepared on a computer to model the behaviour of a real-time control system. SIL part was conducted with the use of the Matlab (2014) software with the model of process automatically generated from the SolidWorks simplified multi-body construction assembly. Simulation models are running on in dSPACE 1005 board which uses generated C code for the control or model in a virtual real-time environment where in future compensating calculations can be carried out using FEA models.

An important reason for using simulation in the loop rather than HIL in this stage of development is safety. An important advantage of a SIL platform is the possibility to directly observe and relate the effective and the measured parameters of the system such as position or speed. The user can adjust the controller parameters in order to obtain the best working conditions. Figure 5.8 shows the Graphical User Interface (GUI) for the simulation and a picture of the actual GEISS machine.

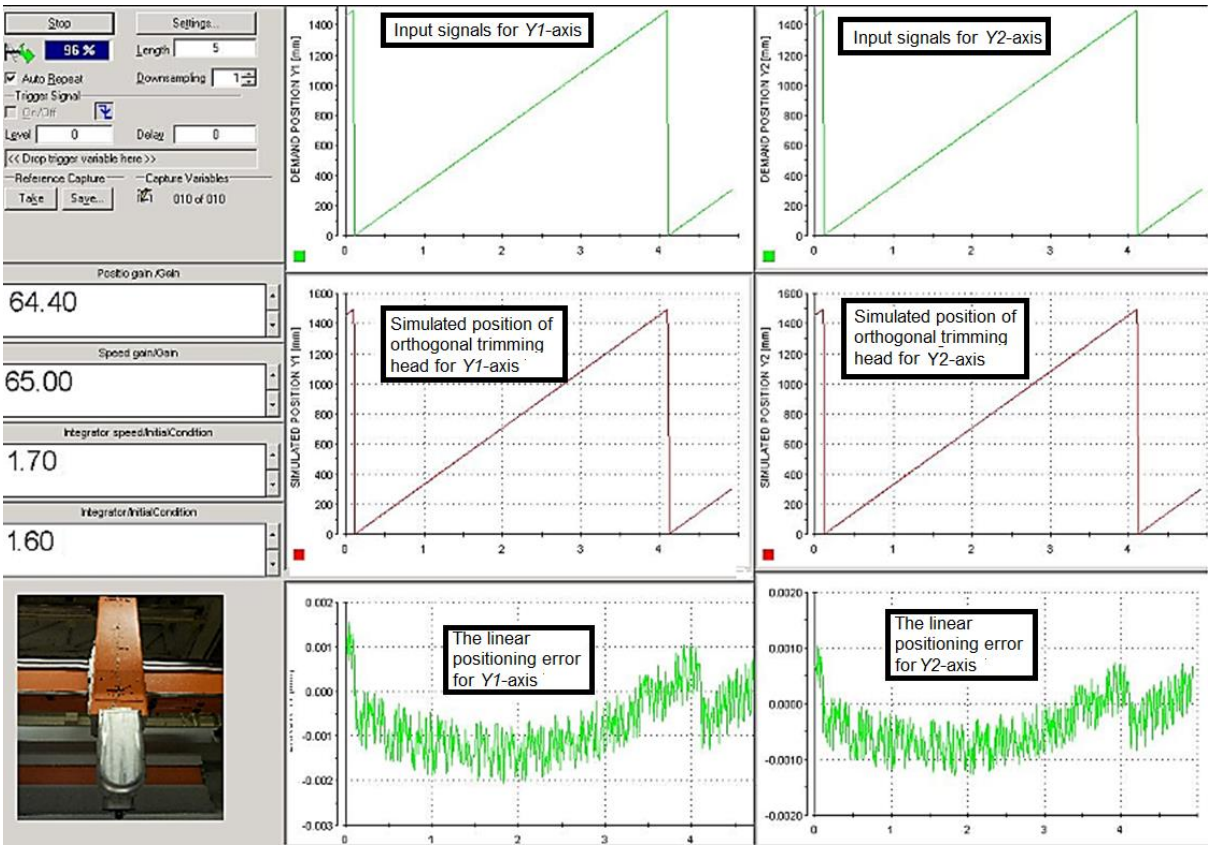

Figure 5-8 SIL GUI for gantry drive using dSPACE real-time system.

Software-in-the-loop can be viewed as Simulation-based Software Evaluation on dSPACE 1005 processor platform. A software system has been executed under measured input conditions to check its functionality. A model-based construction of the simulated machine tool enables an effective verification and assessing reliability problems while improving its efficiency by simplifying the virtual environment. Input signals for *Y1*-axis and *Y2*-axis are presented in left hand top corner and right hand top corner, respectively. Simulated position of orthogonal trimming head for *Y1*-axis is shown in left hand middle graph and for *Y2*-axis in right hand middle graph. The linear positioning error for *Y1*-axis (see Figure 5.8 left hand, bottom corner) and for *Y2*-axis (see Figure 5.8 right hand, bottom corner) is the difference between the position demand and the simulated orthogonal trimming head position. Values for the position demand signal were chosen in accordance with the experimental data from the GEISS machine measured linear position using ServoTrace tool. The position demand requests the travel of orthogonal trimming head for the distance of 1500 mm. The errors are around 1 μm, so they show good correlation between demand signals and simulated position values. The outputs from the model can be used for assessing outputs generated by the code.

5.7 SIL CONCLUSIONS

The results obtained from the simulation were compared with the results from the actual machine using Servo Trace. The procedure for performing Servo Trace is discussed in APPENDIX F. Concluding - the developed SIMULINK model is robust enough to simulate the actual behaviour of the GEISS CNC machine gantry.

The present chapter explains how the experimental data obtained from the data acquisition process using dSPACE real-time system can be used for the development of a machine tool diagnosis and prognosis system that facilitates the improvement of maintenance activities. The health condition of the physical feed drive components can be constantly assessed by using the monitoring data measured by dSPACE to perform on-line system diagnostics and prognostics and estimation of the remaining useful life. SIL allowed to adapt and test the system model with real-time simulation. SIL deals with reproducing the environment where the embedded system will run. Hardware in the loop simulation is usually one of the last steps in the testing procedure, probably before integration and system tests. Whole machine integration with dSPACE system derives later in the project development phases so SIL make use of a software model to test model.

CHAPTER 6 UNCERTAINTY ASSESSMENT RELATED TO THE MEASUREMENTS OBTAINED FROM ACOUSTIC EMISSION SENSOR

This chapter will first review the theory and previous application of acoustic emission (AE) monitoring. It will then describe the piezoelectricity phenomenon under transient elastic waves caused when a material changes in its internal structure. Then it will present details of a typical AE System: the principle of the AE sensors, preamplifier and data acquisition system.

This chapter includes a description of how acoustic emission waves spread in solid materials and how temperature affects the guided waves. By recognising that the acoustic waves diminish in intensity when sound travels through a medium, a distance-attenuation equation is delivered. The installation and choice of couplant material is determined by the particulars of the application

The result of the measurement should be finally related to a stated reference, such as an international standard during the calibration. In reality, errors and uncertainties are always unavoidable in the measurement process. A Bayesian regression technique is used to estimate uncertainties in measurement, in line with the internationally accepted Guide to the Expression of Uncertainty (GUM) (BIPM GUM 2012). Details of the experimental setup and procedure to determine uncertainties are explained. A statistical Bayesian model is developed to describe the relationship between the uncertainty parameters.

A Bayesian network is proposed to dynamically monitor the sensor uncertainness condition of dynamic Bayesian networks (DBN). Estimating the uncertainty associated with the AE measurement will reduce the chance of creating a wrong decision by ensuring that trigger actions are only taken when a measurement conforms, within a high confidence factor.

6.1 DESCRIPTION OF THE DEVELOPED ACOUSTIC EMISSION SYSTEM

Suitable instruments to record the output of the transducer and to process the signal are described. The system used in this research required that the transducer output was amplified, converted using of an analogue to digital converter, and recorded to a computer hard-drive. The data was then analysed in MATLAB. Code to read and interpret the files are attached in Appendix F.

6.1.1 AE SENSOR

The principle of the AE sensors is the use of the piezo-ceramic elements to produce output voltage signals from the presence of stress waves propagated from a source. Figure 6-1 shows the basic construction of an AE sensor.

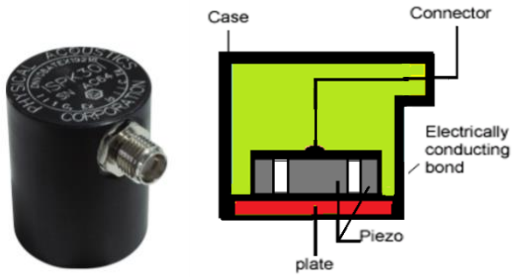

Figure 6-1 Construction of AE sensor Acoustic Emission sensor used in tests (MISTRAS 2015)

The ISPK30I, which was chosen for this research application, resonance frequency is around 300 kHz. Sensor has integral, ultra-low noise and low power preamplifier. The bandpass filtered preamplifier has a gain of 26dB. The sensor has a. PAC a broad-band transducer model 300 kHz calibration curve (sensitivity vs. frequency) is presented on Figure 6-2. Response is relatively smooth and flat, in the frequency band 100 kHz to 1 MHz. AE transducer its sensitivity spectrum does show low separate peaks, but mostly a flat response in a wide frequency band. The wide band frequency spectrum is the superposition of an infinite series of resonant peaks.

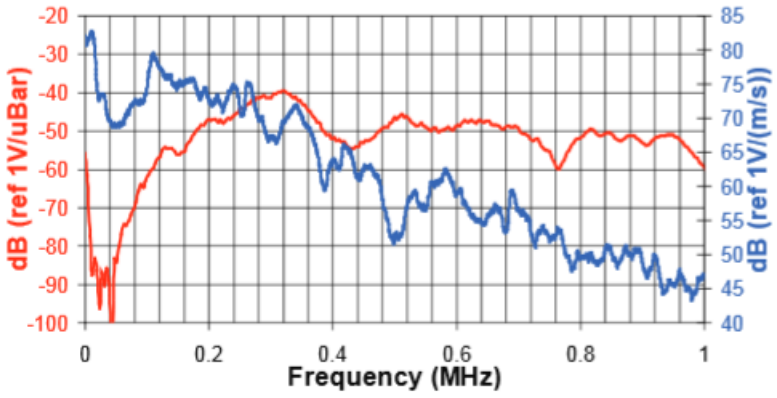

Figure 6-2 Acoustic emission sensor frequency response (MISTRAS 2014)

The location for the transducer was wisely selected Figure 6-3 so that the transducer receive consistent AE signals.

Figure 6-3 AE transducer mounted on the nut

The transducer was mounted on the ballscrew nut. Before attaching the transducer, the contacting surface was cleaned. A Silicone Compound has been used to provide the necessary transducer coupling and mounting and to hold the transducer securely for the duration of the whole test

6.1.2 ACOUSTIC EMISSION PREAMPLIFIER

The sensor is accompanied by a preamplifier so that it increases the signal transmitted. The preamplifier have low noise and moderately gain. Cables connected to the sensor from the pre-amplifier are as short as possible to eliminate noise. The typical unit for an AE signal is indeed voltage or mV.

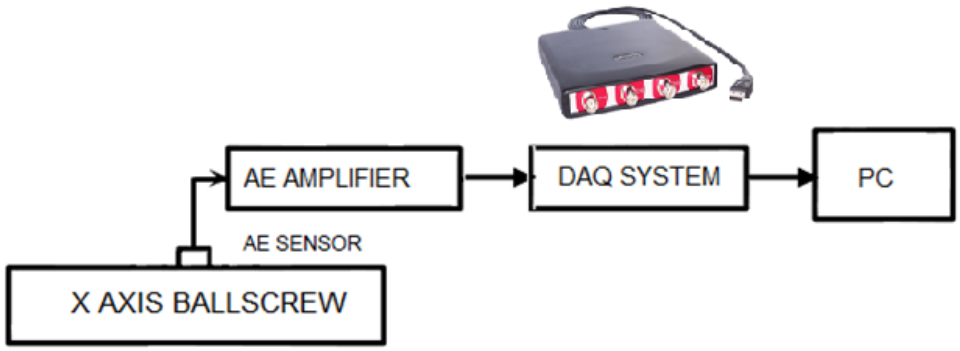

Figure 6-4 Diagram of the data acquisition system

The pre-amplified acoustic emission signals are input simultaneously into a HANDYSCOPE Data Acquisition DAQ (TIEPIE (2015)). Handyscope HS4 is connected to a PC USB 2.0. The complete Handyscope HS4 gain and offset calibrations is controlled by the software. Exporting data is done in ASCII (CSV), so it can be read in a spreadsheet program or MATLAB. Diagram of the data acquisition system is presented on Figure 6-4. Together with each data information file containing all instrument settings are saved. The information file is always in ASCII and can easily be read by MATLAB.

Sampling rate is the speed of the data sampled for the waveforms. Sensor provides signals of 1Mhz resolution. Depending on waveform length required. 1MHz sampling rate is generally sufficient. Data length of the waveform has been set to 131k and processed in MATLAB. Combined with the sampling frequency, the data length will set the duration of your waveform. E.g. 260 kHz and 130k samples results to 0.5 second of data. Sampling rate and data length has been set for maximum efficiency and Nyquist frequency – 800 KHz and 131k length.

Mounting method

When attaching an AE sensor to a measurement surface, a couplant material is used to remove air from the interface. The acoustic impedance of air is high and allows only very small transmission of acoustic energy at the high frequencies typical of AE, thus causing considerable loss in transmission. The use of a couplant greatly improves transmission by around twice at 100 kHz and more than ten times at 500 kHz. Typical gel-based couplants have a high acoustic impedance, approximately four orders of magnitude higher than the one of air. Effectiveness of a couplant is dependent on its acoustic impedance, acoustic attenuation, application thickness and viscosity. Theobald (2016)

Theobald (2016) consider a number of ultra-sonic/AE couplants and compares the sensor response for each couplant to longitudinal and shear waves, demonstrating that a high-performance ultrasonic couplant can improve sensor sensitivity significantly above 400 kHz compared with a grease-type couplant.

Couplant	Couplant type	Clamp	Viscosity	Temperature
Glycerine	Gel	Yes	Medium	Medium
Ultrasonic Gel	Gel	Yes	Medium	Low
Brown Grease	Grease	Yes	High	Low
Silicone Grease	Grease	Yes	High	Medium
Petroleum Jelly	Grease	Yes	High	Low
Silicone	Elastomer Adhesive	No	Elastic Solid	High
Hot melt glue	Elastomer Adhesive	No	Elastic Solid	Low
Cyanoacrylate	Adhesive	No	Rigid	Low
Dental cement	Adhesive	No	Rigid	Low

Table 6-1 National Physical Laboratory table for AE sensor couplants (Theobald 2016)

The AE sensor must be pressed directly against the workpiece for best signal capture. Rating information on AE couplants can be found in a National Physics Laboratory reprt, “Guide on Acoustic Emission Sensor Couplants (Theobald 2016), as shown in Table 6-1.

6.1.3 MOUNTING OF AE SENSOR

The most common adhesive Theobald (2016) used as an AE couplant for industrial applications is silicon rubber compound, which can be applied as a fluid to achieve a thin, bubble free couplant layer and then held in place until cured to provide a permanent bond. Excellent results have been achieved using LOCTITE SI 595 RTV SILICONE SEALANT. It is a waterproof and flexible general-purpose clear sealant which can be applied to horizontal or vertical surfaces. Temperature ranges between -80°F to 450°F. It will set up within hours when set between a sensor and a metal or plastic surface. This couplant installation can be done on rough surfaces. A silicon compound provides good stability in applications where vibration can occur and good resistance to link breakdown where surface movement can take place and provides outstanding transmission with a relatively strong bond. There is risk of damage to the sensor if it is not disconnected carefully, but it is quite flexible, allowing for sensor removal from a surface with a knife blade between the sensor and the measurement surface. Cleaning the silicon residue off both the sensor and the surface will require polishing. The cure time should be checked as the transient acoustic properties of the compound possibly will change through the curing process. Locktite adhesive silicon couplant is ideal for applications where the sensor will not be removed. Clamping is not required for installation due to adhesive properties of the couplant.

The couplant chosen for the semi-permanent application of AE monitoring of the machine tool ballscrew is LOCTITE SI 595 because it's low attenuation and temperature stability.

6.2 ACOUSTIC WAVES IN SOLIDS

Once generated, acoustic emission waves spread under the same rules as any other acoustic wave. They are a shared motion in a set of atoms. The random time of origination and the broad variety of waveforms in separate emissions are primary characteristics of acoustic emission. These factors have a reflective effect on the type of analysis used on the emissions.

The simplest type of acoustic wave is a pressure wave which arises when a material is suddenly compressed by a disturbance in that region. This compression can be either positive or negative. The material in these changes in its density, then that change is then passed to the next by coupling between the atoms. The power of the atomic coupling and the density of the material determine the speed with which the disturbance propagates. The resulting wave occurs in all materials, solids, liquids, gases. (Beattie 2013)

The most familiar depiction of a wave is a sinusoidal curve. If two sine waves are presented in a medium at the same time, their amplitudes will add algebraically. The sum of two waves would be:

$$Y = A1 \sin \omega 1t + A2 \sin \omega 2t \qquad \text{Equation 6-1}$$

It is density of the material, ρ. The elastic constant is determined by the strength of the union between atoms for that exacting kind of motion. Property of the material is the characteristic impedance. The actual relationship is defined by:

$Zi = \rho vi = \sqrt{\rho Ci}$ Equation 6-2

Where Vi is the velocity of the wave and Ci is known as the elastic constant for that wave. Velocities, acoustic impedances, and densities for some materials often seen in acoustic emission tests are showed in Table 6-3 Methods of calibration-comparison

Acoustic velocities and impedances for longitudinal, shear, and Raleigh waves							
Material	V_1	V_s	V_r	ρ	Z_1	Z_s	Z_r
Units	mm/µse	mm/µsec	mm/µsec	mg/mm^3	$Mg/mm^2µse$	$Mg/mm^2µse$	$mg/mm^2µse$
Aluminium	6.42	3.04	2.87	2.7	17.3	8.2	7.7
Brass	4.7	2.11	1.99	8.6	40.6	18.3	17.1
Steel	5.94	3.25	3.03	7.8	46.5	25.4	23.6
Nylon	2.62	1.07	1.01	1.11	2.86	1.18	1.12
Lucite	2.68	1.1	1.04	1.18	3.16	1.3	1.23
Water	1.5	-	-	1	1.5	-	-
Air	0.33	-	-	0.00123	0.0004	-	-

Table 6-2 Acoustic velocities and impedances for longitudinal, shear, and Raleigh waves for several materials (Beattie 2013)

The path of particle under the influence of an acoustic wave can be represented by an ellipse with one of its axes leaning along the direction of the wave's move. The type of wave in immensity materials is determined by the affiliation between the average particle motion and the path of travel of the wave. In materials with boundaries, the exact information of the wave and element motion will be determined by its materials properties, geometry of the sample, and the frequency. (Beattie 2013)

The wave packet (few waves) will alter shape while it travels through the medium so in result, the same acoustic emission may look quite different when detected by the same sensor at different positions. Energy in a wave packet travels at the group velocity. The phase velocity can be defined by:

$Vp = \omega/k$ Equation 6-3

The wavelength is proportional to the velocity of the wave and inversely proportional to the frequency of the wave so a change in frequency will result in a change in wavelength.

6.2.1 ATTENUATION

It is necessary to understand the numerous mechanisms by which the wave energy is intensity diminishes with distance in order to forecast how AE signals can be affected. During the propagation

of AE signal the energy of an acoustic wave is attenuated by several effects. This causes a reduction of the amplitude.

The absorption during the propagation is mainly due to internal friction, losses related to velocity, thermal dissipation and molecular absorption. The inner friction depends on the viscosity of the medium, which add a damping factor to the equation of wave propagation. The thermal dissipation plays a crucial role due to the transient changes, induced by the passing acoustic wave. These waves induce an oscillation of temperature, which can lead to an irreversible energy loss. The molecular inclusion becomes visible during the excitation of the molecules by the wave. The velocity of the energy transfer is a finite value for different degrees of freedom of a molecule. If the waves' frequency matches this relaxation velocity, it leads to an energy loss. Moreover, this effect can change the propagation velocity, which is known as dispersion.

Attenuation of acoustic waves occurs when sound intensity diminishes with its travel distance. Because AE on a ball nut comes from a point of contact and its event rather than a line or an area, the stress wave should propagate as a differing spherical wave. In a consistent medium attenuation normally occur as a fixed percentage of the wave packet energy for each unit length of travel. Scientifically stated by Beattie (2013) this is an exponential decrease in the AE wave amplitude with its traveling distance:

$$A = A_0 e^{-\alpha x} \text{ or } A = A_0 \exp(i\beta t) \qquad \text{Equation 6-4}$$

α - attenuation constant per length,

β - attenuation constant per time.

The two constants are connected by the acoustic velocity:

$$\beta = \alpha V \qquad \text{Equation 6-5}$$

6.2.2 MOUNTING SUMMARY

The AE sensor supplied with preamplifier and noise shielding should be placed as close possible to sensing element. Effective acoustic coupler should be used. Electronic noise directly degrades the detection capability and cable capacitance reduces the signal strength therefore full shielding is mandatory. Acoustic waves diminish in intensity when sound travels through a medium, a distance-attenuation equation is delivered therefore sensor needs to be placed close to source.

6.3 CALIBRATION SOURCES FOR ACOUSTIC EMISSION SYSTEMS

Changes in either the apparatus or the coupling methods can create a very different AE response. AE results obtained from different research centres are not easy to equate making information transfer hard to achieve. To allow transferability of results, various methods of AE calibration are necessary. The procedure of calibration includes a measurement process carried out under specified conditions. Its objective is to make the connection between the value of a quantity as showed by a measuring instrument and the equivalent value from a reference standard. The result of the measurement should be finally related to a stated reference, such as an international standard. (Beattie 2013). To calibrate an AE transducer artificial AE source is needed. AE sources can be classified as:

- **Continuous waves** - generated by exciting piezoelectric, electro-magnetic and electro-static devices;
- **Noise** - produced from, gas jet impact, fracture of silicon particles, stress corrosion cracking;
- **Impulses** - occurs from sparks, breakage of glass capillary, fracture of pencil lead, impact dropping of a steel ball on a hard surface, direct contact resistive heating and laser pulse.

The method for absolute calibration of AE sensors is presented in ASTM E1106 (2015).The standard recommended three main artificial AE sources: a PZT sensor, a gas jet and an impulsive source created by breaking a pencil lead.

In this project, capillary breakage and an air jet were assessed in reference to their suitability as a calibration source for CNC drive system monitoring. Practitioners need a simple method to calibrate an AE system under conditions like to those observed during an experiment or monitoring application.

Nearly ideal transducers *like* laser interferometer, a capacitive transducer and a conical transducer are not useful in industrial applications due to cost and practical limitations. Short review of methods and sources is as presented below.

6.3.1 BREAKING PENCIL LEADS

An acoustic emission calibration method was developed by Nielsen (1980). This involves breaking a 0.5 mm 2H propelling pencil lead like it's presented on Figure 6-5. This generates an intense acoustic signal, quite similar to a natural AE source, which the sensors detect as a strong burst.

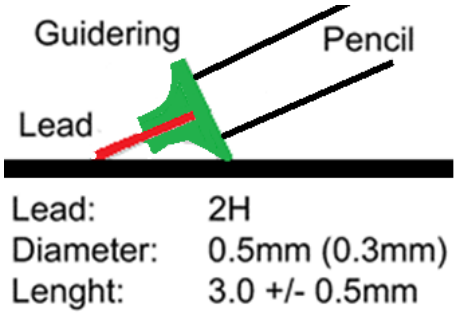

Figure 6-5 Hsu-Nielson Source

A simulator has been adopted as a standard by ASTM (2015) Standard E1067-85.

6.3.2 FRACTURE OF A GLASS CAPILLARY

Burks (2011) used a short length of thin-walled 0.2mm glass capillary to fracture against a large steel cylinder in order to generate an acoustic waveform used for calibration of the sensor. He slowly compressed a tube to failure by a threaded indenter, as a source of standard events (Figure 6-6). When a sufficient force was applied to a glass capillary, a crack was initiated and propagated along the circumference of the glass capillary with a certain propagation velocity. The glass capillary breakage source might be a ramp force with two parameters, rise time and strength. The waveform takes the form of a pseudo-delta-velocity function with a relatively flat frequency range from 50k - 1MHz

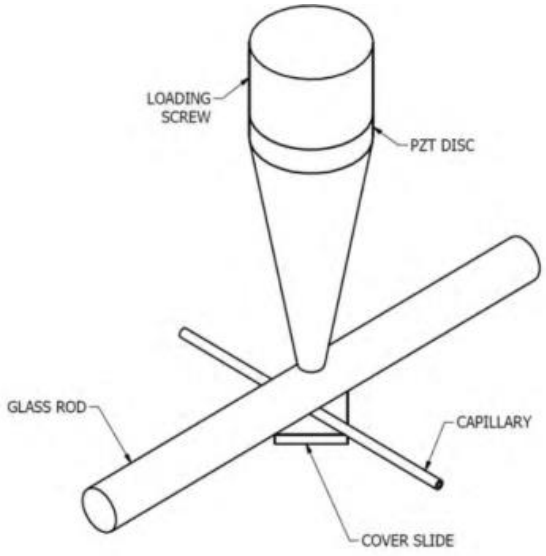

Figure 6-6 Glass capillary AE calibration method (Burks 2011)

Further Hamstad (2011) has studied number of source parameters relating to the fracture of the glass capillary source like value of the rise-time of the force release, temporal shape of the force release, spatial size and spatial distribution of the normal stress on the block surface, and the magnitude of the

force. He has noticed that changes in the spatial distribution and spatial size of the normal stress source from the glass capillary result changes the Rayleigh wave peak amplitude. Changes in the temporal rise time and shape also result in changes in the Rayleigh wave peak amplitude

6.3.3 BALL DROP

AE sensor energy can be calibrated by steel ball drop. McLaskeyet et al. (2012) describes sensor calibration and signal analysis techniques applicable to the method of acoustic emission (AE) and ultrasonic testing. They have illustrated how to perform calibration tests on a thick plate and how to implement two different mechanical calibration sources: ball impact and glass capillary fracture. In this way, the instrument response function can be estimated from theory, without the need for a reference transducer. Author uses a tiny ball dropped onto the surface of the sample as a reference source, or empirical Green's function (EGF). The principle advantage of the ball impact source over other potential EGF sources such as fracture of pencil lead or capillary tube, or piezoelectric pulses, is that the absolute amplitude of the seismic waves can be linked to the momentum of the ball, which is directly measured or easily estimated from the ball mass and drop height. The method relies on a number of simplifications and approximations, but because it does not require the practitioner to model wave propagation or sensor response, it is far simpler than alternative techniques.

6.3.4 OTHER CALLIBRATION METHODS

Helium gas jet

The advantages of the helium gas jet calibration are simplicity, portability, ease of use. It does not create a transient pulse like a real acoustic emission. Continuous AE signal allows direct comparison of system sensitivities in the range 0.2-1 MHz, for any type of signal handling equipment. The magnitude of the resonance peak increase with the air pressure. The distance between the centre of the nozzle and the transducer attenuate the height of the peak. From the preliminary test, the air jet as an artificial AE source holds great promise. (Beattie 2013)

Electric spark discharge

Electric spark discharge source AE calibration method consists of generates a spark wave in air. Absolute calibration of a transducer requires calibration of the spark source against the golden standard.

The reciprocity technique

This method is established on the reciprocity source for electric systems. System is assumed to be reciprocal, if it is reversible. Piezoelectric sensors can be used as a transmitter and receiver. Under certain conditions, this principle is be applied to acoustic measurements and allows to calculate the sensitivity of an acoustic sensor without using any absolutely calibrated reference. The sensors are

calibrated to a “golden standard”. The test setup includes two sensors is similar to the one shown in the power point. The signals are compared and as long as the test unit is within tolerance ~90-95% they are cleared.

6.3.5 SYSTEM CALIBRATION CONCLUSION AND RESULTS

Keprt (2009) reviews the background, the methodology and the standardization of the primary calibration of acoustic emission sensors. He discusses the aims and the purpose of the primary calibration.

The basic problems of calibration are:

- Material displacement of a point at the surface
- Sensor loading effect
- Function is not only dependent on time but also on the position within the measurement area of the transducer.
- Sensor need to be mounted in the same location, using same couplant
- Pencil lead breakage is not repeatable and requires experience for a clean signal to be produced.
- Air jet system is good option but it is necessary to develop the jig to locate and control the air flow
- Calibrated sensor still does not indicate that the results of an acoustic emission experiment will be reproducible therefore uncertainity needs to be predicted.

To qualify as an AE calibration considerations like safety, cost and ease of use should be included. Table 6-3 provides a comparison of different AE calibration sources.

AE CALIBRATION SOURCES	CONVENIENCE	COST	PRACTICALITY	SAFETY
PULSED LASER				
BALL DROPP				
BREAKING PENCIL LEAD				
GAS JET				
FRACTURE OF GLASS CAPILLARY				
THE RECIPROCITY TECHNIQUE				
ELECTRIC SPARK DISCHARGE				

Table 6-3 Methods of calibration-comparison (Beattie 2013)

From there are noticeable better sources. Convenience refers to the ease with which the system can be set up and used. Cost includes both the set-up cost and the operating cost. Safety means the lack of hazard to operators, machines and the environment. They are the breaking pencil lead, the breaking

glass capillary. Since lead pencil break is the low cost basic calibration method used to calibrate sensor for calibration of the AE for ballscrew application. (Beattie 2013)

To succeed transferability of results some method of AE calibration is necessary. The process of calibration includes a measurement procedure carried out on the machine tool under steady conditions. Its objective is to make the connection between the value of a quantity as showed by a measuring instrument and the equivalent value from a reference standard. It is necessary then to carry out the calibration of the AE energy for each installation. Pencil lead breakage was evaluated in reference to their suitability as a calibration source for drive system monitoring. The lead has been broken on the nut housing. Acoustic emission signal gives good fast response when the sensor is placed directly on the machined face of the nut. The registered by the equipment AE signals are characterized by two fundamental parameters: the amplitude and the time of signal duration. Print screen of the results is presented on Figure 6-7.

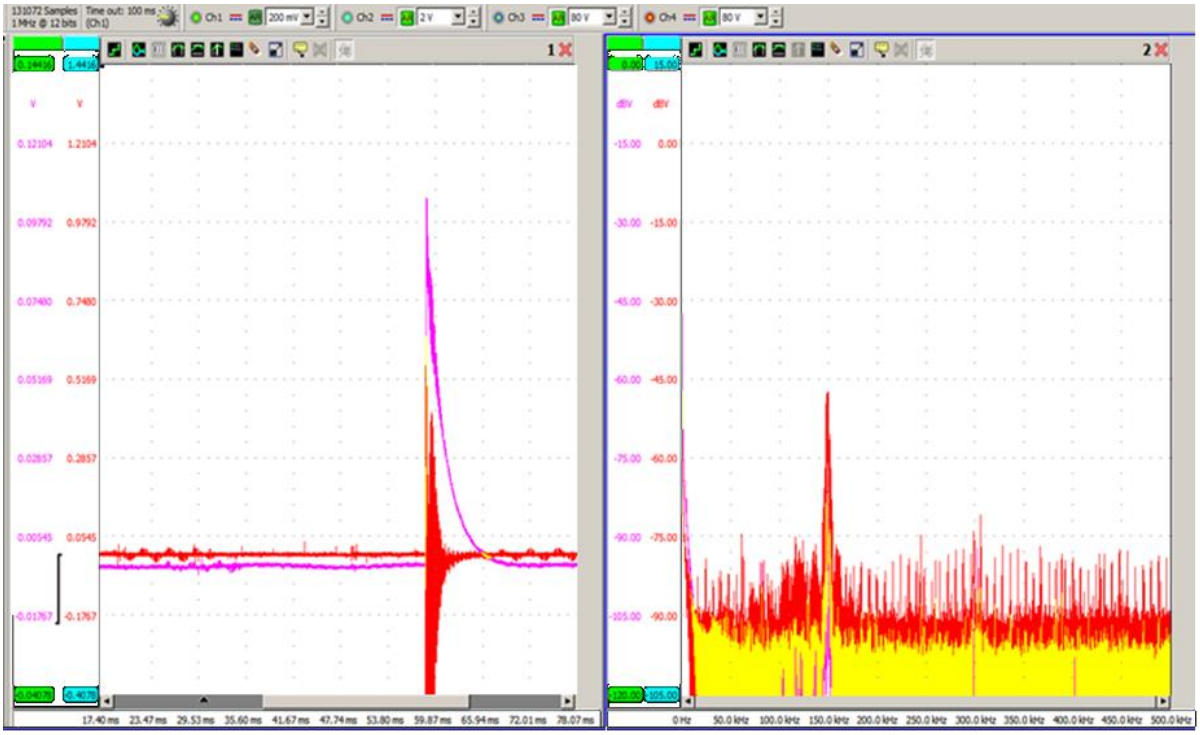

Figure 6-7 Pencil lead break calibration results

6.4 BAYESIAN UNCERTANITY APPROACH

Uncertainty analysis in metrology has been adapted in accordance with the Guide to the Expression of Uncertainty in Measurement (GUM). Is now revised and published by the BIPM GUM (2012) and it defines measurement uncertainty as a parameter that characterizes the dispersion of the values that

might sensibly be qualified to the measurand". It is recommended that measurement uncertainty "reflects the lack of exact knowledge of the value of the measurand". The corresponding state of knowledge is best described by means of a probability distribution over the set of possible values for the measurand.

At this stage, the degree to which factors impact the accuracy is now discussed. The types of uncertainties associated with the limited knowledge of system dimensions and material characteristics, mounting are being considered. Suitable reflexion of uncertainty are essential for carrying out precise estimation.

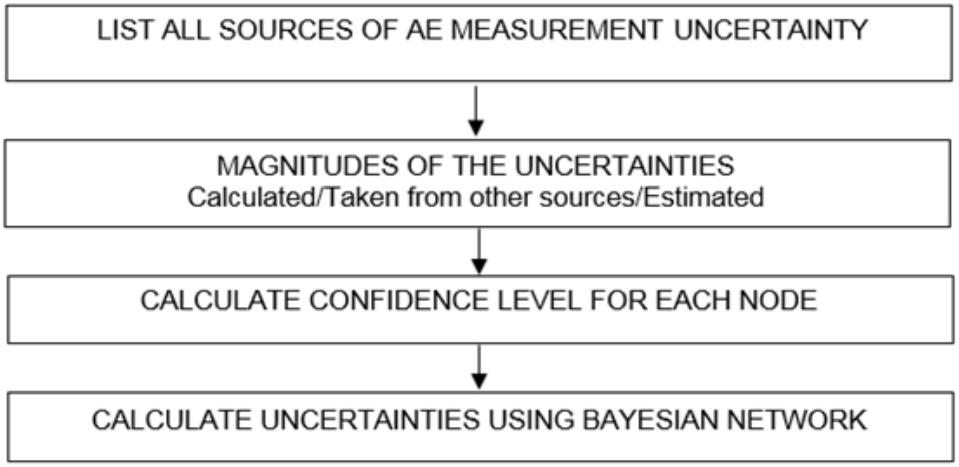

Figure 6-8 Bayesian approach steps

In order to understand AE waveforms Bayesian estimation for AE sensor and system is developed. The Bayesian approach is more complete, universally applicable and more philosophically reliable than the classical approach BIPM GUM (2012). Figure 6-8 shows steps to determine the probability of uncertainties in measurements.

6.4.1 FACTORS THAT INFLUENCES ACOUSTIC EMISSION RESPONSE AMPLITUDE

Measurement uncertainty in AE signals express incomplete knowledge and deviation in the signal. In a typical inspection measurement, the signal is measured using a procedure designed in BIMP GUM (2012) which introduces the likelihood function. This function depends on the specific measurement problem and the measuring system uncertainties.

Factors that influences acoustic emission response amplitude	Influence
Strength of coupling material	High
Ballscrew strain rate/load	Actual results
Sensitivity to the temperature	High
Material discontinuities (Cast materials, air bubble etc...)	Medium
Marten site phase transformations (location of the event)	Medium
Material properties changes	Low
Aperture Effect	Low

Table 6-4 Factors that influences the AE signal energy

Miller (1987) has described some of the factors that influence AE response. Table 6-4 Factors that influences the AE signal energy in ballscrew system. Used approach corresponds to belief that calibrations are identify and inconsistent data eliminate.

6.4.1.1 TEMPERATURE

Special problems are met when PZT material encounter temperature changes. Young's modulus, piezoelectric properties, damping and pyro electric effects are influenced by temperature. AE sensors perform detection by measuring the high frequency energy signals emitted by the contacts between nut and ballscrew. Probability distribution over the possible values for the measurand has been used to represent the knowledge about temperature.

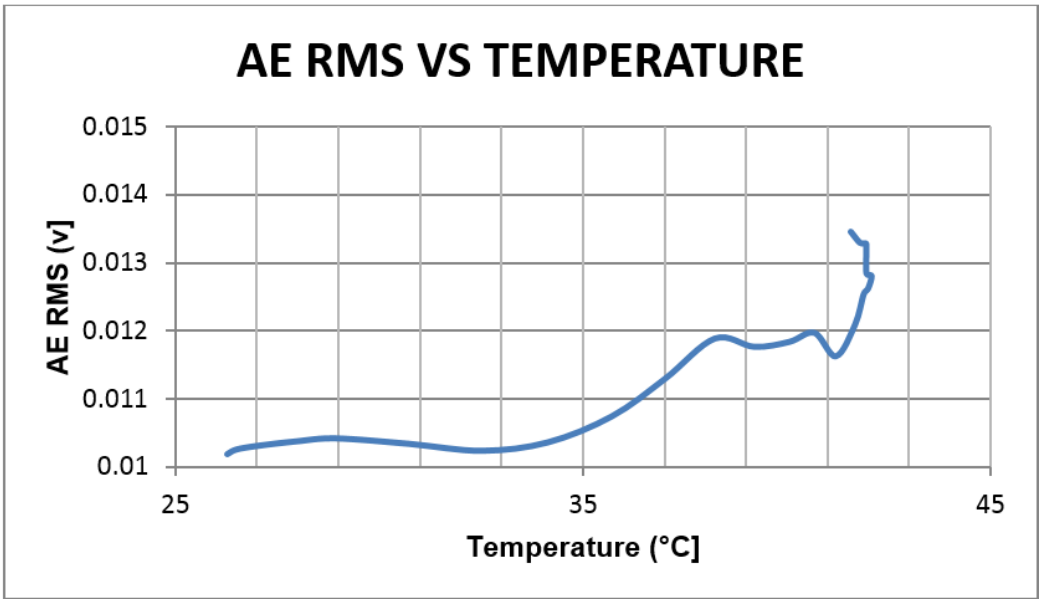

Figure 6-9 Temperature test results

Temperature tests has been prepared to recognize how it influences the reading. Effects are represented in Figure 6 – 9 where the piezoelectric properties change by a maximum of 31% over the temperature range whereas the elastic properties change significantly over the given temperature range. Raghavan et al. (2007) concluded that the amplitude drops significantly with temperature but there is negligible shape distortion. Because the test has been conducted in a short time, there is high possibility of issue that as the temperature of the element (ceramic, quartz, etc.) increases the output signal is going to change. The transfer of heat from the housing to the internals takes time and it takes longer for the element to stabilize.

6.4.1.2 APERTURE EFFECT AND AE EVENT LOCATION

When the displaced surface is a Rayleigh wave, then there are occasions when one or more full wavelength will match the diameter of the piezoelectric element. When this occurs, the average movements may give a zero output. This effect, called the Aperture Effect, has been carefully measured by Keprt (2009).

The output voltage is described as follows:

$$U(t) = \frac{1}{A}\int_S^\infty \int u(x,y,t)r(x,y)dydx \qquad \text{Equation 6-6}$$

Where $r(x,y)$ the local sensitivity of transducer is face in S region in (m^2) and $u(x,y,t)$ is the displacement (m) on the surface (Theobald 2016)

In real life one sensor may identify multiple AE signals coming from different AE sources as one AE event The situation that AE event is created by multiple AE is not considered (Figure 6-10) otherwise it would create incorrect test result. In order to improve the measurement accuracy, an AE event determination method based on using a few AE sensors should be used. It is too expensive to include sensor clustering, so Bayesian uncertainty estimation becomes crucial.

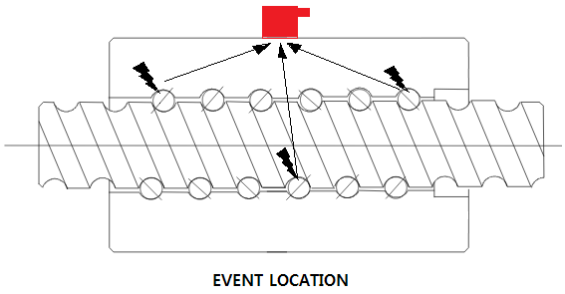

Figure 6-10 Multiple AE sources

AE cluster is a set of AE sources that take place close in the same position on one structure. A growing damage should in theory generate a sequence of emissions. Errors in the arrival times, resonant, noise can emerge as a cluster of sources. It is difficult to define the clusters during the test. The actual starting

place of those emissions may be a localized and that defines a cluster. The occurrence of an AE cluster shows a region on the ballscrew that is generating AE.

6.4.1.3 ATTENUATION AND COUPLING UNCERTAINTY

Loss of AE energy has several causes but invariably results in creating uncertainty in the signal measurement. It has been described in Chapter 6. Received signal will have lower amplitude than the signal generated on the ballscrew or the nut.

Attenuation properties of distance in an ideal system is described by equation:

$$PAE_2 = PAE_1 - 20log\left(\frac{R_2}{R_1}\right)^2 \qquad \text{Equation 6-7}$$

Where PAE_1 is the AE Power Level at distance "R1" from point of origin and PAE_2 is the AE Power Level at distance "R2" event origin. The acoustic impedance mismatch between the sensor and the nut is included in probability model.

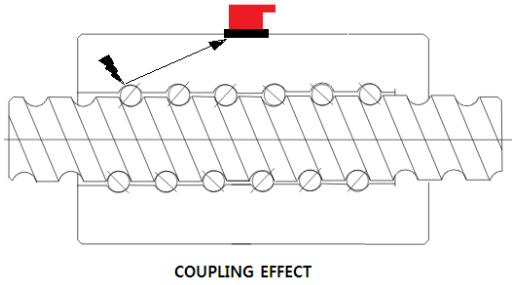

Figure 6-11 Attenuation and coupling effect

A coupling layer is essential between the measuring element and the AE sensor (Figure 6-11). Air for has an acoustic impedance by 5 orders of magnitude lower than the metals and polymers, and ceramics from which the sensor elements, nut are made.

6.4.1.4 BALLSCREW STRAIN RATE LOAD AND MARTENSITIC PHASE TRANSFORMATION

Martensitic transformation is a true and energetic source of acoustic emission and is caused by the change of crystal structure is accommodated by a so-called "diffusion-less" shear transformation. Diffusion, if it occurs, is over a very short range; of the order of the lattice parameter.

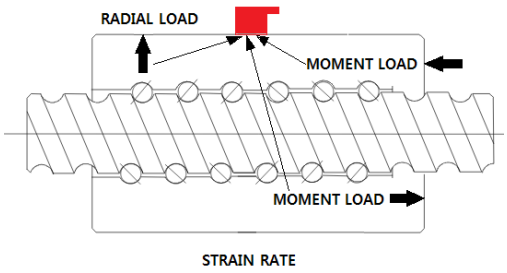

Figure 6-12 Strain rate load and martensitic phase transformation

When there are mowing errors or distortion forces may be generated between the screw shaft and the nut, as illustrated on Figure 6-12. This could cause the shortened service life, generate of low frequency noise or vibrations

6.4.1.5 NOISE UNCERTAINTY

Machine shop area can produce unexpected sources of electrical noise Figure 6-13 which are problematic because AE is looking for high frequency wide band signals in microvolt level. That's one of the main problems in direct measurement of ballscrew is the considerable level of disturbing acoustic emission produced by other components of the transmission. AE signals occur randomly and have no definite characteristics. Unwanted noise must be distinguished from events associated with ballscrew damage. Probability of noise in detecting damage in the ballscrew and the stage needs to be included.

This causes uncertainty when measuring the sound power. Many electronic methods of noise reduction are not possible so it's necessary to will include noise as a factor. The signal-to-noise ratio is U(f)

Where Vs and Vn are the signal and noise, respectively. A bandwidth is usually given for SNR

$$snr(t) = \frac{Vs}{Vn}$$ Equation 6-8

The SNR should be calculated before the start of the system

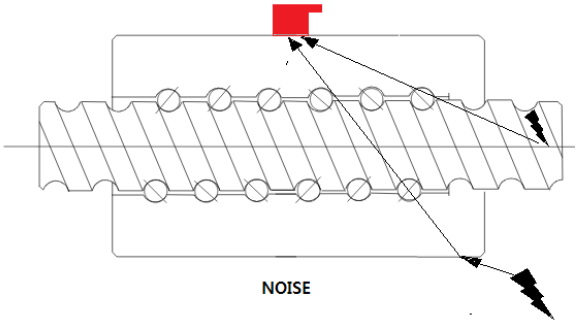

Figure 6-13 AE noises

Electromagnetic signals looks like short, spiky signals which last less than milliseconds. Kurtosis analysis is a good method to recognise them. Filtering is a method to avoid this without removing any important acoustic signals.

The main sources of noise generated by a transmission system have been identified as:

- impact sound, which is generated by collisions
- sound due to transverse vibration of machine;
- noise generated by the pulley vibration;
- noise due to ejection of air between belt and pulley;
- various frictional noises.

6.4.2 UNCERTAINTY CALCULATION

Keprt and Benes (2009) present and describe the influence of the main sources of the uncertainties. They found that the main source of uncertainty is the accuracy in the measurement of amplitude of their signal analyser.

Source of uncertainty	Uncertainty (%)
Temperature	8.1
Time stability of couplant	1.6
Mounting method/couplant	17
Remounting sensor	31
Sensor characteristics- Sensitivity	5
Incorrect placing the sensor	21.7
Wave travel path	10
Geometry	8

Table 6-5 Comparison influences on uncertainty of various sources in reciprocity calibration

Table 6-5 Comparison influences on uncertainty of various sources in reciprocity calibration. First shows influence of temperature. Second is obtained by leaving sensor for a few days. Third shows the influence of couplant and mounting method. One of the largest influences was the remounting of the pair sensor showed in fourth row. Fifth shows the sensor characteristic by approximating the sensitivity. Sixth shows the influence of incorrect positioning on the surface. Seventh and eighth estimates wave travel path and its system geometry.

6.4.2.1 WHOLE SYSTEM TRANSFER FUNCTION

AE waveforms are obtained as convolution of functions of source (seal face friction), propagation media (attenuation from source to sensor), sensor (frequency and dB sensitivity) and acquisition system (baseline noise) in the time domain,

$$X(f)= D(f)*T(f)*S(f)*Y(f)-U(f) \qquad \text{Equation 6-9}$$

X(f), are Fourier transforms of detected AE waveforms,
S(f), AE source,
D(f), propagation media,
T(f), sensor transfer function linearized by narrowing frequency and adding temperature factor
Y(f), acquisition system,
U(f) is a transfer function which represents ratio to determine noisier seal
Respectively. *S(f)* in is the target to quantify the damage using PM data driven equation

For each AE energy is associated with a standard deviation. If ballscrew test is repeated several times, a number of mean AE energy values would be obtained and these mean values would themselves show a small random variation. It is then possible to estimate the standard deviation of these mean values using the following equation:

$$u_c(m) = \frac{1}{((n)^{1/2})s(x)}$$ Equation 6-10

where $u_c(m)$the uncertainty of the mean and provides a measure of the width of the distribution of mean values that would be expected and s(x) is the standard deviation. (Mukhopadhyay (2012))

6.5 BAYESIAN UNCERTAINTY ANALYSIS

Uncertainty analysis in metrology has been accomplished in accordance with the Guide to the Expression of Uncertainty in Measurement (BIPM GUM 2012), which has led a revolution in uncertainty analysis in metrology. The GUM originally published by the ISO has increased emphasis on the specification of a measurement model and to quantifying influence variables and sources of uncertainty. It fails to give satisfactory guidance on the handling of non-linearity's and corrections of systematic effects, products of errors distributed about zero, asymmetric error distributions ,and multidimensional outputs such as for complex quantities. So GUM can be look at as a good set of guidelines. The Bayesian approach is claimed to be more complete and more philosophically consistent than the classical approach. (BIPM GUM 2012)

Numerous developed procedures differ in computational simplicity of algorithms have been researched and theoretical parameter estimation is used.

In its simplest form Bayes' theorem are defined as follows:

$$Pr(A|B) = \frac{Pr(B|A)Pr(A)}{Pr(B)}$$ Equation 6-11

• A is the vector of parameters to be estimated - probability if sensor is faulty.

A= {Pt,Pi,Pm}.

• $Pr(A)$is the prior distribution of model parameters.

•B denotes the set observations to be used in the updating process.

•p (B) is the marginal probability of B, and acts as a normalizing constant.

• $Pr(B|A)$is referred to as the likelihood function, as it describes the conditional probability of observed data given the model parameters.

When the probability distributions involved are continuous

$$Pr(A|B) = \frac{Pr(B|A)Pr(A)}{\int(Pr(B|A)*Pr(A)dA)}$$ Equation 6-12

The denominator is simply a normalising factor in this case whole equation can be described like posterior probability ∝likelihood function×prior probability

Where A represents having the disease, B represents testing positive for the disease

It is easier to carry the equation numerically so *Bayesian software* has been used to calculate probability using advanced algorithms. Bayesian network is proposed to dynamically monitor the sensor uncertainness condition a DBN. Figure 6-14 shows the created representation of the system in Bayes software (2015)

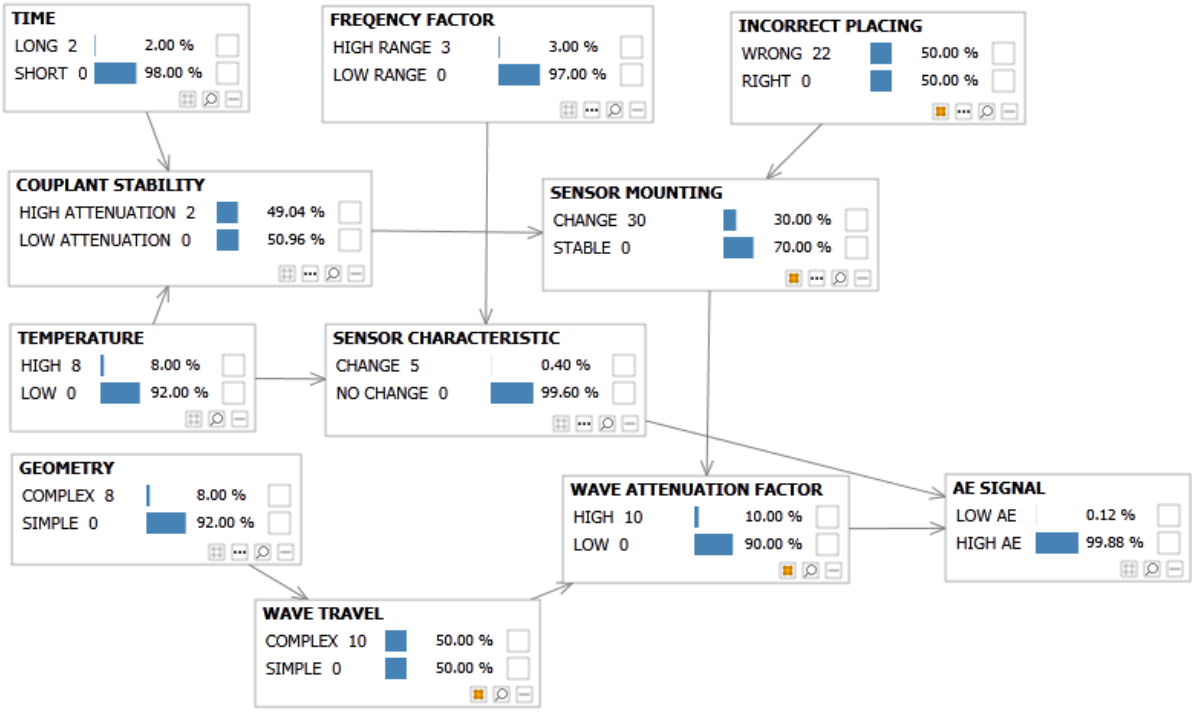

Figure 6-14 Bayesian network for sensor uncertainty condition

Acceptance limit probability rules are chosen following BIPM (GUM 2012) standard as to manage the undesired consequences of incorrect decisions Decision is based on measured percentage values. The true value of a measurable property of an item is specified to lie in a tolerance interval defined by limits (TL; TU). The item is accepted as conforming if the measured value of the property lies in n acceptance interval defined by limits (AL;AU) its discarded as non-conforming otherwise.

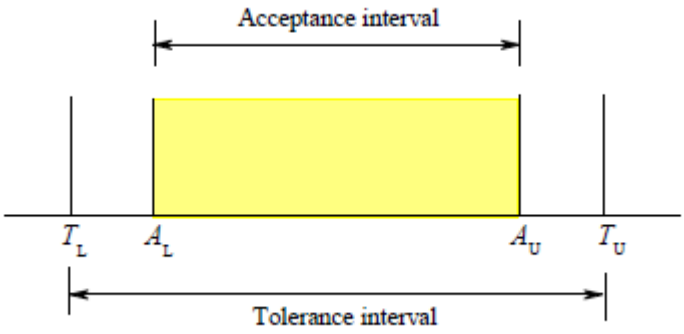

Figure 6-15 Confidence probability (BIPM GUM 2012)

In conformity assessment, a measurable property is considered as a random variable with possible values denoted by uncertainty. Signal sensible belief in its possible values is characterized by a BAYES model whose form is independent of the measuring system. According to Figure 6-15, if the whole measuring system was accurate then and all risks would be zero. Increase in probability percentage is proportional with an increase in measurement uncertainty and that measurement is incorrect. Probability is greatest when measured values are close to the tolerance limits. Unknown values have been estimated then probabilistically assessed the response of the whole sensor system. Gaussian standard uncertainty corresponds to a confidence probability of 92.8%.

6.6 SUMMARY AND CONCLUSIONS

Keeping CNC machine tools accurate and in best condition is important to produce parts to tight tolerance. Condition monitoring sensors are used to develop automated, unmanned manufacturing systems. This chapter has included a description of how acoustic emission waves spread in solid materials and how temperature affects the guided waves. By recognising that the acoustic waves diminish in intensity when sound travels through a medium, a distance-attenuation equation is delivered.

AE sensor has been found to give valuable results only when the mounting is correct. It's necessary to include all environmental effects which can interfere the signal. In more practical environment like shop flor the application of acoustic signal may not possible due to high noise level and signal processed by filtering and useful information. On other side AE high frequencies can inhibit the low noise interferences effectively therefore improve diagnosis. The use of acoustic emission systems enables user to limit maintenance check-ups.

AE uncertainty probabilistic risk measurement based on information from the tests and literature has been developed. Bayesian fusion was demonstrated. Most of the outcomes of this Bayesian estimation and methodology are standard so general and can be applied to other systems. The presented method

should be very effective in identifying false readings therefore Bayesian approach is claimed to be more complete and more philosophically consistent than the classical approach therefore has been used to calculate the risk off acquiring validate results. Estimating the uncertainty associated with the AE measurement will reduce the likelihood of creating an incorrect decision.
The part of development is Bayesian uncertainty assessment to evaluate the uncertainty related to the estimates obtained from measured data.
Calibration of the AE sensor needs to be done in order to validate sensibility of the sensor. Various calibration techniques has been tested. Both caterpillar method and pencil lead breakage can be used to validate the mounting of the AE sensor. During the initial tests various couplants has been used. A silicon compound has been chosen for this application to machine tools because it provides good stability in measurement- temperature, rigidity where vibration can occur and good resistance to link breakdown where surface movement can take place and provides outstanding transmission with a relatively strong bond.
A Bayesian network is proposed to dynamically monitor the sensor uncertainness condition of dynamic Bayesian networks (DBN). Estimating the uncertainty associated with the AE measurement will reduce the chance of creating a wrong decision by ensuring that trigger actions are only taken when a measurement conforms, within a high confidence factor.

The result of the measurement are related to a Guide to the Expression of Uncertainty (GUM) (BIPM GUM 2012) and AE calibration. In reality, errors and uncertainties are always unavoidable in the measurement process. Details of the experimental setup and procedure to determine uncertainties are explained. A statistical Bayesian model is developed to describe the relationship between the uncertainty parameters.

By combining the reference model approach developed in previous chapters with AE sensing that has been evaluated and described in next chapter, a systematic approach to the condition monitoring of precision machine tools can be achieved. Cumulative failure data are considered as a health report of ballscrew system.

CHAPTER 7 MONITORING THE DEGRADATION OF A BALLSCREW DURING MACHINE OPERATION USING AE SENSORS

The most frequent reason for failure of a ballscrew is high load or dry running, usually recognized at the last minute by a fault flagged by the control system, by dimensional inaccuracy or bad machined surface finish. This is caused by gradual degradation of the metal atomic surface of the balls in the nut race and the metal surface of the ballscrew shaft. This frequent interaction over a long period of time leads to a deterioration of the metal surface and wear. This wear is exacerbated due to impact force and vibration during machining.

As a feed drive condition worsens the atomic fragments enters the ballscrew lubrication system and spread across the whole length. Lubrication has a massive impact on the lifetime of the ballscrew. Unfortunately over-lubrication can also be problematic - too much oil can cause rise in pressure in the return system. Other cause is misalignment of the gantries, other is catastrophic failure due to an exceptional force due to shock load or crash.

Acoustic emission (AE) monitoring has been used as the technique to monitor the feed drive system. Periodical check the ballscrew system with AE can detect changes in energy due to abrupt excessive load and rapid deceleration. The results obtained in this chapter suggest that features extracted from properly filtered AE signals can be correlated. This thesis section seeks to identify the defect as soon as possible. An added machine intelligence to allow for easy detection of features changes in the machine operations are described in next chapter.

The experimental data generated in this chapter will be used to infer the parameters of CNC model. Once the hardware in the loop model is fully developed, it will be used to investigate the ballscrew condition and the AE parameters used for it.

7.1 ACOUSTIC EMISSION SIGNAL & FEATURES

Feature extraction is a significant subject in sensor-based condition monitoring of systems. The frequency response function (FRF) results from the solution of the differential equation of motion for the Single-degree-of-freedom (SDOF) system. This equation is obtained by setting the sum of forces acting on the mass equal to the product of mass time’s acceleration. Acoustic emission signals were first collected during feed drive movement operations, next enveloped and processed.

7.1.1 ACOUSTIC EMISSION FREQUENCIES

The AE signal frequencies cover a wide spectral range varies between 50 to 500 kHz in metals. High pass filter needs to be used to restrict a low frequency around 20 kHz to exclude much of the unnecessary noise produced by machine. The low pass filter is usually determined by the test. Typical frequency are used with metals, and lower range - 20 to 100 kHz with composites.

7.1.1.1 SPECTRAL ANALYSIS

Spectral analysis has developed from heat conduction studies performed by Jean-Baptiste Fourier in nineteenth century. Fourier was capable to get a solution for his temperature flow problem in the form of trigonometric series.

The discussion of data acquisition concept of spectral analysis when aliasing and windowing were explained by Beattie (2013) hinting that the knowledge of the frequency content of a signal was important. Frequency spectrum displays information will often reveal details of signal that are too subtle to observe in the time domain, in spite of the fact that the frequency spectrum of a signal has no more information in it than the time domain signal. This analytical power of spectral analysis makes it an attractive technique for characterizing acoustic emission signals because each source mechanism should have characteristic frequency spectrum based upon its size and speed of operation.

7.1.2 AE FEATURE

Main acoustic emission characterization parameters and application are described shortly in table 7.1

PARAMETER	MEANING
HIT	Signal over a threshold
EVENT	Regional change emitting AE
RINGING	Times of oscillation near threshold
AMPLITUDE	Maximum AE waveform value
RMS	Root mean square value
ASL	Mean during sampling time
DURATION	Time of event
RISE TIME	Time to reach maximum amplitude
COUNTS OF PEAK	number of times the acoustic emission signal surpasses threshold
AE SIGNAL DURATION	last crossing of the threshold by signal
AE SIGNAL RISE TIME	between AE signal start and the peak amplitude
AE SIGNAL START	the beginning of an AE signal as

Table 7-1 Acoustic emission terminology

7.1.3 THE PARAMETERS ANALYSIS OF AE SIGNALS

Parameter analysis is a method related to the full waveform analysis method. This time based analysis has many advances such as the RMS, rise time, amplitude, peak, duration value average, standard deviation, skewness, and kurtosis are included in work.

7.1.3.1 MAXIMA AND MINIMA

The maxima and minima of a function are the biggest and smallest values of the function, either within a given range or on the entire domain of a function. Limitless sets such have no minimum or maximum.

7.1.3.2 ROOT MEAN SQUARE

Mathematically the root mean square of the raw AE signal is calculated by Equation 7.1

$$AErms = \sqrt{1/\Delta T \int_0^{\Delta t} AE^2(t)dt \sum_{i=1}^{N} AE(i)^2} = \sqrt{1/N \sum_{i=1}^{N} AE(i)^2} \qquad \text{Equation 7-1}$$

Where:

ΔT - integration time constant and

N -the number of discrete AE data within time ΔT.

AE RMS is obtained digitally by calculating with a chosen ΔT according to the equation. There is no general rule in selecting suitable ΔT to obtain AE RMS, however has been found that ΔT=10ms delivers a reasonable resolution for current research.

7.1.3.3 MEAN VALUE

The mean value is used synonymously to one measure of the dominant tendency either of the random variable characterized by that distribution. The mean of variable X is equal to the sum over every value weighted by the probability of that value given by equation:

$$MEAN = \mu = \frac{1}{N} \sum_{1}^{N} x \qquad \text{Equation 7-2}$$

N - the number of data points

X - the data at each point in time.

7.1.3.4 VARIANCE

Variance measures spread out set of numbers. A variance of zero specifies identical values. Variance is always positive. The variance is a parameter that describes an observed population of numbers by equation:

$$VARIANCE = \frac{1}{N}\sum_{1}^{N}\left[x_i - \mu\right]^2$$ Equation 7-3

7.1.3.5 STANDARD DEVIATION

Standard deviation (SD) is a measure that is used to quantify the amount of variation or dispersion of a set of data values. SD close to 0 indicates data points close to the mean. High SD indicates data points spread out over a wider range of values. The standard deviation of a data is the square root of its variance.

$$\sigma = \sqrt{\frac{1}{N}\sum_{1}^{N}\left[x_i - \mu\right]^2}$$ Equation 7-4

(σ) s-tandard deviation with mean value μ

Unlike the variance, standard deviation is expressed in the same units as the data.

7.1.3.6 KURTOSIS AND SKEWNESS

Kurtosis and skewness are utilized as an indicator to the acoustic emission variations. Sudden changes in the AE signal may result in spikes in these statistics. The Equation 7-5 shows the calculation of an x signal.

$$KURTOSIS = \frac{1}{N}\sum_{1}^{N}\left[\frac{x_i - \mu}{\sigma}\right]^4 - 3$$ Equation 7-5

Similarly, the expression given in Equation 7-6 is used to calculate skewness

$$SKEWNESS = \frac{1}{N}\sum_{1}^{N}\left[\frac{x_i - \mu}{\sigma}\right]^3$$ Equation 7-6

7.2 TESTS ON A BALLSCREW NUT

Distinguishing between different AE sources imposed many limitations of the tests. Largest possible bandwidth has been used to record the data in order to acquire the maximum data baseline to extract the signal features.

The main objectives of the preliminary test are:

- To measure noise released from the surrounding.
- To understand the limitations of the equipment.
- To select the continous time interval to record data and measure the progression of ballscrew events.

- To eliminate the level of acoustic emission background noises.

There are a number of experimental approaches and processing methods used to characterize damage using AE, such as:

- Apply calibration factors to attenuate the dependency on variations between data acquisition units and their amplifiers.
- Apply normalization factors to attenuate the effects of operational variations or configuration changes; e.g. normalize the effects of changes in speeds, temperatures, loads, weights, etc.
- Derive a synchronized average signal from the raw signal as follows: a machine tool signal obtained using servo trace measuring software is used to produce a synchronous signal.
- Derive envelope spectra: If a signal consists of high frequencies whose amplitudes change at a low frequency over time, the envelope is the low frequency signal with values corresponding to the peaks of the high frequency signal. It is often calculated as the magnitude of an analytic signal of a band-pass-filtered signal.
- Features extracted from synchronized average signals would obscure ballscrew feed rate faults.
- Envelope detection and amplitude demodulation techniques are used to derive diagnostic features for ballscrew.
- Invert the spectra back to its time domain. Enhanced signals emphasise fault related features and ignore the normal features of shaft and meshing frequencies, which can obscure the fault features.

The raw AE signals received from the AE sensors are analogous with alternating current (AC) signals and this is regarded as not user friendly. The most common initial stage of analysis is to average the raw waveforms to represent smoother dynamic profile of the signal. When averaging techniques are used, it is important to use an appropriate sample length, averaging with too high a time constants will inevitably reduce the high frequency dynamic features of the waveform. Data has been collected for various ballscrews at 5 main constant rotational speeds so that AE signals are excited equally. Laser interferometer has been used for position measurement of the actual position and to interpret it with energy and to show mechanical system imprecisions.

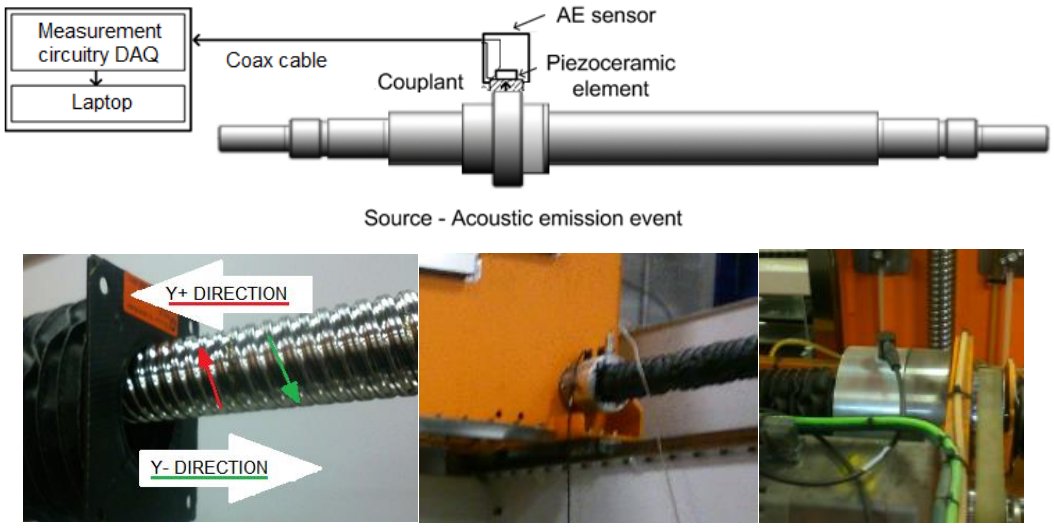

Figure 7-1 Mounting method diagram and actual installation on the Geiss machine

A Geiss CNC milling machine as described in section 2 was used for initial tests. Mounting diagram and sensors locations are presented on Figure 7-1. The machine moving process was automatically controlled by the CNC's native language (G-code program). In order to make a direct comparison of the signals, a trigger has been used to synchronise them in a repeatable manner. While the ballscrew is rotating in steady mm/min the measuring system continuously acquires position and AE data. The analysis of the data was implemented in the MATLAB (Appendix E). Ten feed rates (machining test 1-10) were selected in preliminary tests with the specification as shown in Table 7-2:

	Feed rate (ballscrew mm/min)		Feed rate (ballscrew mm/min)
Machine test 1	2500	Machine test 6	30000
Machine test 2	5000	Machine test 7	35000
Machine test 3	10000	Machine test 8	40000
Machine test 4	15000	Machine test 9	45000
Machine test 5	20000	Machine test 10	50000
Machine test 6	25000		

Table 7-2 Preliminary machine tool tests

Simultaneous AE data acquisition has been conducted at least twice by means of two different AE sensors: wideband ISPK PAC and resonant ISPK15I AE sensor. Two transducers for signal pickup allows a compared analysis to be performed on signals gathered at the same time on both gantry axes.

7.2.1 VIBRATION

Vibration of a machine can be characterised in the time domain in terms of its amplitude measured as acceleration. Further analysis has been be done in frequency domain to find leading frequencies. Vibration signature analysis should determine the general condition of a ballscrew, which is based on measurement of vibration level.

Machine vibration may vibrate quickly, slowly, and with or without perceptible sound. Vibrations in a CNC ballscrew can occur due to the rotation of imbalanced, misaligned, damage, or improperly driven machine nut. An accelerometer has been used in initial test. It is producing an electrical signal that is proportional to the acceleration of the vibrating section where the accelerometer is mounted.

At first, a visual comparison between AE and vibrations signals has been performed. The comparison of the envelope analysis of acoustic emission and vibration signals in order to demodulate and to emphasize the peaks resultant to the shocks shows no clear indication from vibration signals. This result means that viability in using AE for early detection is much better than with vibration signal.

7.3 AE TESTS RESULTS

Numerous techniques such as higher order statistics, etc., could be employed to AE to aid diagnosis. All attempts has been made to keep the method of diagnosis simple so it can be easily implemented in the field. A few main techniques were applied for acoustic emission signals. Simple descriptors were extracted and the results presented in Table 7-3 show the efficiency of acoustic emission technique for detection.

Averaged test results for gantry slave and master axis					
Feedrate (mm/min)	10000	20000	30000	40000	50000
Gantry slave axis Y- **direction**					
Energy Y- axis	1.793	5.063	17.086	30.016	54.214
Kurtosis Y- axis	3.158	5.243	7.138	6.921	5.745
RMS Y- axis	0.004	0.006	0.011	0.014	0.019
Skewness Y- axis	-0.010	-0.007	0.009	-0.009	0.008
Gantry slave axis Y+ direction					
Energy Y+ axis	1.792	6.273	26.768	57.742	91.619
Kurtosis Y+ axis	3.342	5.230	9.710	7.709	6.759
RMS Y+ axis	0.004	0.007	0.014	0.020	0.024
Skewness Y+ axis	-0.012	-0.021	-0.029	-0.012	-0.002
Gantry master axis Y- direction					
Energy Y- axis	1.747	5.542	20.820	57.507	82.399
Kurtosis Y- axis	3.014	7.970	9.946	12.407	6.866
RMS Y- axis	0.004	0.007	0.012	0.020	0.028
Skewness Y- axis	0.032	0.009	-0.040	-0.030	-0.013
Gantry master axis Y+ direction					
Energy Y+ axis	1.598	14.341	68.899	122.860	168.48
Kurtosis Y+ axis	3.136	16.729	10.189	8.799	9.542
RMS Y+ axis	0.004	0.0107	0.022	0.0286	0.031
Skewness Y+ axis	-0.033	-0.072	-0.073	-0.039	-0.083

Table 7-3 Test average results for gantry slave and master axis

Gantry Y axis test has been carried for 5 different ballscrew feederates. Calibration of the sensor has been concluded prior the test. Every run has been conducted at least two times. At a feedrate of 50000 mm/min Figure 7-2 AE is the highest possible traverse for GEISS machine. Results of enveloped AE data shows that noise baseline is established around 100 (mV). The axis's was tested separately in the positive and negative directions, because the point of contact of the thrust force is different on both the nut and ballscrew races for each direction. Y+ direction is nosier. It can be due to the fact that nut balls are rolling upward the ball grove (Figure 7-1) so coefficient of friction is be different than Y- direction. This would be even more critical on a vertical axis, where gravitational forces have a significant influence.

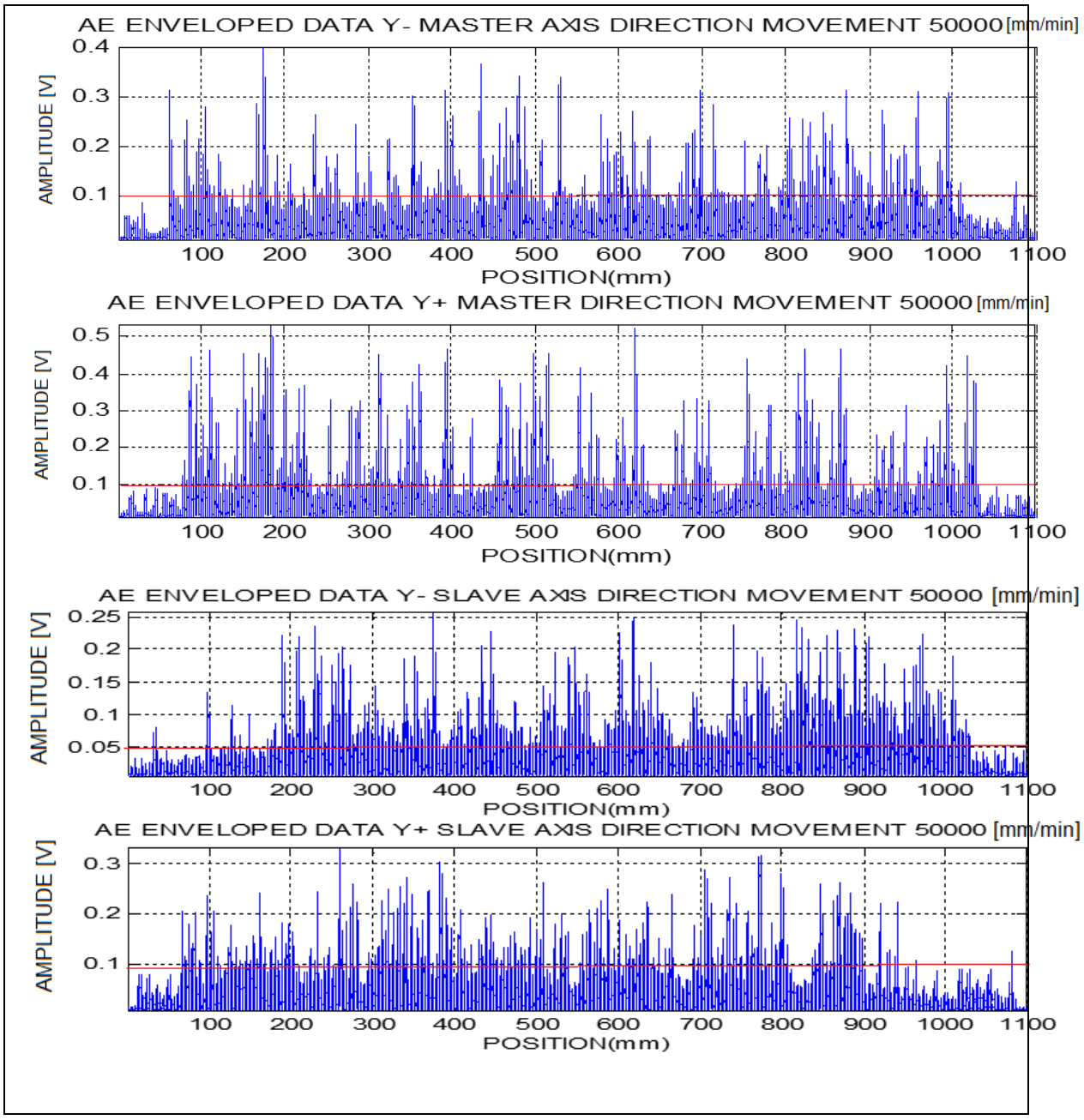

Figure 7-2 AE Enveloped signal for 50000 mm/min feedrate

Conditions during the early stages of movement (balls sliding) are unlike from those once inertia and stiction have been overcome. After a longer sliding time, the average friction coefficient, AE magnitude, surface roughness tend to become constant.

From the Table 7-3 Test average results for gantry slave and master axis can be recognised that 40000 and 50000 mm/min results seems to be too excessive for conclusive tests. That feeds are not common

to use in normal working operations. High level of energy and RMS indicates that there is higher friction and possible damage to the ballscrew.

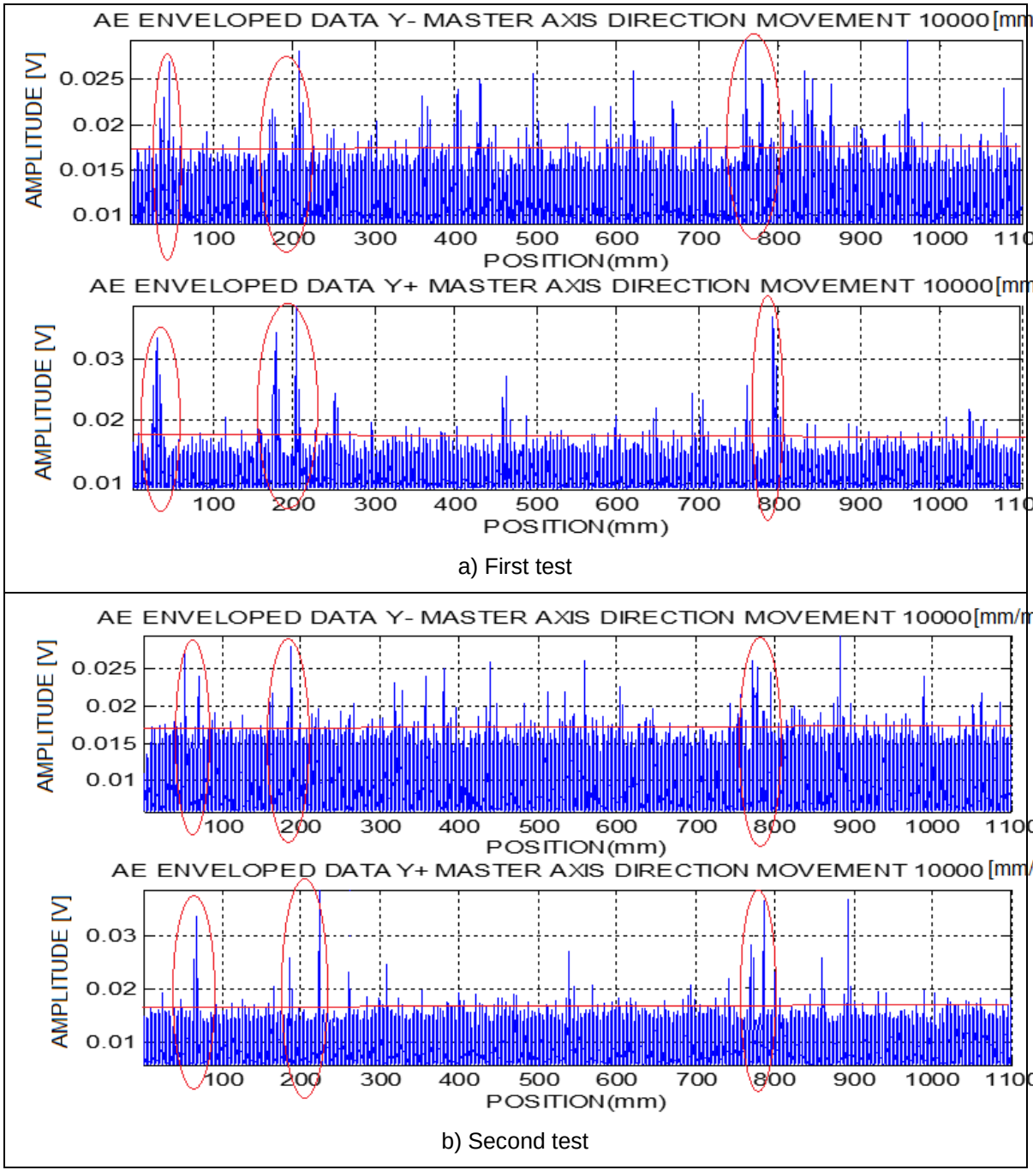

Figure 7-3 Enveloped AE data for 10000 mm/min Y master gantry axis for two tests

Lubrication is more stable in lower speeds. 10000 and 30000 mm/min speeds shows good signal to noise ratio. Envelope peaks are above baseline level and noises therefore can be easily distinguished. The highest peaks are visible is at around 80mm, 200mm, 800mm on master axis Figure 7-3 Enveloped

AE data for 10000 mm/min Y master gantry axis for two testsand Figure 7-4 AE Enveloped signal for 10000 mm/min. Master axis executes trajectories directly from the numeric controller NC code. Master feedback encoder is used also as the master encoder for the parallel slave motor. Alignment of the ballscrews is not perfect so slave gantry axis is a bit noisier than the master. Most likely this is due to design of the machine.

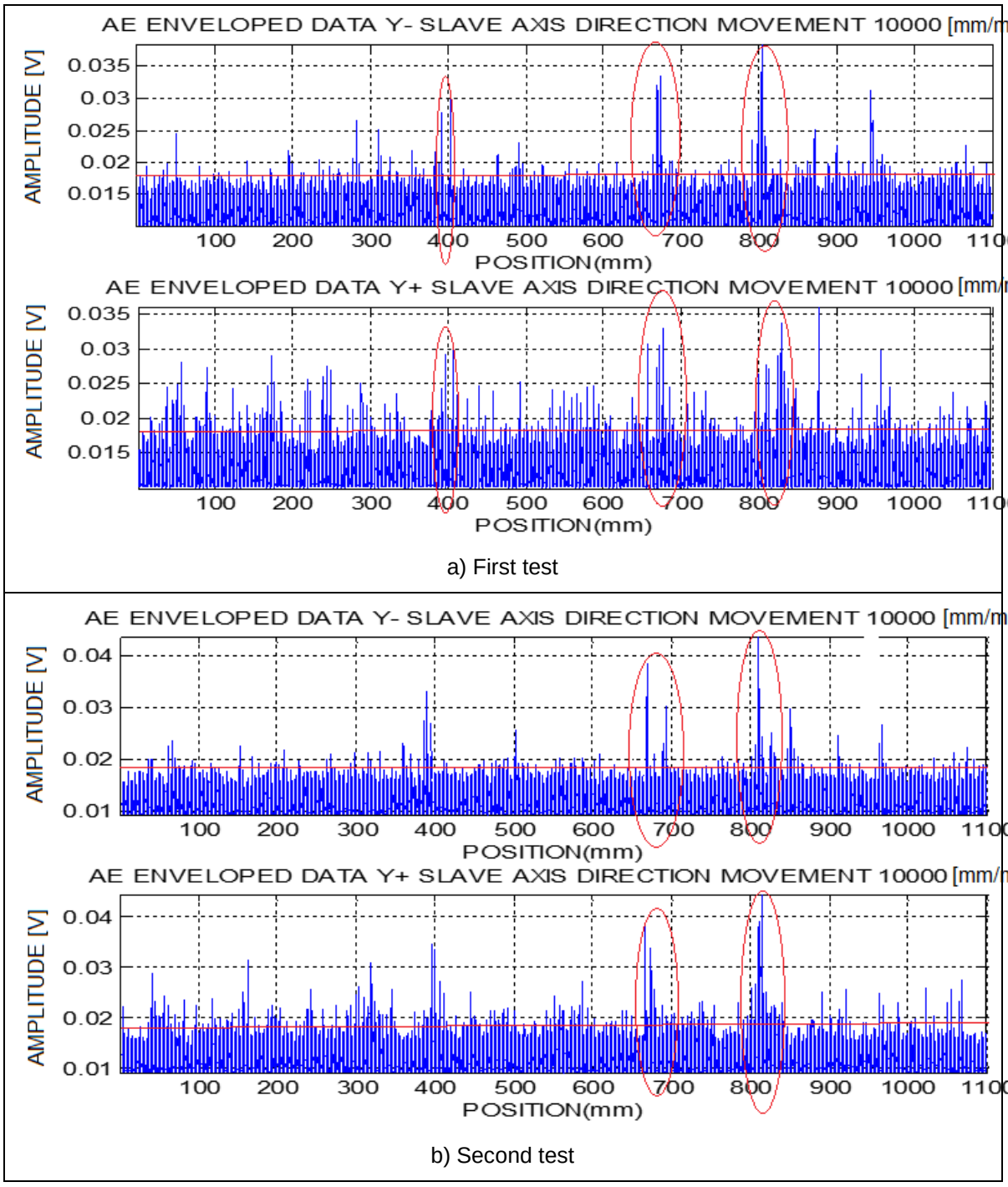

Figure 7-4 AE Enveloped signal for 10000 mm/min Y slave gantry for two tests

The advantage of taking the AE for the whole ballscrew length is that it is influenced by the occurrence of some burst events, which are most often due to high friction events and material imperfectness/defects during the travel. The kinematics of a ballscrew and nut does not support direct comparison of time-based signals like it's presented on Figure 7-5 . At the instant of triggering, all the balls would needs to be in the same location each time. Due to slip of the balls and backlash of the nut it can be anticipated that this is not possible. It's hard to establish accurate position of the wear due to length of the nut and amount of balls acting on the damage.

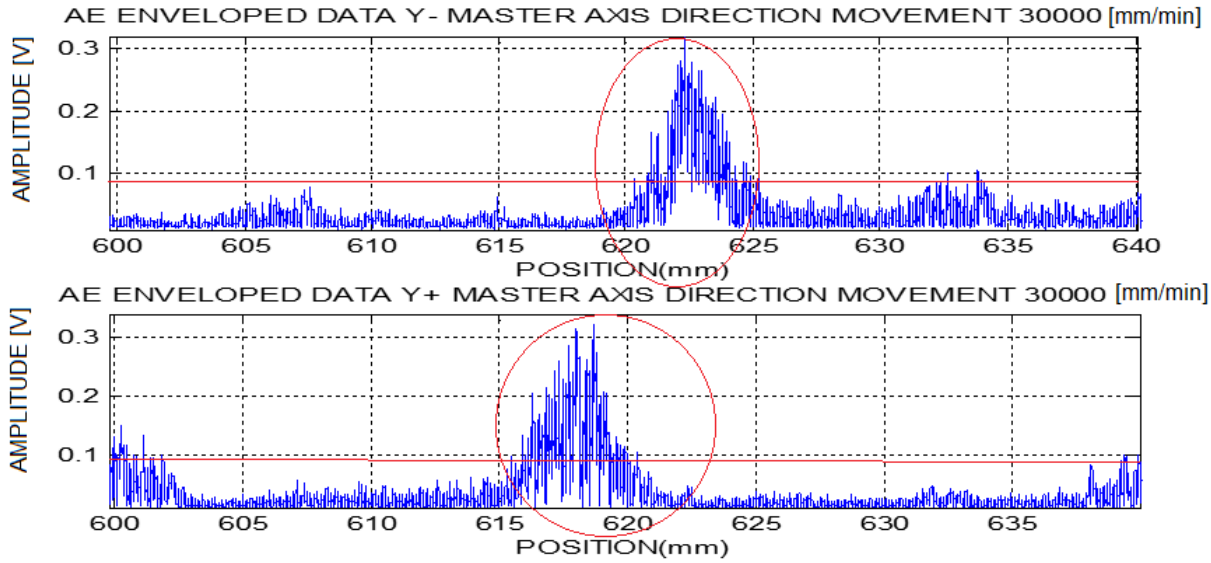

Figure 7-5 Forward and backward direction triggering location

Average AE RMS and Energy are reliable and meaningful. If those values will change it will mean that ballscrew or nut condition has changed due to lubrication, friction or other faults. The burst energy doesn't perfectly match when the machine is traversed in each direction. This could be due to length of the nut and position of linear encoder.

Test average results for X axis			
FEEDRATE (mm/min)	**10000**	**30000**	**50000**
X- direction			
Energy X- axis	3.249	67.678	215.522
Kurtosis X- axis	0.009	7.948	6.972
RMS X- axis	0.066	0.025	0.042
Skewness X- axis	0.010	-0.066	-0.089
X+ direction			
Energy X+ axis	5.365	223.717	463.380
Kurtosis X+ axis	0.009	10.455	7.037
RMS X+ axis	-0.012	0.045	0.060
Skewness X+ axis	0.009	-0.169	-0.087

Table 7-4 Test average results for X axis

Burst AE signal always exist, but when the frequency of AE is so high that the signal is not separable in time domain, it becomes continuous AE signal. The amplitude of the acoustic emission signal is directly related to the energy released while friction occurred.

Figure 7-6 AE enveloped data for X axis tests. The signal has been enveloped to visualise more features. It shows comparable results to Y axis. The burst AE signal is a time domain separable waveform, which consists of high amplitude, incoherent and duration for microseconds signals.

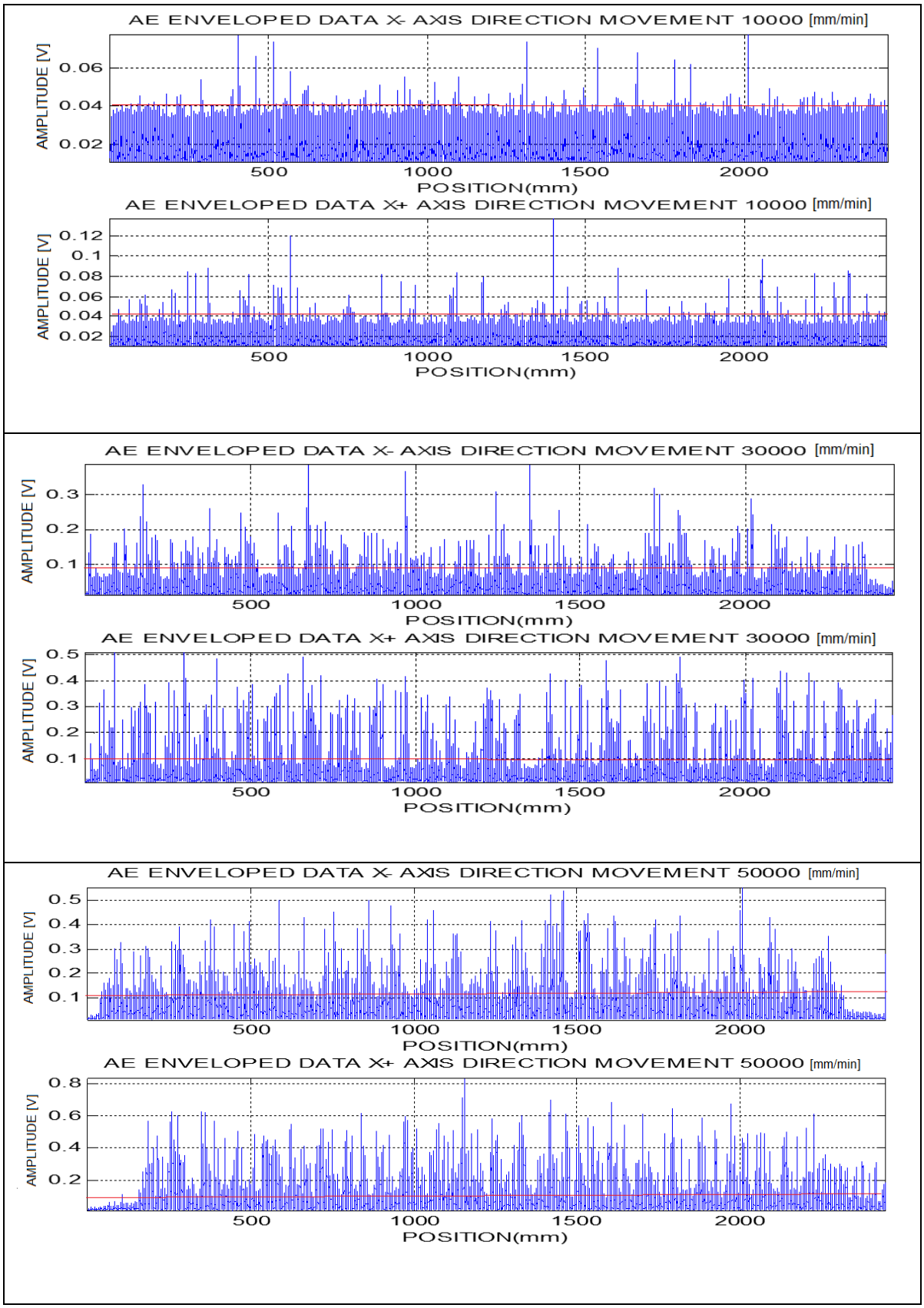
AE ENVELOPED DATA X- AXIS DIRECTION MOVEMENT 10000 [mm/min]
AMPLITUDE [V]
0.06
0.04
0.02
500
1000
1500
2000
POSITION(mm)
AE ENVELOPED DATA X+ AXIS DIRECTION MOVEMENT 10000 [mm/min]
AMPLITUDE [V]
0.12
0.1
0.08
0.06
0.04
0.02
500
1000
1500
2000
POSITION(mm)
AE ENVELOPED DATA X- AXIS DIRECTION MOVEMENT 30000 [mm/min]
AMPLITUDE [V]
0.3
0.2
0.1
500
1000
1500
2000
POSITION(mm)
AE ENVELOPED DATA X+ AXIS DIRECTION MOVEMENT 30000 [mm/min]
AMPLITUDE [V]
0.5
0.4
0.3
0.2
0.1
500
1000
1500
2000
POSITION(mm)
AE ENVELOPED DATA X- AXIS DIRECTION MOVEMENT 50000 [mm/min]
AMPLITUDE [V]
0.5
0.4
0.3
0.2
0.1
500
1000
1500
2000
POSITION(mm)
AE ENVELOPED DATA X+ AXIS DIRECTION MOVEMENT 50000 [mm/min]
AMPLITUDE [V]
0.8
0.6
0.4
0.2
500
1000
1500
2000
POSITION(mm)

Figure 7-6 AE enveloped data for X axis tests

The figures in Appendix G shows more results in the time domain. As described in previous chapters, it is hard to distinguish exactly where an event occurs. The kinematics of a ballscrew drive do not act in repetitive manner. It is necessary to set up the trigger for DAQ system and measurement, otherwise all moved elements of ballscrew system must be in the same points each time. The variance between the present condition and the baseline condition of the ballscrew is considered.

7.3.1 FREQUENCY RESPONSE

The frequency domain may include magnitudes of certain frequencies, power of certain frequencies, the integral of the power spectrum of a processed signal, etc. Previous studies described in **Error! Reference source not found.** have showed that by observing the spectrum analysis of the broad-band AE sensors, it was possible to categorize different sources with different frequency bands. Depending on the objective, a good balance of sampling speed and record length is required to capture the required features. For spectrum analysis in the high frequency range it is necessary to sample as high it's possible, however at a cost of a short sample length. For observing rotating periodic features, it is important to have a sampling length large enough to cover a good number of nut and its balls revolutions. Parameters has been chosen to maximise efficiency of the whole system. Those are presented in the next paragraph.

7.3.1.1 FAST FURIER TRANSFORM (FFT) PARAMETERS

The most efficient FFT algorithms works on a "power of two" number of samples therefore "nf" samples - defined below are used by the FFT algorithm. The frequency domain analyses presented in the following section are applied to centred AE signals; i.e. the average of each signal was subtracted from the values of the signal samples. The frequency domain analyses also consider the following parameters:

- nf = the "power of two" number of samples just below the available number of samples.
- The resolution = the sampling rate/nf.
- The frequency below which mains/DC frequencies exists = 100Hz.
- The high pass frequency= 50,000 Hz.
- The low pass frequency = 500,000 Hz.
- The band width over which the sum of the squares of the FFT amplitudes is named "energy01, energy02, etc. = 50,000 Hz.

The raw AE signal is an AC voltage signal that has a burst-like feature. The data presented on Figure 7-7 has been collected at the highest points in envelope response for each motor mm/min and then they peaks are compared with baseline (low/medium envelope response). Moved elements are not in the same position each time. However, amplitude and phase position can be separated in frequency

domain so the effect of signal attenuation due to interference avoided. The AE response for 10000 mm/min is low due to good ballscrew lubrication.

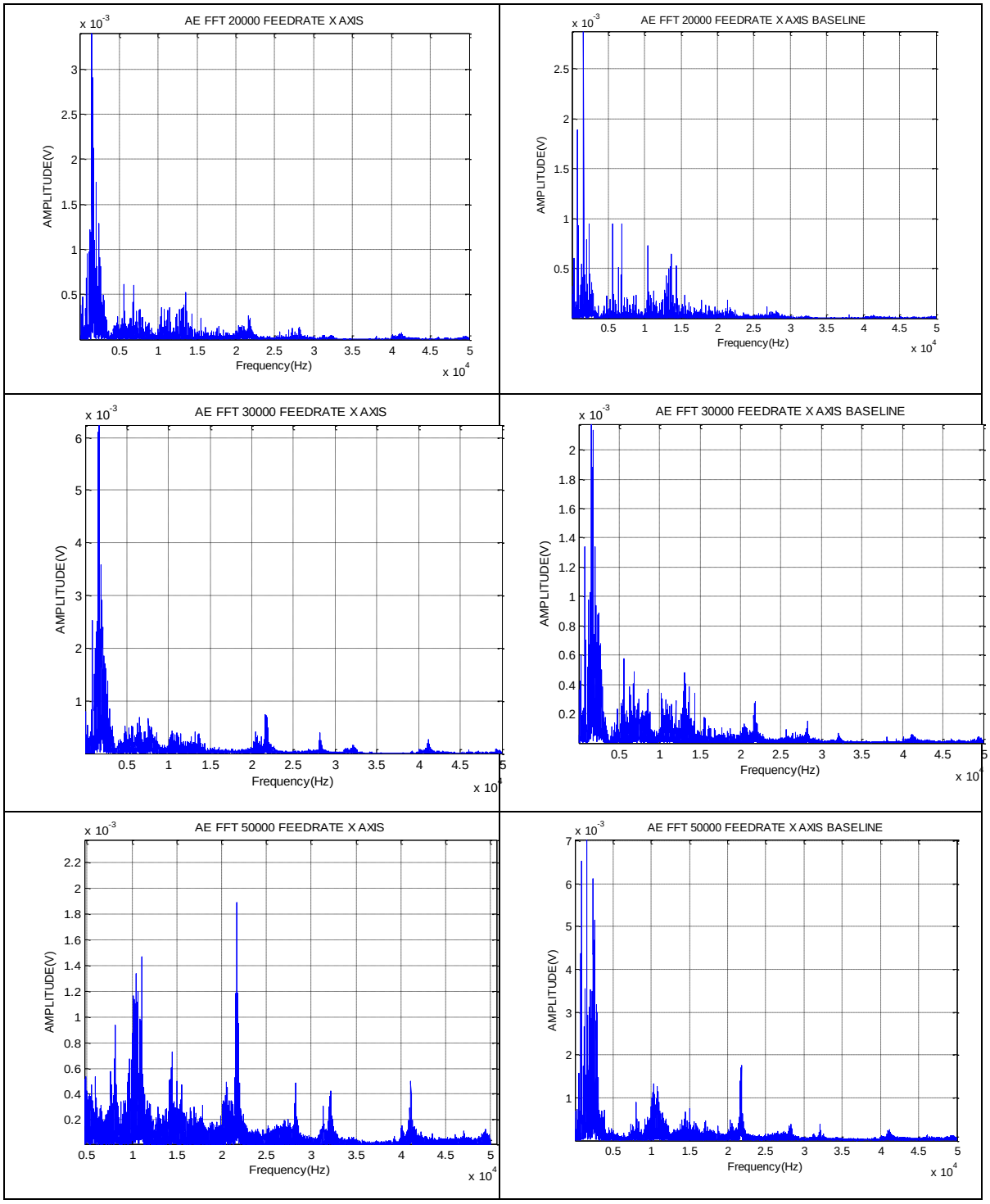

Figure 7-7 Frequency response for 20000, 30000 and 50000 mm/min highest AE peak point on X - axis

The goal is the condition monitoring of balls and grove systems with wear. The AE technique is efficient in detecting transient events due to ball nut inner race mechanisms. Figure 7-7 shows that there is no change in frequency response due to speed change It can be seen that a frequency has increased amplitude when compared with its baseline. The analysis anxieties the real behaviour of the CNC machine tool under destructive conditions shows that forced and self-excited both vibration problems can happen. Forced vibration is typically analysed in the frequency-domain unlike the free vibration which is represented in the time-domain.

7.4 CONCLUSIONS

The lubricate film prevents contact between the surfaces. This works when the system is running in a constant mode. When the machine is turned on or off, the balls will touch the nearby surfaces. Contact can occur if the direction of motion is changed. So lubrication must be considered in the issue of machine lifetime span. AE technique will be used to detect those contacts and establish wear factor for proposed condition monitoring system.

AE parameters have been extracted from AE events. These events were ordered, selected and normalised using Matlab code which was created during this research. Continuous time interval to record data and measure the progression of ballscrew events has been chosen. Appropriate understanding of the AE response during the test was performed using the waveform features. Envelope is the low frequency signal with values corresponding to the peaks of the high frequency signal. It has been used It to calculate the magnitude of an analytic signal of a band-pass-filtered signal

AE technique is a non-directional and non-invasive method for onsite monitoring tool. In this research AE were effectively applied to detect CM features in signal. The identification of noise sources and other uncertainties was essential part of the work. Calibration tests has been performed before each test to minimise the errors. Two type of sensors has been used to find if there is a shift in frequency domain and amplification, although there was no significant difference in results. It has been proven that AE waveforms carries information about the source that produces.

In this chapter, AE measurements were successfully applied to detect impairment in ballscrew. Alignment of the ballscrews is not perfect so slave gantry axis is a bit noisier than the master. The amplitude of the acoustic emission signal is directly related to the energy released while friction occurred. The analysis anxieties the real behaviour of the CNC machine tool under high feedrate conditions shows that problems can happen.

CHAPTER 8 DEFINITION OF AN MODEL-REFERENCE CONDITION MONITORING STRATEGY

The designed condition based monitoring (CBM) systems acquire Acoustic Emission (AE) data over few steady running conditions, e.g. during periods of steady feed rate and spindle speed, to provide diagnostics for drive-train components including nut, bearings and a ballscrew. Time and frequency domain Condition Indicators (CIs) are extracted from both the acquired raw AE signals and from the signals after processing them. The CIs are extracted after subtracting the average of the signal from the raw or processed AE signal under consideration. The time domain CIs can include: the Root Mean Square (RMS) of the signal, the four statistical moments of the signal (average, standard deviation, skewness, and kurtosis), the difference between the maximum and minimum values, and the maximum rate of change.

Friction between the moving components of the monitored assembly (ballscrew, balls and nut), may cause serious problems in accuracy and production. Friction, which is produced due to complex kinematics of the ball nut, is undesirable because it may cause machine failure.

The physical process of acoustic emission occurs in varied materials and under a wide range of conditions. The method promises to be very useful as a real-time detection on-line monitoring tool. Sensors can cover only identified faults so diagnostic system cannot be fully developed without knowledge of all failures. To secure the value of measurements, AE sensor should be regularly calibrated.

8.1 CONDITION BASED MONITORING

Monitoring involves maintaining regular investigation over features that can lead to or indicate faults. These factors include temperatures, pressures, speeds accelerations, loads etc. Usually, the monitoring function implements algorithms to monitor undesirable events such as over-speeding or over-pressurizing. The monitoring function can also include prognostic relationships that indicate the accumulative progressive effects on the health state of the operational parameters (or undesirable events).

Assessment involves the use of detection and/or monitoring results with strategy information and material properties to determine the current health status. Assessment can also include prognostics where the future conditions of the monitored components are forecasted and/or the remaining life of components estimated from fault progression relationships.

Detection is a crucial part which involves finding the existence, location and magnitude of undesirable displacement or plastic deformation. The detection tasks require data from dedicated sensors.

8.1.1 FAILURE MODES OF MACHINE COMPONENTS

The failure of a component occurs as a result of components interactions and other external effects. Damages caused by wear, thermal cycles, overloads are causing events detectable by AE sensor. The 'bath tub' failure probability curve, provides a general model that encompasses the main causes of failure and describes how the probability of failure can change with time, Figure 8-1 (Azzam (2016))

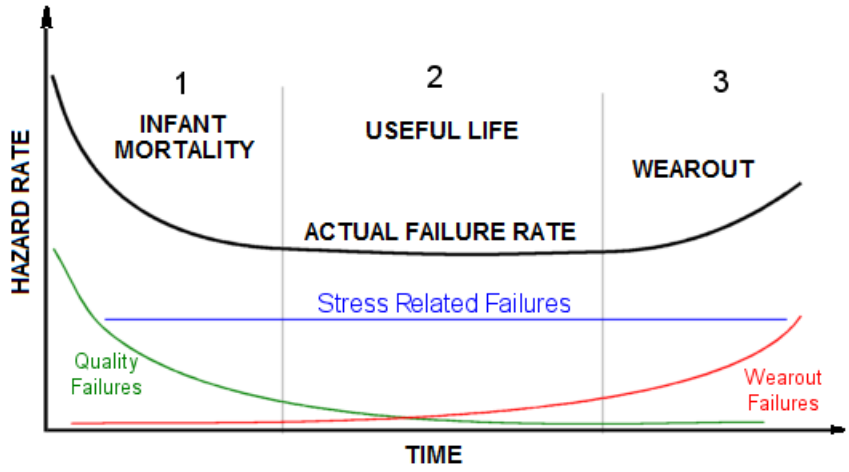

Figure 8-1 Bath tub' failure probability curve (Azzam (2016))

The failures in tool components occur due to three main causes:

- inherent weakness- that's when hazard rate is high in stage 1 – infant mortality

- gradual deterioration – its useful life range

- wear out – when ballscrew condition is really bad

- missue- unexpected damage – hard to predict

Only failures of gradual deterioration are suitable for ballscrew condition monitoring purpose. AE monitoring can provide information of its condition and rate of deterioration. This has achieved by selecting suitable parameters like RMS and Energy, recording their values at in comparison with basleine data from the model.

8.1.2 CONDITION MONITORING SYSTEM

Filev et al., (2010) have analysed practical framework for independent monitoring of industrial equipment based on novelty detection. Costa et al. (2015) presents two-stage algorithm for real-time

fault detection and identification. Both approaches provide the opportunity to incorporate novel detected faults to the monitoring system. Both methods the incorporation is limited to update the known data base, but an adaptation of the numerical features analysed is not considered.

Saravann (2003) states that use of appropriate condition monitoring technique for sub-systems of the machine tools is helpful in identifying and predicting the failures. Table 8-1 presents various methods for condition monitoring of rotating machinery and their fields of application. According to this table it is possible to monitor the entire machine tool by applying various possible combinations of these techniques as a multi-sensor and multi-parameter approach. Acoustic emission is suitable to monitor bearing, lubrication and tool wear.

Condition monitoring methods and their fields of application						
	Vibration	Oil analysis	Thermal	Ultrasonic	Sound	Acoustic
Rolling bearing	GOOD	GOOD	AVERAGE	AVERAGE		GOOD
Sliding Bearing	GOOD	GOOD	AVERAGE	AVERAGE		GOOD
Gears	GOOD	GOOD			AVERAGE	GOOD
Shafts	GOOD		AVERAGE			AVERAGE
Electrical			GOOD			
Lubrication		GOOD		GOOD		GOOD
Tool	AVERAGE				GOOD	GOOD

AVERAGE
GOOD

Table 8-1 Various methods for condition monitoring and their fields of application (Saravann 2003)

The proposed method has the principle that data of the healthy operation of the machine is initially available and fault scenarios will eventually develop. Continuous monitoring framework where the initial information available is the healthy operating condition includes confidence factor which is a pattern recognition technique that quantifies the similarity of the measured peaks to the expected fault peak frequencies and pattern.

Investigating the evidence of the faults during the monitoring process could advance the identification of a most adequate set of different features. Progressively identified faults discriminate the possible upcoming or already detected scenarios.

If the Confidence Factor is low then it most likely means that the specific fault is not present. If it is high, then it is a safe bet that the fault indicated is real. Therefore it provides a strong indication of whether a measurement actually represents a real fault or damage. This approach has the advantage of providing a most adequate situation for real time adaptation.

8.1.3 BALLSCREW SYSTEM FAILURE AND AE

It problematic to predict and model the characteristics of friction because of its nonlinear behaviour. Load, so the friction and AE signal becomes larger as the feed rate increases. Wear or drastic damage on the ball contact area of the ballscrew be caused by abrasive materials absorbed by the ball nut lubricant. If any of damaging conditions are detected by system user need to immediately take corrective action. Misalignment can be detected by AE energy signal rise caused by the balls sliding in erratic way. The difference between modelled value and actual value should be calculated in real time.

Component type	Function	Failure mode	Root Causes	Failure Potential Effects	Detection type
Ball bearings	Various	Wear	Misassemble; dirt, material defect	Reduced lifespan	High motor current / AE
Drive shaft	Connect motor and spindle	Wear	Dirt; aging		
Seal system	Seal rings etc...	Break	Stress corrosion	Possible outage extension for rive repair	Inspection
Drive shaft	Couples motor and spindle	Break	Misassemble stress	loss of drive	Indication
Ball nut rollers	Support ball nut	Breaks, seizes, increases friction	Impact	Excess motor torque	motor current AE
Ballscrew	Drives ball nut & rod	Distorts; increased friction & wear	Residual stress	Excess motor torque	motor current AE
Ball nut	Spindle rotation to ballscrew motion	Balls jam, friction, wear	Ball failure, crud, foreign object	Misplaced	AE Current position
Nut return tube	Retain and recirculate balls	Breaks, balls Wear	Stress corrosion; over–pressure	Rotation interference	AE Current position
Motor	Drives ball nut & rod	Stall	Short, open winding; bearing seizure	Motor- driven function	Indicator

Table 8-2 Ball screw feed drive system possible failures

Ballscrew is design to convert rotational motion to linear movement by rolling the balls between the screw and the nut. The rolling elements eliminate sliding friction so smooth accurate motion. Rolling motion is efficient and easier to control therefore its and precise and cost effective. A failure of the

ballscrew usually leads to a total breakdown of the machine. The reasonable life of this component is an important factor.

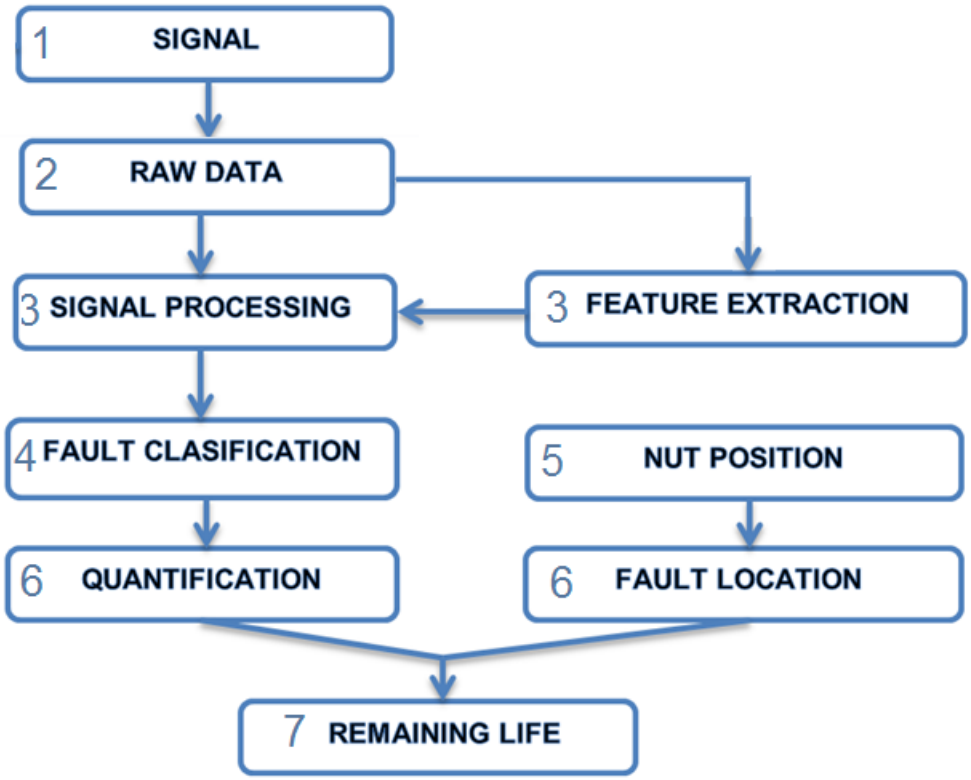

Figure 8-2 Condition Monitoring implementation method

Figure 8-2 shows the stages of implementation for condition monitoring of the ballscrew. First stage (1) is acquisition of the signal. AE pulse analysis of measured data is used for fault detection. Raw data needs to be computed or analogue feature extraction where signal processing method. Different computational approaches are used to categorize the types of faults. Fault classification which is commonly refereed as fault diagnosis is the next stage. Quantification of AE feature and recognition of fault nature is done on this level. Third stage is measurement of the position and locating measurement for this particular point. AE and position measurement has been synchronised using DAQ trigger to precise locate the event. Position has been measured using Renishaw laser interferometer. Fourth stage (6) is quantification of damage. It has been done in Matlab and its computation code is described in Appendix F. Results are giving the magnitude fault. Last stage (7) is estimating the remaining useful life based on AE measurement of the component and removing this time from useful life estimation table of identification of fault location. This is described in next paragraph.

8.1.4 BALLSCREW LIFE

In presented research condition monitoring is applied to ballscrew system. The balls serve as rotating medium within a feed drive, the motion and behaviour of these balls provide very useful information,

such as degree of wear, lubrication and breakage. Ballscrew system is a complex device. Its life depends on lubrication, nut condition therefore its suitable for remaining useful life calculation.

The friction force has nonlinear characteristics and it is position-dependent as well as speed dependent so AE sensor has been employed to detect the exact location and level. Health monitoring systems require information about position of the nut and measured signals using integrated AE sensors to estimate the exact position of damage.

Ballscrew's life is defined by the manufacturers as a total number of rotations it can sustain without showing any deterioration. Ballscrew life can be calculated with Dynamic Load Rating *C*a and *Life* formula.

$$L_{na} = a_1 * a_2 * a_3 * a_4 \left(\frac{c}{p}\right)^p (Hrs) \qquad \text{Equation 8-1}$$

L_{na}: Adjusted life rating in hours for reliability, material and conditions

a_1 Material/construction factor

a_2 Lubrication Factor

a_3 Misalignment factor

a_4 Load distribution

C

P

AE energy changes when any of $Lna= a_1 * a_2 * a_3 * a_4 \left(\frac{c}{p}\right)^p (Hrs)$

Equation 8-1 factors varies. Therefore a_{AE}: AE load factor firmly depends on the lubrication, misalignment and load. So it can be assumed that AE load factor can represent those three variables.

$$L_{na} = a_1 a_{AE} \left(\frac{c}{p}\right)^p (Hrs) \qquad \text{Equation 8-2}$$

Rolling contacts show AE wear signatures in a typical enveloped sequence. Ballscrew wear and other damaging factors causing events which release AE, therefore possible to accumulate it over time and compare it with baseline signal. Ballscrew baseline AE signals can be determined by running machine in low, stable federate – in our case 10000 mm/min is on the level of 0.005 which can be found on Figure 8-3. Material/construction factor a_1 is obtained from manufacturer specification.

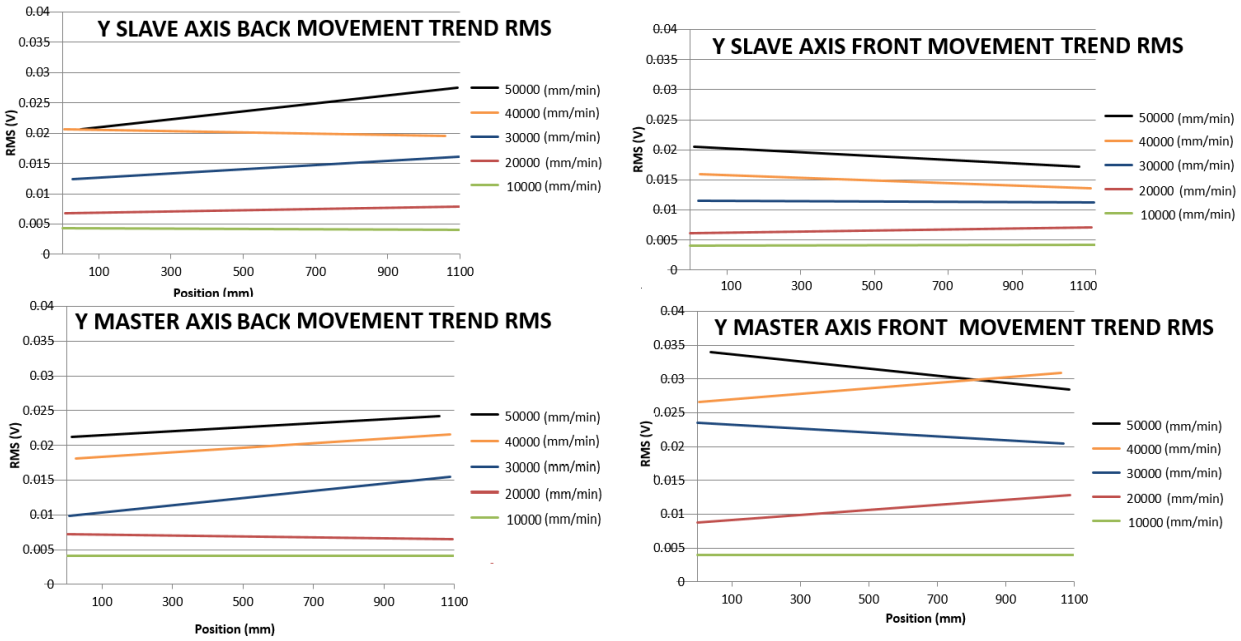

Figure 8-3 RMS trend for gantry axis

Ballscrew service life is very important because failure can cause the problems with accuracy and downtime. AE load factor will be similar to load factor supplied by ballscrew system manufacturer Table 8-3. Five times AE baseline will match movement causing high wear so load factor to calculate remaining useful life will be 1.5. Normal working conditions occurs when federate is not higher than 30000 (mm/min) and load factor of AE is not higher twice the baseline.

Conditions	Load factor = AE load factor	AE load factor threshold
Movement with high wear	1.5 – 2.5	Baseline *5
Normal movements	1.2 – 1.5	Baseline *3
Smooth movement without wear	1.0 – 1.2	Baseline *2

Table 8-3 AE load factor and its threshold

The total life of the ballscrew will be calculated using the formula hours.

$$L_h = \frac{L}{60 n_m} \qquad \text{Equation 8-3}$$

$$n_m = \frac{\sum_i (n_i l_i)}{\sum_i l_i} \qquad \text{Equation 8-4}$$

Where L: Rotation life (rev), L_h: Life time (hr), n_m: mean rotational speed (min-1), ni: rotational speed at phase i (min-1), i: distance travelled at phase i (m)

8.2 CONCLUSIONS

In order to save high maintenance costs and to increase manufacturing output ballscrew monitoring system has been method has been proposed. The balls serve as rotating medium within a feed drive, the motion and behaviour of these balls provide very useful information, such as degree of wear, lubrication and breakage. The relation between contact AE energy and ballscrew wear calculated and used to estimate the life.

The prescribed levels are based on theoretical results therefore major concerns will include future tests. It is difficult to distinguish ballscrew wear AE emission from the noises generated by cutting process, environmental sources. The ballscrew system emissions characteristics are not fully researched and known. Emissions characteristics can differ from feed drive to feed drive so user do not know what frequencies to listen without initial testing a particular system. Even with the same ballscrew emissions characteristics can change with a change in operating conditions and can change with time as the balls surfaces change due to wear. Thus, even if the condition can be isolated and identified, their interpretation become difficult.

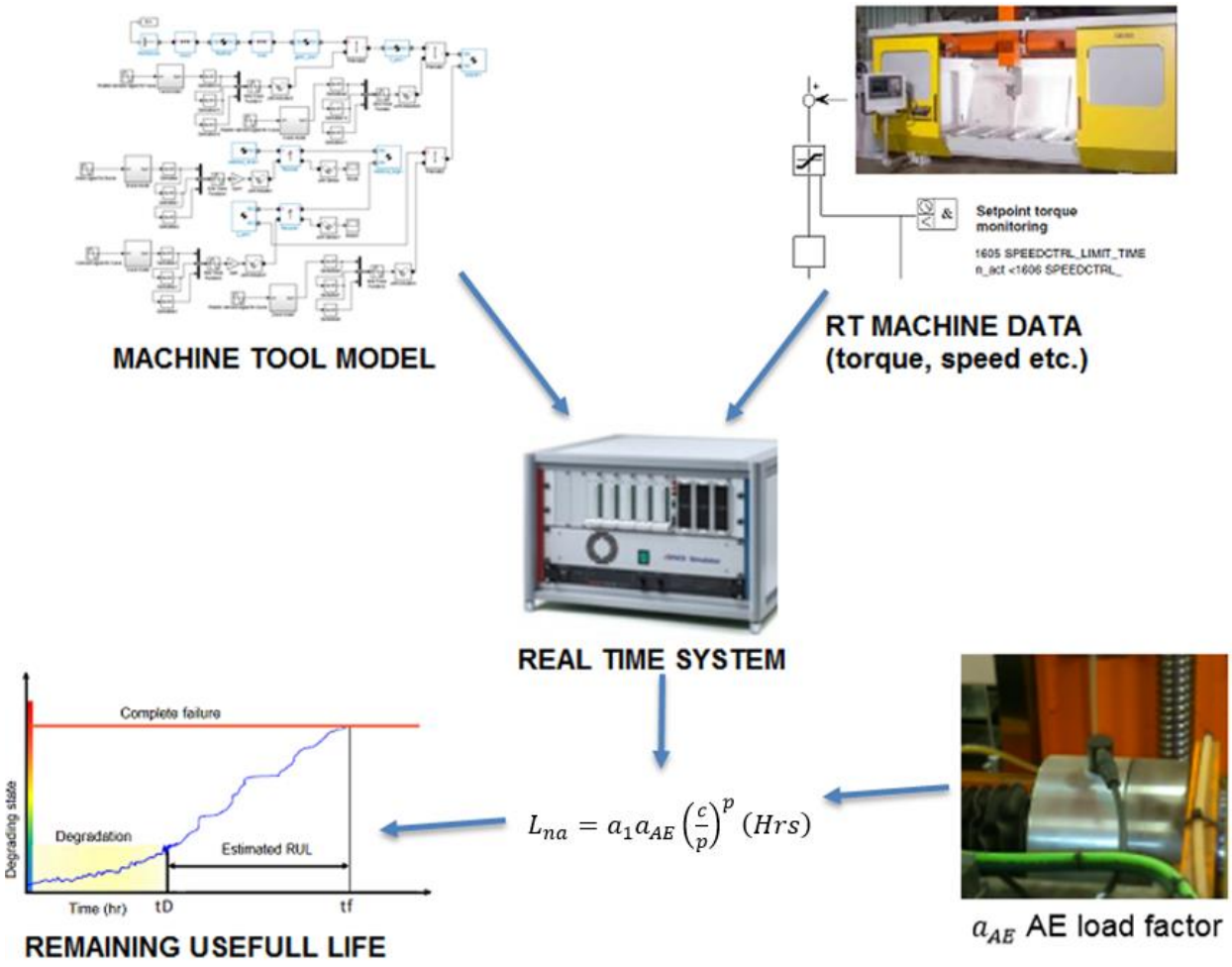

Figure 8-4 Model based Real time

Figure 8-4 Model based Real time system. Real time machine data needs to be used with developed machine model to estimate loads on the system. Experimental data should be used to establish AE factor levels. Those loads should be used with proposed AE factor to calculate remaining useful life. Results can be then been plotted against time. Anyway proposed method needs to be validated.

CHAPTER 9 CONCLUSIONS AND FURTHER WORK

The aim of modern industry is to achieve intelligent factory in wchich all machines communicate with another and optimize itself. As a consequence the productivity, efficient improves. Components are cructial parts of the system. Proposed condition monitoring system is suitable for wear parts monitoring. Since five axises are in operation per machine and the failure of single one shuts down whole machine for weeks or months the condition of the ballscrew drives should be monitored continiusly. The intention of the model-based approach is to determine the loads which are acting on the machine in order to calculate remaining useful life span. If the system is implemented it can improve productivity even by several percent. Novel methods has been proposed to achieve this aim. Work attempted includes modelling using various software packages – like Matlab, SolidWorks and dSPACE. Real time application has been deeply studied.

This thesis applies recent modelling techniques to represent all parameters which affect the accuracy of a component produced automatically. The motion control system is described and the elements, which compose the axis drives including both the electrical components and the mechanical ones, are analysed. SIMULINK models have been developed to represent the majority of the dynamic behaviour of the feed drives from the actual CNC machine tool. Development of a mechatronic hybrid model for five-axis CNC machine tool using Multi-Body-System (MBS) simulation approach is described. The model is experimentally validated by using speed and position signals then various load torque have been applied to the motor to show their behaviour. Analysis of CNC machine tool performance under non-cutting conditions is developed.

Health monitoring system is necessary to detect defects in machine components in order monitor machinery performance and to avoid malfunction. Fault-driven and time-based methods are widely recognized. In fault- driven approach, there wouldn’t be any maintenance in the system till an apparent failure would occur which indicates this approach is reactive rather than being proactive. Run to failure method is when repair work is performed on a piece of machinery after an equipment failure without any prior maintenance. The issue is having a spare parts inventory - organization has to rely vendors for the delivery of the parts or store the parts. In time-based method inspection and maintenance is conducted regularly.

9.1 INTRODUCTION

Machine tools are valuable, keeping them running is important because non-productive time costs money. Keeping them accurate is important to produce parts to tight tolerance which meets the grooving customer needs. Condition monitoring is one of the steps in developing automated, unmanned manufacturing systems.

Computer Numeric Control (CNC) machines are and more complex and sophisticated. Their maintenance is a major issue in the industry. The model is a simplification of a real machine to visualize the dynamics of a mechatronic system. The main aim of further developing machine tools is the improvement of accuracy and reducing maintenance resources. It is essential to reduce the machine downtime by condition monitoring.

There is a trend in manufacturing systems to a structure consisting of small, intelligent and flexible units with monitoring capabilities which increases the demand to monitor quality and performance

The main benefits of model based condition monitoring system of machine tool feed drive system:

- Lower maintenance costs
- Less downtime
- Reduced stock of spare parts
- Longer machine tool life
- Increased accuracy and production, Reduced equipment life cycle cost Therefore the model needs to be implemented

This thesis presents the development of a full representation of the feed drives model for a five-axis CNC machine. The analysis of the operation of a case-study CNC five-axis gantry machine is presented and the derivation of the mathematical equations describing the dynamic behaviour of machine is explained. The model is implemented in SIMULINK using SimPowerSystems toolbox. The simulated angular rotor position compares with the experimental data measured from the machine so the proposed model is validated. The SIMULINK model was designed to emulate the machine having a specific motor and ballscrew specification. The generic nature of the method means that the model was extended to other axes for the same or different CNC machine with limited alteration - the motor specifications, ballscrew parameters (pitch, friction, damping etc...) and control parameters (proportional constant, integral constant etc.) for position, speed & current controllers. This transition was successfully applied to the other four geometric axes of the case study machine.

The research carried out has led to the general conclusion that the selected software/hardware solution gives sufficient support to perform the tasks. The conceptual link between the modelling and

prototyping phases has to be taken to account when evaluating various approaches and it seems to be addressed best in SIMULINK.

A preliminarily study of the dSPACE Real Time Workshop was performed in Chapter 5 as part of the hardware-in-the-loop (HIL) implementation exercise. Using software-in-the-loop (SIL) simulation systems, the model of the machine controller, SimMechanics models for mechanical elements and SIMULINK models for feed drives accurately simulated the range of movement of the tool. By the use of SIL in dSPACE, both the velocity and the position were measured. The ControlDesk graphical analysis was used to compare the results by unifying the all the captured and simulated data used in the model.

This approach provides a test environment offering modelling support for dynamic environments that may reduce significant cost within the NC controller during design and training. Simulation therefore reduces the burden on valuable machining capacity, there is no risk of damaging equipment by using manual inputs and the space required is much lower.

The misuse and interaction events can initiate mechanical faults then the exposure to normal operational. The future course of the controlled signal can be calculated only if a model of the process is known. Therefore, predictive control is often called model-based predictive control. The virtual environment created on accurate model of the feed drives presents advantages:

- It allows testing and validating in real time simulation novel control architectures.
- it allows through SIL simulation automatic selection the finest set of tuning values for parameters to provide stability and accuracy
- Those are strong motivations in favour of the model developed and described in previous chapters, which

Conducted experiments shows that the AE sensor in fault identification was more reliable than accelerometer. In more practical environment like shop floor the application of acoustic signal may not vialable due to high noise level and signal processed by filtering and useful information. The part of development is Bayesian uncertainty assessment to evaluate the uncertainty related to the estimates obtained from measured data. This high frequency system has capabilities in early fault detection of the direct lubrication therefore is well suitable in hi high speed linear positioning systems. The severity of the changes can be indicated by rising in appear in AE feature levels over long time period.

By using an acoustic emission (AE) sensor, data can be acquired during the normal operation of the machine without interrupting the machining processes. AE is effectively used in diagnosis systems for ballscrew positioning system as an indicator of operation condition. There is high business value attached to research in such areas. By developing a universal model, HIL implementation becomes

more feasible and marketable as a product. Testing and reengineering becomes easier and down times can be greatly reduced.

To detect performance drifts it is essential to extract references from the simulation environment and compare them with AE features. The AE signature for a healthy ballscrew was obtained as a function of feedrate for the full range of operational conditions. Envelope analysis technique was applied to the acoustic emission signals to investigate patterns and correlate them with specific faults. The chosen analysis method has been shown for the assessment of feed drive system subcomponents. AE is used for ballscrew estimating the probabilities of consistent operations.

From the data obtained, the following conclusions were determined and summarized:

- Acquired acoustic emission signals present obvious characteristics of time-varying nonlinear and pulsating.
- Acoustic emission in friction is commonly attributed to changes in the stress-strain state of contact spots.
- AE signal is good to establish friction between nut and screw.
- AE features are more significant higher
- It was detected that AE energy and RMS increased with increasing speed of the nut.
- It is evident from the results that Acoustic signal trends can be correlated with local foults
- AE analysis establishes a better understanding of individual machine ballscrew characteristics.
- Present work highlighted the procedure for identification of higher friction and defect in the ballscrew.
- Further study can be carried out for finding exact location of defects in the ballscrew.
- Higher AE intensity values should be typical for adhesive wear of the ballscrew.
- If the nut was damaged then enveloped signal should show visible pattern.

The ballscrew is perhaps the most prevalent CNC machine subsystem and the condition of each element is critical to the success of a machining operation. So there is a great need for a timely knowledge of the health status of ballscrew, bearings and nut. The feed drive examined is based on the typical mechanical structures in the machine tool. The condition monitoring strategies have been offered with the advantage of a model of the system in real time. Acoustic emission analysis of machines has been carried out to determine the deterioration of the ballscrew. Degradation of feed drive mechanical components is critical for active maintenance judgement.

Some condition indicators in define period can be used to estimate the ballscrew damage. The condition of the feed drive can be determined by comparing the peak AE values to baseline. There is clear correlation between a weakening condition of the feed drive lubrication and increasing AE events. It is possible to assign energy amplitude and position which were sustained by damage. The main capability of system is to insight of future health states of a system. The main step is detection and to

the assessment of severity of degradation. Then forecasting degradation trends to estimate the future remaining useful life (RUL) using time series techniques. It is promising to describe the condition of a ballscrew in terms of AE and load.

9.2 CONTRIBUTION TO KNOWLEDGE

- Development of a novel multi-body mechatronic model for five-axis CNC machine tool

  The full model for the five-axis machine including the horizontal, vertical and rotary axes drives which represent the behaviour of electrical and mechanical elements in a single simulation environment has been developed in this work. Physically-based parameter identification for the feed drives of the CNC machine tool has been performed. Design a detailed CAD model for the GEISS machine in SolidWorks and develop Multi-body simulation MBS approach in SimMechanics to examine interactions that occur between machine tool components and the motion dynamic properties obtained with regard to elapsed time. This approach to modern maintenance practice can be used on various CNC machines with similar feed drive systems

- The work presented in this dissertation adds value to pioneering projects in the world of HIL testing for the CNC machine.

  This condition monitoring solution relies on the capabilities of simulation software such as SIMULINK. An HIL model is inconclusive in the absence of a reliable SIL model. In Software in the loop (SIL) simulation, the software can reproduce the NC control unit which reacts to errors between real input from CNC and model. The approach has been shown to be scalable to other axes, giving it widespread applicability. The steps for data acquisition using ControlDesk and HIL hardware-in-the-loop implementation of the feed drive models in dSPACE real-time system has been described. It has been explained how the experimental data obtained from the data acquisition process using dSPACE ControlDesk can be used for developing machine tool diagnosis and prognosis systems.

- Establish acceptable degree and locate higher AE peaks on the ballscrew

  Vital phase of detection and Condition Monitoring requires a robust identifier which simulates dynamic measuring systems by extracting relevant AE features. Bayesian uncertainty assessment and study in influences of external factors on AE measurement.

- Measure the degradation of ballscrew during cutting trials using Acoustic Emission (AE) sensors.

  The research for the condition monitoring of the defects in ballscrews is still almost blank. This approach to modern maintenance practice promises to reduce unforeseen failures, downtime and

maintenance cost. Describe how the developed multi-body mechatronic model for Geiss five-axis CNC machine tool can be used for condition monitoring purposes. Condition monitoring strategy which employs the dSPACE real-time system and machine model has been defined. Assessment of severity of AE energy has been combined with SIMULINK model to estimate remaining useful life (RUL) of feed drive system using time series techniques

- Opening new opportunities for Industry 4.0 condition monitoring

  To prevent unwanted downtime some manufacturers exchange damaged components on regular basis. Presented solution allows the useful life of the machine tool feed drive to be exploited and future maintenance scheduled. AE measured system works with high frequency waves. This state of art technology can be easily implemented on the ballscrew nut.

- Propose RUL calculation algorithm and validated by real field data and simulation data

  The proposed method has dominant strengths. Approach does not assume the degradation, it calculates certain distribution and it can adapt to feed rate changes therefore it benefits RUL prediction.

9.3 CONCLUDING REMARKS AND SUGGESTIONS FOR FUTURE WORK

The work in this thesis has investigated methods suitable for condition monitoring of machine tools to maintain their availability to produce precision parts.

By combining the reference model approach developed in this research with additional sensing, such as the AE system that has been evaluated, a systematic approach to the condition monitoring of precision machine tools can be achieved. Cumulative failure data are considered as a health report of ballscrew system.

The work in this thesis has created the software-in-the-loop solution. Further development is required to integrate the full model into a hardware-in-the-loop closed-loop system to maintain condition. Research will be required to take the experimental data obtained from signals in the SINUMERIK 840d SL controller directly into the dSPACE platform to be compared with the simulated data in real time. This would represent a considerable contribution to the condition monitoring techniques which could be used to improve the five-axis machine performance and be a platform for a tuning of the machine's controller.

In order to get the real time information from the NC control side, the interface must be able to access the data from Siemens SINUMERIK 840D during the operation, collect the necessary information and pass it in real time to dSPACE 1005 DSP board. The desired model configuration is built for the

dSPACE target hardware and are run directly using ControlDesk. One procedure for data acquisition using ControlDesk from dSPACE system was developed for three-axis CNC machine tool (Sztendel et al. 2009). A similar approach will be applied when the measured data from five-axis machine should be included in dSPACE system in the future. This research has successfully created a healthy SIL model, working and ready to be implemented into HIL architecture. The main components of the HIL system are: the drive model simulation (real-time simulation of the drive dynamic characteristics) and I/O (input – output) modules for receiving the real time controller outputs and responding with simulated signals from the drive model back to the controller with the aim to improve the quality of machine operation. Conducting this work would be timely, since the growing integration of the "Internet of Things" (IoT) is driving manufacturers to make such signals more readily available.

As part of future work, this model can further be improved to have an agile design. Realism of the SIMULINK feed drive models can be improved by inserting the spectral density of noise measured from the actual five-axis CNC machine tool and the effect of mass distribution on the dynamic behaviour of the system, etc. Essentially what this means is that there would be one block with a set of parameters. The user will have to input these parameters and determine how the block is supposed to work. So the same model could be used for various machines for a specified set of parameter configuration. The key is identifying these unique sets of parameters.

The next step is a calibration process which is used to improve the physical system model accuracy. In order to compare the results and to analyse the differences, the measures collected need to be transformed in the right format and then processed using MATLAB showed in the work. Using the ControlDesk software parameters of a design such as gain can be varied and the effects of such changes can be monitored in real-time to compare simulation results, and on the other hand, the measurements.

Feed drives with ballscrews can be periodically examined using the system to find the affected elements, how much they are worn and to approximate their remaining lifetime. Further analytical methods could be found to include more features, especially when processed in conjunction with other signal inputs.
It is almost impossible to achieve a natural wear of the feed unit in a short time. Wearing of the feed unit is an expensive and time-consuming process. For future experimental analysis, wear can be accelerated by contamination of the lubricant with harsh materials or eliminating the lubrication. Then it would be more possible to follow the location and evolution of the damage.

In future wavelet packets which gives better time-frequency resolution than other transforms can be used to de-noise the signal and retrieve any desired frequency range. Then AE signal features can be extracted by envelope detection. Wevelet packets can give better time-frequency resolution than other transforms, it is more suitable for locating defects also which is a major application of AE testing.

Further tests needs to be carried to establish if AE bursts will disappear after the establishment of the fault (material removal and less friction) and if vibration method will be suitable. Vibration is able to detect the faults later however it is been proven good tool for analysis and diagnostic of the fault.

The analysis should been done by comparing the signals of encoder – indirect measurement then real time model based compared with acquired AE involved. The stimulation of the wear properties as well as the determination of patent in frequencies occurring during the different phases of damage should be investigated. More comprehensive trials to prove robustness to different faults in different situations should be part of the further work.

REFERENCES

Al-Bender F., V. Lampaert, J. Swevers, (2005). A generalized Maxwell-slip friction model: a novel model for friction simulation and compensation, IEEE Transactions on Automatic Control 50 (11) Pages 1883–1887.

Al-Bender F., V. Lampaert, J. Swevers, (2004). Modelling of dry sliding friction dynamics: from heuristic models to physically motivated models and back, Chaos: An Interdisciplinary Journal of Nonlinear Science 14 (2) Pages 446–460.

Altintas Y., A. Verl, C. Brecher, L. Uriarte, G. Pritschow, (2011). Machine Tool Feed Drives. CIRP Annals - Manufacturing Technology, Volume 60, Issue 2, Pages 779–796

ASTM (2015) Standard Test Method for Primary Calibration of Acoustic Emission Sensors, Active Standard ASTM E1106 | Developed by Subcommittee: E07.04 Book of Standards Volume: 03.03

Bayes server (2015). Bayesian Network software for artificial intelligence Retrieved from: http://www.bayesserver.com/

Beattie A.G., (2013). Acoustic Emission Non-Destructive Testing of Structures using Source Location Techniques, SANDIA REPORT, SAND 2013-7779

BIPM GUM JCGM 106 (2012). Evaluation of measurement data – The role of measurement uncertainty in conformity assessment Joint Committee for Guides in Metrology 106:2012

Arroyo E.L.C., (2006). Modelling and simulation of permanent magnet synchronous motor drive system. MSc Thesis, University of Puerto Rico Mayaguez Campus.

Azzam H., McFeat, (2016). Development, Validation, Verification and Certification of Structural Health Monitoring Systems for Military Aircraft MASAAG Paper 123 Issue 2a January 2016

Baracos P. Murere, G. Jin W. (2001). “Enabling pc-based HIL simulation for automotive applications,” IEEE International Electric Machines and Drives Conference, Pages 721 -729.

Bhuiyan M. Choudhury, I. Nukman, Y. (2012). Tool condition monitoring using acoustic emission and vibration signature in turning. Proceedings of the World Congress on Engineering 2012 Vol III

Boer S.E., D. Hoopen, R.G.K.M. Aarts, W.B.J. Hakvoort, J.B. Jonker, (2013). Model Reduction for Efficient Time-Integration of Planar Flexible Multibody Models, International Journal of Non-Linear Mechanics Volume 53, July 2013, Pages 75-82

Boothroyd G., Knight, W. (2006). Fundamentals of Machining and Machine Tools (3rd). United States of America: CRC Press

Burks B., (2013). Re-Examination of NIST Acoustic Emission Sensor Calibration: Part I - Modeling the loading from glass capillary fracture Journal-AE Session: Volume 29

Canudas de Wit, C., H. Olsson, K.J. Astrom, P. Lischinsky, (1995). A new model for control of systems with friction, IEEE Trans. Automat. Control 40 Pages 419–425.

Choi J., S. Rhim, J.H. Choi, (2013). A General Purpose Contact Algorithm using a Compliance Contact Force Model for Rigidand Flexible Bodies of Complex Geometry. International Journal of Non-Linear Mechanics, Volume 53, July 2013, Pages 13-23

Delgado A.S., E. Ozturk, N. Sims, (2013). Analysis of Non-Linear Machine Tool Dynamic Behaviour. Procedia Engineering, Volume 63, 2013, Pages 761-770

Dougal R., A. Monti, (2000). "High level virtual prototyping with hardware in the loop," IEEE VIMS00, Annapolis, MD,

dSPACE GmbH, (2013). Test and Experiment Software / ControlDesk", Rathenaustraße 26, 33102 Paderborn, Germany," Retrieved from: http://www.dSPACE.com.

dSPACE, (2015). DS1005 PPC Board (online) Retrieved from http://www.dspace.ltd.uk/ww/en/ltd/home/products/hw/modular_hardware_introduction/processor_boards/ds1005.cfm

Eidelberg P., Pilock, B., Thomas Haran, T., (2015). Keeping gantries on the straight and narrow: economical misalignment-compensation techniques prevent bearing overload and premature gantry failure.(Motion Control) Penton Media, Inc., Penton Business Media, Inc. Machine Design VOLUME: 87

Essid El-Alej M. (2014). Monitoring Sand Particle Concentration in Multiphase Flow Using Acoustic Emission Technology PhD thesis, Cranfield University

Feng G., D. Zhen, X. Tian, F. Gu, and A. Ball, (2015). A Novel Method to Improve the Resolution of Envelope Spectrum for Bearing Fault Diagnosis Based on a Wireless Sensor Node. In: Vibration Engineering and Technology of Machinery. Springer, pp. 765-775. ISBN 978-3-319-09918-7

Fleischer J., A. Broos, M. Schopp, J. Wieser, H. Hennrich, (2009) Lifecycle oriented component selection for machine tools based on multibody simulation and component life prediction. In: CIRP Journal of Manufacturing Science and Technology, Jahrgang 1, Heft/Band 3, Verlag Elsevier, Amsterdam, The Netherlands, ISBN/ISSN 1755-5817, Pages 179-184.

Fortunato A., A. Ascari, (2013). The Virtual Design of Machining Centers for HSM: Towards New Integrated Tools. Mechatronics, Volume 23, Issue 3, Pages 264-278

Fredin J., A. Jonsson, G. Broman, (2012). Holistic Methodology using Computer Simulation for Optimization of Machine Tools. Computers & Industrial Engineering Volume 63, Issue 1, Pages 294-301

Frey S., A. Dadalau, A. Verl, (2011). Expedient Modelling of Ballscrew Feed Drives. Production Engineering Research and Development WGP Vol. 6/2

Garcia J., E. Bayo, (1994). Kinematic and Dynamic Simulation of Multibody Systems: The Real-Time Challenge. Springer-Verlag New York, Inc. Secaucus, NJ, USA 0941-5122

GEISS. (2014). GEISS Trimming Spindle ER16. Retrieved from http://www.geiss-ttt.com/www_geiss/rangeofproducts_millingmachines_optionalequipments_e_5.1_408_103_0_f.htm?query=

Gu F., X. Tian, Z. Chen, I. Rehab, A. Ball, (2014). Fault severity diagnosis of rolling element bearings based on kurtogram and envelope analysis. International journal of structural analysis & design, 1 (2). ISSN 2372 – 4102

Hansen J., F. Drews, (2006). – Soft and Firm Real-Time Systems (or Kinder, Gentler Real-Time). 14 WPDRTS 2006, Greece.

Hanson B., M. Levesley, K. Watterson, P. Walker, (2007). Hardware-in-the-loop-simulation of the cardiovascular system with assist device testing application, Medical Engineering & Physics, vol. 29, no. 3, Pages 367-374.

Hanwu H., W. Yueming, (2009). Web-based Virtual Operating of CNC Milling Machine Tools. Computers in Industry Volume 60, Issue 9, December 2009, Pages 686-697

Hamstad M. A. (2011). RE-EXAMINATION OF NIST ACOUSTIC EMISSION ABSOLUTE SENSOR CALIBRATION: Part II-Finite element modelling of acoustic emission signal from glass capillary fracture J. Acoustic Emission, 29, 175 Acoustic Emission Group

Heidenhain (2012). "Heidenhain- Rotary encoders," Retrieved from: http://www.auto-met.com/heidenhain/08PDF/Rotary%20Encoders.pdf.

Herrmann S., M. Kaehler, R. Souffrant (2012). "HiL simulation in biomechanics," A new approach for testing total joint replacements, Computer Methods and Programs in Biomedicine, vol. 105, no. 2, Pages 109-119.

Holroyd, G. (2007). The modelling and Correction of Ballscrew Geometric, Thermal and Load Errors on CNC Machine Tools, Doctoral Thesis, University of Huddersfield

Hornstein A., (2005). Dynamical modelling with application to friction phenomena, Dissertation, Univesity of Gottingen

Hujun I., (2013). Intelligent Data Engineering and Automated Learning – IDEAL 14th International Conference, IDEAL, Hefei, China

Isermann R. (2003). Mechatronic Systems Fundamentals. Great Britain: Springer 978-1-85233-930-2

Janschek K. (2012). Mechatronic System Design: Methods, Models, Concepts. Germany: Springer-Verlag Berlin Heidelberg, ISBN 978-3-642-44466-1

Juvva K. (1998) "Real-Time Systems, 18-849b Dependable Embedded Systems," Carnegie Mellon University, Spring London

Kadir A.A., X. Xu, E. Hammerle, (2010). Virtual Machine Tools and Virtual Machining - A Technological Review, Robotics and Computer-Integrated Manufacturing, Volume 27, Issue 3, Pages 494-508.

Kaiser J. (1953). “Erkentnisse und Folgerungen aus der Messung von Geraeuschen bei Zugbeanspuruchung von metallischen Werkstoffen”, Archiv fuer das Eisenhuettenwesen, 24, Pages 43-45

Kang I.S., J.S. Kim, M.C. Kang, K.Y. Lee, (2008). “Tool condition and machined surface monitoring for micro-lens array fabrication in mechanical machining,” Journal of Materials Processing Technology, vol. 201, no. 1–3, Pages 585–589

Keprt J., P. Benes, (2009). “Determination of Uncertainty in Calibration of Acoustic Emission Sensors”, International J. of Microstructure and Material Properties, Vol. 4, Pages 85-103.

Kholkin A.L., N.A. Pertsev, A.V. Goltsev (2008). Chapter 2 Piezoelectricity and Crystal Symmetry Springer-Verlag US, ISBN 978-0-387-76540-2

Laxalde D., and F. Thouverez, (2009). Complex non-linear modal analysis for mechanical systems: Application to turbo machinery blading with friction interfaces Journal of Sound and Vibration 322, Pages 1009–1025.

Labview (2015). National Instruments, LabVIEW Basics Introduction, Course Manual, U.S.A Retrieved from: https://www.ni.com/getting-started/labview-basics/

Law M., Y. Altintas, A. Srikantha Phani, (2013). Rapid Evaluation and Optimization of Machine Tools with Position-Dependent Stability. International Journal of Machine Tools and Manufacture Volume 68, Pages 81-90.

Lee R.S., Y.H. Lin, (2009). Development of Universal Environment for Constructing 5-Axis Virtual Machine Tool based on Modified D-H Notation and OpenGL. Robotics and Computer-Integrated Manufacturing Volume 26, Issue 3, Pages 253-262.

Li B., B. Luo, X. Mao, H. Cai, F. Peng, H. Liu, (2013). A new approach to Identifying the Dynamic Behaviour of CNC Machine Tools with respect to Different Worktable Feed Speeds, International Journal of Machine Tools and Manufacture Volume 72, Pages 73-84.

Li R., S.U. Seckiner, D. He, E. Bechhoefer, P. Menon, (2012). "Gear Fault Location Detection for Split Torque Gearbox using AE Sensors," IEEE Transactions on Systems, Man and Cybernetics –Part C: Applications and Reviews, Vol. 42, No. 6, Pages 1308-1317.

Liao L., P. Radu, (2012) Machine Tool Feed Axis Health Monitoring Using Plug-And-Prognose Technology, Conference of the Society for Machinery Failure Prevention Technology, Proceedings of the 2012 Conference of the Society for Machinery Failure Prevention Technology

Liu Y., T. Zhao, H. Zhang, (2010). Hybrid Dynamic Modelling of a High-Speed Ballscrew Drive System - Department of Precision Instruments and Mechanology, Tsinghua University, Beijing, China.

Loutas T.H., D. Roulias, E. Pauly, V. Kostopoulos, (2011). "The Combined use of Vibration, Acoustic Emission and Oil Debris on-line Monitoring towards a more Effective Condition Monitoring of Rotating Machinery," Mechanical Systems and Signal Processing, Vol. 25, Pages 1339-1352.

López de L.N. Lacalle, A. Lamikiz, (2009). Machine Tools for High Performance Machining ISBN: 978-1-84800-380-4

Maj R, F Modica, G Bianchi, (2006). Machine Tools - Mechatronic Analysis. Proc. IMechE, Part B, 220 Pages 345-353

Maier D., U. Heisel, (2011). A comparison of model and signal based condition monitoring and mode separation for predictive maintenance of feed drives Journal of Machine Engineering, Vol. 11, No. 4, Pages 138-151

Mayer J.R.R., (2000). Optical Encoder Displacement Sensors. The measurement, instrumentation, and sensors handbook, J.G Webster, CRC press, Boca Raton FL

Mathew J., Kennedy, J., Ma, L., Tan, A., Anderson, D., (2006). Engineering Asset Management Proceedings of the 1st World Congress on Engineering Asset Management (WCEAM) SBN: 978-1-84628-583-7

Mártona, L., B. Lantos, (2009). Control of mechanical systems with Stribeck friction and backlash Systems & Control Letters 58 Pages 141-147.

MathWorks. (2014). MATLAB: The Language of Technical Computing. Retrieved from http://www.mathworks.com/products/matlab/

MathWorks. (2014). SIMULINK: Simulation and Model-Based Design. Retrieved from http://www.mathworks.com/products/SIMULINK/

MathWorks. (2014). SimMechanics: Model and Simulate Multibody Mechanical Systems. Retrieved from http://www.mathworks.com/products/simmechanics/

MathWorks. (2014). SimPowerSystems for use with SIMULINK. Retrieved from http://www.mathworks.com/help/releases/R13sp2/pdf_doc/physmod/powersys/powersys.pdf

MathWorks. (2014). SimPowerSystems: Model and Simulate Electrical Power Systems. Retrieved from http://www.mathworks.com/products/simpower/

McLaskey G.C., D. Steven (2012). Glaser Acoustic Emission Sensor Calibration for Absolute Source Measurements J Nondestruct Eval DOI 10.1007/s10921-012-0131-2

Merzouki R., J.A. Davila, L. Fridman, J.C. Cadiou, (2007). Backlash phenomenon observation and identification in electromechanical system Control Engineering Practice, Vol 15, Issue 4, Pages 447-457

Miller R., K. McIntire, P (1987). Nondestructive Testing Handbook. Volume 5: Acoustic Emission Testing. American Society for Nondestructive Testing. 603 p. ISBN0-931403-02-2

MISTRAS, PAC sensor (2015). Retrieved from http://www.physicalacoustics.com/by-product/sensors/ISPK15I-150-kHz-Intrinsically-Safe-AE-Sensor-with-Low-Power-Integral-Preamp

Montazeri-Gh M., M. Nasiri, S. Jafari, (2011). "Real-time multi-rate HIL simulation platform for evaluation of a jet engine fuel controller," Simulation Modelling Practice and Theory, vol. 19, no. 3, Pages 996-1006.

Mukhopadhyay, C.K., T. Jayakumar, B. Raj, B.S. Venugopa. (2012). Statistical analysis of acoustic emission signals generated during turning of a metal matrix composite. J. Braz. Soc. Mech. Sci. & Eng. vol.34 no.2 Print version ISSN 1678-5878

Nassehi A. S.T. Newman, (2012). Modelling of Machine Tools using Smart Interlocking Software Blocks. CIRP Annals - Manufacturing Technology Volume 61, Issue 1, Pages 435-438

Nelson (2012). MULTI-AXIS drive applications using common DC BUS, Siemens E&A Production Machines Retrieved from: https://www.industry.usa.siemens.com/drives/us/en/electric-drives/ac-drives/ac-drives-apps/multi-axis-common-dc-bus/Documents/Common_DC_bus_paper.pdf

Neugebauer R., C. Scheffler, M. Wabner, M. Schulten, (2010). Advanced State Space Modelling of Non-Proportional Damped Machine Tool Mechanics. CIRP Journal of Manufacturing Science and Technology Volume 3, Issue 1, Pages 8-13

Neugebauer R., C. Scheffler M. Wabner, (2011). Implementation of Control Elements in FEM Calculations of Machine Tools. CIRP Journal of Manufacturing Science and Technology Volume 4, Issue 1, Pages 71-79

Neugebaue R., P. Klimant, M. Witt, (2012). Realistic Machine Simulation with Virtual Reality. Procedia CIRP Volume 3, Pages 103-108

Neugebauer R., S. Ihlenfeldt, U. Frieβ, M. Wabner, S. Rauh, (2012). New High-Speed Machine Tool Structure by Holistic Mechatronic Systems Design. Retrieved from Procedia CIRP Volume 1, 2012, Pages 307-312

Nielsen A., (1980). Acoustic emission source based on pencil lead breaking, The Danish Welding Institute Publication, vol. 15.

Ozevin D., J. Cox, W. Hardman, S. Kessler, A. Timmons (2014). Fatigue Crack Detection at Gearbox Spline Component using Acoustic Emission Method, Annual Conference of the Prognostics and Health Management Society, Publication Control Number: 014

Parey A.M., El Badaoui, F. Guillet, N. Tandon (2006). Dynamic modelling of spur gear pair and application of empirical mode decomposition-based statistical analysis for early detection of localized tooth defect Journal of Sound and Vibration, Vol. 294, Issue 3, Pages 547-561.

Pislaru C. (2001). Parameter Identification and Hybrid Mathematical Modelling Techniques Applied to Non-linear Control Systems., PhD Thesis, University of Huddersfield

Pislaru C. (2013). A Review on Real-Time Simulation of CNC Machine Tool Dynamics, Retrieved from: http://eprints.hud.ac.uk/18405/1/2-67-1379752218-4._Mech-IJME-_A_Review_on_Real-Time_-Pislaru_-UK.pdf

Prasad B. S. Sracar, M. M. M. Satish, B. (2011). Real-time tool condition monitoring of face milling using acousto-optic emission – an experimental approach. International Journal of Computer Application in Technology, vol. 41, no. 3–4, Pages 317–325.

Pürzel F, P Klimant, V Wittstock, M Kuhl (2013). Real NC Control Unit and Virtual Machine to Improve Operator Training Int. Conf. on Virtual and Augmented Reality, Pages 98–107.

Prevost, D., S. Lavernhe C. Lartigue, (2010). Feed Drive Simulation for the Prediction of the Tool Path follow up in High Speed Machining. Retrieved from http://arxiv.org/ftp/arxiv/papers/1004/1004.4722.pdf

Raghavan A., C. Cesnik, (2007). The Shock and Vibration Digest, 39, Pages 91-114.

Raharjo, P., B. Tesfa, F. Gu, A. Ball, (2012). A Comparative Study of the Monitoring of a Self-Aligning Spherical Journal using Surface Vibration, Airborne Sound and Acoustic Emission. Journal of Physics: Conference Series, 364. 012035. ISSN 1742-6596

Rexroth Bosch Group, Manual, (2006) Retrieved from: https://www.boschrexroth.com/ics/cat/?&id=&cat=Linear-Motion-Technology-Catalog&u=si&o=Desktop&p=g255180,g255583,g302780,g301380

Russer P., (2000). The transmission line matrix method, in Applied Computational Electromagnetics, ser. NATO ASI Series, Springer, Berlin, pp. 243–269

RecurDyn (2013). RecurDyn. Retrieved from: http://www.functionbay.de/why-multibody-dynamics-simulation.html

Reynolds, O. 1886. On the Theory of Lubrication and Its Application to Mr. Beauchamp Tower's Experiments, Including an Experimental Determination of the Viscosity of Olive Oil. *Philosophical Transactions of the Royal Society of London*.

Saravanan S., G.S.Yadava, P.V. Rao (2003) Machine Tool Failure Data Analysis For Condition Monitoring Application Retrieved from: 11th National Conference on Machines and Mechanisms, IIT Delhi

Siemens, (2008), Sinamics S120/s150 List Manual, Retrieved from: http://www.pogoni.etf.bg.ac.rs/VezbeRP/Sinamics%20S120-manual.pdf

Srinivasa B., S. Prasad, D. Prasad, A. Sandeep, G. Veeraiah, (2013). Condition Monitoring of CNC Machining Using Adaptive Control (J). International Journal of Automation and Computing, vol. 10, no. 3, Pages 202-209.

Suh S.H., S.K. Kang, D.H. Chung, I.A. Stroud, (2008). Theory and Design of CNC Systems Springer Publishing Company, Incorporated ISBN: 1848822111 9781848822115

Sztendel S., C. Pislaru, A.P. Longstaff, S. Fletcher, A. Myers, (2012). Five-Axis Machine Tool Condition Monitoring Using dSPACE Real-Time System, Journal of Physics: Conference Series 364, 25th International Congress on Condition Monitoring and Diagnostic Engineering

Sztendel S., C. Pislaru, A. Poxton, D.G. Ford, A. Myers, (2009). Developing Mechatronic Models Of Modern CNC Machine Tools For Real-Time Implementation. Proc. LAMDAMAP 2009, Brunel, Pages 147-155.

Urbanek J., T. Barszcz, J. Antoni (2014). Integrated modulation intensity distribution as a practical tool for condition monitoring. Applied Acoustics, 77, Pages 184 – 194

Uhlmann E., J. Eβmann, J-H. Wintering, (2012). Design- and Control-Concept for Compliant Machine Tools based on Controller Integrated Models. Retrieved from: CIRP Annals - Manufacturing Technology Volume 61, Issue 1, Pages 347-350

University of Copenhagen. (2014). Welcome to Physical Modelling. Retrieved from http://www.itu.dk/stud/speciale/segmentering/Matlab6p5/help/toolbox/physmod/mech/mech_intro2.html

Yanada H., Y. Sekikawa, (2008). Modelling of dynamic behaviours of friction Mechatronics, Vol 18, Pages 330-339

Yang J., Y. Altintas, (2013). Generalized Kinematics of Five-Axis Serial Machines with Non-Singular Tool Path Generation. Retrieved from: International Journal of Machine Tools and Manufacture Volume 75, Pages 119-132

Yeung C.H., Y Altintas, K. Erkorkmaz, (2006). Virtual CNC System - Part I: System Architecture, Int. J Mach Tools and Manuf 46. 1107-1123.

Walsh J., Bashir, I., Thies P. R., L. Johanning., Blondel, Ph., (2015). Acoustic emission health monitoring of marine renewables: Illustration with a wave energy converter in Falmouth Bay (UK) MTS/IEEE Oceans15, At Genova, Italy

Wei N., F. Gu, T. Wang, G. Li, Y. Xu, L.Yang, A. Ball, (2015). Characterisation of Acoustic Emissions for the Frictional Effect in Engines using Wavelets based Multi-resolution Analysis. In: Proceedings of the 21st International Conference on Automation and Computing (ICAC). IEEE. ISBN 978-0-9926801-0-7

Whalley R., A.A. Abdul-Ameer, and K.M. Ebrahimi, (2011). The Axes Response and Resonance Identification for a Machine Tool. Mechanism and Machine Theory Volume 46, Issue 8, Pages 1171-1192

Widiyarto M.H.N., C. Pislaru, D.G. Ford A.P. Longstaff, A. Myers, (2005). Hybrid Modelling Technique Applied to Digital Feed Drives, Proceedings of the 7th LAMDAMAP. European Society for Precision Engineering and Nanotechnology, Pages 454-463. ISBN 1861941188

TIEPIE (2015) High accuracy measurement products Retrieved from: http://www.tiepie.com/en/products/Oscilloscopes

Theobald P. (2016) Guide on Acoustic Emission Sensor Couplants Retrieved from http://www.npl.co.uk/acoustics/ultrasonics/research/guide-on-acoustic-emission-sensor-couplants

Tummescheit H., C. Haugstetter (2003). Hardware-in-the-Loop Simulation & Analysis Retrieved from: https://www.cds.caltech.edu/help/uploads/wiki/files/12/HIL-DGC100.pdf

Zaeh, M., D. Siedl, (2007). A New Method for Simulation of Machining Performance by Integrating Finite Element and Multi-body Simulation for Machine Tools ANNALS- CIRP 2007, VOL 56; NUMBER 1, Pages 383-386

Zirn O, J. Nowak, B. Hiller, (2007) Dynamic coupling force compensation for direct-driven machine tools IEEE Ind. Applications Society Annual Meeting (New Orleans)

Zirn, O. (2008). Machine Tool Analysis - Modelling Simulation and Control of Machine Tool Manipulators, Habilitation Thesis, ETH Zurich, Institute of Machine Tools and Manufacturing.

APPENDIX A AE SENSORS COMPARISON

VALLEN

Electrical Data

max. voltage:	U_i = 13,8 V_{DC}
max. current:	I_i = 60 mA
max. power:	P_i = 0,3 W
max. internal capacity:	C_i = 65 nF
max. internal inductivity:	L_i = 1 µH

Mechanical Specifications

Protection class (EN60529)	IP68 (cable connected)
Ambient temperature	-20 … +60 °C
Case material	Stainless steel 1.4571
Max. surface temp. (worst case fault)	< 85°C at 60 °C ambient temperature
Dimension	53,5 W x 56 L x 47,5 H mm, Cover diameter: 46,5mm For ISAS3-030 add 7,5mm height
Weight	0,25 kg (sensor) 0,17 kg (magnet holder)
Mounting aid	Magnet holder MAG4IS, see ISAS3-SpecMount

ISAS3 is equipped with an integral preamplifier that has 20dB gain. It is suitable for driving long distances (up to 2km) of BNC cable. The integral preamplifier supports Automatic Sensor Test (AST) for judging sensor coupling.

Score Dunegan SE150-MI-IS & SE900-MWBI-IS

They have +20dB internal preamplifiers and must be used with the 500J-IS power adapter and barrier to achieve proper IS protection. The adapter provides power and signal conditioning for the IS AE sensors. It is for operation in safe areas or unclassified locations, typically installed in an instrument cabinet or rack, and is certified associate apparatus cULus

Aperture size:	Diameter 0.675 inch (17.14 mm)
Case Material:	Stainless Steel
Physical Dimensions:	Diameter 0.993 inch (25.23 mm)
	Height 1.000 inch (25.4 mm)
Weight:	45 grams
Temperature:	- 40 to + 75 °C

$725.00

https://score-atlanta.com/products/Intrinsically%20Safe%20AE%20Products

KISTLER

Type	Unit	8152B111/121	8152B21/22sp
Sensitivity	dBref 1V/(m/s)	57	48
Frequency Range ±10dB	kHz	50 ... 400	100 ... 900
Ground Isolation	MΩ	>1	>1
Environmental:			
Shock Limit (0,5ms pulse)	gpk	2000	2000
Temperature Range Operating	°C	-40 ... 60	-40 ... 60
Output:			
Bias nom.	VDC	2,2	2,5
Impedance	Ω	<10	<10
Voltage full scale	V	±2	±2
Current	mA	2	4
Source:			
Voltage (Coupler)	VDC	5 ... 36	5 ... 36
Constant Current	mA	3 ... 6	3 ... 6
Construction:			
Sensing Element	type	ceramic	ceramic
Housing/Base	material	stainless steel	stainless steel
Sealing-housing/connector	type	hermetic	hermetic
Viton Cable Bend Radius, max.	mm	15,24	15,24
Weight (without cable)	grams	29	29
Mounting Torque	Nm	9±1	9±1

PAC

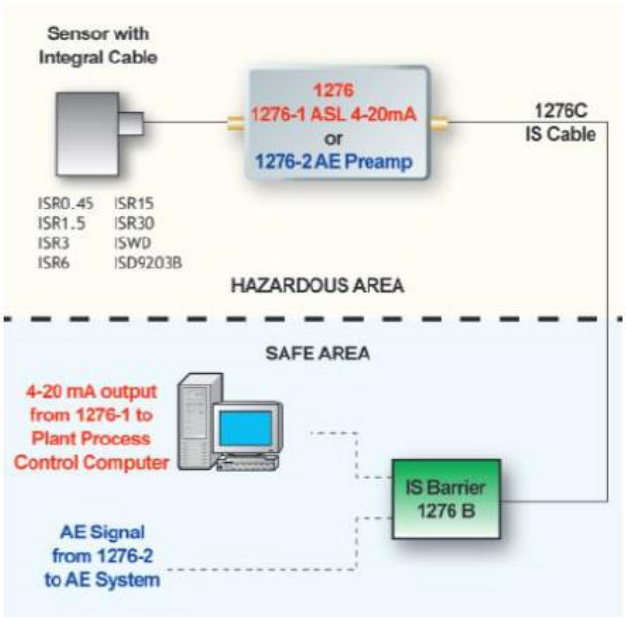

- **Noise:** < 2 mV RTI
- **Output:** 2 V p-p into 50 Ω
- **Power:** 11 – 11.5 VDC
- **Operating Current:** 20 mA
- **Operating Temp.:** -40°C to +70°C
- **Dimensions:** 5.92"(L)x2.50"(W)x1.38"(H) (15.04cm x6.35cm x 3.50cm)
- **Weight:** 0.81lb(360 grams)

Roxar Sand monitor

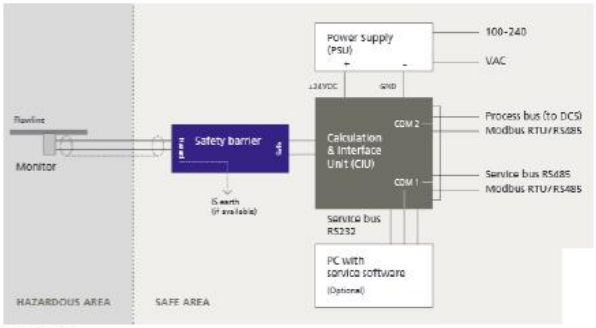

EMERSON.
Process Management

Detector unit

Power consumption:	Maximum 0.6W
Supply voltage:	11-18 V (supplied with 24 V DC via Safety barrier)
Hazardous area classification:	EEx ia
Location:	Hazardous area, Zone 0, 1 or 2
Pipe surface temperature range:	-40 to + 115°C (or higher with high-temperature fixture)
Ambient temperature range:	-40 to +80°C
Dimensions:	88 (OD) x 100 mm
Weight:	3.0 kg
Ingress protection:	IP 67
Installation:	Clamped onto pipe
Material:	Stainless steel 316

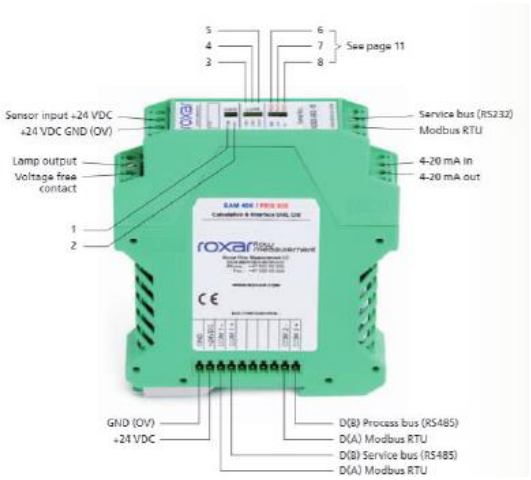

SIEMENS

Acoustic sensor for solids flow detection

SITRANS AS100

- Non-invasive
- Screw in, bolt on, weld, or bond in place
- Analog output
- High and low sensitivity range of operation

Enclosure	Compact 304 or 303 stainless steel, IP68
Sensor mounting	Sensor non-invasive: glue or weld-on disc, bolt or weld-on tab, drill and tap
Operating temperature	-20 ... +80 °C (-4 ... +176 °F)[1]
Power requirements	20 ... 30 V DC, 18 mA
Approvals	CE, C-TICK, CSA/FM Class II, Div. 1, Group E, F, G optional, ATEX II, 2GD, 3D optional, GOST-R

Pulsarguard 201x series

The sensor listens to the high frequency sound generated by impacts, cavitation and friction within a system. 100 to 600kHz is the bandwidth of the sensor making it immune to audible noise or vibration caused by plant machinery.

`Product Name	Comment
PULSARguard 2010HT	High temperature version -40 °C to +125 °C. Identified by "HT" stamped on mounting tab.
PULSARguard 2011Z	Suitable for use with Zener barriers only (Certificate No. Sira 04ATEX2121X). This system requires connection to an intrinsically safe earth. Zener barriers are a cheaper option to galvanic isolating barriers. Identified by "Z" stamped on mounting tab.
PULSARguard 2011G	Suitable for use with Galvanically isolating barriers only (Certificate No. Sira 04ATEX2121X). This system does not require connection to an intrinsically safe earth. Galvanic isolating barriers are a more expensive option to zener barriers. Identified by "G" stamped on mounting tab.

http://www.pulsar-pm.com/

AVT

The IS series of high performance, ATEX certified, acoustic emission transducers offer high sensitivity-low noise measuring capability for a wide range of industrial applications in designated hazardous areas. There are three basic models each with its own temperature rating which are available in four versions covering the frequency range from 70 to 650 kHz.

IS2000:	Ex II 1 G EEx ia IIC T6 (-20°C ≤ T_a ≤ +80°C) (Baseefa03 ATEX0197)
IS2200:	Ex II 1 G EEx ia IIC T4 (-20°C ≤ T_a ≤ +115°C) (Baseefa03 ATEX0198)
IS2201:	Ex II 1 G EEx ia IIC T3 (-20°C≤ T_a ≤ +190°C) (Baseefa03 ATEX0199)
IA2100:	Ex II 1 G EEx ia IIC T4 (-20°C ≤ T_a ≤ +70°C) (Baseefa03 ATEX0195X)
IF410:	Ex II (1) G [EEx ia] IIC (Baseefa03 ATEX0194)

http://www.avtechnology.co.uk/products.php?record_id=8

APPENDIX B SIMULATION SOFTWARE COMPARISON

LMS,

LMS gives direct coupling of multibody model with MATLAB and Simulink. Its flexible body modeling based on FEA modes , solid model user interface for part and assembly construction and ability to directly connect multibody results to durability and acoustic analysis.

Virtual.Lab Motion is the connection to MATLAB and Simulink is a solution for connecting multibody dynamic equations of motion with control and hydraulic models to produce more complete and accurate coupled dynamic systems. The product is used to solve the constrained nonlinear equations of motion and report the positions, velocities, accelerations, and reaction forces of all parts in the system.

Simulink models of control systems can link them with Virtual.Lab Motion using the S-Function feature. All outputs from Virtual.Lab Motion (position, velocity, and acceleration of parts), and all inputs to Virtual.Lab Motion (forces or torques acting on parts) are passed through a single S-Function element. MATLAB solver performs the integration of the combined equations of motion and control state equations to produce time-domain results for position, velocity, acceleration, and reaction forces from the mechanical system, and control states from Simulink. Results can be plotted as normal in MATLAB, and mechanical system results in Virtual.Lab Motion. The complete model can be animated in Virtual.Lab Motion.

Integration with Dassault Systèmes' CATIA V5, LMS Virtual.Lab Structures eliminates the need to translate the original geometry to an intermediate meshable geometry format. With integrated drivers for industry-standard solvers, such as Nastran (MD, MSC, NX, NEi), Abaqus, LSDyna and Radioss.

SIMPACK

With the powerful FE-interface FEMBS, SIMPACK has the reputation to be the technology leading multi-body system for the integration of flexible bodies. The multi-level interfaces SIMAT and MATSIM make SIMPACK the perfect partner for Matlab Simulink when 3D-mechanical systems have to be connected to a 1D block-oriented simulation. CAD data can be used in multi-body simulation using SIMPACK's CAD interfaces. SIMPACK can also represent the missing link between FE- and CAD-data that is required by Simulink. FEMBS, the SIMPACK-Interface to finite element programs enables the user to incorporate Finite-Element-models into SIMPACK for the representation of flexible bodies in mechanical systems.

Ricardo

Ricardo is used in the field of engine and vehicle engineering. It links between ANSYS FLUENT and WAVE gives ANSYS FLUENT users the ability to execute simultaneously with WAVE through the Ricardo API. There are occasions when it is not possible to model the entire flow domain in an engine using 3D CFD due to the excessively large mesh and subsequent run-time. In these instances it is extremely advantageous to be able to model the majority of the engine using the simpler 1D approach and only the critical parts where real important 3D flow phenomena are expected. In addition, the 2-way coupling allows feedback between the simulations allowing for more accurate results.

CAE analysis programs with the ability to communicate during the simulation are the most effective tools to design fully integrated systems. An Application Program Interface (API) has been developed to enable WAVE to be linked to other industry-standard commercial programs including Matlab/Simulink, EASY5, Matrixx/Systembuild and VECTIS and ANSYS FLUENT.

SDT

An interface between ANSYS and the Structural Dynamics Toolbox really reads element mass and stiffness matrices so that can both assemble the full model or consider modifications. An example application is to generate flexible body models to be used in ADAMS or SYMULINK.

National instruments

NI INSIGHT can be used to import any model that can be saved into the VRML format (.wrl), which works with most major CAD and CAE software packages including SolidWorks, ProEngineer, CATIA, NX I-deas,NASTRAN and ANSYS. You can easily pass measurement data directly to the NI INSIGHT environment through LabVIEW automation commands to map live measurements directly to CAD/CAE models for instant design validation and simulation verification. The open, flexible architecture of LabVIEW means that you can connect to virtually any type of measurement device.

APPENDIX C GEISS CNC MACHINE TECHNICAL DATA

GEISS AG	
Project	FZ61990
Plant designation	2000 x 1000 D sl
Supply	230/400V/50Hz/41KW/61A
Control voltage	230VAC/24VDC
Model	2008
Motion controller	SIEMENS SINUMERIK 840D SL
Electrical drive	SINAMICS S120
Motor	SIEMENS 1FK7083-5AF71 CT, HARMONIC DRIVE FHA-32C-50-H-C1024-B and FHA-40C-50-H-C1024-B
Rotary encoder	INBUILT ENCODER WITH SMI MODULE
Linear encoder	HEIDENHAIN LC 183

Table C -1 Data for GEISS CNC machine tool

Technical data for X-axis Y-axis, Y2-axis Z-axis, and B-axis C-axis		
Siemens double motor module 2 x 9A 6SL3120-2TE21-0AA3 (booksize format)		
Output current	Rated current I_{rated} (A)	2 x 9
	For S6 duty (40%) I_{S6} (A)	2 x 10
	Base-load current I_H (A)	2 x 7.7
	I_{max} (A)	2 x 18
Type rating[1)]	Based on I_{rated} (kW (HP))	2 x 4.8 (5)
	Based on I_H (kW (HP))	2 x 4.1 (5)
DC link current I_d[2)] (A)		22
Current carrying capacity	DC link busbars (A)	100
	24V DC busbars (A)	20
DC link capacitance (µF)		220
Current requirement with 24V DC, max. (A)		1.0
Weight, approx.	With internal air cooling (kg (lb))	5.3 (11.7)
	With external air cooling (kg (lb))	5.8 (12.8)

Table C-2 Technical data for double motor module (Siemens, 2008)

Technical data for 1FK7 motors			
Motor type	Permanently excited synchronous motor		
Magnet material	Rare-earth magnet material		
Siemens motor 1FK7083 CT			
Technical data	Code	Units	-5AF71
Rated speed	n_N	RPM	3000
Number of poles	2p		8
Rated torque (100K)	$M_{N(100K)}$	Nm	10.5
Rated current	I_N	A	7.4
Stall torque (60K)	$M_{0(60K)}$	Nm	13.3
Stall torque (100K)	$M_{0(100K)}$	Nm	16
Stall current (60K)	$I_{0(60K)}$	A	8.6
Stall current (100K)	$I_{0(100K)}$	A	10.4
Moment of inertia (with brake)	J_{mot}	$10^{-4}kgm^2$	35.9
Moment of inertia (without brake)	J_{mot}	$10^{-4}kgm^2$	27.3
Optimum speed	n_{opt}	RPM	3000
Optimum power	P_{opt}	kW	3.3
Max. permissible speed (mech.)	n_{max}	RPM	6000
Max. torque	M_{max}	Nm	50
Peak current	I_{max}	A	37
Torque constant	K_T	Nm/A	1.52
Voltage constant	K_E	V/1000 RPM	97
Winding resistance at 20°C	R_{ph}	Ohm	0.4
Rotating field inductance	L_D	mH	6.0
Electrical time constant	T_{el}	ms	15
Shaft torsional stiffness	C_t	Nm/rad	105000
Mechanical time constant	T_{mech}	ms	1.41
Thermal time constant	T_{th}	min	50
Weight with brake	m	kg	16.5
Weight without brake	m	kg	14

Table C-3 Technical dataforSiemens Motor 1FK7083-5AF71 CT(Siemens, 2005)

Dimensions for FAR drive units without side drive timing belt and motor (mm)									
D_1	D_5 h6	D_6	D_7	D_{T1}	G_1	L_{FAR}	L_{G1}	L_{ZF}	L_1
20	80	65	M8	h6	M20x1	120	31	108	77
L_3	D_L -0.018	K_L	d_{L3} +0.3/-0.1	t_L	S	S_L	B_L	D_N	B_N
11	145	120	8.8	8x45°	8	M6	49	75	16

Technical data for FAR drive unit with side drive timing belt and AC servo motor with brake								
Size	Motor				Mass moment of inertia		Weight	
	Motor type**	Torque		Rated rotary speed* (n_K) (min^{-1})	Motor J_M (kgm^2) x 10^{-4}	Brake J_{BR} (kgm^2) x 10^{-4}	Motor M_{BR} (Nm)	Brake m_M (kg)
		M_{MN} rated (Nm)	M_{Mmax*} maximum (Nm)					
32x32 Rx3.969-3	MKD 090B-047	12	43.5	3200	43	3.5	14	1.1

FAR drive unit with side drive timing belt and AC servo motor with brake									
Dimensions (mm)							Side drive timing belt reduction i_{RV}	Reduced mass moment of inertia at the motor journal J_{RV} (kgm^2)10^{-4}	Weight of side drive timing belt m_{RV} (kg)
S_1	D_N	D_L	W_1	W_2	L_E	H_E			
13	75	145	47	60	313	140	1	79	8.6

Table C-4 FAR drive unit with side drive timing belt and AC servo (Rexroth Bosch Group, 2006)

Technical data for FHA-32C-50-H-C1024-B B-axis and FHA-40C-50-H-C1024-B (C-axis)				
Excitation		Permanent magnet		
Number of pole pairs		6		
Actuator		Unit	FHA-32C-50-H	FHA-40C-50-H
Ratio			50	50
Maximum output torque		Nm	281	500
Maximum output speed		min^{-1}/rpm	80	70
Continuous stall torque		Nm	73	122
Continuous stall current		Arms	1.7	2.4
Maximum current		Arms	6.0	8.9
No load current		Arms	0.5	0.72
Torque constant (at output)		Nm/A	51	61
Torque constant (motor)		Nm/A	1.11	1.33
Motor terminal voltage		Vrms	430	430
Mechanical time constant (20°C)		ms	7.1	9.6
Electrical time constant (20°C)		ms	1.3	1.97
Moment of inertia without brake		kgm^2	1.87	5.0
Moment of inertia with brake		kgm^2	2.2	5.7
Moment of inertia at motor without brake		$kgm^2 \times 10^{-4}$	7.5	20
Moment of inertia at motor with brake		$kgm^2 \times 10^{-4}$	8.9	22.6
Rated motor speed		min^{-1}/rpm	2500	2500
Maximum motor speed		min^{-1}/rpm	4000	3500
Resistance (L-L, 20°C)		Ω	7.8	5.6
Inductance (L-L)		mH	9.9	11.1
Weight without brake		kg	6.7	12.2
Weight with brake		kg	7.6	14.2
Brake voltage		VDC	24 ± 10%	24 ± 10%
Brake holding torque (at output)		Nm	75	108
Hollow shaft diameter		mm	35	45
Transmission accuracy		arcmin	< 0.7	< 0.7
Torsional stiffness		$Nm/rad10^3$	150	300
Ambient operating temperature		°C	0…40	0…40
Output bearing	Dynamic radial load	N	6250	11644
	Dynamic axial load	N	9328	17379
	Dynamic tilt moment	Nm	530	690

Table C-5 Technical data for motors FHA-32C-50-H and FHA-40C-50-H (Harmonic Drive, n.d.)

Parameters for three-phase source block	
Phase-to-phase rms voltage (V)	400
Phase angle of phase A (degrees)	0
Frequency (Hz)	50
Internal connection	Yg
Source resistance (Ohms)	0.02
Source inductance (H)	0.05e-3
Base voltage (Vrmsph-ph)	25e3
Generator type of load flow	swing
Parameters for three-phase diode rectifier block	
Number of bridge arms	3
Snubber resistance Rs (Ohms)	10e3
Snubber capacitance Cs (F)	20e-9
Power electronic device	diodes
Ron (Ohms)	1e-3
Lon (H)	0
Forward voltage Vf (V)	1.3
Parameters for braking chopper block	
Chopper activation voltage (V)	320
Chopper shutdown voltage (V)	310
Braking chopper frequency (Hz)	4000
DC bus capacitance (F)	2000e-6
Braking resistance (ohms)	8
Parameters for three-phase inverter block	
Ron (Ohms)	1e-3
Source Frequency (Hz)	50
PMSM-Inductances (Ld(H) Lq(H))	(8.5e-3,8.5e-3)
PMSM-Flux induced by magnets (Wb)	0.175
PMSM-Stator resistance Rs (ohm)	0.2
PMSM-Pairs of poles p	6

Table C-6 Parameters for B-axis drive

Configuration and parameters for PMSM block	
Number of phases	3
Back EMF waveform	sinusoidal
Rotor type	round
Mechanical input	Torque Tm
Preset model	No
Stator phase resistance Rs (ohm)	7.8
Armature inductance (H)	0.0099
Flux linkage established by magnets (V.s)	0.175
Inertia, viscous damping, pole pairs, static friction (J(kg.m^2) F(N.m.s) p() Tf(N.m))	(0.089,0.005,6)
Initial conditions (wm(rad/s) thetam(deg) ia,ib(A))	(0,0,0,0)
Rotor flux position when theta = 0	90 degrees behind phase A axis (modified Park)
Parameters for vector controller block	
Motor pairs of poles	6
Flux induced by magnets (Wb)	0.175
Sampling time (s)	75e-6

Table C-7 Parameters for B-axis drive

Parameters for three-phase inverter block	
Data is presented only for the three-phase inverter, PMSM, and vector controller block of X-axis, because the parameters of other blocks are similar to those of B and C-axis drive.	
Ron (Ohms)	1e-3
Source Frequency (Hz)	50
PMSM-Inductances (Ld(H) Lq(H))	(8.5e-3,8.5e-3)
PMSM-Flux induced by magnets (Wb)	0.175
PMSM-Stator resistance Rs (ohm)	0.2
PMSM-Pairs of poles p	8
Configuration and parameters for PMSM block	
Number of phases	3
Back EMF waveform	sinusoidal
Rotor type	round

Mechanical input	Torque Tm		
Preset model	No		
Stator phase resistance Rs (ohm)	0.4		
Armature inductance (H)	0.006		
Flux linkage established by magnets (V.s)	0.175		
Inertia, viscous damping, pole pairs, static friction (J(kg.m^2) F(N.m.s) p() Tf(N.m))	(0.15,0.005,8)		
Initial conditions (wm(rad/s) thetam(deg) ia,ib(A))	(0,0,0,0)		
Rotor flux position when theta = 0	90 degrees behind phase A axis (modified Park)		
Parameters for vector controller block			
Motor pairs of poles	8		
Flux induced by magnets (Wb)	0.175		
Sampling time (s)	75e-6		
Parameters for the mechanical part of X-axis			
Parameters for belt and pulley		Parameters for inertia	
Gear ratio	1.5	Inertia (kg·m^2)	0.0058
Parameters for ball-screw		Initial velocity (rad/s)	0
Screw lead (m)	271.5	Mass	
Screw helix type	Right-hand	Mass (kg)	8
Friction model	Constant efficiency	Initial velocity (m/s)	0
Lead angle (degrees)	15	Spring rate (N/m)	1/9.8
Acme thread half angle (degrees)	14.5	Initial deformation (m)	0.00001
Friction coefficient	0.08	Parameters for ideal translational motion sensor (linear encoder)	
Linear velocity threshold (m/s)	0.001		
Viscous friction coefficient (N·m/(rad/s))	25·96	Initial position (m)	0

Table C-8 Parameters for the mechanical part of X-axis

Parameters for speed controller block	
Regulation type	Speed regulation
Speed reference ramp (rpm/s) (deceleration, acceleration)	(-1000,1000)
Proportional gain	5
Integral gain	100
Speed measurement - low-pass filter cutoff frequency (Hz)	100
Controller output torque saturation (N.m) (negative, positive)	(-17.8,17.8)
Controller sampling time (s)	2·75e-6
Parameters for position controller block	
Form	parallel
Time domain	Continuous-time
Proportional	Kp
Y-axis	
Data is presented only for the inertia and mass blocks of Y-axis, because the parameters of other blocks are similar to those of X-axis drive.	
Inertia (kg·m^2)	0.008
Initial velocity (rad/s)	0
Mass (kg)	50
Initial velocity (m/s)	0
Z-axis	
Inertia (kg·m^2)	0.007
Initial velocity (rad/s)	0
Mass (kg)	30
Initial velocity (m/s)	0
Gantry axis	
Mass	500kg
Maximum travel	1410mm
Technical data for spindle CLASSIC 126 400V/60A 6SL3120-1TE26-0AA3	
With external air cooling (kg (lb))	13.4 (29.5)
With cold plate cooling (kg (lb))	9.1 (20.1)

Table C-9 Parameters for blocks of the feed drive

Configuration and parameters for PMSM block	
Data is presented only for the PMSM block of C-axis, because the parameters of other blocks are similar to those of B-axis drive.	
Number of phases	3
Back EMF waveform	sinusoidal
Rotor type	round
Mechanical input	Torque Tm
Preset model	No
Stator phase resistance Rs (ohm)	5.6
Armature inductance (H)	0.011
Flux linkage established by magnets (V.s)	0.175
Inertia, viscous damping, pole pairs, static friction (J(kg.m^2) F(N.m.s) p() Tf(N.m))	(0.1,0.005,6)
Initial conditions (wm(rad/s) thetam(deg) ia,ib(A))	(0,0,0,0)
Rotor flux position when theta = 0	90 degrees behind phase A axis

Table C-10 Configuration and parameters for PMSM block of C-axis drive

APPENDIX D SIMULATION RESULTS

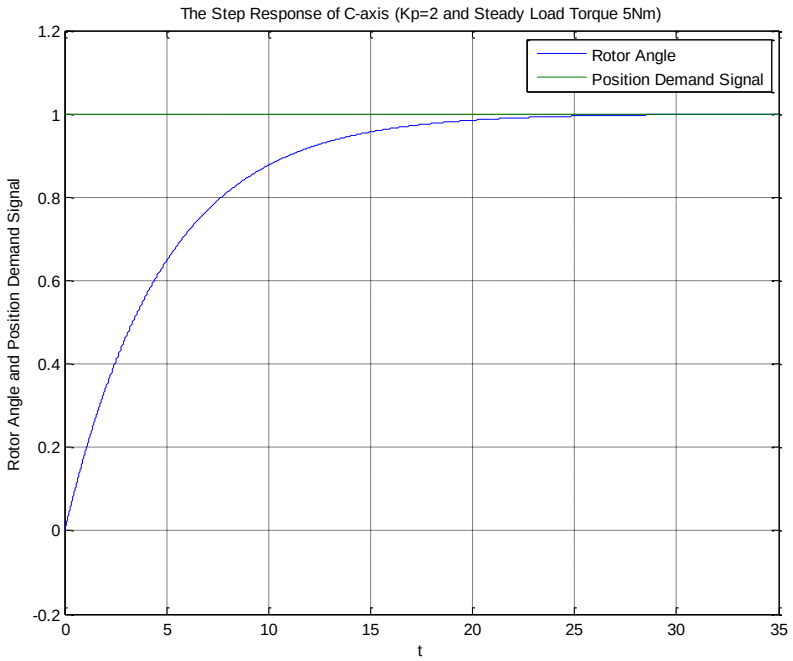

a

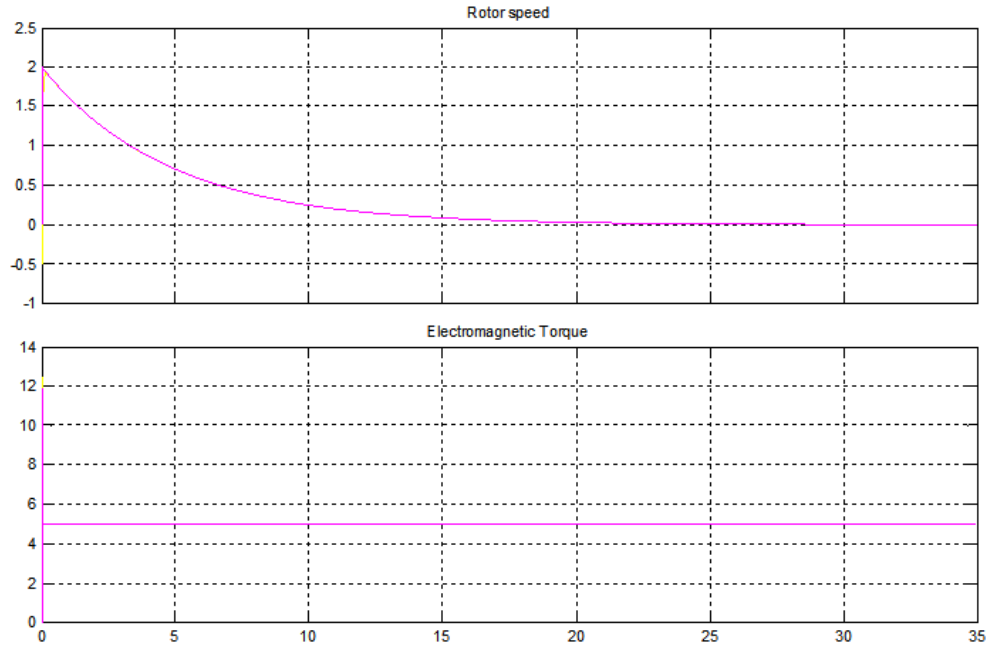

b

a)The unity step response b) Rotor speed with nominal speed (above) and electromagnetic torque with reference torque

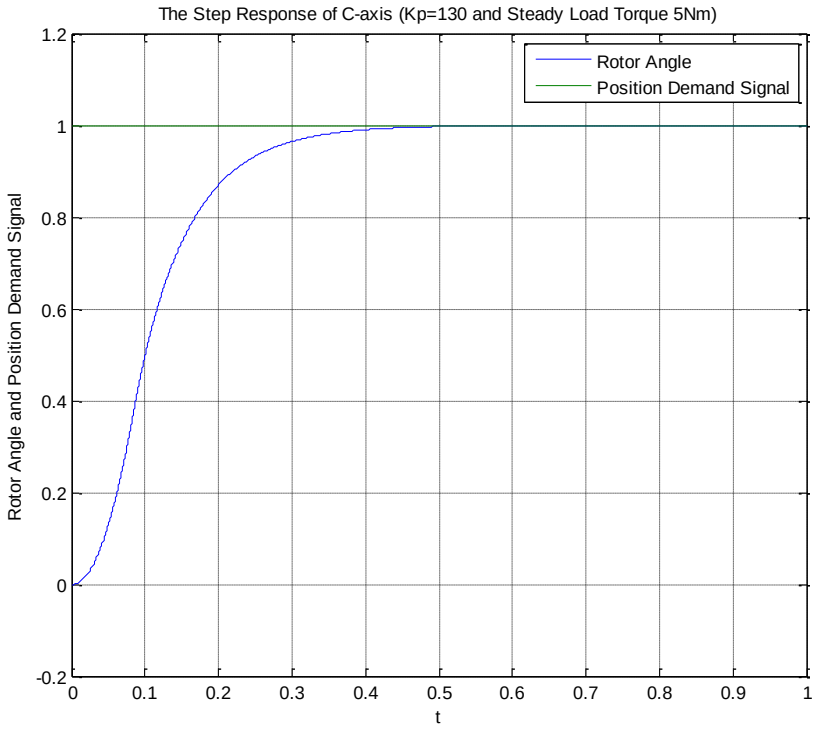

a

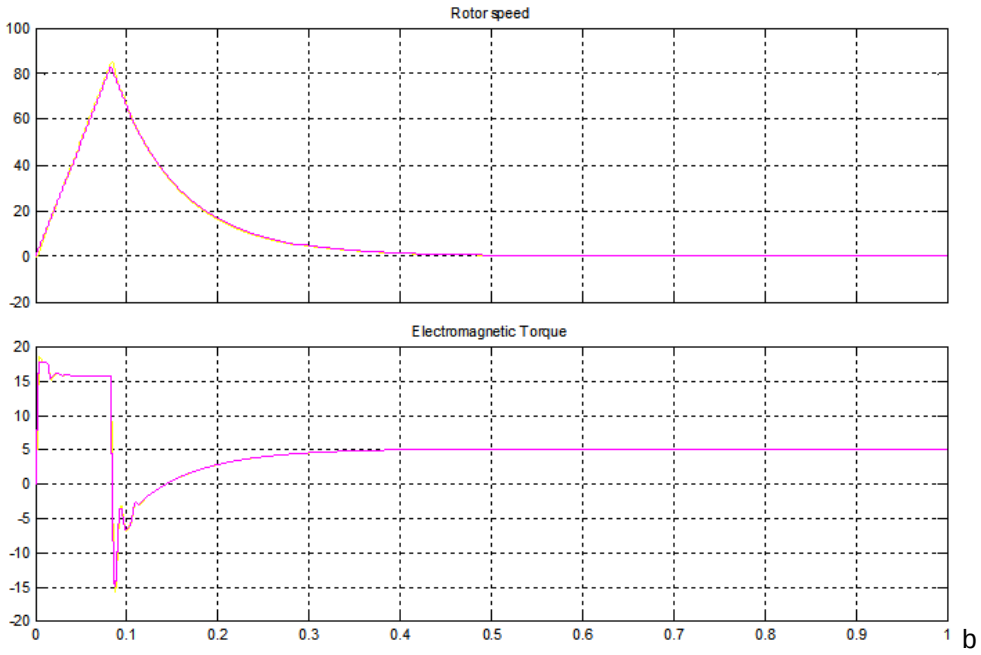

b

The unity (a) step response of C-axis for a steady load torque 5 Nm and Kp=130 Rotor speed with nominal speed (above) and (b) electromagnetic torque with reference torque (below) for a step input, steady load torque 5Nm, and Kp=130

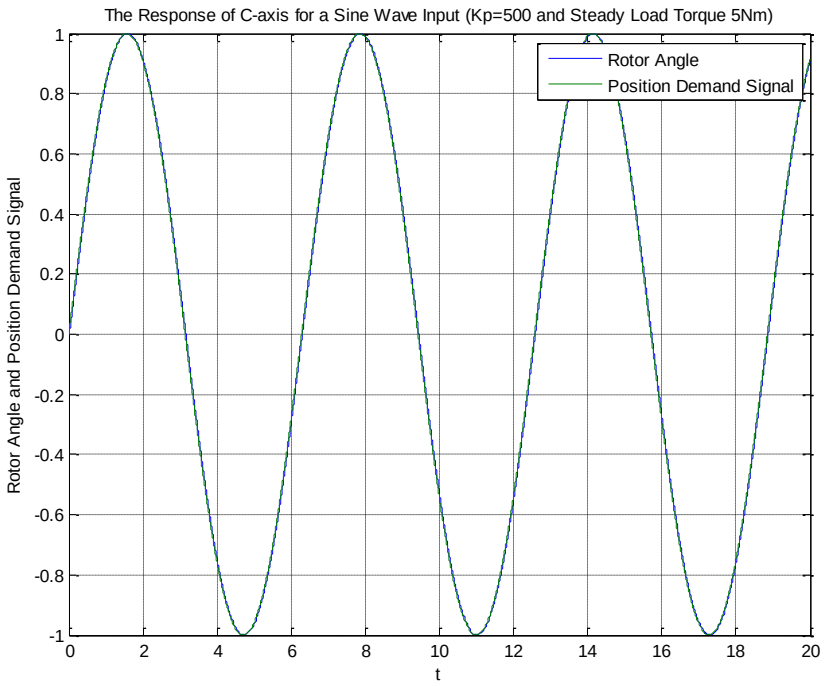

a

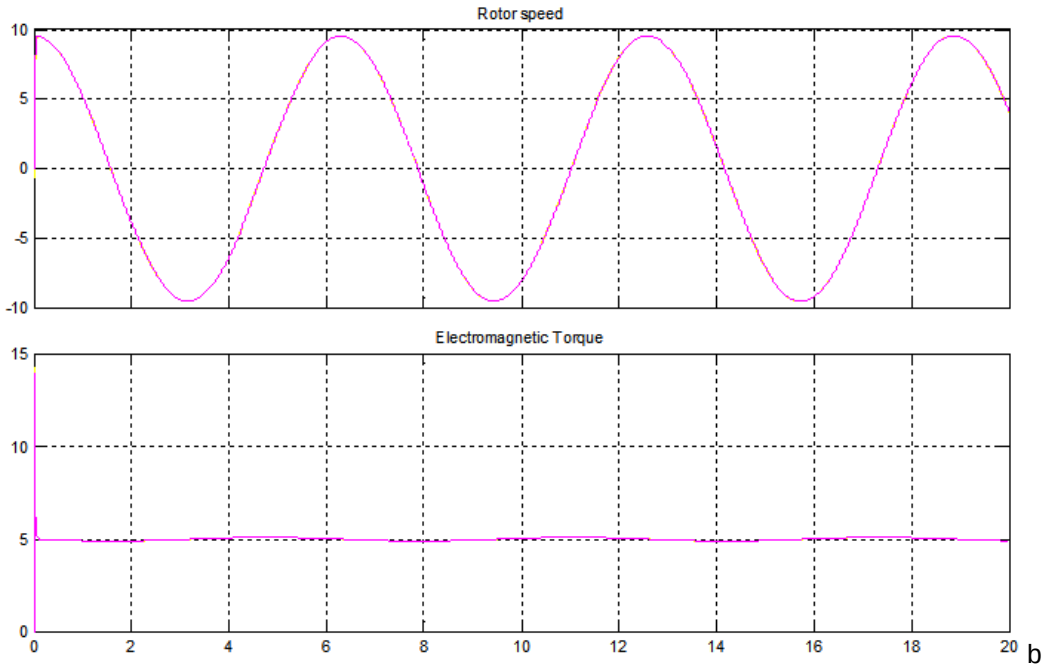

b

The response of C-axis for a sine wave input, steady load torque 5Nm, and Kp=500
Rotor speed with nominal speed (above) and electromagnetic torque with reference torque (below) for a sine wave input, steady load torque 5Nm, and Kp=500

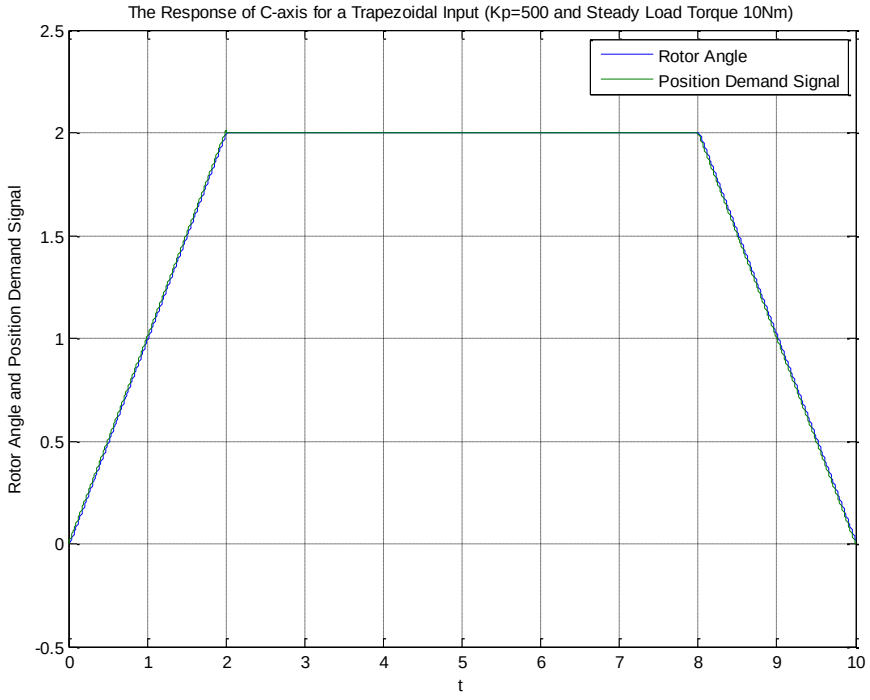

a

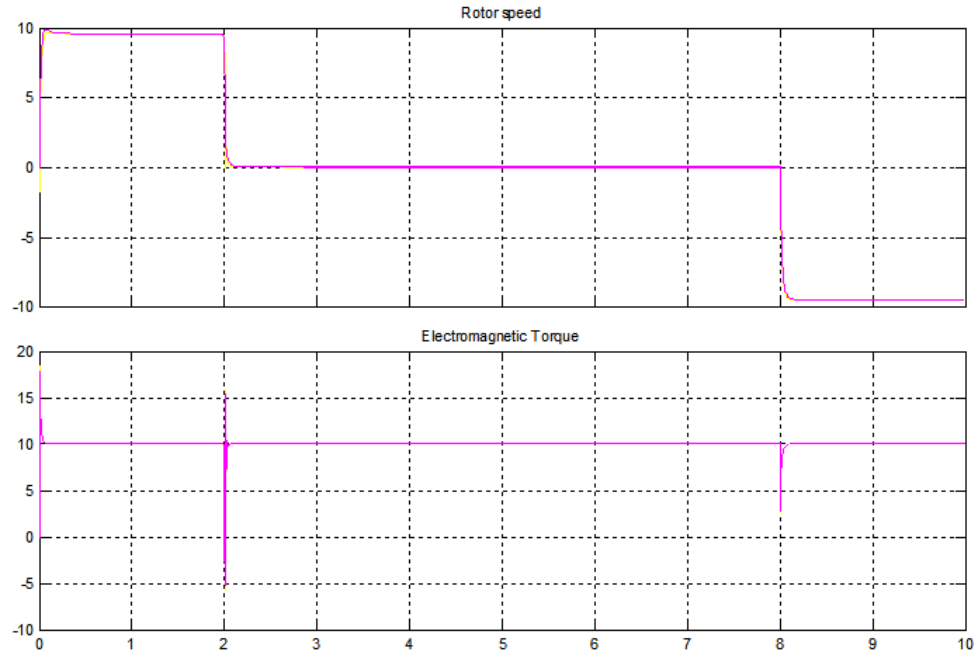

b

a) The response of C-axis for a trapezoidal input, steady load torque 10Nm, and Kp=500 b)Rotor speed with nominal speed (above) and electromagnetic torque with reference torque (below) for a trapezoidal input, steady load torque 10Nm, and Kp=500

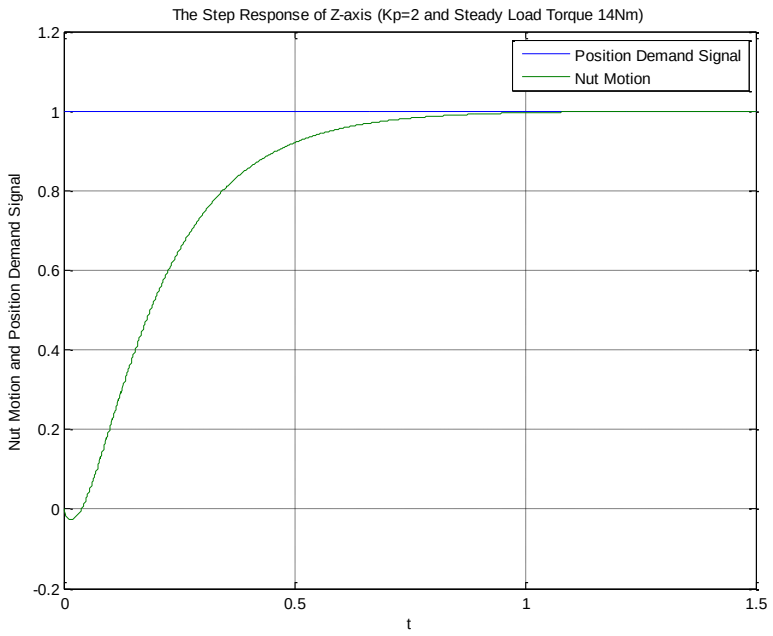

a

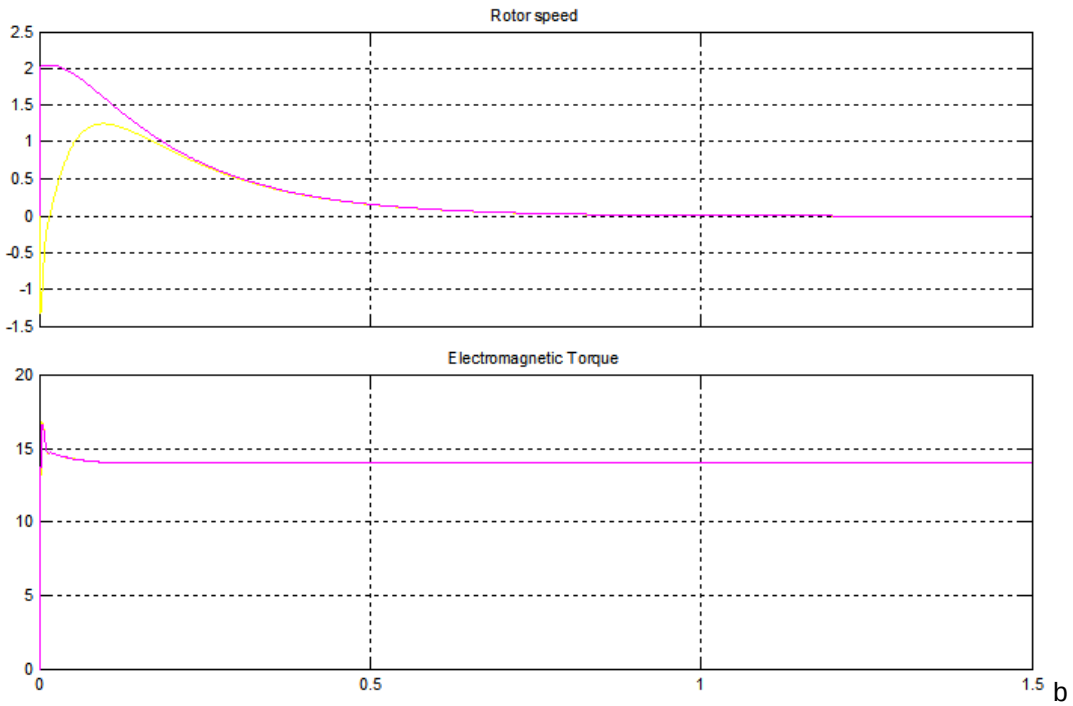

b

a) The step response of Z-axis for a steady load torque 14Nm and Kp=2

Rotor speed with nominal speed (above) and electromagnetic torque with reference torque (below) for a step input, steady load torque 14Nm, and Kp=2

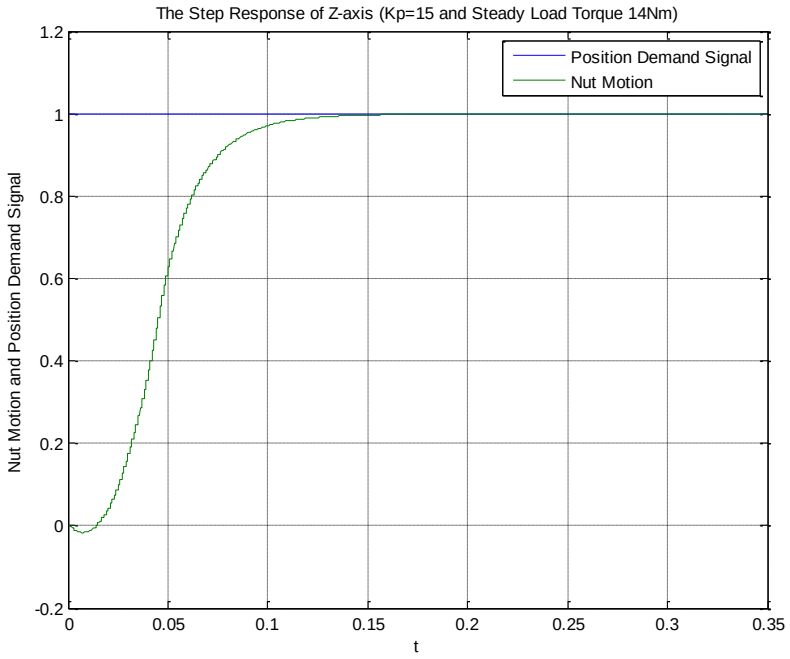

a

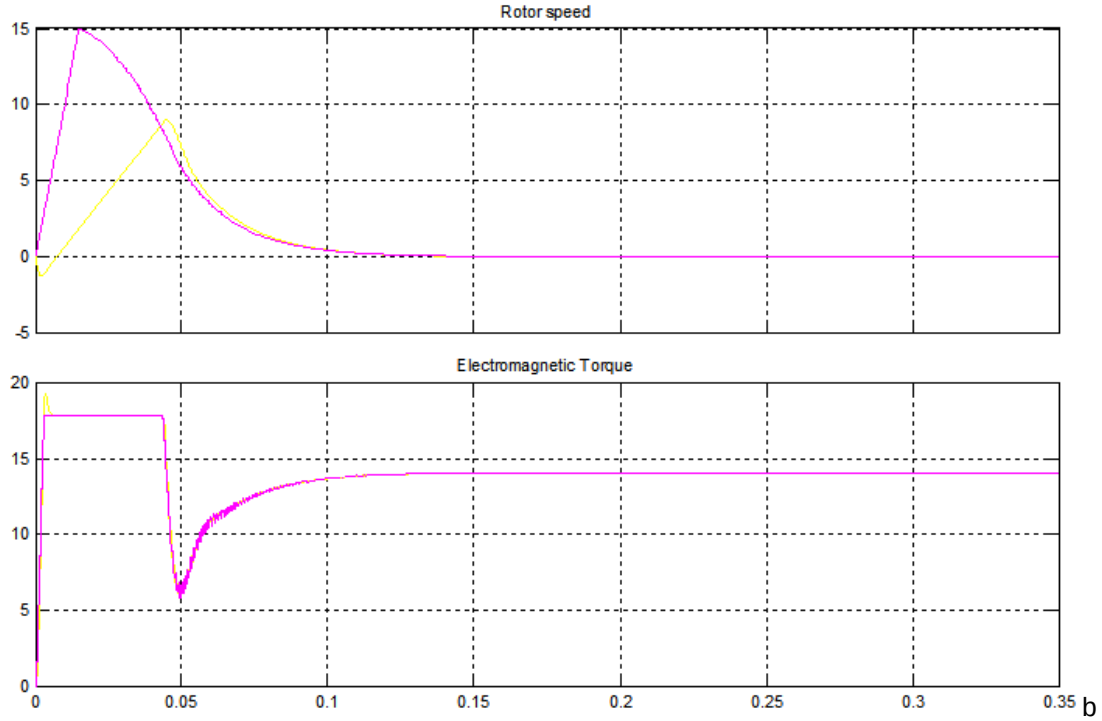

b

a) The step response of Z-axis for a steady load torque 14Nm and Kp=15

Rotor speed with nominal speed (above) and electromagnetic torque with reference torque (below) for a step input, steady load torque 14Nm, and Kp=15

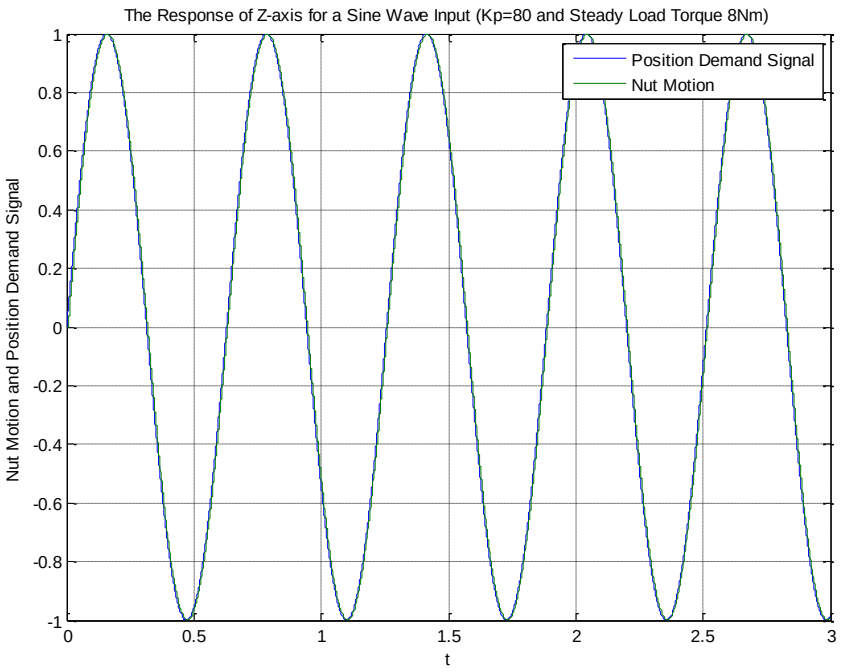

a

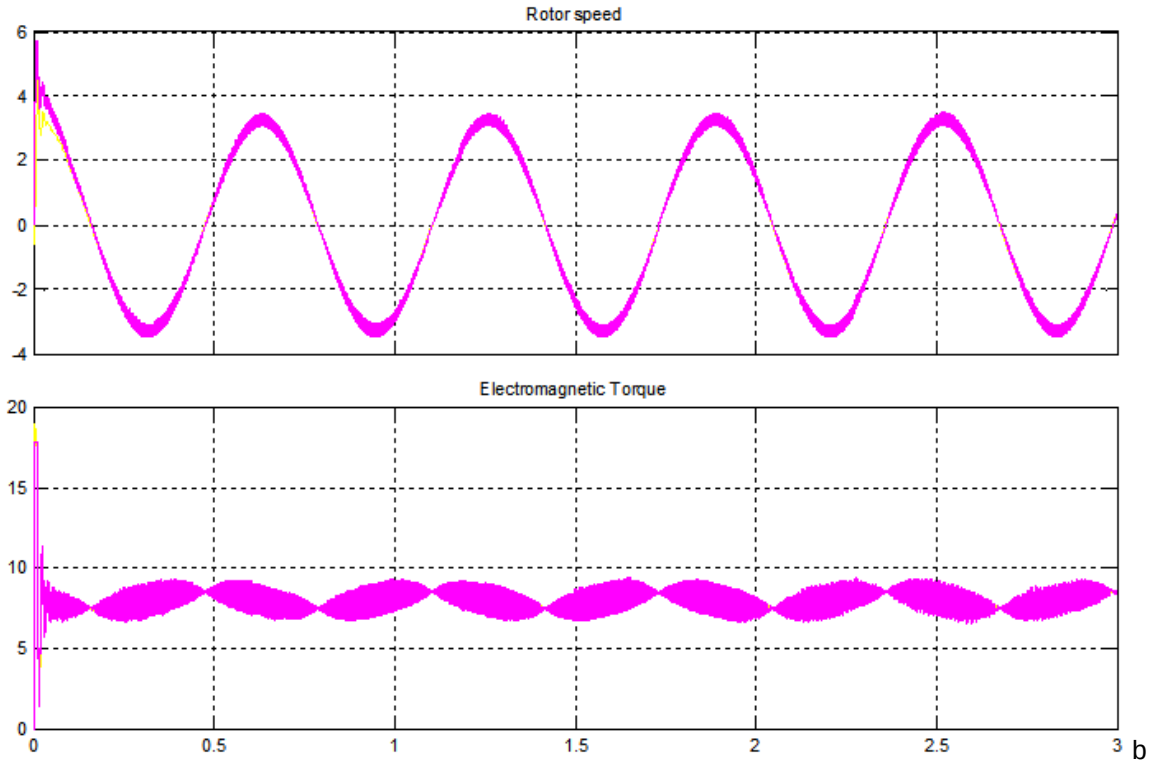

b

a) The response of Z-axis for a sine wave input, steady load torque 8Nm, and Kp=80

Rotor speed with nominal speed (above) and electromagnetic torque with reference torque (below) for a sine wave input, steady load torque 8Nm, and Kp=80

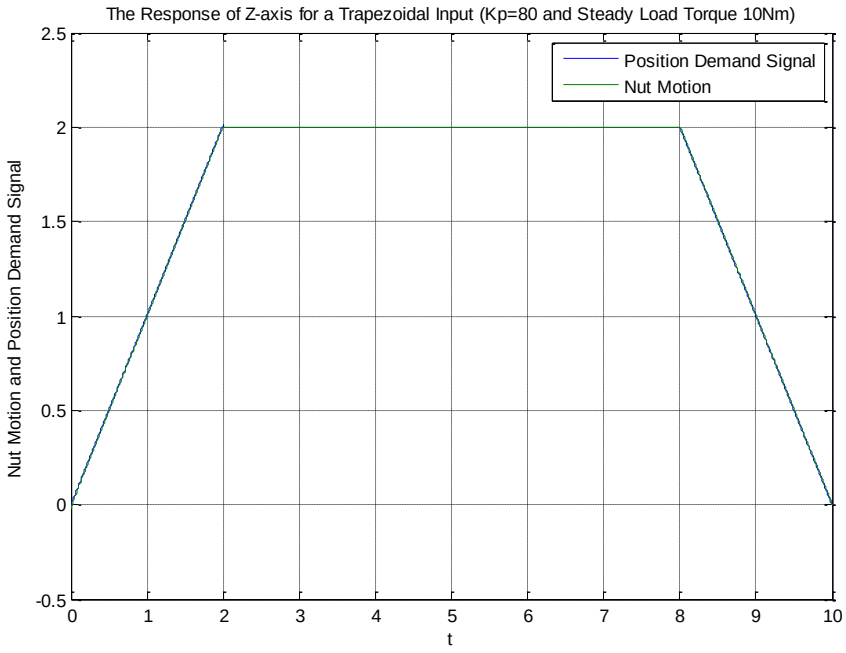

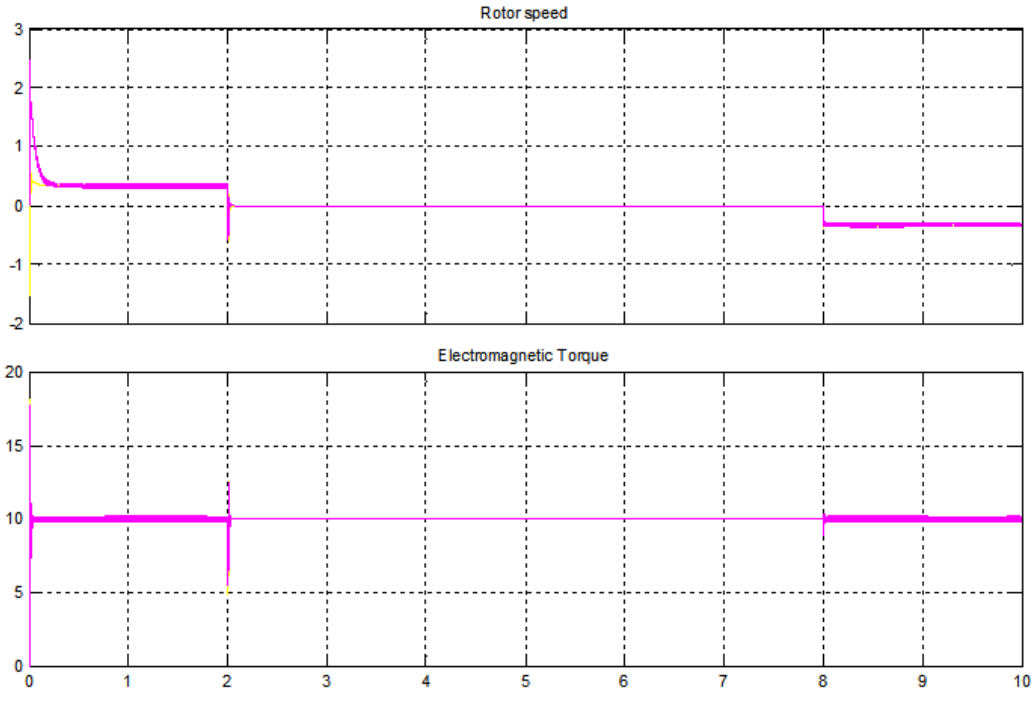

a) The response of Z-axis for a trapezoidal input, steady load torque 10Nm, and Kp=80

Rotor speed with nominal speed (above) and electromagnetic torque with reference torque (below) for a trapezoidal input, steady load torque 10Nm, and Kp=80

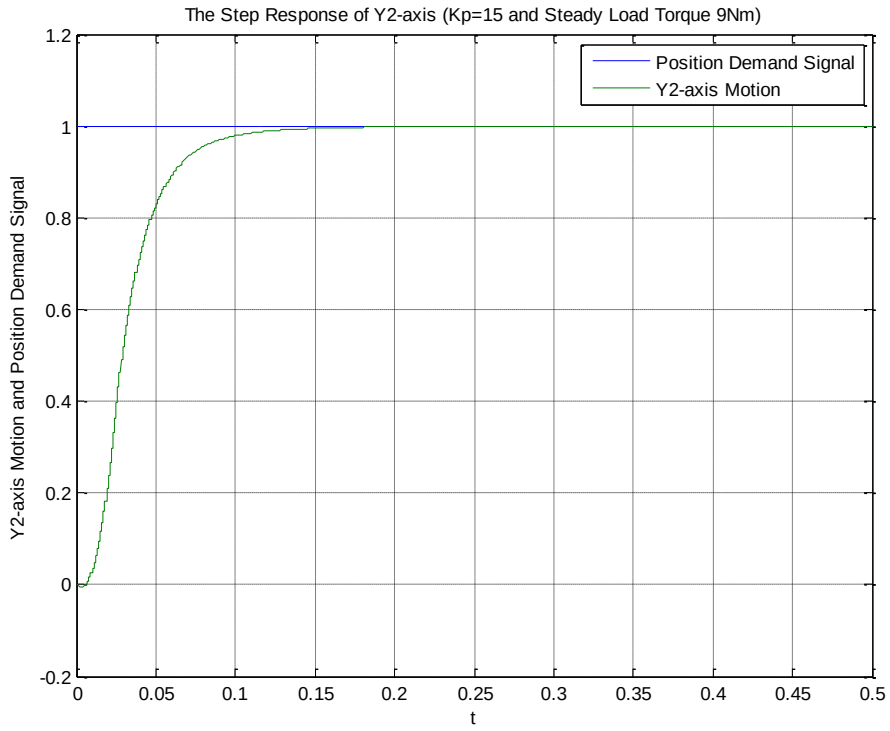

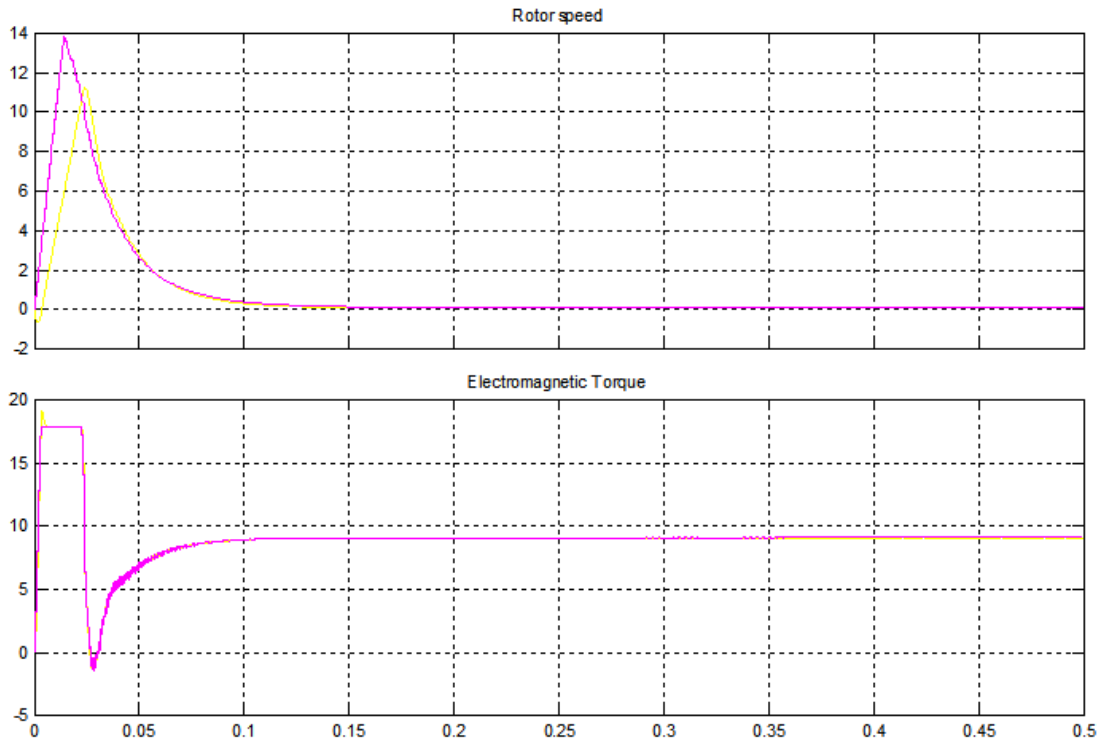

a) The step response of Y2-axis for a steady load torque 9Nm and Kp=15

Rotor speed with nominal speed (above) and electromagnetic torque with reference torque (below) for a step input, steady load torque 9Nm, and Kp=15

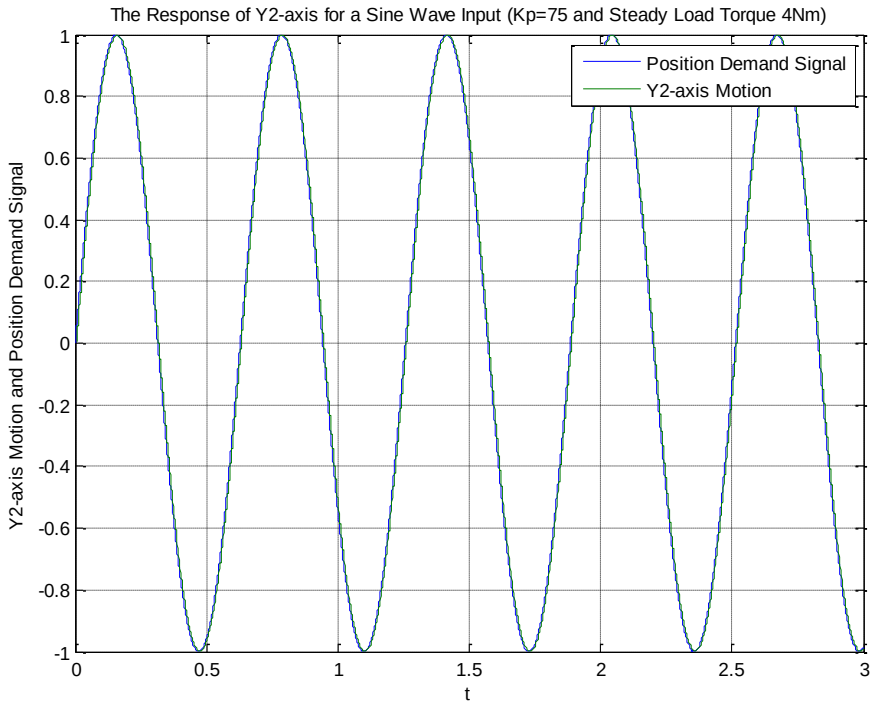

a

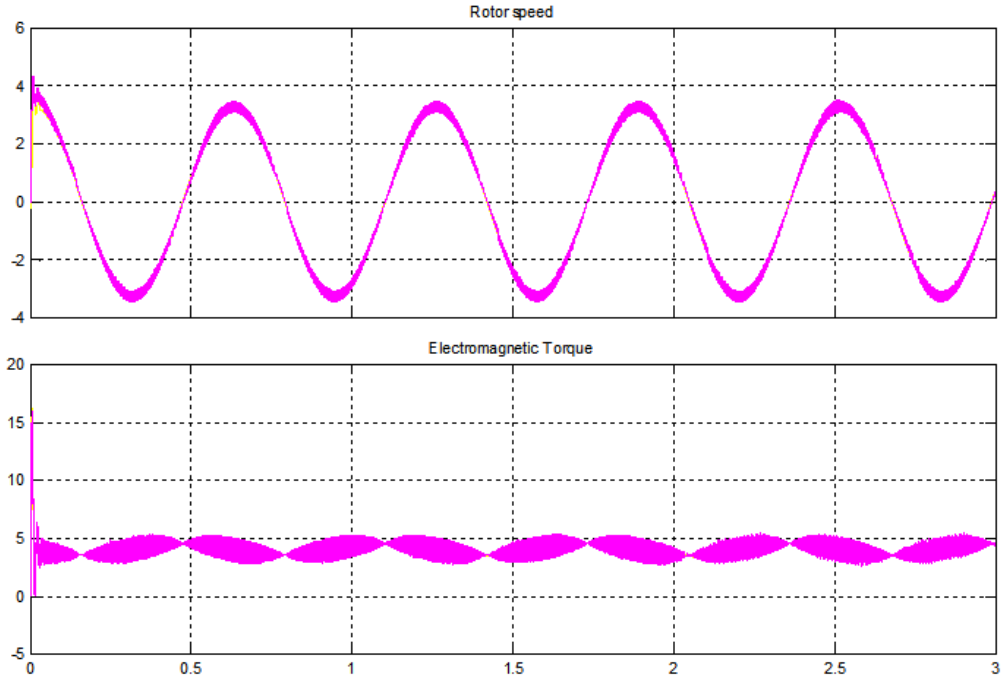

b

a) The response of Y2-axis for a sine wave input, steady load torque 4Nm, and Kp=75

Rotor speed with nominal speed (above) and electromagnetic torque with reference torque (below) for a sine wave input, steady load torque 4Nm, and Kp=75

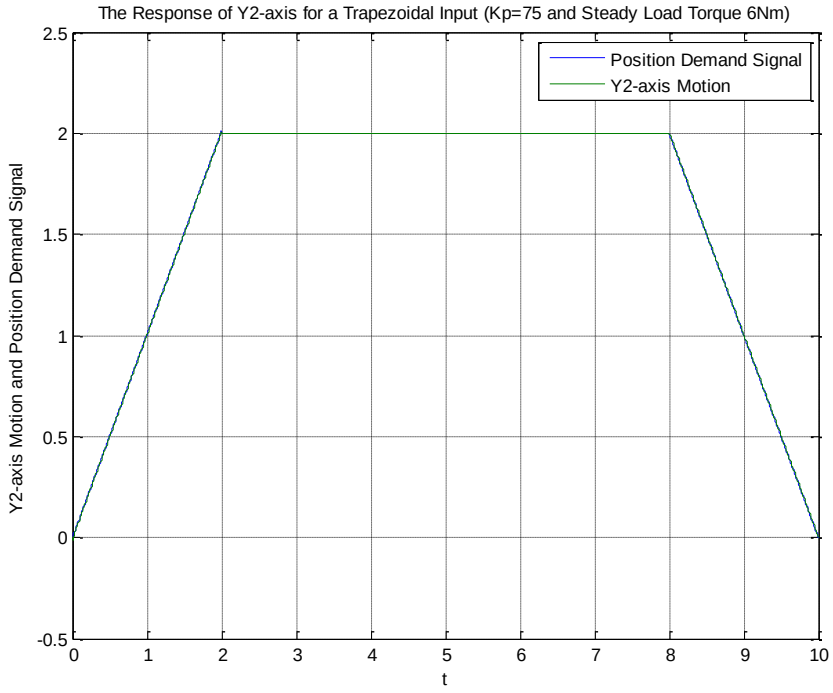

a)

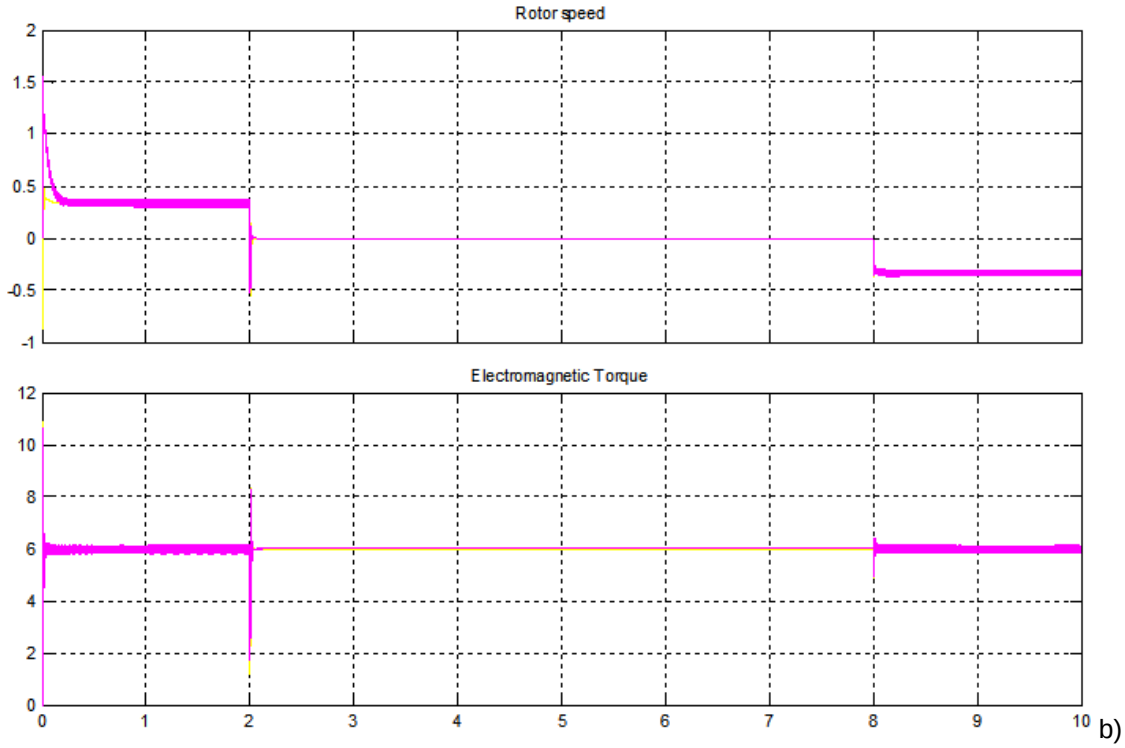

b)

a) The response of Y-axis for a trapezoidal input, steady load torque 6Nm, and Kp=75

Rotor speed with nominal speed (above) and electromagnetic torque with reference torque (below) for a trapezoidal input, steady load torque 6Nm, and Kp=75

APPENDIX E DSPACE SYSTEM TECHNICAL DATA

Parameter	Specification	
	Board Revision DS 1005-09	**Up to Board Revision DS 1005-09**
General	Power PC 750 FX running at 800 MHz	Power PC 750 FX running at 480 MHz
	Building processor systems with further DS 1005PPC boards: Up to 20 DS 1005 boards High-speed link via one DS910 Gigalink Module on each DS 1005 Possible cable length of up to 100 m	
Processor	Power PC 750 FX 800 MHz(up to four parallel instructions, 32 KB L1 data cache, 32 KB L1 instruction cache)	Power PC 750 480 MHz (up to four parallel instructions, 32 KB L1 data cache, 32 KB L1 instruction cache)
	Temperature sensor for the PPC: triggers an exception if the temperature exceeds 100 ° C (emergency shutdown). →Program execution is interrupted and the processor is set to power save mode. Note: Only operating in the stated ambient temperature range ensures that the board works correctly.	
Memory	512 KB level 2 (L2)cache Cache running at processor clock	1 MB level 2 (L2) cache
	128 MB SDRAM global main memory 16 MB flash memory: Consisting of 64 blocks of 256 KB each; At least 100,000 erase cycles possible; 15 MB can be used for a user-specific application ○ 1 MB reserved for the boot firmware	
Timer	2 general-purpose timers Synchronous Time Base Unit (STBU) for multiprocessor systems	
Serial Interface	RS232 interface with standard UART allowing transfer rates of up to 115.2 kBaud	
DS910 Gigalink Module for multiprocessing (optional)	4 optical, high-speed communication ports (Gigalinks), each providing: ○ 16 bidirectional interrupt lines ○ 16 bidirectional data channels (2 KWords width on each channel) I/O access speed of send operations adapted to Gigalink's capabilities: data is sent directly without a FIFO buffer Gross transfer rate: 1.25 GBit/s 32-bit or 64-bit read/write operations allowed: ○ 32-bit access for single 32-bit (or shorter) data words ○ Fast 64-bit access for block transfer functions as far as possible	
Host interface	One full-size 16-bit ISA slot required Via eight 16-bit I/O ports (ISA bus) Bidirectional interrupt line (PPC ↔ host PC) Plug & Play support	
Cooling	DS1005: passive cooling DS910 Gigalink Module: active cooling (fan)	
Power supply	+5 V ±5%, 4 A (without DS910 Gigalink Module) +5 V ±5%, 5.5 A (with DS910 Gigalink Module)	

Table E.1. DS1005 (PPC Board) Data Sheet

Parameter		**Specification**
General		32 A/D input channels (single-ended) 2 independent A/D converters (ADCs) with separate sample-and-hold (S/H), 16 multiplexed inputs each Hold mode; 4-, 8-, 12-, or 16-bit resolution (programmable) 1.5, 2.7, 3.8, 5.0 µs ADC conversion time (resolution dependent) 5 V or 10 V input voltage range (programmable) Interrupt controller
ADCs	Conversion time	5.0 µs
	S/h acquisition time	0.9 µs to 0.01% of FSR (full-scale range)
	Multiplexer settling time	1.2 µs to 0.01% of FSR
	Offset error	±2.0 mV
	Gain error	± 0.2 % of FSR
	Offset drift	± 4 ppm of FSR/K
	Gain drift	± 25 ppm of FSR/K
	Linearity error	± 0.003% of FSR
	Differential linearity error	± 0.002% of FSR
	Missing codes	No missing codes at 14-bit resolution.
	SNR (signal-to-noise-ratio)	78 dB
	Channel crosstalk	-75dB (at 10 kHz signal frequency)
	Input impedance	1 MΩ
	Input overvoltage protection	Up to ± 15 V
	Warm-up time	2 min.
Interrupt controller		2 interrupts on end of A/D conversion (one for each A/D converter)
Host Interface		One 8- or 16-bit ISA slot (power supply only)
Physical size		340 x 125 x 15 mm (13.4 x 4.9 x 0.6 in.)
Ambient temperature		0…70 °C (32…158 °F)
Power supply		+5 V ±5%, 2.5 A OR ±12 V ±5%, 150mA

Table E.2. DS2002 (Multi-channel A/D Board) Data Sheet

Parameter		Specification
General		6 independent incremental encoder interface channels Differentia inputs for encoder phase lines and an index line on each Channel Synchronized sampling of multiple channels Encoder power supply line per channel On-board line termination
Encoder signal types		Sinusoidal signals: 1 V_{pp} differential or 11μA_{pp} differential Digital signals: single-ended (TTL) or differential (RS422) Selectable individually for each channel 250 ns min. index pulse width
Position counters		32 bit resolution, Max. 750 kHz input frequency, i. e., fourfold pulse counts up to 3 MHz; Counter reset or preload via software
Encoder Power supply lines		5 V, 200 mA max. per channel; Voltage regulation with sense lines
Input performance	ADC	12-bit resolution; 800 ns data conversion time
	Offset error (PHI0, PHI90)	±4 mV for V_{pp} (±0.08 % position error) ±75 nA for 11 μA_{pp} (±0.14 % position error)
	ADC nonlinearity	±0.06 % resulting position error ; No missing codes
	Gain match (PHI0, PHI90)	±0.25 (±0.025 % position error) of 1 V_{pp} ±0.6 (±0.06 % position error) of 11 μA_{pp}
	Common mode rejection ratio (PHI0, PHI90 in 1 V_{pp} mode only)	±2.5 m V/V (±0.05 %/V position error) each channel
Host interface		One 8- or 16-bit ISA slot (power supply only)
Physical size		340 x 125 x 15 mm (13.4 x 4.9 x 0.6 in.)
Ambient temperature		0…70 °C (32…158 °F)
Power supply		+5 V ±5%, 2.0 A • ±12 V ±5%, 200 mA plus 200 mA for each channel in use

Table E.3. DS3002 (Incremental Encoder Interface Board) Data Sheet

Parameter		Specification
General		96 bidirectional digital I/O lines arranged in three ports (A,B,C) of 32 lines each Interrupt controller with up to 7 interrupt inputs Release output for external release logic I/O error monitor output and I/O error request input for error monitoring of external devices 2 customization module connectors (pin-headers) supporting digital I/O lines and power supply of port B and C
Digital I/O	Lines	Each of the three ports (A, B, C) provides: 32 I/O lines programmable in 8-bit groups (as non-strobed input, strobed input or output) 1 strobe input 2 handshake lines for acknowledge and output ready
	Voltage range	TTL input/output leve
	Output current	Max. -15 mA/+24 mA
Interrupt controller	Interrupt sources	3 user interrupts (one per port) 3 strobe interrupts (one per port) 1 interrupt on I/O error
	Voltage range	TTl input level
Host interface		One 8- or 16-bit ISA slot (power supply only)
Physical size		340 x 125 x 15 mm (13.4 x 4.9 x 0.6 in.)
Ambient temperature		0…70 °C (32…158 °F) The board requires three brackets
Power supply		+5 V ±5%, 1,5 A without customization modules/external loads)

Table E.4 DS4003 (Digital I/O Board) Data Sheet

APPENDIX F MATLAB CODE

```
clear all
close all

ENERGY=();
RMS=();
MAXAMP=();
MINAMP=();
MEAN=();
KURTOSIS=();
VARIANCE=();
STANDARDDEVIATION=();
SKEWNESS=();
TIME=();
TS=();
waterfall=();
baselineremoved=();
MeanBaselineRemoved=();

s=1;
wc =0.1;
(B,A) = butter(6,wc,'high');

% Load AE data from folder
pname = uigetdir; pname = (pname '\');
dir_names = dir((pname '*.mat'));
for k = 1:length(dir_names);
        names{k} = getfield(dir_names,{k,1},'name');
end;
clear k ; names = names';

if isempty(names);
    disp ('No .tdms files found in this directory');
else
    disp(('Number    of    .tdms    files    in    selected    directory:    '
num2str(length(names))));
end

for fl = 1:length(names);
    z=length(names);
    disp((names{fl} '.   File ' num2str(fl) ' of ' num2str(length(names))
'.'))
    matFileName=(pname names{fl});
 FileName=(pname names{fl});
    %matFileName(names);
    %load (matFileName -regexp '^(?!tpd)...');

    % Import the file
newData1 = load(FileName);


% Create new variables in the base workspace from those fields.
vars = fieldnames(newData1);
```

```
for i = 1:length(vars)
    assignin('base', vars{i}, newData1.(vars{i}));

    for n = 1:length(tpd);
    ti=(newData1.tpd(n,:).DateTime);%show            time            stamp
http://blogs.mathworks.com/videos/2013/07/18/working-with-dates-in-
matlab/?s_tid=Blog_Videos_Category
    (year, month, day, hour, minute, second)=datevec(ti);
    minutesecond=(hour,minute,second);

    Time=datenum(ti);
    ts = timeseries(minutesecond);

    %DATA

    data=(newData1.tpd(n,:).Data);
    Energy=trapz(data.^2);
    rmss=rms(data);
    kurt = kurtosis(data);
    %waterfall=(waterfall repmat(data,i,1));
    %plot(waterfall);%%,(1 1 1),'Edgecolor',(0 0 1)); %plot water
    min_amp=min(data);
    max_amp=max(data);
    mean_val=mean(data);
    var_val=var(data); %returns the variance of the elements of Aalong the
first array dimension whose size does not equal 1.
    sdeviation=std(data);%standard deviation of the elements
    skewness_val=skewness(data);
    %energy=(energy Energy);

    ENERGY=(Energy ENERGY);
    RMS=(rmss RMS);
    MINAMP=(min_amp MINAMP);
    MAXAMP=(max_amp MAXAMP);
    KURTOSIS=(kurt KURTOSIS);
    MEAN=(mean_val MEAN);
    VARIANCE=(var_val VARIANCE);
    STANDARDDEVIATION=(sdeviation STANDARDDEVIATION);
    SKEWNESS=(skewness_val SKEWNESS);
    %Mean=mean(data);
    %baselineremoved=(data-Mean baselineremoved);

    %MeanBaselineRemoved=mean(baselineremoved);
    %MeanBaselineRemoved=(MeanBaselineRemoved baselineremoved);
     %%t(s)=Time;
     TIME=(Time TIME);
     TS=(ts, TS);

    s=s+1;
  %%fft decomposition
  fa=fft(data);
  %fa(20:end)=0;
  N=length(data);%how many decomp;
  fa=fa(1:ceil(N/2));
  mag=2*abs(fa).^2; %calculate energy
  reconstr=real(ifft(fa));
   %% save('test1111.mat','data','-append');
```

```
    end
end

end
 energy1=transpose(ENERGY);
%figure(1)=figure('Position', (100, 100, 1024, 1200));
figure(1);
ha(1)=subplot(3,1,1);%get the axes handle when you create the subplot
plot(TIME,MAXAMP,'b','LineWidth',2); % plot the data,
title('AE MAXIMUM AMPLITUDE');
ylabel('AMPLITUDE(V)');
%xlabel('Time(s)');
axis tight;
grid on;
datetick('x','HH:MM:SS','keeplimits');% give the a xaxis time label ticks..
hold on;

figure(1);
ha(2)=subplot(3,1,2);%get the axes handle when you create the subplot
plot(TIME,MINAMP,'b','LineWidth',2);% plot the data,
title('AE MINIMUM AMPLITUDE');
ylabel('AMPLITUDE(V)');
%xlabel('Time(s)');
axis tight;
grid on;
datetick('x','HH:MM:SS','keeplimits');% give the a xaxis time label ticks..
hold on;

figure(1);
ha(3)=subplot(3,1,3);%get the axes handle when you create the subplot
plot(TIME,MEAN,'b','LineWidth',2);  %# Update the y data of the line
title('AE MEAN');
ylabel('MEAN(V)');
xlabel('TIME(s)');
axis tight;
grid on;
datetick('x','HH:MM:SS','keeplimits');


figure(2);
ha(4)=subplot(3,1,1);%get the axes handle when you create the subplot
plot(TIME,RMS,'b','LineWidth',2);  %# Update the y data of the line
title('AE RMS VALUE');
ylabel('RMS(V)');
%xlabel('Time(s)');
axis tight;
grid on;
datetick('x','HH:MM:SS','keeplimits');

figure(2);
ha(5)=subplot(3,1,2);%get the axes handle when you create the subplot
plot(TIME,KURTOSIS,'b','LineWidth',2);  %# Update the y data of the line
title('AE KURTOSIS');
ylabel('KURTOSIS(V)');
%xlabel('Time(s)');
```

```
axis tight;
grid on;
datetick('x','HH:MM:SS','keeplimits');

figure(2);
ha(6)=subplot(3,1,3);%get the axes handle when you create the subplot
plot(TIME,SKEWNESS,'b','LineWidth',2);  %# Update the y data of the line
title('AE SKEWNESS');
ylabel('AMPLITUDE(V)');
xlabel('TIME(s)');
axis tight;
grid on;
datetick('x','HH:MM:SS','keeplimits');

figure(3);
ha(7)=subplot(3,1,2); %get the axes handle when you create the subplot
plot(TIME,VARIANCE,'b','LineWidth',2);  %# Update the y data of the line
title('AE VARIANCE');
ylabel('AMPLITUDE(V)');
%xlabel('Time(s)');
axis tight;
grid on;
datetick('x','HH:MM:SS','keeplimits');

figure(3);
ha(8)=subplot(3,1,1);%get the axes handle when you create the subplot
plot(TIME,STANDARDDEVIATION,'b','LineWidth',2);  %# Update the y data of the
line
title('AE STANDARDDEVIATION');
ylabel('AMPLITUDE(V)');
%xlabel('Time(s)');
axis tight;
grid on;
datetick('x','HH:MM:SS','keeplimits')

figure(3);
ha(9)=subplot(3,1,3);%get the axes handle when you create the subplot
plot(TIME,ENERGY,'b','LineWidth',2);
title('AE ENERGY');
ylabel('AMPLITUDE(V)');
xlabel('TIME(s)');
axis tight;
grid on;
datetick('x','HH:MM:SS','keeplimits')% plot the data,
linkaxes(ha, 'x');% Link all axes in x
   % give the a xaxis time label ticks..
hold on;
%%drawnow                %# Force the graphics to update immediately
hold off;
```

APPENDIX G ANALYSED AE DATA RESULTS

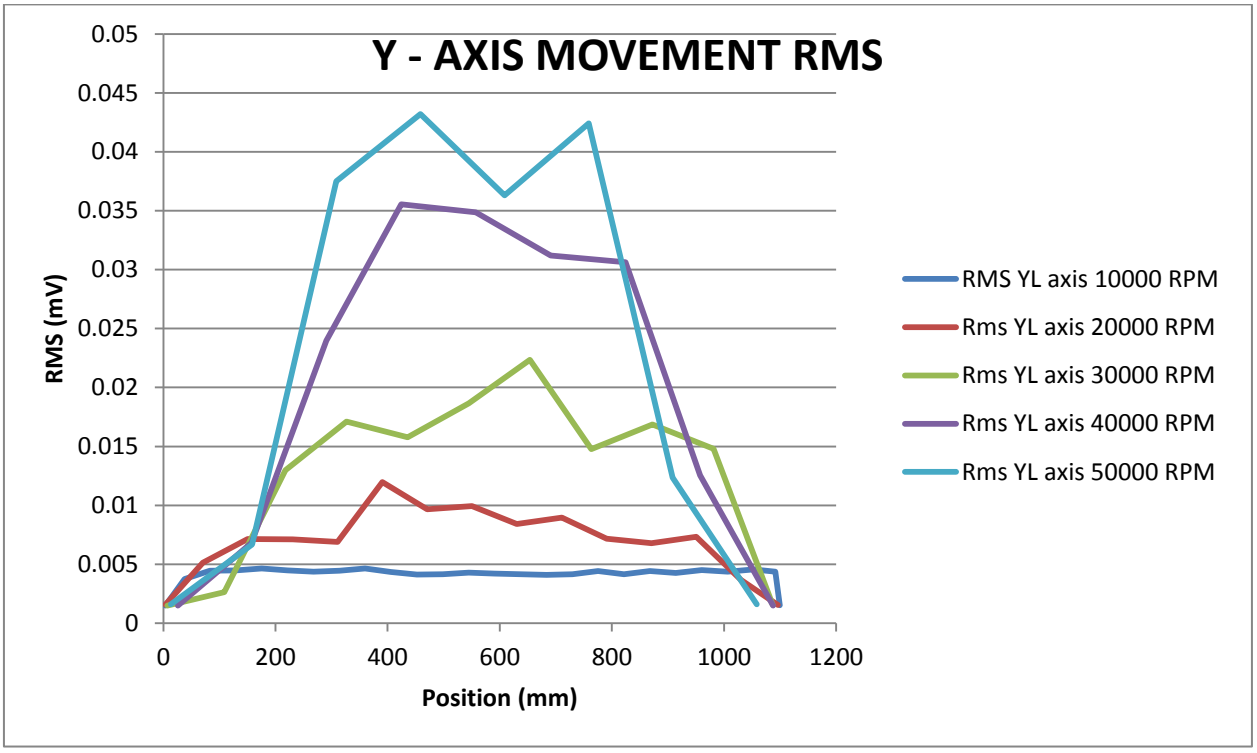

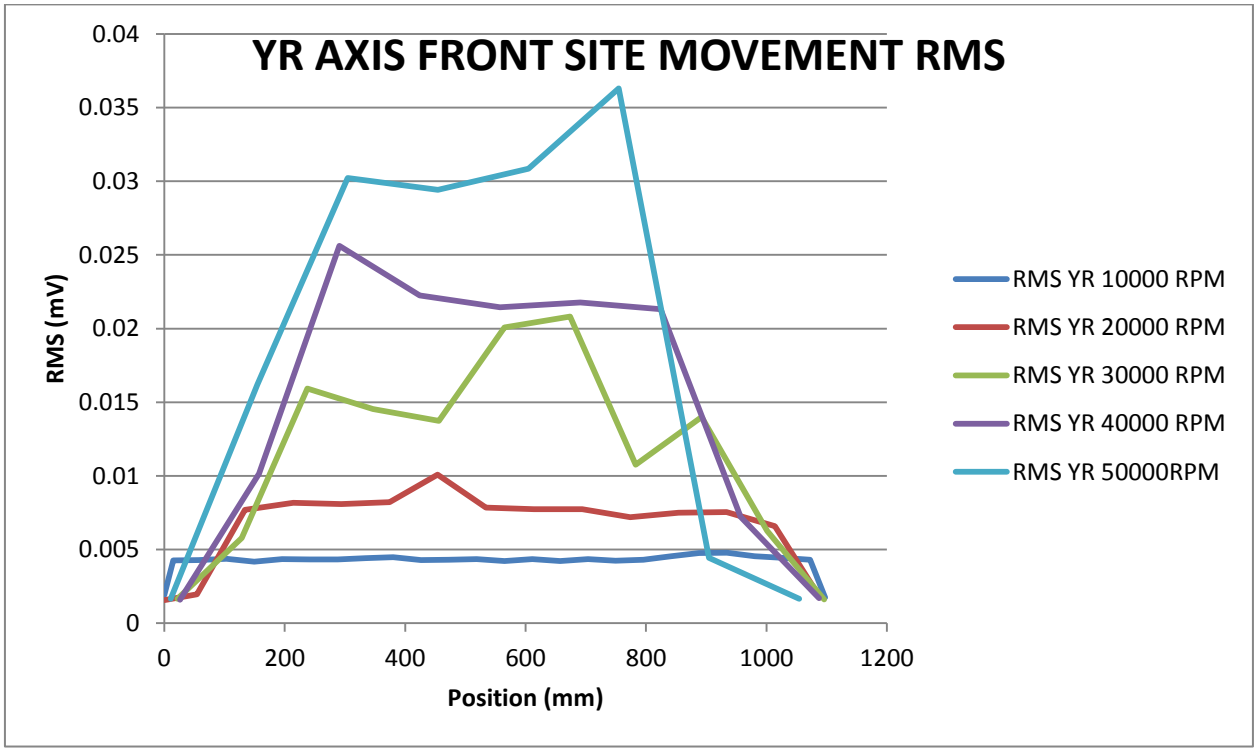

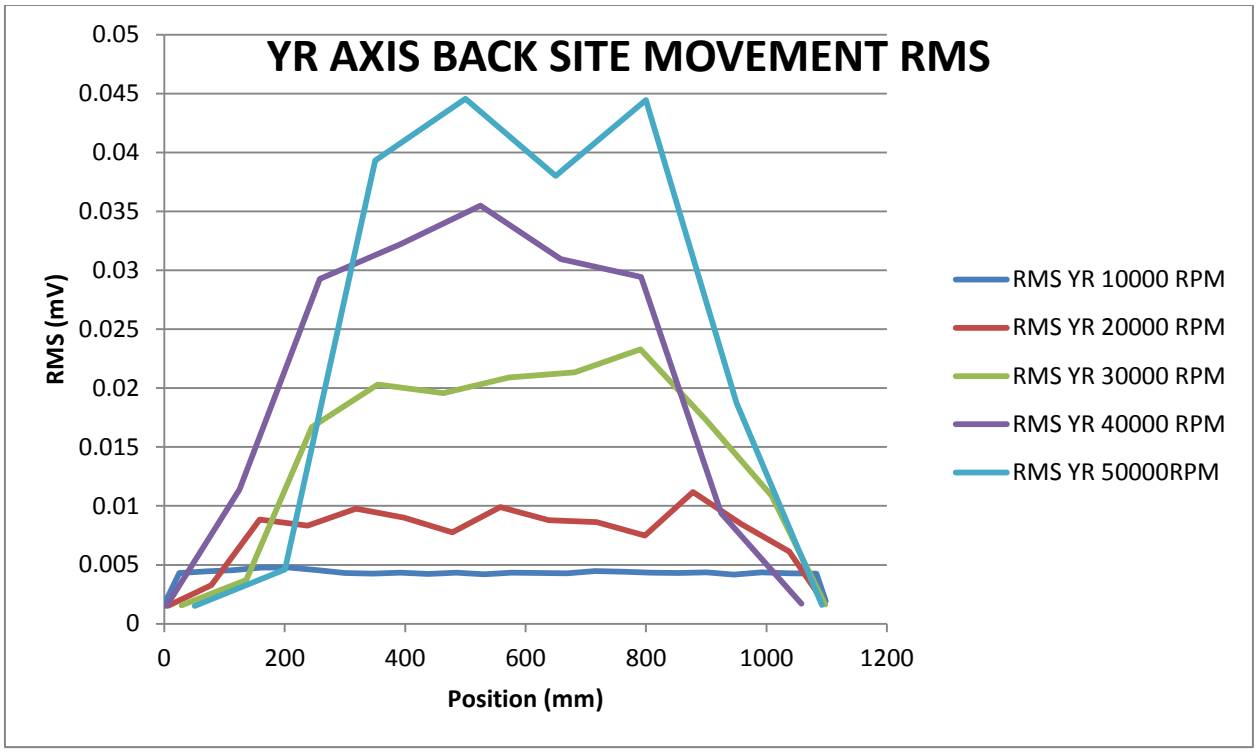
YR AXIS BACK SITE MOVEMENT RMS
RMS (mV)
0.05
0.045
0.04
0.035
0.03
0.025
0.02
0.015
0.01
0.005
0
0
200
400
600
800
1000
1200
Position (mm)
RMS YR 10000 RPM
RMS YR 20000 RPM
RMS YR 30000 RPM
RMS YR 40000 RPM
RMS YR 50000RPM

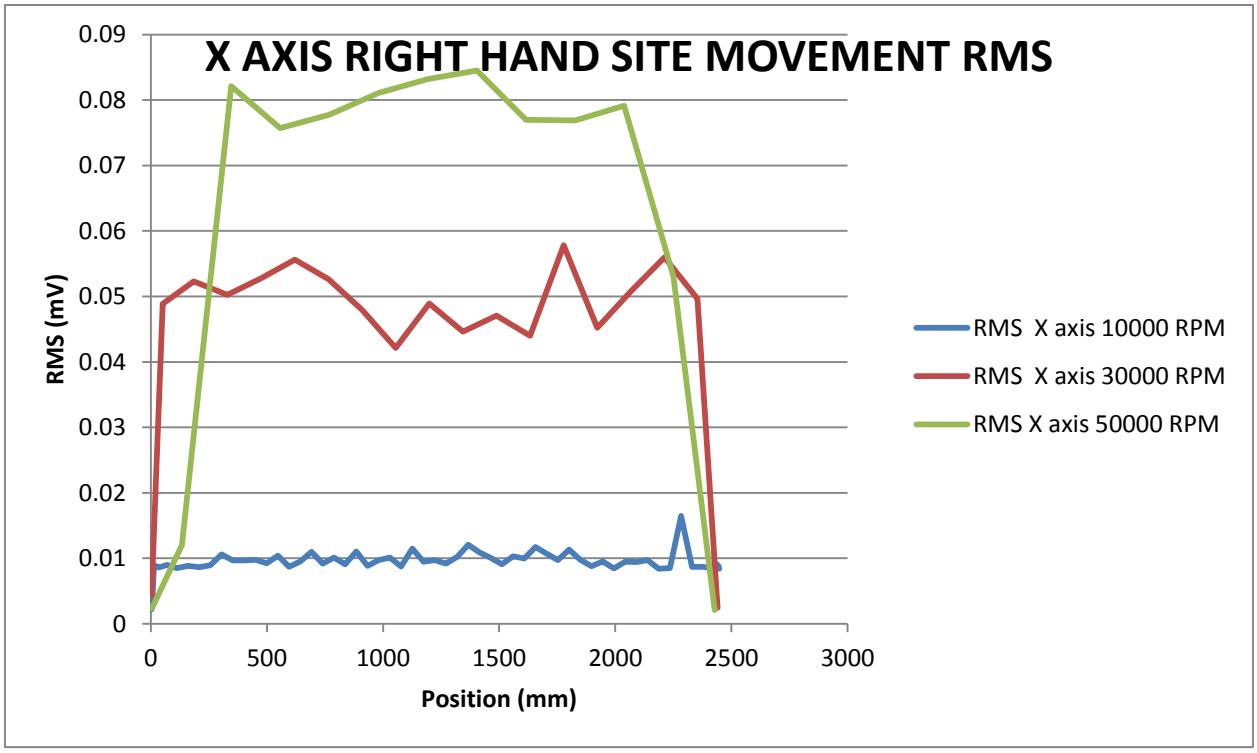
X AXIS RIGHT HAND SITE MOVEMENT RMS
RMS (mV)
0.09
0.08
0.07
0.06
0.05
0.04
0.03
0.02
0.01
0
0
500
1000
1500
2000
2500
3000
Position (mm)
RMS X axis 10000 RPM
RMS X axis 30000 RPM
RMS X axis 50000 RPM

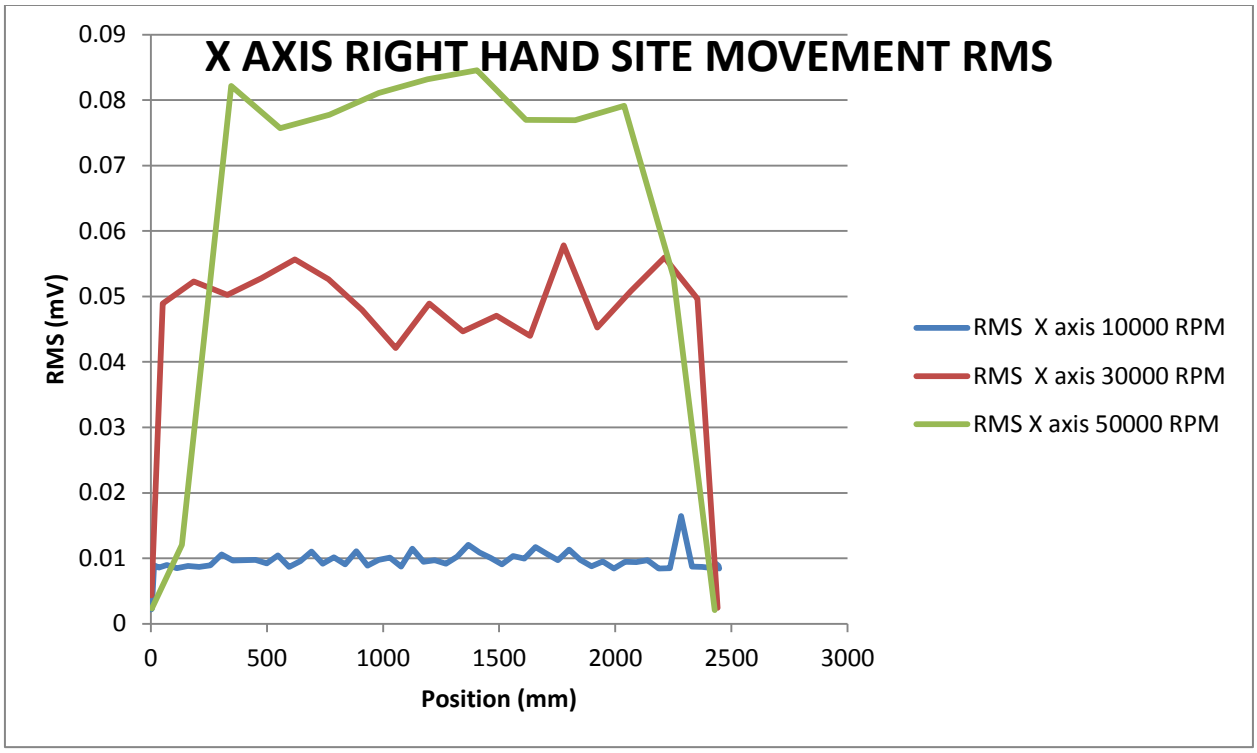
X AXIS RIGHT HAND SITE MOVEMENT RMS
RMS (mV)
0.09
0.08
0.07
0.06
0.05
0.04
0.03
0.02
0.01
0
0
500
1000
1500
2000
2500
3000
Position (mm)
RMS X axis 10000 RPM
RMS X axis 30000 RPM
RMS X axis 50000 RPM

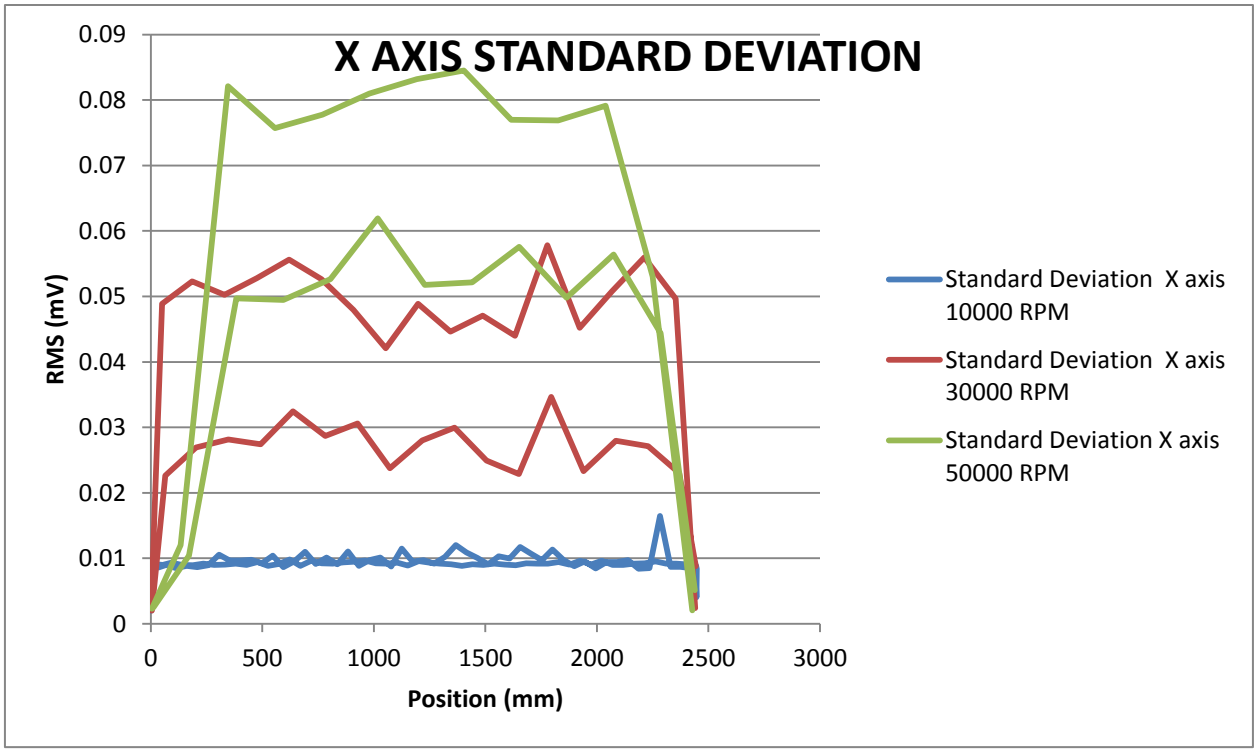
X AXIS STANDARD DEVIATION
RMS (mV)
0.09
0.08
0.07
0.06
0.05
0.04
0.03
0.02
0.01
0
0
500
1000
1500
2000
2500
3000
Position (mm)
Standard Deviation X axis 10000 RPM
Standard Deviation X axis 30000 RPM
Standard Deviation X axis 50000 RPM

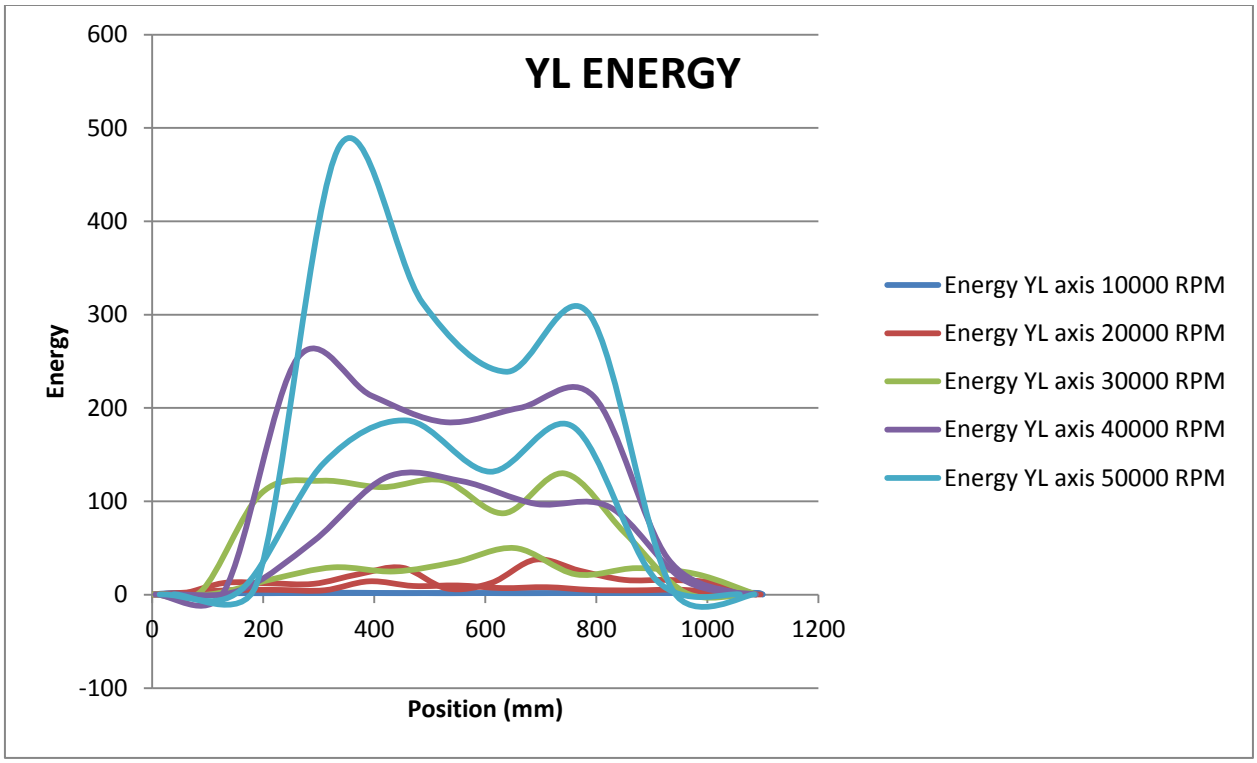
YL ENERGY
600
500
400
300
200
100
0
-100
Energy
0
200
400
600
800
1000
1200
Position (mm)
Energy YL axis 10000 RPM
Energy YL axis 20000 RPM
Energy YL axis 30000 RPM
Energy YL axis 40000 RPM
Energy YL axis 50000 RPM

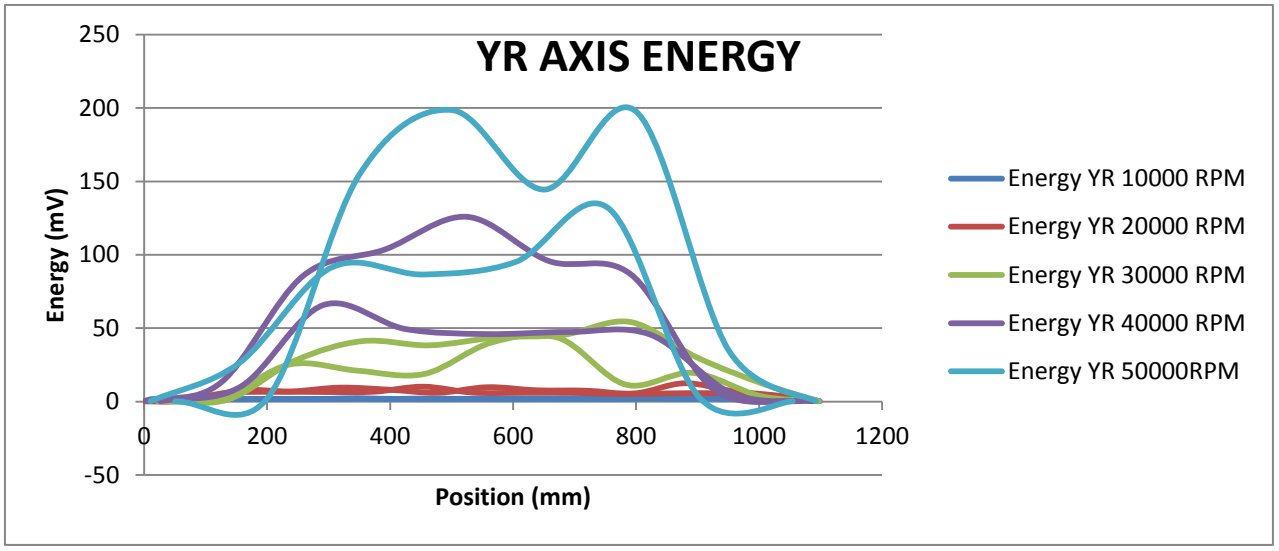
YR AXIS ENERGY
250
200
150
100
50
0
-50
Energy (mV)
0
200
400
600
800
1000
1200
Position (mm)
Energy YR 10000 RPM
Energy YR 20000 RPM
Energy YR 30000 RPM
Energy YR 40000 RPM
Energy YR 50000RPM

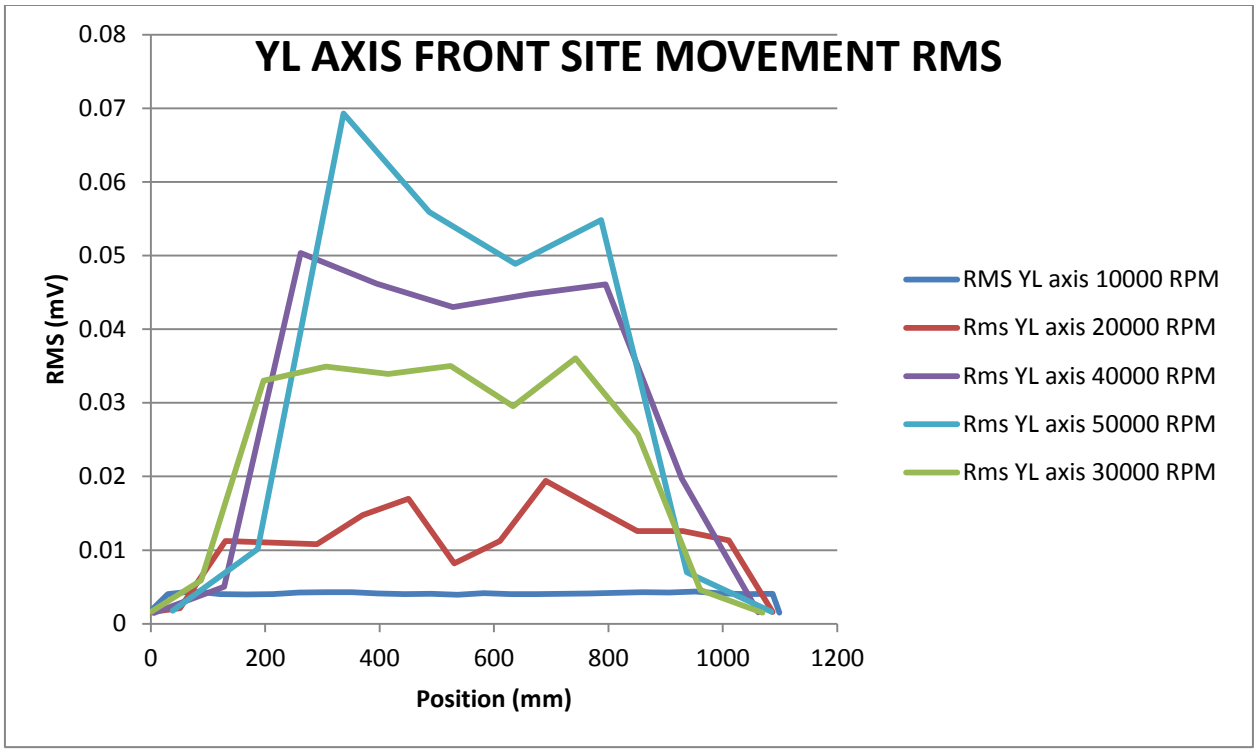
YL AXIS FRONT SITE MOVEMENT RMS
RMS (mV)
0.08
0.07
0.06
0.05
0.04
0.03
0.02
0.01
0
0
200
400
600
800
1000
1200
Position (mm)
RMS YL axis 10000 RPM
Rms YL axis 20000 RPM
Rms YL axis 40000 RPM
Rms YL axis 50000 RPM
Rms YL axis 30000 RPM

APPENDIX H SERVO TRACE MEASUREMENT

The selected signals are also active after POWER ON.

Machine→Menu Select →Start up→ Drives Servo → Servo Trace

In the basic display you can select:

Machine→Menu Select →Start up→ Drives Servo → Servo Trace → Measurement

Under the window following objects can be selected:

The axis/spindle to measure

The signal to measure

The duration of measurement

The threshold time and the type of triggering

To run the measure parameters use following steps:

Machine→Menu Select →Start up→ Drives Servo → Servo Trace → Start Measurement

To save/load/delete measured data:

Machine→Menu Select →Start up→ Drives Servo → Servo Trace → File Functions → Save Data

Create **"New directories"** in the "Service" area.

Under **"Directory"** frame select the directory under which file has to be saved.

In the "Data" frame select the data type. Possible to choose:

-Parameter -Drive MD

-Bit graph -Graph1-Graph2

-Axis MD -Graph 1 & 2

Access to display of the trace function:

Machine→Menu Select →Start up→ Drives Servo → Servo Trace → Display → Start

In the **"File"** frame select an existing file from the dropdown list or enter one in the text field underneath.

To copy saved data go under **"DOS SHELL"**

Machine→Menu Select →MMC→ DOS SHELL

Type DOS commands to get directory and save data. In our case it's:

cd .. /Input

cd dh /Input

d dg.dir /Input % “cd” sometimes also available as chdir (change directory), is a command line command to change the current working directory in DOS

cd seb.uma /Input

cd svtrc.dir /Input

cd svtrg1.dir /Input

copy *filename*.st1 a: /Input % “Copy” file to a directory

Press **“Menu Select”** to come back from DOS